IDENTIFYING THERAPEUTIC AGENTS FOR THE TREATMENT OF DIFFUSE LARGE B-CELL LYMPHOMA

Marissa Lynn Cann

A dissertation submitted to the faculty at the University of North Carolina at Chapel Hill in partial fulfillment of the requirements for the degree of Doctor of Philosophy in the Department of Pharmacology in the School of Medicine.

Chapel Hill
2017

Approved by:

David S. Lawrence

Lee M. Graves

Gary L. Johnson

Kristy L. Richards

John E. Sondek

ABSTRACT

Marissa Lynn Cann: Identifying Therapeutic Agents for the Treatment of Diffuse Large B-cell Lymphoma
(Under the direction of David S. Lawrence)

Diffuse large B-cell lymphoma (DLBCL) can be categorized into two clinically relevant subtypes: activated B-cell (ABC) DLBCL and germinal center B-cell (GCB). Patients with ABC DLBCL have a worse prognosis, and are defined by chronic, overactive signaling through the B-cell receptor and NF-κB pathways. Signaling through the B-cell receptor is heavily dependent on the Src family kinases (SFKs), and NF-κB signaling is dependent on the proteasome.

In Chapters 2 and 3, we examined the effects of the SFK inhibitor dasatinib in a panel of ABC and GCB DLBCL cell lines, with a focus on changes in the kinome (Chapter 2) or the proteasome (Chapter 3). In Chapter 2, we found that the ABC DLBCL cell lines are much more sensitive to dasatinib than the GCB DLBCL cell lines. However, both subtypes display inhibition of the SFKs in response to dasatinib treatment. Subsequent analyses revealed several cell cycle kinases to be inhibited by dasatinib treatment in the ABC DLBCL subtype, but not in the GCB DLBCL subtype. In Chapter 3, we found that treatment with dasatinib results in a decrease in the proteasome's chymotrypsin-like (ChL), trypsin-like (TL), and caspase-like (CaL) activities in the ABC but not GCB DLBCL cell lines. Furthermore, it appears that association between the proteasome 20S core particle and 19S regulatory particle is disrupted in the ABC DLBCL cell lines after dasatinib treatment.

In Chapter 4, we explored the utility of site-specific inhibitors of the proteasome's TL and CaL activities in a variety of cancer cell lines. We found that the TL/ChL and CaL/ChL ratios of proteasome activity correlate with sensitivity to TL and CaL inhibitors, respectively. In addition, the two hematological malignancy cell lines studied are most sensitive to the site-specific inhibitors. Furthermore, the combination of the TL or CaL site-specific inhibitors with bortezomib or carfilzomib is synergistic in all cell lines examined.

The studies presented in this thesis have important implications for the clinical use of dasatinib and site-specific proteasome inhibitors for the treatment of DLBCL, either alone or in combination with other agents. These inhibitors show promise and warrant further exploration.

To my fiancé, Garrett Berry,
who keeps me on my toes
&
To parents, James and Cori Cann,
who never stopped believing in me

ACKNOWLEDGMENTS

First and foremost, I would like to thank the members of my thesis committee, starting with my thesis mentor, David Lawrence. David has been a wonderful mentor to me during my time at UNC. He has pushed me to think about my research from different perspectives, encouraged all my grant writing adventures, and his snarky sense of humor has always helped make the lab a brighter place. I would not be the scientist I am today without his guidance and support. I would also like to thank Kristy Richards, who served as my clinical co-mentor as part of UNC's Training Program in Translational Medicine. Her input and advice has been critical for the development of my thesis project. I would also like to thank Lee Graves, my committee chair. He has been like a second mentor to me the past few years, and I am grateful for his support and advice regarding my endeavors both in and outside the lab. I would also like to thank the other members of my thesis committee, Gary Johnson and John Sondek, whose questions and critiques have been invaluable in carrying out my thesis work.

I would like to thank my labmates, both current and former members of the Lawrence lab. Melanie Priestman played an essential role in my development as a scientist, and I am grateful for her wisdom and advice. My work with Weichen Xu when I first joined the Lawrence lab is what kickstarted my thesis project, and I am grateful to her for my beginnings. It has been a pleasure working with Robert Hughes, Qunzhao Wang, Nate Oien, Luong Nguyen, Weston Smith, Zach Rodgers, Colin O'Banion, Song Ding, Anwesha Goswami, Christina

Marvin, Emilia Zwyot, Amber Lee, Brianna Vickerman, and Josh Welfare. I wish you all the best of luck in your lives and careers.

I would also like to thank my collaborators in the Graves lab and the UNC Proteomics Core facility. Laura Herring and Karim Gilbert were instrumental in helping me with my proteomics experiments, and I greatly appreciate all of the time Laura spent chatting with me about my data and experiments. Ian McDonald, Mike East, and Denis Okumu were always fun to chat with whenever I had to pop into the Graves lab (and their requests for cookies were always flattering!).

The administrative staff in the Department of Pharmacology also deserve a shout-out. In particular, Nicole Arnold and Arlene Sandoval have been critical for keeping the Department of Pharmacology running. They are always willing to help folks in the department, and have truly helped make the Department of Pharmacology feel like a home to me. Their dedication to the department and the graduate students is felt and appreciated by all of us.

One of the best parts of graduate school has been the friends I've made, and I am grateful for all of the wonderful people I have met during this journey. James Shellhammer has been my pharmacology buddy since day one, and I wish him the best of luck in his post-doc in Ireland. I am also thankful for the close friendships I have formed with Emily Tegowski, Cassandra Hayne, and Meagan Ryan. They have been incredible friends, and I am grateful to have enjoyed many a girls' night with them. I look forward to our future escapades. I would also like to thank my friends from Michigan State University, especially Lauren Luethy and Chelsea Cojocari, who have always lent an understanding ear during the trials of graduate school.

I would like to thank my parents, Jim and Cori Cann, and my brother, Shane, for their love and support during my time in graduate school. Their belief in me and my future success

has meant much to me while I progressed in graduate school. I always got a kick out of my dad asking how "my little amoebas were doing", even though they're a completely different organism from what I've studied for the past 6 years. I am lucky to have such a loving and supportive family. I would also like to thank my future in-laws, Paula, Wayne, Colton, and Kira, who have been just as supportive of my journey as they have been of my fiancé's. It was always nice to hear Paula brag about how her "babies are going to be scientists". I am grateful to become part of their family.

Most importantly, I would like to thank my fiancé, Garrett Berry. He has been with me every step of the way regarding graduate school, from studying for the GRE all the way to writing and defending my dissertation. He has kept me grounded, been a comfort during the bad days in lab (we all have them), celebrated my triumphs, and has been there to push me when my tendencies toward procrastination threatened to get the better of me. I can honestly say I could not have done this without him. Garrett, I thank you for everything you are and what you have done for me, and I am honored and thrilled to become your wife.

Last, but not least (okay well maybe least), I would like to thank my handy-dandy laptop. She's been with me since the beginning of my undergraduate career and, while she may be slow and ancient in computer years, she has been my trusty sidekick all throughout my undergraduate and graduate careers. She hasn't given me her last blue screen of death yet, but when that time comes, may she rest in peace.

TABLE OF CONTENTS

LIST OF TABLES

LIST OF FIGURES

LIST OF ABBREVIATIONS

°C	degree(s) Celsius
%	percent
λ_{ex}	excitation wavelength
µg	microgram(s)
µL	microliter(s)
µm	micrometer(s)
µM	micromolar
x g	multiples of the standard acceleration due to gravity
AB40	acid blue 40
ABC	activated B-cell
ABP	activity-based probe
ACN	acetonitrile
ADP	adenosine diphosphate
AGC	AGC kinase family; family of protein kinases containing 60 members, including cAMP-dependent kinase (PKA), cGMP-dependent kinase (PKG), and protein kinase C (PKC)
AML	acute myelogenous leukemia
ANOVA	analysis of variance
AnnV	annexin V
AS	analog-sensitive
ATP	adenosine triphosphate
AURKA	Aurora kinase A (gene name)
AURKB	Aurora kinase B (gene name)
BCA	bicinchoninic acid

BCR	B-cell receptor
BioID	proximity-dependent biotin identification
BSA	bovine serum albumin
Btk	Bruton's tyrosine kinase
CaL	caspase-like
CAMK	CAMK kinase family; family of kinases named after Ca^{2+}/calmodulin-dependent protein kinase
CD20	B-lymphocyte antigen cluster of differentiation 20
CDK	Cyclin-dependent kinase (protein family)
CE	capillary electrophoresis
CE-LIF	capillary electrophoresis with laser-induced fluorescence detection
ChL	chymotrypsin-like
CHOP	chemotherapy cocktail of cyclophosphamide, doxorubicin (also known as hydroxydaunorubicin), vincristine (brand name Oncovin), and prednisone
CK1	casein kinase 1 (CK1) family of kinases
cm	centimeter(s)
cm^2	square centimeter(s)
CMGC	CMGC kinase family; family of kinases including cyclin-dependent kinases (CDKs), mitogen-activated protein kinases (MAP kinases), glycogen synthase kinases (GSK), and CDK-like kinases)
CML	chronic myelogenous leukemia
CO_2	carbon dioxide
CP	core particle
C-terminal	carboxy-terminal
DLBCL	diffuse large B-cell lymphoma
DMSO	dimethyl sulfoxide

DNA	deoxyribonucleic acid
DPBS	Dulbecco's phosphate-buffered saline
DTT	dithiothreitol
EC_{50}	effective concentration of 50% inhibition
ECL	enhanced chemiluminescence
EDTA	ethylene diamine tetraacetic acid
EGFR	epidermal growth factor receptor
EGTA	ethylene glycol tetraacetic acid
ELISA	enzyme-linked immunosorbent assay
ERK	extracellular signal-regulated kinase
FAK	focal adhesion kinase
FBS	fetal bovine serum
FDA	U.S. Food and Drug Administration
FDR	false discovery rate
Fmoc	9-fluoroenylmethoxycarbonyl
FP	fluorescence polarization
FRET	fluorescence resonance energy transfer
FU	fluorescence units
GAPDH	glyceraldehyde-3-phosphate dehydrogenase
GCB	germinal center B-cell
HCD	higher-energy collisional dissociation
HCMV	human cytomegalovirus
HEPES	4-(2-hydroxyethyl)-1-piperazineethanesulfonic acid
h	hour(s)
HRP	horseradish peroxidase

HTRF	homogeneous time resolved fluorescence
IκB	inhibitor of kappa B (inhibitor of NF-κB)
IKK	inhibitor of kappa B (IκB) kinase
IP	immunoprecipitation
ITAM	immunoreceptor tyrosine-based activation motif
KCl	potassium chloride
kDa	kilodalton(s)
LANCE	lanthanide chelate excitation
LC	liquid chromatography
LFQ	label-free quantification
LIF	laser-induced fluorescence
M	molar
MAPK	mitogen-activated protein kinase
mg	milligram(s)
$MgCl_2$	magnesium chloride
mg/mL	milligram(s) per milliliter
MIB	multiplexed inhibitor bead
MIB/MS	multiplexed inhibitor beads combined with mass spectrometry
mIg	membrane immunoglobulin
min	minute(s)
mL	milliliter(s)
mM	millimolar
M-PER	mammalian protein extraction reagent (from Thermo Scientific)
MRM	multiple reaction monitoring
MS	mass spectrometry

m/z	mass to charge ratio
Na_3VO_4	sodium orthovanadate
NaCl	sodium chloride
NADH	nicotinamide adenine dinucleotide
NaF	sodium flouride
ND	not detected
NEK	NimA-related kinase family of kinases
NF-κB	nuclear factor kappa-light-chain-enhancer of activated B-cells
NHL	non-Hodgkin lymphoma
nL/min	nanoliter(s) per minute
nm	nanometer(s)
nM	nanomolar
N-terminal	amino-terminal
PAGE	polyacrylamide gel electrophoresis
PBS	phosphate-buffered saline
PCA	principal component analysis
pH	potential of hydrogen
PI	propidium iodide
PI3K	phosphoinositide 3-kinase
PKCβ	protein kinase C, β isoform
PLC γ	phospholipase C γ
PLK1	Polo-like kinase 1 (gene name)
PRM	parallel reaction monitoring
PVDF	polyvinylidene fluoride
R-CHOP	chemotherapy cocktail of rituximab, cyclophosphamide, doxorubicin (also known as hydroxydaunorubicin), vincristine (brand name Oncovin), and

	prednisone
RFDD-PCR	restriction fragment differential display polymerase chain reaction
RFU	relative fluorescence units
RNA	ribonucleic acid
RP	regulatory particle
RPMI-1640	Roswell Park Memorial Institute 1640 medium
Rpn	regulatory particle non-ATPase
RPPA	reverse phase protein array
Rpt	regulatory particle triple-ATPase
SD	standard deviation
SDS-PAGE	sodium dodecyl sulfate polyacrylamide gel electrophoresis
SFK	Src family kinase
SH	Src homology
STAT	signal transducer and activators of transcription
STE	STE family of kinases
Syk	spleen tyrosine kinase
TBS	Tris-buffered saline
TCA	trichloroacetic acid
TK	Tyrosine kinase (TK) family of kinases
TKL	Tyrosine kinase-like (TKL) family of kinases
TL	trypsin-like
Tyr	tyrosine
X	multiples of the standard concentration
Y	tyrosine

CHAPTER 1: INTRODUCTION[1]

1.1 Diffuse Large B-cell Lymphoma

Lymphomas and leukemias are cancers of the immune system, with lymphomas generally presenting as solid tumors of immune cells in lymph nodes and leukemias generally presenting as overgrowths of immune cells in the blood or bone marrow. Roughly 90% of lymphomas are classified as Non-Hodgkin lymphoma (NHL), which is the seventh most common cancer in the United States (1-3). Non-Hodgkin lymphoma can be further categorized into several different subtypes, with diffuse large B-cell lymphoma (DLBCL) comprising roughly one-third of NHLs (2,3). Despite DLBCL being the most common subtype of NHL, there is still a lot of heterogeneity within this disease.

By gene expression profiling, DLBCL patients can be categorized into two clinically relevant subtypes: activated B-cell (ABC) and germinal center B-cell (GCB) (4). Patients with ABC DLBCL generally have much shorter (poorer) median overall survival time and progression-free survival time than those with GCB DLBCL (5,6). Despite these distinctions, there are currently no significant treatment differences between these two subtypes. The standard treatment of DLBCL is a cocktail of chemotherapeutic agents called R-CHOP, which includes the following compounds: rituximab, an anti-CD20 antibody; cyclophosphamide, a DNA alkylating agent; doxorubicin (also known as hydroxydaunorubicin), a DNA intercalating

[1] Section 1.5 of this chapter previously appeared as an article in the Journal of Cellular Biochemistry. The original citation is as follows:
Cann ML, McDonald IM, East MP, Johnson GL, Graves LM. Measuring Kinase Activity – A Global Challenge. J Cell Biochem. 2017 Nov;118(11):3595-3606.

agent; vincristine (brand name Oncovin), a microtubule polymerization inhibitor; and prednisone, an immune suppressant. However, roughly 10% of DLBCL patients will be refractory (non-responsive) to this therapy, and a substantial 40% of DLBCL patients who do respond to R-CHOP will relapse within 5 years (7). Although the standard R-CHOP chemotherapy regimen has a relatively high cure rate for patients with a good prognosis (2,8), patients with refractory and relapsed DLBCL pose a significant challenge to effective treatment.

The CHOP backbone of the R-CHOP cocktail has been in use since the 1970s, and rituximab was added as part of the cocktail in the early 2000s. In an era where personalized medicine is gaining recognition as a means for treating cancer, it is surprising that recent advances in the treatment of DLBCL have been limited. Chronic, overactive signaling through the B-cell receptor (BCR) and the anti-apoptotic NF-κB pathway are hallmarks of the ABC but not the GCB DLBCL subtype (9,10), and could therefore be particularly important for promoting tumor progression and drug resistance. In fact, several therapies targeting aspects of these pathways are currently under investigation in clinical trials for the treatment of DLBCL, including bortezomib (proteasome inhibitor) (11,12), ibrutinib (Btk inhibitor) (13), fostamatinib (Syk inhibitor) (14), lenalidomide (immunomodulatory agent) (15), enzastaurin (PKCβ inhibitor) (16), ruxolitinib (Janus kinase inhibitor) (17), and idelalisib (PI3K inhibitor) (18). Although some of these therapeutic agents have shown preferential activity in the poorly-prognosed ABC subtype (19,20), none of these agents are FDA-approved for use in DLBCL. A better understanding of the cellular processes that contribute to tumor progression and drug resistance in DLBCL would complement ongoing studies of promising therapeutic agents and could lead to the identification of additional therapeutic targets for the treatment of relapsed and refractory DLBCL.

1.2 The Src Family Kinases (SFKs)

Kinases are crucial cellular signaling enzymes that catalyze the transfer of a phosphoryl group from ATP to amino acid residues on protein substrates. They are categorized based on the amino acid residues they phosphorylate: serine/threonine kinases or tyrosine kinases. The tyrosine kinases can be further categorized based on whether they can also function as receptors (receptor tyrosine kinases) or not (nonreceptor tyrosine kinases).

The Src family kinases (SFKs) are a family of nine nonreceptor tyrosine kinases that include Blk, Hck, Fgr, Frk, Fyn, Lck, Lyn, Src, and Yes in mammals (21,22) (Table 1.1). The prototypical family member, Src, was discovered in the 1970s as the first molecularly-defined proto-oncogene. Mutations of the Src gene were captured in the genome of the avian Rous sarcoma virus, giving rise to the oncogene v-Src (23,24). This gene was identified as the transforming protein of the oncogenic Rous sarcoma virus, which caused tumor growth in chickens (21,22). Later, the evidence that the Src protein possesses tyrosine kinase activity launched a search for related protein kinases, and the additional members of the SFKs were discovered (23). Many subsequent studies of the SFKs demonstrated that these kinases play a role in a multitude of cellular signaling pathways (21-25).

The SFKs can be subdivided into three groups, based their expression patterns. Src, Fyn, and Yes are expressed in most tissues (23). A second group including Blk, Fgr, Hck, Lck, and Lyn are primarily found in hematopoietic cells (26). Lastly, Frk is primarily expressed in epithelial-derived cells (22). Despite differences in expression, the SFKs are highly related to one another and have significant sequence homology. Each of the SFK members have four key Src homology (SH) domains: SH1, the kinase domain; SH2, a phospho-tyrosine binding domain; SH3, a domain that binds proline-rich amino acid sequences; and SH4, which contains a

myristoylation site important for membrane anchoring (21,22) (Figure 1.1). In addition to these domains, each SFK member has a C-terminal tail, containing an autoinhibitory tyrosine phosphorylation site, and a unique N-terminal region whose function remains unclear. The structure of the SH1 kinase domain of the SFKs is comparable to that of most kinases, and is composed of an N-terminal lobe and a C-terminal lobe (27). The binding of ATP and the transfer of the phosphoryl group occur at the cleft between these two lobes. The C-terminal lobe contains the substrate binding site and an activation loop (27), another common feature of kinases.

Within the aforementioned domains, there are two key regulatory phosphorylation sites: Tyr416 in the kinase domain activation loop and Tyr527 on the C-terminal tail (21,22). Although the amino acid number of each phosphorylation site differs slightly among the various SFK members, the nomenclature refers to them based on the amino acid numbers of the first SFK member to be identified, chicken Src. Phosphorylation of Tyr527 by Csk is known to be autoinhibitory (21-23). Phosphorylation of Tyr527 causes binding of the C-terminal tail by the SH2 domain, a conformational change that also favors binding of the kinase domain by the SH3 domain, leading to a tightly bound closed configuration that covers the kinase domain and reduces its potential for substrate interaction (28). In contrast, dephosphorylation of Tyr527 weakens the intramolecular interactions and allows for autophosphorylation at Tyr416. This autophosphorylation helps activate the kinase, opening the protein and freeing the SH2 and SH3 domains to interact with SFK binding partners and substrates. Activity of the SFKs is commonly measured by simply examining the levels of phospho-Tyr416 (active) and phospho-Tyr527 (inactive) SFK. It should be noted that, due to the high level of sequence homology between

SFK members, antibodies that target these phosphorylation sites are unlikely to differentiate between SFK members.

1.3 The SFKs and B-cell Receptor (BCR) Signaling

Upon activation, the SFKs are involved in a multitude of normal cellular processes, such as proliferation, survival, motility and adhesion, differentiation, and more (21-25,29). They are key mediators of signaling through immune recognition receptors, several receptor tyrosine kinases, integrins, and even some G-protein coupled receptors (22). Some examples of SFK substrates are Syk, Abl, cyclins D and E, focal adhesion kinase (FAK), members of the MAPK pathway, phospholipase C γ (PLC γ), and signal transducers and activators of transcription (STATs) (22,23,30,31).

In the context of B-cells, the SFKs are key mediators of B-cell receptor (BCR) signaling (32-34) (Figure 1.2). The BCR is composed of membrane immunoglobulin (mIg) molecules associated with Igα and Igβ (also known as CD79a and CD79b) heterodimers. Under resting conditions, the SFKs are anchored to the plasma membrane and weakly interact with the Igα/Igβ heterodimers (35). Upon binding of antigen, BCRs will aggregate and induce a conformational change in the Igα/Igβ proteins that promotes phosphorylation of their immunoreceptor tyrosine-based activation motifs (ITAMs) by the SFKs, namely Lyn (36). Phosphorylation of the ITAMs promotes recruitment of the nonreceptor tyrosine kinase Syk, which becomes active upon binding (33,34). Activated Syk can then phosphorylate the nonreceptor tyrosine kinase Btk. This ordered activation of the Lyn (or other SFKs), Syk, and Btk is required for proper BCR signal transduction, and leads to the activation of many different pathways, including the PI3K/Akt, NF-κB, and MAPK pathways (32).

1.4 Role of the SFKs in Cancer and Lymphoma

The SFKs play a role in signaling from many receptors, facilitating several proliferation, survival, and cell motility pathways (22,23,29). Based on SFK involvement in these signaling pathways, it is not surprising that the SFKs have been implicated in progression and drug resistance in many cancers, including lymphoma (9,29,37,38). Interestingly, many of the pathways in which the SFKs play a role are the types of pathways often found to be aberrant in cancer cells (39). Although much of the aberrant signaling observed in cancer cells can be attributed to gene mutations, the SFKs are rarely mutated in cancer (40-43). Rather, they are often found to have higher activity or be more highly expressed in several cancers (44). For example, Src, Lyn, and Fgr are expressed at high levels in malignant tissues and primary cell cultures derived from the prostate (45,46), and increased Src activity is correlated with more invasive forms of prostate cancer (47). Other studies have heavily implicated Src and Yes in the progression of colorectal cancer (48,49). The SFKs have also been implicated in breast, lung, head and neck, and pancreatic cancer (29). In the context of hematological malignancies, there is increasing evidence that Lyn and other SFK members play a role in several types of leukemia and lymphoma, including DLBCL (37,50-56). For example, Lyn is often found to be overexpressed and/or overactive in chronic myelogenous leukemia cells with the Bcr-Abl mutation (52,56,57).

As described earlier, chronic, overactive signaling through the B-cell receptor (BCR) and the anti-apoptotic NF-κB pathway are hallmarks of the ABC but not the GCB DLBCL subtype (9,10), and could therefore be particularly important for promoting tumor progression and drug resistance. Signaling through the BCR triggers the activation of many pro-survival and anti-apoptotic signaling pathways, including the anti-apoptotic NF-κB pathway. Important mediators

of BCR signaling are Syk and Btk, both of which have inhibitors in clinical trials for the treatment of DLBCL as well as other types of lymphoma (58). The importance of activation of Lyn (or other SFKs), Syk, and Btk for BCR signaling is well known, and deficiencies in any one of these tyrosine kinases results in defective or aberrant B-cell function and development (59-61). Therefore, it stands to reason that SFK inhibition in the context of ABC DLBCL may provide a valuable option for the treatment of this disease.

Unsurprisingly, the significant amount of evidence that implicates the SFKs in cancer progression has led to the development and exploration of many SFK inhibitors. Perhaps the most notable SFK inhibitor is BMS-354825, or dasatinib (Sprycel, Figure 1.3A). Dasatinib is a dual SFK/Abl inhibitor (62), and was initially pursued in clinical trials to overcome resistance to the Bcr-Abl inhibitor imatinib (Gleevec) in chronic myelogenous leukemia (CML) (63). Like many kinase inhibitors, dasatinib is a rather nonspecific kinases inhibitor, but its primary targets are the SFKs and Bcr-Abl (64). Despite this promiscuity, dasatinib is FDA-approved for the treatment of CML and is currently being evaluated in clinical trials for other hematological malignancies and several solid tumors. Two other notable SFK inhibitors are saracatinib (AZD0530, Figure 1.3B) and ponatinib (AP24534, Figure 1.3C). These inhibitors, while still having some level of promiscuity, are reported to be more specific for the SFKs and Abl than dasatinib (65,66).

Although there have not been many studies exploring SFK inhibition in the context of DLBCL, there are some preliminary studies that demonstrate the potential utility of targeting the SFKs in this disease. Ke *et al.* demonstrated that dasatinib is capable of inhibiting the growth of B-cell lymphomas both *in vitro* and *in vivo* (37). Moreover, Davis *et al.* demonstrated that dasatinib is capable of killing cell lines that are dependent on chronic BCR signaling, but has

little effect on GCB DLBCL cell lines (9). In another study, Yang *et al.* demonstrated that dasatinib is capable of inhibiting cell proliferation in some DLBCL cell lines, but not others, and that activity of Syk and PLCγ2 correlated with dasatinib sensitivity (38).

1.5 Measuring Kinase Activity – A Global Challenge

1.5.1 Introduction

Kinases and the proteins that they phosphorylate constitute the virtual "wiring diagram" of the cell. Collectively, the kinases or kinome dictate key aspects of cell function in normal and disease states (67,68). Understanding the connections and relationships between these cellular components is a major objective of current phosphorylation research. Kinase networks are beginning to emerge and the dynamic nature of the kinome is now readily accepted (69-71). Ultimately, a more complete kinase network map, and better knowledge of the events regulated by kinases, will improve the design and application of targeted kinase inhibitor strategies for the treatment of disease. Essential to this goal is the ability to measure changes in kinase activity, either as isolated enzymes or as part of the greater kinome (72). The objective of this section is to discuss some recent advances in these methods and to evaluate their applications, advantages, and disadvantages (Figure 1.4).

Since the original studies of Casnellie and Krebs (73,74), methods to quantitatively measure kinase activity remain in demand and have continued to evolve to meet current needs (75,76). Significant progress has been made in the development of methods to measure kinase activity in live cells and in a high-throughput, kinome-wide manner. These developments have been fueled by advances in peptide chemistry, fluorescent methodologies, mass spectrometry, and other technologies (77-79). Much of this emphasis is motivated by a need to evaluate kinase

inhibitor potency and specificity against the kinome. This need has been met with both commercial and academic developments, some of which will be discussed herein (Table 1.2).

1.5.2 Early Methods

The majority of the early methods relied on the use of radioactivity and incorporation of ^{32}P into proteins or peptide substrates (73,74). Later, some of these methods shifted to the use of ^{33}P because of the desirable properties of this isotope, particularly for array-based assays (80). Advantages of array-based assays included increased rapidity, versatility, and the quantitative nature of these assays. Disadvantages included the burdensome maintenance and disposal of radioactive waste, as well being limited to purified kinases and/or substrates. The principle of these assays was based on selective binding of the phosphorylated substrate to paper or other matrices. Commonly employed methods used acid precipitation of protein substrates (casein, myelin basic protein, histones) followed by extensive TCA washes to remove free ATP. To account for kinase autophosphorylation, substrate negative controls were absolutely necessary. Additionally, substrate peptide binding to phosphocellulose (P-81) paper was dependent on basic charge and required sufficient basic residues to allow binding in the presence of phosphoric acid (74). One of the advantages of this approach is that peptide substrates can be engineered based on known kinase specificity to optimize the measurement of kinase activity either from lysates or enriched samples (81-83). Either approach can be successfully applied to quantitatively measure kinase activity. However, a disadvantage of these methods is that they are not suitable for measuring the kinase activity of a large number of kinases at the same time.

More recently, these methods have been optimized for high-throughput applications with the general goal of testing for inhibitor specificity (84). One technology of note is the HotSpot^{SM} methodology that utilizes miniaturized platforms and purified kinases (578) for inhibitor

screening (Reaction Biology Corporation). Thus, these and other similar assays remain versatile approaches to study kinase activity and inhibitor specificity.

1.5.3 The Emergence of Fluorescent and Luminescent Methods

Because of the negative implications of the use of radioactivity, non-radioactive methods for measuring kinase activity have become increasingly popular. Many of these methods are based on the measurement of fluorescent peptide substrates and take advantage of altered fluorescent properties upon phosphorylation (85). Furthermore, some of these fluorescent- and luminescent-based methods are amenable to studies in cell lysates and live cells, providing a more natural environment for studying kinase activity. A very large variety of these *in vitro* kinase assays are now available; for an excellent resource the reader is referred to the review of Jia *et al.* (86). In general, the fluorescent and luminescent peptide-based kinase assays can be broken down into multi-component sensors and unimolecular sensors. Some of these methods are briefly described below.

1.5.3.1 Multi-component Fluorescent and Luminescent Methods

The multi-component fluorescent and luminescent methods for measuring kinase activity include both direct and indirect measurements of kinase activity. The more direct measurements generally involve a fluorescently-labeled peptide substrate specific for the kinase of interest and a secondary component whose binding alters the fluorescence of the peptide substrate. The more indirect measurements utilize enzyme-coupled assays to measure the depletion of ATP or production of ADP after the kinase reaction. The multi-component techniques are best used with purified protein, and possibly cell lysates.

1.5.3.1.a HTRF/LANCE/AlphaScreen

The majority of the multi-component sensors for kinase activity depend on binding of a phosphorylated peptide substrate by a phospho-specific antibody (Figure 1.5A). Commonly used assays, like HTRF (homogeneous time resolved fluorescence) or LANCE (lanthanide chelate excitation), measure the generation of a fluorescence resonance energy transfer (FRET) signal induced by substrate phosphorylation (87-89). In these assays, the peptide substrate is labeled with a FRET acceptor molecule, generally via streptavidin-biotin binding. Upon substrate phosphorylation, a phospho-specific antibody labeled with a donor molecule can bind, thus bringing the donor and acceptor molecules close enough to generate the FRET signal. The AlphaScreen (amplified luminescent proximity homogeneous assay) utilizes a similar bead-based setup, but produces a luminescence signal rather than fluorescence (90,91). Advantages of these assays include high sensitivity and applicability to high-throughput formats. Limitations include the reliance on europium- or other conjugated phospho-specific antibodies, which can be costly. Furthermore, there may be limitations to which substrates have a corresponding phospho-specific antibody.

1.5.3.1.b Fluorescence Polarization (FP) and Time-Resolved FP

While fluorescence polarization (FP) techniques also utilize a phospho-specific antibody, they are based on a well-established principle of fluorescence anisotropy, rather than FRET (92). When polarized light excites the fluorophore of a fluorescently-labeled peptide, the excited fluorophore can rotate rapidly, and therefore emits light in many planes (depolarized light). However, when the fluorescently-labeled peptide is phosphorylated and bound to phospho-specific antibodies (93) or metal complexes (94), the excited fluorophore rotates more slowly, thereby emitting more polarized light. FP techniques measure the ratio of fluorescence emissions

in different planes in order to determine the level of polarization, which is indicative of substrate phosphorylation. These techniques are amenable to high-throughput screening, but they are subject to potential compound interference and require a large amount of phosphorylated substrate to effectively determine FP. However, the application of time-resolved anisotropy measurements can be used to improve the quality of information obtained from these assays.

1.5.3.1.c Metal Ion Coordinated Fluorescence Quench Assays

While the phospho-specific antibody-based assays can provide sensitivity and the potential for high-throughput studies, the need for specific antibodies can be costly and limit the kinases/substrates that can be studied. Metal ion coordinated fluorescence quench assays are a form of multi-component kinase activity sensors that do not depend on a phospho-specific antibody. Instead of measuring an increase in fluorescence, these assays use a decrease in fluorescence as the measure of substrate phosphorylation (95,96). In these assays, the phosphorylation site of a fluorescently-labeled peptide substrate coordinates with a metal ion. The metal ion is associated with a quencher molecule, thus bringing the quencher in close enough proximity to absorb the fluorescence of the peptide's fluorophore, and causing a decrease in fluorescence. A major advantage of these assays is the lack of a phospho-specific antibody, thus making them more cost-effective and easily applicable to a variety of kinases/substrates. Some disadvantages are that the reagents used may be sensitive to excessive levels of ATP or the chelation agents often used to halt a kinase assay, such as EDTA.

1.5.3.1.d Enzyme-Coupled Assays

Enzyme-coupled assays are more versatile than peptide-based substrate assays, as they depend solely on the amount of ATP or ADP present after the kinase reaction and do not require a synthetic peptide substrate tailored to a given assay and kinase of interest. The ATP-

dependent assays measure ATP depletion via luminescence, in which the remaining ATP is used to catalyze a luciferase reaction (97). Thus, luminescence is inversely related to kinase activity. The ADP-dependent assays measure ADP accumulation via fluorescent or colorimetric signals, in which a pyruvate kinase and lactate dehydrogenase system uses accumulated ADP and NADH oxidation to convert phosphoenolpyruvate to lactic acid (98). In these assays, the readout is dependent on NADH concentration, therefore fluorescence/absorbance is inversely related to kinase activity. Since the enzyme-coupled assays generally require cessation of the kinase reaction prior to ATP/ADP measurement, another limitation of these assays is that they are fixed-timepoint assays, rather than real-time. However, some work has been done to adapt these assays to a kinetic readout (99). Despite these adaptations, the main disadvantage of the enzyme-coupled assays is that they are indirect measurements of kinase activity and require purified protein and substrate in order to reduce interference. Furthermore, if the kinase assays are being used to investigate the effects of a compound, the coupled assays may be subject to off-target interference by the compound.

1.5.3.2 Unimolecular Fluorescent Methods

While multi-component assay technologies have proven to be extremely useful, a major drawback is the need for multiple components, which requires additional optimization and limits the utility of these assays in more physiologically relevant systems, such as cell lysates and living cells. The development of unimolecular fluorescent-based methods for measuring kinase activity allows for a more straightforward measurement of kinase activity in cell lysates and living cells.

1.5.3.2.a Genetically -Encoded FRET Sensors

Genetically-encoded sensors for kinase activity are generally FRET-based, following the original design by Roger Tsien's group (100,101). These single-chain constructs consist of a kinase substrate sequence (tailored to the kinase of interest), a corresponding phospho-amino acid binding domain, a FRET pair of autofluorescent proteins, and flexible linkers where needed (Figure 1.5B). The FRET proteins are located on opposite ends of the construct, so they will not interact when the kinase substrate sequence is unphosphorylated. Once the substrate sequence is phosphorylated, the phospho-amino acid binding domain binds the phospho-substrate, thus bringing the FRET pair into close proximity and producing a FRET signal. The major advantage of this technique is that it can be used in live cells, thus allowing the study of kinase activity in its native environment. Furthermore, targeting sequences can be implemented to study kinase activity in specific cellular compartments (102-104). Some of the drawbacks of this technique are low sensitivity and being genetically-encoded, which means a lack of temporal control and control over the level of expression.

1.5.3.2.b Environmentally-Sensitive Fluorophores

To avoid the complications of a genetically-encoded construct, environmentally-sensitive peptide sensors are a useful alternative. These sensors consist of a kinase substrate sequence labeled with an environmentally-sensitive fluorophore located close to the phosphorylation site (Figure 1.5C). Phosphorylation of the peptide substrate creates a change in the charge near the fluorophore, inducing a change in fluorescence intensity or wavelength of the fluorophore (57,105-107). Similarly, chelation-sensitive fluorophores can coordinate with a metal ion in response to phosphorylation of a nearby site on a peptide substrate, resulting in a change in fluorescence (106,108). The benefits of environmentally-sensitive sensors are that they can be

synthetically produced, avoiding the complications of recombinant systems, and they can provide more temporal control and dynamic range than the genetically-encoded sensors. Furthermore, these sensors can be made light-activatable, thereby providing precise temporal control (109). They can be used in whole cells using microinjection, but are more easily applied to cell lysates. The major disadvantage of this technique is that the environmentally-sensitive fluorophore must be in close proximity to the phosphorylation site of the peptide substrate, which has the potential for interference with kinase binding and phosphorylation. In addition, the need for microinjection when studying kinase activity in live cells requires special equipment and training.

1.5.3.2.c Electrophoretic Mobility Shift Assays

The electrophoretic mobility shift assays are perhaps the simplest form of unimolecular sensors of kinase activity. They utilize a fluorescently-labeled peptide substrate, in which the fluorophore is always fluorescent regardless of phosphorylation status of the peptide substrate. The addition of a phosphate group to the peptide alters its charge and mass, so the phospho-peptide will migrate differently from the unphosphorylated peptide in an electric field (Figure 1.5D). Thus, total amounts of phosphorylated and unphosphorylated peptide can be determined at various timepoints throughout a kinase reaction. Examples of electrophoretic mobility shift assays include standard CE-LIF (capillary electrophoresis with laser-induced fluorescence) approaches (110) and the Caliper Life Sciences LabChip technology, which is a miniaturized high-throughput version of CE-LIF (111). The electrophoretic mobility shift assays avoid the need to position the fluorophore in close proximity to the phosphorylation site, and provide a very sensitive detection method with the potential for multiplexed analyses. The CE-LIF sensors can be adapted for use in living cells through the use of genetically-encoded

constructs (112), microinjection (113), or cell-penetrating peptides (114), but they are more easily applicable to cell lysates. A disadvantage of the electrophoretic mobility shift assays is that they are fixed-timepoint assays rather than real-time assays. The use of electrophoresis also requires specialized instruments and more time and data analysis than some of the sensors with phosphorylation-dependent fluorescence changes.

1.5.4 Kinome-Wide Methods

The realization that the kinome is an integrated network of kinases has spurred the development of methods to measure changes in the kinome "en masse". The majority of the focus has been on the human kinome, which is composed of approximately 500 unique members, including the less well-characterized pseudokinases (115). A number of different approaches have recently been developed and the pros and cons of these methods are discussed below.

1.5.4.1 RPPA and Phosphoprotein Arrays

Multiple commercial products and services are available for the large-scale profiling of the kinome or their substrates based on protein phosphorylation. These include antibody arrays for measuring changes in receptor and non-receptor kinase activity, serine/threonine kinases, and their substrates. Popular among these is the reverse phase protein array (RPPA) technology for profiling phosphoproteins, in which many cell lysate samples are "printed" on a nitrocellulose membrane and probed with an antibody of interest (116,117). Some of the advantages of the antibody array methods include high sensitivity, speed, and the lack of need for expensive equipment, such as mass spectrometers.

A number of commercial vendors offer services and reagents for phosphoprotein array assays, including R&D Systems, RayBiotech, Kinexus, Full Moon Bio, Cell Signaling (PTMScan) and others. Kinexus has developed bioinformatics analyses to complement their

discovery-based assays for kinases and kinase substrates (118). DiscoverX also offers a variety of kinase assay and profiling methods including those for measuring receptor kinase activity (PathHunter) and kinase inhibitor specificity assays (KinomeScan) (119).

The advantages of these array-based approaches are the rapidity and simplicity of analysis. Both total protein and phosphoprotein detection can be quantified in a specific and sensitive manner. Disadvantages pertain to potential artifacts when measuring total phosphorylation changes, such as those obtained with anti-phosphotyrosine arrays. In this case, both positive and negative regulatory sites may be simultaneously detected.

1.5.4.2 KinoBeads

Originally developed by Cellzome scientists, based on the work of Daub and others (120), the KinoBeads technology has proven to be a powerful approach to study the kinome (121,122). Based on the concept of kinase capture by kinase inhibitors immobilized on Sepharose beads, the inclusion of multiple pan kinase inhibitors of differential specificity and affinity allows the capture of a large percentage of the kinome in a single experiment. The captured kinases can then be eluted and identified via mass spectrometry or Western blotting. Derivatization of kinase inhibitors to include reactive amines or other groups facilitates the rapid coupling of these inhibitors to modified Sepharose (ECH) or other supports, and many of these derivatized inhibitors are now commercially available. Thus, inhibitor bead composition can be tailored to meet the needs of a particular experiment.

Numerous studies have explored the utility of the KinoBead approach to examine the kinome. Initially, the vast majority of the studies were used to profile kinase inhibitor specificity, as discussed in these reviews (69,123,124). Other studies used the KinoBead approach to profile changes in the baseline kinome of different cancer cell lines and other cells

(121,125,126). In some instances, this has been effectively combined with phosphoproteomics (127,128) and used to investigate changes in the kinome during the cell cycle (129). However, no claims were made regarding the ability of these reagents to measure the actual activation state of individual kinases in the kinome. A comparison of kinase capture by KinoBeads to ATP and ADP probe-based methods (Desthiobiotin, described below) has been made. Interestingly, a high degree of complementarity between these two methods was observed in these studies (130). Further development led to the emergence of commercial ventures like Ambit/DiscoverX, which provides large-scale inhibitor specificity screening services. This remains a popular and powerful approach to investigate inhibitor specificity in a "kinome-wide" manner.

1.5.4.3 Multiplexed Inhibitor Beads

The Multiplexed Inhibitor Beads (MIBs) approach is an adaptation of the original KinoBead technology. In short, this method uses individual, layered immobilized kinase inhibitors in a column-based approach (70) (Figure 1.6). The philosophy behind layering the MIBs was that more abundant kinases could be absorbed onto more highly selective inhibitors (top layers), thereby providing additional binding "space" for lower abundance kinases. The original composition of MIBs included the following immobilized inhibitors layered from top to bottom: Bisindoylmaleimide-X, SB203580, Lapatinib, Dasatinib, Purvalanol B, VI16832, and PP58. More recent adaptations of this method have included additional inhibitors (131) in an effort to extend the coverage of the kinome. The advantages and disadvantages of these alterations are discussed below.

Combined with quantitative methods of mass spectrometry (MS), MIB/MS was used to measure changes in the kinome in response to targeted kinase inhibitors and acquired drug resistance (70,132-136). Based on changes in MIB kinase binding in response to EGF and

pervanadate, the ability of MIB/MS to measure changes in the activity of individual kinases was reported. Similarly, kinome changes associated with acquired resistance to imatinib in a model of chronic myeloid leukemia was determined. In both studies, kinases were detected that showed dependence on the phosphorylation and activation state of the kinase (70,132). While the number of kinases that displayed activity-dependent binding was limited, these were verified with phosphoantibodies and other methods. This was particularly evident for some members of the MAPK and IKK pathways (132). Thus, the property of inhibitor beads to capture kinases in an activity-dependent manner is based on the potential structural changes that result in altered affinity of the kinase for an immobilized type 1 inhibitor.

The ability of MIB/MS to measure kinase activity changes was recently challenged (137). This study compared the ability of similar inhibitor bead mixtures to capture kinases in an activity-dependent manner. Based on their data, the authors concluded that these beads were not capturing active kinases preferentially to inactive ones. Instead, they report that changes in kinase abundance were responsible for the difference in kinase capture and quantification.

While the majority of kinases probably do not show activity-dependent binding with published inhibitor bead combinations, there is a fraction that appear to, but this may depend on the specific properties of the immobilized inhibitor and the assay conditions. Unpublished studies from the Graves lab at UNC support this premise. As shown in Figure 1.7, the capture of EGF-activated EGFR depends heavily on the inhibitor bead composition. Of four individual inhibitor beads that captured EGFR, three (PP58, Purvalanol B, and Shokat Inhibitor) show increased capture of EGFR by several-fold upon EGF stimulation. The fourth immobilized inhibitor, CTx-0294885, shows no increase in EGFR capture. Moreover, inclusion of CTx-0294885 in a mixture of six inhibitor beads is sufficient to suppress any observed increase in

EGFR binding. Comparison of activity dependent binding of other kinases within the EGFR/MAPK signaling pathway shows similar dependency on inhibitor bead composition. Thus, the activation state of a kinase may strongly influence or have no detectable effect on MIBs binding depending on the composition of the immobilized inhibitors used. This premise was supported by the recent study of Urisman *et al.* (131), where kinase capture was compared to the phosphorylation status of the given kinase. From these studies, the authors conclude that there is an element of activity-dependent binding to inhibitor beads.

In summary, the strength of this approach is its ability to capture and quantify hundreds of kinases in a single experiment, including members of the understudied kinome (138). Interestingly, MIB/MS was recently used to profile kinome changes in response to viral infection (139) and to examine the kinome of *Chlamydomonas* (140), demonstrating the versatility of this approach. Combined with analysis of kinase phosphorylation (either by mass spectrometry or immunological methods), this technique provides extensive insight into properties of the "functional" kinome of a given cell type or tumor. Thus, it appears that the utility of this method to investigate global changes in the kinome remains high.

1.5.4.4 DigiWest

Recent advances have extended the application of kinase capture on immobilized kinase inhibitors, with the power of Luminex immunodetection. The DigiWest technology is a multistep process that begins with running samples on an SDS-PAGE gel and transferring to a nitrocellulose membrane (141). The separated, membrane-bound proteins are then biotinylated, and each lane of the membrane is cut into 96 strips that cover a wide range of molecular weights. The proteins are then eluted from the strips and labeled with Neutravidin-coated Luminex beads with distinct color-codes for each molecular weight. The bead-labeled protein samples from a

given lane can then be combined, aliquots can be used to probe with hundreds of different antibodies, and samples are analyzed using flow cytometry, wherein the signals represent the different molecular weights of the initial SDS-PAGE lane. To use the DigiWest technology to the study of the kinome, high-affinity kinase capture beads, such as KinoBeads, are applied to the cell lysates prior to the initial SDS-PAGE. The application is simple in concept and could provide a rapid and sensitive new approach to study the kinome in depth. The authors demonstrate the application of this approach to detect low levels of kinase from small amounts of tissue material (141). This may be a particularly useful approach when sample amounts are limiting, such as clinical biopsies or laser capture microdissection.

1.5.4.5 ATP Probes

1.5.4.5.a Desthiobiotin ATP

An alternative approach to the inhibitor-based capture methodology described above is the application of affinity-based tagging of kinases, as described by Patricelli and co-authors (142,143). This elegant technology takes advantage of reactivity with conserved lysine residues found in the majority of protein kinase ATP-binding pockets. Desthiobiotin ATP reacts with these lysines, resulting in a biotin-tagged kinase. The biotinylated kinase peptides are purified by streptavidin affinity chromatography and analyzed by mass spectrometry. Applying principles of Multiple Reaction Monitoring (MRM) or Parallel Reaction Monitoring (PRM) MS, these peptides can be rapidly identified and quantified (144). The tremendous advantage of this approach is that the binding of desthiobiotin ATP shows preference for the "activated" kinase, and thereby provides a covalent probe to tag only active kinases. The technology has been commercialized and is available either as a service (KiNativ) or as a kit-based format (145).

1.5.4.5.b Shokat Approach

A well-accepted approach to study kinase specificity was developed by Kevan Shokat (146). Based on the application of modified ATP analogs and kinases mutated to accept only the modified ATP molecules, the authors demonstrated that this approach can be used to identify direct substrate targets for desired kinases. Known as the analog-sensitive (AS) approach, this methodology has shown great application to identify novel substrates for kinases like PKA, SRC, CDK2, EPHA4, and many more. In fact, this approach has been successfully applied to the study of over 80 kinases (for an excellent review see (147)). In addition to providing insight into global analysis of kinase substrates in yeast, mammalian cells, and multicellular organisms, this approach has also contributed significantly to kinase inhibitor design.

1.5.4.5.c Other Covalent Approaches

The recent study of Zhao and co-authors (148) describe the design of cell-permeable, lysine-directed kinase inhibitor probes. These molecules are based on sulfonyl fluoride reactivity and provide a method to "tag" kinases in live cells, under physiological ATP concentrations and conditions. Using these probes to test dasatinib potency, the authors show a greater selectivity of dasatinib than would have been predicted based on conventional kinase inhibitor screens. The development of chemically reactive kinase probes offers significant potential for a better understanding of kinase targets.

1.5.5 Assessing Kinase Interactors and Substrates by Biotinylation: BioID Approach

The BioID (proximity-dependent biotin identification) technique relies on the fusion of the kinase being studied to a mutated, promiscuous form of BirA, a biotin ligase from *Escherichia coli* (149). The BirA gene used for BioID has a point mutation that results in a ligase (BirA-R118G (BirA*)) with decreased affinity for biotinyl-5'-AMP, the highly reactive

intermediate of the biotinylation reaction (150). When a BirA*-kinase fusion protein is expressed in cells grown in media supplemented with biotin, the biotinyl-5'-AMP molecule is released by BirA* and irreversibly biotinylates lysine residues on proximal proteins (within ~10 nm), with no required biotinylation consensus sequence (151,152) (Figure 1.8). Biotinylated proteins can then be captured with streptavidin Sepharose and identified by mass spectrometry, to ultimately identify proximal proteins and candidate kinase substrates. Comprehensive protocols are available as guides for implementation of the BioID technique (149,152-154).

When using the BioID technique, careful consideration must be taken to ensure that the fusion of BirA* to the kinase of interest does not affect subcellular localization. A potential alternative is a smaller biotin ligase from *Aquifex aeolicus* (designated BioID2), which is less likely to affect normal subcellular localization of fusion proteins than the original BioID construct, and thus may be useful for kinases with N- or C-terminal localization domains (155). However, the BirA* used in BioID2 is also capable of catalyzing the biotinylation of proteins using much lower concentrations of biotin than the original BioID construct. BioID2 is therefore unsuitable for any time-sensitive experiments, such as those involving cell cycle synchronization or drug treatment (155).

The BioID technique has been used previously to identify novel interactors of the kinase EphA2 and a novel substrate of Plk4 (156,157). It is important to note that, using BioID, complementary approaches must be used to determine whether interactors are bona fide substrates, or merely proteins in close proximity. This technique has also been used to validate the physiological relevance of kinase interactions that were identified by other means (158,159). Extensive reviews emphasizing the capabilities and limitations of the BioID approach have been published recently (160,161).

1.5.6 Future Directions

The power of assaying the kinome "en masse" is just beginning to be realized. Emerging areas include applying these approaches to study host-viral interactions and the impact of parasitic infections, the development of brain pathologies like Alzheimer's disease, probing stromal/tumor cell interactions, illuminating the basis of rare diseases (including those driven by kinase fusions or mutations), determining kinome-wide specificity of uncharacterized kinase inhibitors, and elucidating kinome adaptions to loss of key proteins like Ras and p53. Ultimately, these studies are expected to define the unique kinome "fingerprints" that arise from these perturbations, with the hope that novel therapeutic targets can be identified. For example, the recent study of Arend *et al.* (139) applied this approach to identify kinase adaptations in response to human cytomegalovirus (HCMV) infection. Using this information, existing kinase inhibitors were selected and effectively demonstrated to have anti-viral activity (139).

Future applications include combining these technologies with targeted mass spectrometry approaches, such as multiple reaction or parallel reaction monitoring (MRM/PRM). This approach has the value of greatly improved sensitivity and reproducibility, making it an attractive option for rare or low-abundance clinical samples. The study of Miao and co-authors (162) demonstrated the quantification of 328 kinases by MRM and measured their response to methylgloxal stimulation. Recently, MIB kinome capture was successfully combined with PRM mass spectrometry (131). These studies investigated the adaptive responses to MEK and Erk inhibitors in colorectal cancer cells. In addition to quantifying over 800 peptides from 150 kinases, these authors demonstrated a compensatory activation of the TGF-beta family receptors to these inhibitors. Thus, these types of technical adaptions have the potential to greatly extend the application of kinome analysis to important clinical problems.

1.5.7 Conclusion/Discussion

The need to quantitatively and specifically measure kinase activity across the kinome remains important for many areas of biology. With the emergence of global methods to measure RNA and DNA, it is even more important to be able to measure proteins and their substrates. This is particularly relevant given the low degree of correlation between protein and RNA expression. Kinases, as a class of enzymes, are one of the most diverse groups of enzymes because of the multitude of events that they control. A deeper understanding of how this important network is regulated will contribute extensively to our comprehension of cell signaling.

1.6 The Proteasome

The ubiquitin-proteasome system is critical for the quality control of most, if not all, proteins within a cell. It serves as the primary proteolytic system for the degradation of misfolded or damaged proteins and proteins targeted for downregulation. As part of the ubiquitin-proteasome pathway, proteins destined for degradation are labeled with polyubiquitin chains, which can then be recognized and bound by the proteasome. The proteasome then unfolds these proteins in an ATP-dependent manner and trypsinizes them (163).

The proteasome is a multi-subunit protein, with its proteolytic activity being derived from the 20S core particle. The 20S core particle is a barrel-shaped structure comprised of two heteroheptameric outer α-rings and two heteroheptameric inner β-rings (164) (Table 1.3, Figure 1.9). The core particle has three distinct proteolytic activities: caspase-like (CaL), trypsin-like (TL), and chymotrypsin-like (ChL), which are provided by its β1, β2, and β5 subunits, respectively (163). In immune cells, or in nonimmune cells in the presence of interferon or

tumor necrosis factor, each of these subunits can be replaced by immunoproteasome subunits β1i, β2i, and β5i, respectively, resulting in either mixed proteasomes, with one or two subunits replaced, or the full immunoproteasome when all three are substituted (163,165). This produces a proteasome with altered cleavage patterns favoring the production of peptides involved in antigen presentation (163,166,167).

Although the 20S core particle has proteolytic activity, it is generally unable to degrade folded proteins without a regulatory particle cap, as the N-terminal tails of some of the α subunits form a gate at the entrance to the 20S core particle (168,169). Binding of a regulatory particle to the 20S core particle induces a conformational change that displaces the α subunit tails and opens the gate to the 20S core particle (170). In addition to opening the gate, the regulatory particles serve as a lid to the 20S core particle and facilitate binding, unfolding, and entry of proteasome substrates. There are four different regulatory particles that can bind to the 20S core particle: PA700 (also known as 19S), PA28αβ, PA28γ, and PA200 (163). Considering the variety of regulatory particles and catalytic 20S subunits, there is potential for several forms of the proteasome to exist within a given tissue, or even within an individual cell (171,172). However, the most well-studied and predominant form of the proteasome is the 26S proteasome, which includes the 20S core particle and one or two 19S regulatory particle(s) (Table 1.3, Figure 1.9).

1.7 Role of the Proteasome in Cancer and Lymphoma

The function of the proteasome within the cell can be likened to that of a garbage disposal. As a garbage disposal chops up and disposes of unwanted food, the proteasome is responsible for degrading proteins that are damaged or no longer needed (173). It plays a role in a number of signaling pathways, including cell cycle regulation (174), transcription (175), and

signal transduction (176). The proteasome is therefore critical for maintaining the health and viability of a cell. As such, it is not surprising that aberrant proteasome activity is linked with disease. For example, proteasome activity is often upregulated in cancer (172,177,178), but downregulated in neurodegenerative diseases (179). Consequently, there has been and continues to be a high level of interest in the proteasome as a therapeutic target.

In addition to the SFKs, the proteasome has also been implicated in cancer and drug resistance due to its degradation of various antitumor-related proteins (180,181). Notable proteins regulated by the proteasome include IκB, the tumor suppressor p53, the cyclin-dependent kinase (CDK) inhibitors p21 and p27, and members of the MAPK pathway (180). As noted earlier, the ABC subtype of DLBCL is heavily dependent on chronic BCR and NF-κB signaling (9,10). The anti-apoptotic NF-κB signaling pathway is heavily dependent upon the proteasome because negative regulator of NF-κB, IκB, is degraded by the proteasome in response to phosphorylation by IκB kinase (IKK). Thus, there is potential use for proteasome inhibitors in the treatment of ABC DLBCL.

There are currently three FDA-approved proteasome inhibitors: bortezomib (PS-341 or Velcade, Figure 1.10A), carfilzomib (PR-171 or Kyprolis, Figure 1.10B), and ixazomib (MLN-2238 or Ninlaro, Figure 1.10C) (182). These inhibitors preferentially target the β5 subunit of the proteasome, which confers the proteasome's ChL activity (183-186). Bortezomib and ixazomib are slowly reversible inhibitors, whereas carfilzomib is an irreversible proteasome inhibitor (186,187). All three inhibitors are indicated for the treatment of multiple myeloma, a cancer of plasma B-cells, and are currently in clinical trials for other hematological and solid malignancies. In fact, both bortezomib and carfilzomib are currently in clinical trials for the treatment of DLBCL. Several preclinical studies have demonstrated cytotoxic and/or antitumor activities of

proteasome inhibitors in various hematological malignancies (11,188,189). Furthermore, there is evidence that when combined with standard chemotherapy, bortezomib has a significant effect on ABC DLBCL but not on GCB DLBCL patients (12,190).

Interestingly, several studies have demonstrated synergy between proteasome inhibitors and many other agents, including tyrosine kinase inhibitors, particularly within hematological cells (191-195). The Btk inhibitor ibrutinib (PCI-32765) has garnered interest for the treatment of DLBCL (34), and Dasmahapatra *et al.* have shown that ibrutinib and bortezomib demonstrated synergy in DLBCL and mantle cell lymphoma cells (194). The combination of ibrutinib with proteasome inhibitors and standard chemotherapy (R-CHOP) is currently under investigation in a Phase I/II clinical trial. Considering the proximity of Btk activation to SFK activation in BCR signaling, it stands to reason that SFK inhibitors, such as dasatinib, may prove to be synergistic with proteasome inhibitors in DLBCL.

1.8 Strategies for Measuring Proteasome Activity

The 20S core particle of the proteasome has three proteolytic activities, caspase-like (CaL), trypsin-like (TL), and chymotrypsin-like (ChL), which are provided by its β1, β2, and β5 subunits, respectively (163). Several methods have been developed to assays these activities (Table 1.4).

1.8.1 Fluorogenic Peptide Substrates

The most commonly cited method for profiling proteasome activity is the use of peptide substrates that are biochemically acted upon by one of the proteasome's three proteolytic activities. These substrates are fluorescently labeled, but the fluorescence is internally quenched in the intact peptide (196). Upon cleavage by the specific proteasome active site, part of the

fluorophore-labeled peptide may dissociate, thus allowing an increase in fluorescence. Therefore, changes in fluorescence are directly related to proteasome activity. The most common fluorescent tag used with the fluorogenic peptide substrates is 7-amino-4-methylcoumarin. While other fluorescent tags have been used, they tend to have similar photophysical properties, which limits the ability to measure multiple proteasome activities simultaneously (197-199). There is a variation of this assay that utilizes a coupled luminescent readout instead of fluorescence (200), but it is still subject to the same limitations of the fluorescent-based assay.

1.8.2 Site-specific Activity-based Probes

Site-specific activity-based probes (ABPs) will target and irreversibly bind to the catalytic subunits of the proteasome. The covalently bound ABS can then be detected using antibodies directed against part of the ABP (201) or fluorescent labeling of the probe (202). Several of these probes have been described and used to assess the functional proteomics of the proteasome (201,203,204). The advantage of these probes is that they can be made cell-permeable, thus allowing assessment of proteasome activity in a more native environment (196,201). However, their main disadvantage lies in the nature of suicide substrates, which will inactivate an enzyme and may prevent a true readout of enzymatic activity.

1.8.3 Molecular Imaging

Molecular imaging is meant to be a non-invasive process that allows the measurement of proteasome activity in live cells and potentially *in vivo*. The approaches utilizing this technique have generally used either exogenously-delivered probes or genetically-encoded probes (196). In both cases, the probes can serve as proteasome substrates and will display a change in fluorescence or bioluminescence upon proteasomal processing. Examples of these probes

include ubiquitin-firefly luciferase (Ub-FL) and ubiquitin-green fluorescent protein (UbG76V-GFP) (205,206). The advantage of the molecular imaging technique is that it allows for a measurement of proteasome activity with respect to whole proteins, as opposed to peptide substrates. However, the need to exogenously introduce or genetically encode these constructs is not ideal and may perturb cells, or may not even be feasible for some cell types.

1.8.4 RFDD-PCR and Proteomics

On a more global level, restriction fragment differential display polymerase chain reaction (RFDD-PCR) and proteomics can be used to identify differentially expressed genes and study the structure and function of related proteins, respectively (196,207). This technique allows a global comparison of changes in gene expression with changes in protein expression. However, it technically is not a direct measure of proteasome activity.

1.8.5 Immunological Methods

In addition to traditional western blotting, enzyme-linked immunosorbent assays (ELISA) can be used to quantify the 20S core particle of the proteasome (196,208). Although at its first use this technique was limited to purified 20S proteasome, it has since been adapted for use in cell extracts and crude lysates as well as for the identification of the 26S proteasome (208,209). The advantages of this technique are that the protocols are easy to follow and it can be carried out in most laboratories. However, this assay cannot distinguish between single- or doubly-capped 26S proteasomes, and measures the amount of proteasome as opposed to its actual activity.

1.8.6 Simultaneous Measurement of All Three Proteasome Catalytic Activities

Fluorogenic peptide substrates provide the best means for directly measuring the proteasome's three catalytic activities, but are severely limited in the ability to measure more

than one activity at a time. Thus, there is considerable interest in identifying probes that discriminate between and simultaneously assess the catalytic subunits of the proteasome (210-212). In this regard, our group has previously reported the first example of a set of fluorescent, real-time, peptide-based sensors capable of simultaneously monitoring all three of the proteasome's proteolytic activities (Figure 1.11) (213). Each sensor is comprised of a fluorophore, a peptide specific for one of the three proteasome activities, and a quencher. These proteasome sensors possess photochemically distinct fluorophores: fluorescein (λ_{ex} = 488 nm) for the ChL sensor, tetramethylrhodamine (λ_{ex} = 550 nm) for the TL sensor, and DyLight633 (λ_{ex} = 633 nm) for the CaL sensor, appended to the N-terminus of the recognition sequences selective for each proteasomal activity [ChL: Fluorophore-His-His-Ser-Leu-Lys(Quencher); TL: Fluorophore-Leu-Arg-Arg-Lys(Quencher); CaL: Fluorophore-norLeu-Pro-norLeu-Asp-Lys(Quencher)]. A broad-spectrum quencher, an acid blue 40 derivative (AB40) (214), is appended to the C-terminal lysine residue on each sensor. In the intact sensor, the fluorescence of the fluorophore is internally quenched by a covalently appended dye (AB40), but upon proteolysis of the peptide, the fluorophore dissociates from the quencher and becomes fluorescent, furnishing a fluorescent enhancement of 30- to 140-fold for each peptide (213).

1.9 Potential Cross Talk Between the SFKs and the Proteasome

Although the proteasome and the SFKs each appear to independently play a role in promoting a neoplastic phenotype in primarily ABC DLBCL over GCB DLBCL, there is evidence for cross talk between these proteins. Treatment with proteasome or SFK inhibitors reduces the growth of lymphoma cells *in vitro* and *in vivo* (11,37,38,215,216), indicating that both the SFKs and the proteasome could be valuable targets for targeted DLBCL chemotherapy.

A recent study by Crawford *et al.* (192) demonstrated that treatment of chronic myelogenous leukemia cells with tyrosine kinase inhibitors and proteasome inhibitors produces a synergistic effect. There is some evidence of cross talk between the SFKs and the proteasome (Figure 1.12), but there is much more to learn about the mechanisms connecting these proteins. The SFKs are involved in many signaling pathways that feed into the proteasome, such as NF-κB and MAPK/ERK signaling (217-220). In addition, the SFKs themselves are degraded by the proteasome (221,222). However, direct links between SFK activity and proteasome activation are not well understood. The proteasome can be transcriptionally activated by Jak/STAT signaling (223,224). In *C. elegans*, EGF signaling through the Ras-MAPK pathways has been shown to activate the proteasome (225). The SFKs can promote both Jak/STAT and EGF signaling (226), and may therefore promote proteasome activation. One study demonstrated that treatment with the SFK inhibitor dasatinib led to decreased gene expression of several STAT proteins (227). Thus, there is evidence that the SFK and proteasome pathways are connected.

1.10 Scope of Dissertation

The following chapters of this dissertation will explore potential chemotherapeutic agents for the treatment of DLBCL, notably the SFK inhibitor dasatinib and site-specific inhibitors of the proteasome. Chapter 2 will explore sensitivity to dasatinib and the effects of dasatinib on the kinome in a panel of ABC and GCB DLBCL cell lines. This chapter is in preparation to be submitted as a manuscript to the *Journal of Proteome Research*. Chapter 3 will explore the effects of dasatinib on the proteasome in the same panel of cell lines. Chapter 4, which is submitted as a manuscript to *ACS Chemical Biology*, will examine the sensitivities of several different cancer cell lines to site-specific inhibitors of the β2 and β1 proteasome subunits.

1.11 Tables and Figures

SFK Member	Pattern of Expression	Isoforms
Blk	B-cells	-
Fgr	Myeloid cells, B-cells	-
Fyn	Ubiquitous	T-cell specific isoform (FynT)
Frk	Primarily epithelial cells	-
Hck	Myeloid cells	Two different translational starts
Lck	T-cells, NK cells, brain	-
Lyn	B-cells, myeloid cells, brain	Two alternatively spliced forms
Src	Ubiquitous	Two neuron-specific isoforms
Yes	Ubiquitous	-

Table 1.1: Src family kinase members
List of SFK members, their primary expression patterns, and known isoforms (22).

Technology Name	Basic Principle	Applicable Kinase Samples	Read Type	Detection Method	Amenable to HTS?	Potential for Multiplexed Analysis?
Radiometric assays	[γ-^{32}P]- or [γ-^{33}P]-labelled ATP	Purified protein, cell lysates	Endpoint	Scintillation counting	Yes	No
HTRF/LANCE	Phospho-specific antibodies and FRET	Purified protein, cell lysates	Endpoint	Fluorescence plate reader	Yes	No
AlphaScreen	Phospho-specific antibodies and luminescence	Purified protein, cell lysates	Endpoint	Luminescence plate reader	Yes	No
Fluorescence polarization	Phospho-specific antibodies and fluorescence anisotropy	Purified protein	Endpoint or kinetic	Fluorescence plate reader	Yes	No
Metal ion coordinated fluorescence quench	Metal ion coordination and fluorescence quenching	Purified protein, cell lysates	Endpoint or kinetic	Fluorescence plate reader	Yes	No
Enzyme-coupled assays	ATP depletion or ADP accumulation	Purified protein	Endpoint or kinetic	Luminescence, fluorescence, or absorbance plate reader	Yes	No
Genetically-encoded sensors	Phospho-substrate binding domains and FRET	Live cells	Kinetic	Fluorescence microscopy	No	Yes
Environmentally-sensitive fluorophores	Charge- or chelation-sensitive fluorophores	Purified protein, cell lysates, live cells	Endpoint or kinetic	Fluorescence plate reader, fluorescence microscopy	No	Yes
Electrophoretic mobility shift assays	Charge alters electrophoretic migration	Purified protein, cell lysates, live cells	Endpoint	Capillary electrophoresis with laser-induced fluorescence	Somewhat	Yes
RPPA and phosphoprotein assays	Immune detection of known proteins and phosphorylation sites	Purified protein, cell lysates	Endpoint	Luminescence, fluorescence, or chemiluminescence	Yes	Yes
KinoBeads	Kinase capture on immobilized kinase inhibitor beads	Purified protein, cell lysates	Endpoint	Mass spectrometry	No	No
Multiplexed inhibitor beads (MIBs)	Kinase capture on layers of immobilized kinase inhibitor beads	Purified protein, cell lysates	Endpoint	Mass spectrometry	No	No
DigiWest	Kinase capture on immobilized kinase inhibitor beads followed by immune detection of known proteins and phosphorylation sites	Purified protein, cell lysates	Endpoint	Flow cytometry (luminescence)	Yes	Yes
Desthiobiotin ATP	Covalent modification of active kinases	Purified protein, cell lysates, live cells	Endpoint	Mass spectrometry	No	No
Shokat approach	ATP analog assay of kinase specificity	Purified protein, cell lysates, live cells	Endpoint	Mass spectrometry	No	No
BioID	In cell biotinylation of neighboring proteins	Live cells	Endpoint	Mass spectrometry	No	No

Table 1.2: Summary of technologies for measuring kinase activity
As discussed in Section 1.5.

Subparticle		Protein Name	Gene Name	Major Function
20S CP	α-ring	α1	PSMA6	
		α2	PSMA2	
		α3	PSMA4	
		α4	PSMA7	
		α5	PSMA5	
		α6	PSMA1	
		α7	PSMA3	
	β-ring	β1	PSMB6	Caspase-like proteolysis
		β2	PSMB7	Trypsin-like proteolysis
		β3	PSMB3	
		β4	PSMB2	
		β5	PSMB5	Chymotrypsin-like proteolysis
		β6	PSMB1	
		β7	PSMB4	
		β1i	PSMB9/LMP2	Caspase-like proteolysis (immunoproteasome)
		β2i	PSMB10/LMP10	Trypsin-like proteolysis (immunoproteasome)
		β5i	PSMB8/LMP7	Chymotrypsin-like proteolysis (immunoproteasome)
		β5t	PSMB11	Chymotrypsin-like proteolysis (thymoproteasome)
19S (PA700) RP	base	Rpt1	PSMC2	ATP-dependent protein unfolding; binds to 20S CP α-ring
		Rpt2	PSMC1	ATP-dependent protein unfolding; binds to 20S CP α-ring
		Rpt3	PSMC4	ATP-dependent protein unfolding; binds to 20S CP α-ring
		Rpt4	PSMC6	ATP-dependent protein unfolding; binds to 20S CP α-ring
		Rpt5	PSMC3	ATP-dependent protein unfolding; binds to 20S CP α-ring
		Rpt6	PSMC5	ATP-dependent protein unfolding; binds to 20S CP α-ring
		Rpn1	PSMD2	Ubiquitin receptor (Rpn10) docking
		Rpn2	PSMD1	Ubiquitin receptor (Rpn13) docking
		Rpn13	ADRM1	Ubiquitin receptor/Binding of ubiquitinated proteins
	lid	Rpn10	PSMD4	Ubiquitin receptor/Binding of ubiquitinated proteins
		Rpn3	PSMD3	
		Rpn5	PSMD12	
		Rpn6	PSMD11	
		Rpn7	PSMD6	
		Rpn8	PSMD7	
		Rpn9	PSMD13	
		Rpn11	PSMD14	Deubiquitinase
		Rpn12	PSMD8	
PA28αβ RP		PA28α	PSME1	
		PA28β	PSME2	
PA28γ RP		PA28γ	PSME3	
PA200 RP		PA200	PSME4/PA200	

Table 1.3: Proteasome subunits and their function
List of the proteasome's 20S core particle subunits and various regulatory particle subunits. Note: the β1i, β2i, β5i, and β5t 20S core particle subunits are not necessarily expressed in every proteasome, but are induced in certain cell types after certain stimuli, such as IFNγ. CP = core particle; RP = regulatory particle; Rpt = RP triple-ATPase; Rpn = RP non-ATPase.

Technology Name	Basic Principle	Applicable Proteasome Samples	Read Type	Detection Method	Proteasome Activity Measured
Fluorogenic peptide substrates	Degradation of fluorescent peptides increases fluorescent signal	Purified	Endpoint or kinetic	Luminescence or fluorescence plate reader	Individual: β1 (CaL), β2 (TL), or β5 (ChL)
Activity-based probes (ABPs)	Suicide substrates irreversibly bind to proteasome, detected via antibodies or fluorescent labeling	Purified or live cells	Endpoint	Fluorescence plate reader or fluorescence microscopy	Individual: β1 (CaL), β2 (TL), or β5 (ChL)
Molecular imaging	Degradation of fluorescent or luminescent proteins decreases fluorescent or luminescent signal	Live cells	Endpoint or kinetic	Fluorescence microscopy	Whole proteasome
RFDD-PCR	Global changes in proteasome gene expression	Extracted RNA	Endpoint	Electrophoresis of PCR products	None (measures amount)
Proteomics	Global changes in proteasome protein expression	Cell lysates	Endpoint	Mass spectrometry	None (measures amount)
Immunological methods	Antibodies detect levels of proteasome protein (western blotting or ELISA)	Purified or cell lysates	Endpoint	Chemiluminescence, fluorescence or absorbance plate reader	None (measures amount)
Priestman *et al.* fluorogenic peptide substrates (213)	Degradation of fluorescent peptides increases fluorescent signal	Purified	Kinetic	Fluorescence plate reader	Simultaneous: β1 (CaL), β2 (TL), and β5 (ChL)

Table 1.4: Summary of technologies for measuring proteasome activity
As discussed in Section 1.8.

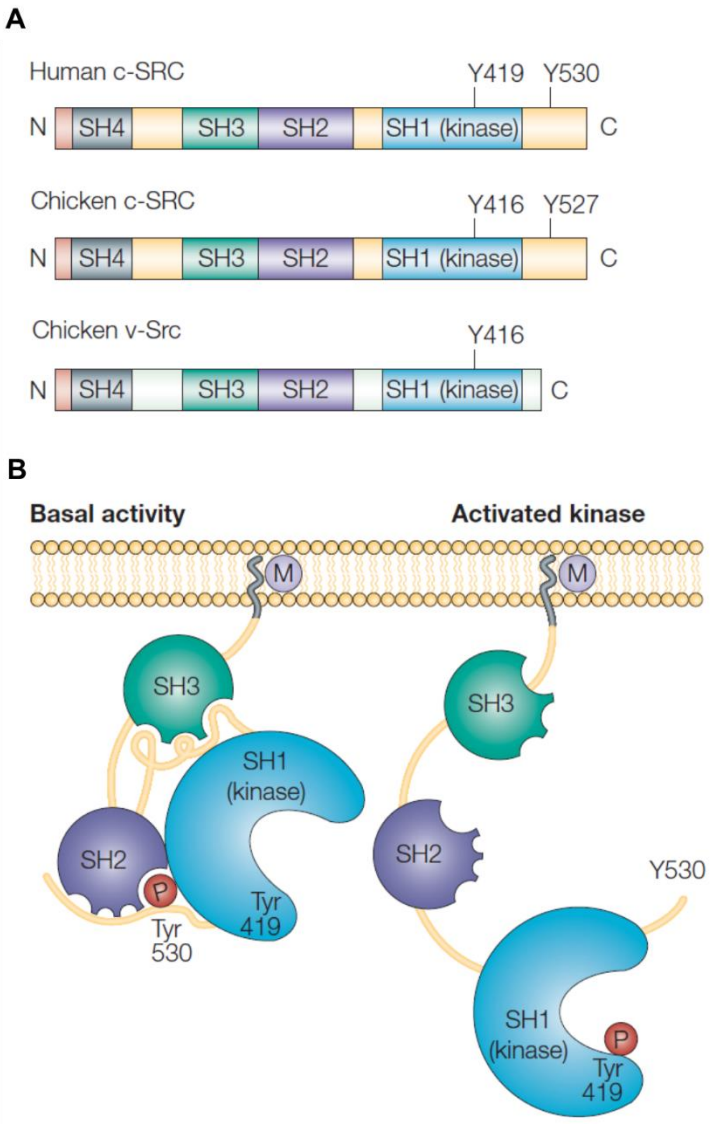

Figure 1.1: Structure and activation of the Src family kinases
Schematic representation of SFK domain structure and protein folding. (*A*) Comparison of the molecular structures of human Src, chicken c-Src, and chicken v-Src. Each of the SFK members have four key Src homology (SH) domains: SH1, the kinase domain; SH2, a phospho-tyrosine binding domain; SH3, a domain that binds proline-rich amino acid sequences; and SH4, which contains a myristoylation site important for membrane anchoring. In addition to these domains, each SFK member has a C-terminal tail, containing an autoinhibitory tyrosine phosphorylation site, and a unique N-terminal region whose function remains unclear. (*B*) Inactivation of human Src occurs when its C-terminal Tyr530 is phosphorylated and it binds back to the SH2 domain. This interaction and an interaction between the SH3 domain and the kinase domain result in a closed molecular structure with diminished access of substrates to the kinase domain. Conversely, Src activation occurs with removal of the C-terminal phosphotyrosine, displacement of inhibitory intramolecular interactions, and opening of the Src molecular structure. Full activation involves phosphorylation at Tyr419. M, myristoylation; P, phosphorylation. Figure adapted and reprinted with permission from the publisher (21).

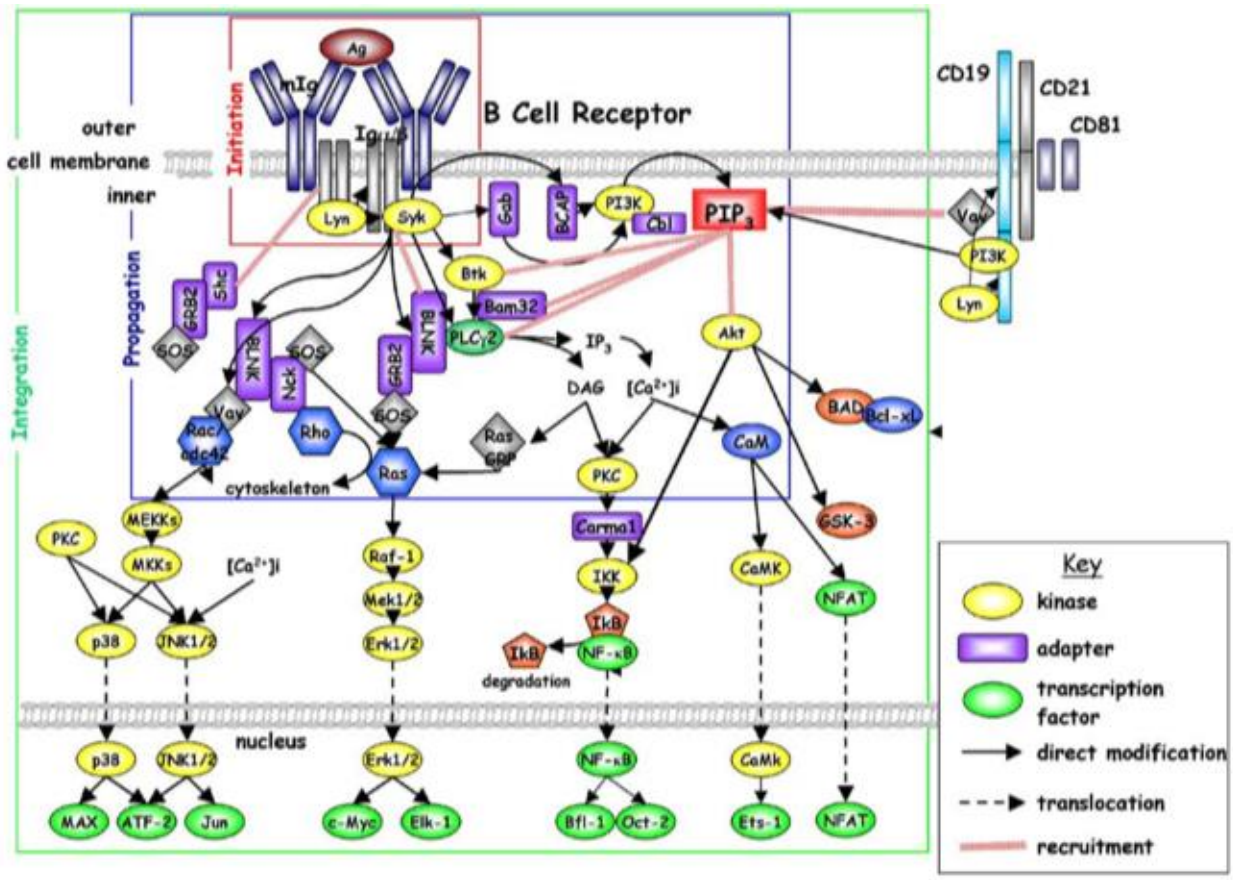

Figure 1.2: B-cell receptor signaling
Signal transduction initiates at the cell membrane following ligand-induced aggregation of the membrane immunoglobulin (mIg) and associated signal transducing elements Igα and Igβ. Signals are then propagated by means of protein phosphorylation, modification, and interaction. The culmination of the signaling cascade is the regulation of transcription factor activation and gene expression. Figure reprinted with permission from the publisher (32).

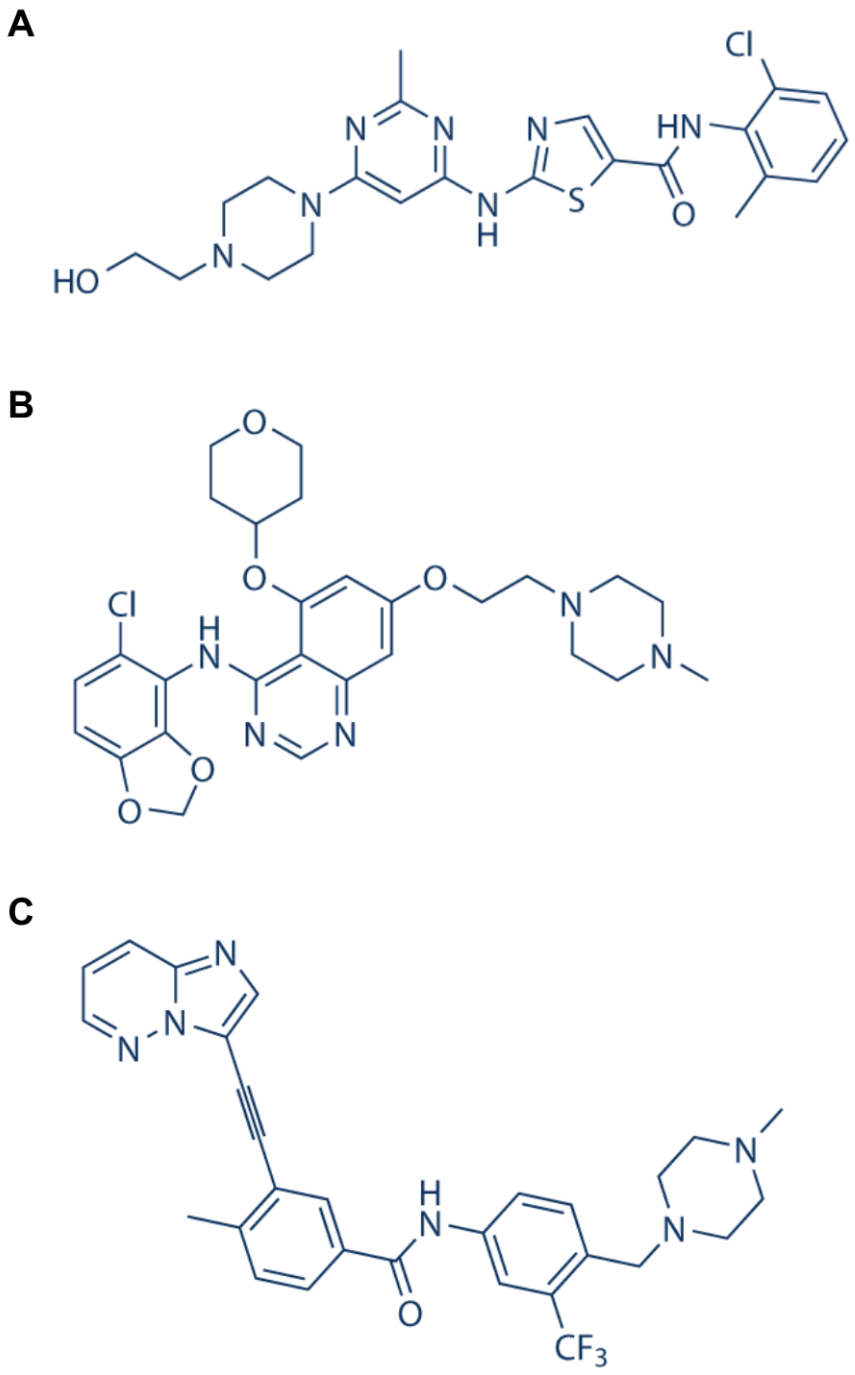

Figure 1.3: Chemical structures of SFK inhibitors
Chemical structures of the SFK inhibitors (*A*) dasatinib, (*B*) saracatinib, and (*C*) ponatinib.

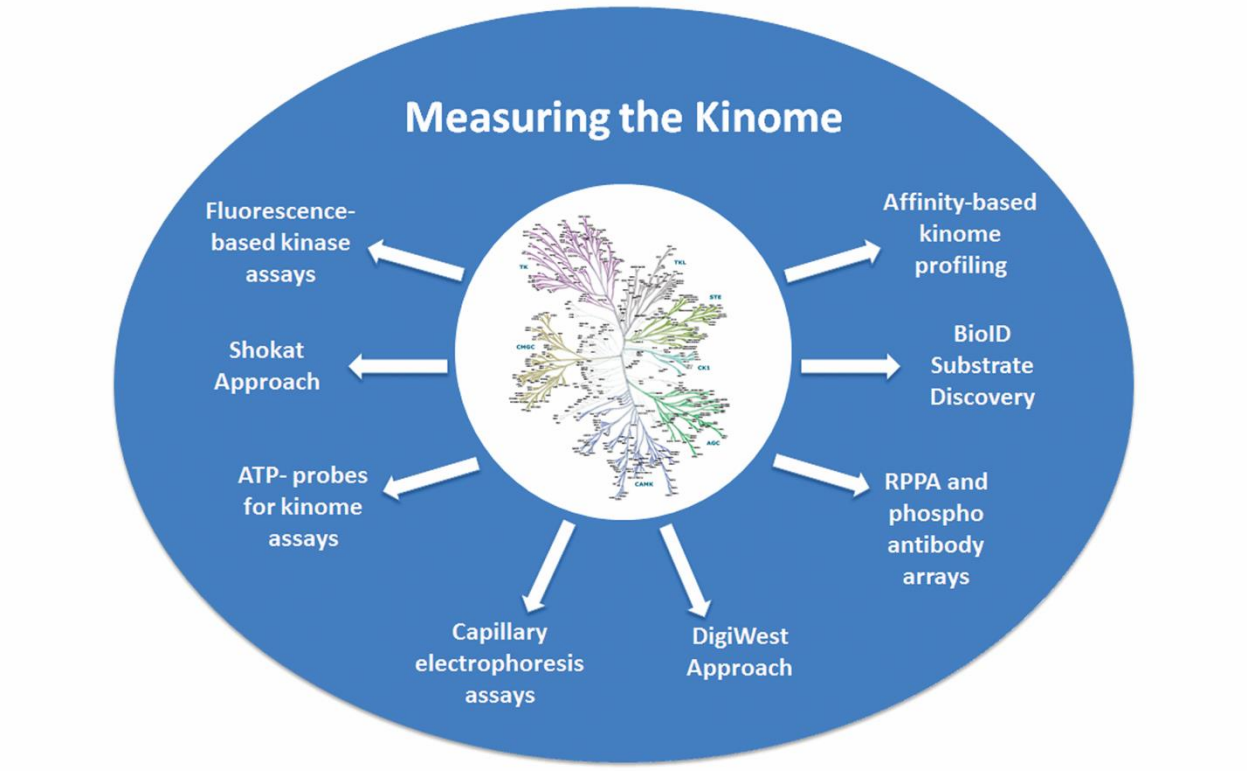

Figure 1.4: Measuring the kinome
Graphical representation of the various technologies for measuring kinase activity that are discussed in this section.

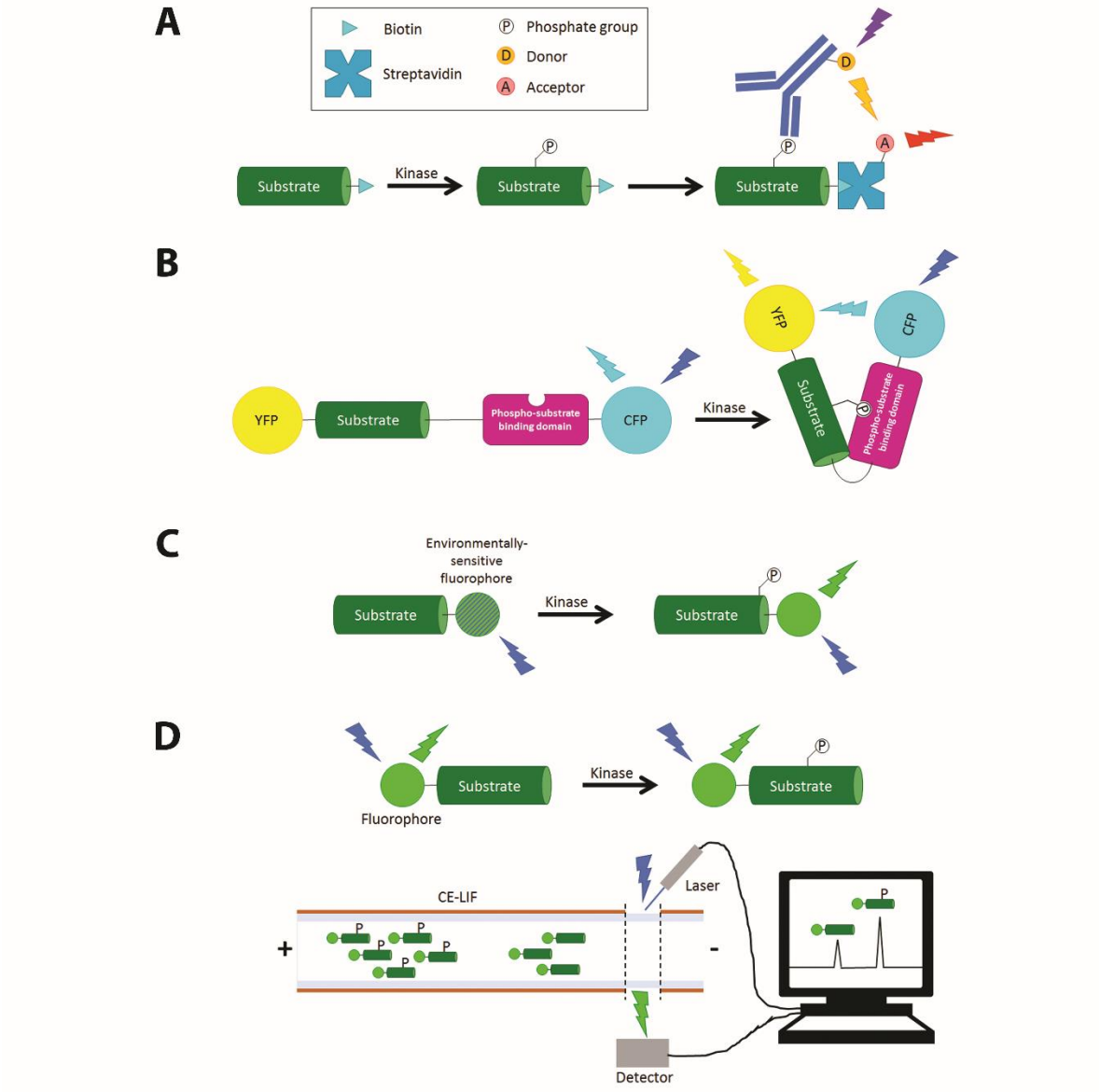

Figure 1.5: Schematics of several of the peptide-based sensors for kinase activity
(*A*) Example of a multi-component assay that uses a phospho-specific antibody, such as HRTF or LANCE. After phosphorylation of the substrate, binding of a pair of FRET molecules (via labeled antibody or biotin-streptavidin) brings the donor and acceptor molecules into close enough proximity to generate a FRET signal. (*B*) Example of a genetically-encoded unimolecular sensor. Upon phosphorylation, the phospho-substrate binding domain binds to the phosphorylated substrate, bringing a pair of FRET proteins in close enough proximity to generate a FRET signal. YFP = yellow fluorescent protein, CFP = cyan fluorescent protein. (*C*) Example of a peptide sensor with an environmentally-sensitive fluorophore. Added charge from the phosphorylation of the substrate causes a change in the fluorescent properties of the fluorophore. (*D*) Example of an electrophoretic mobility shift assay. Permanently fluorescent substrates are separated into phosphorylated and nonphosphorylated substrates by an electric field and quantified based on fluorescence at different migration times.

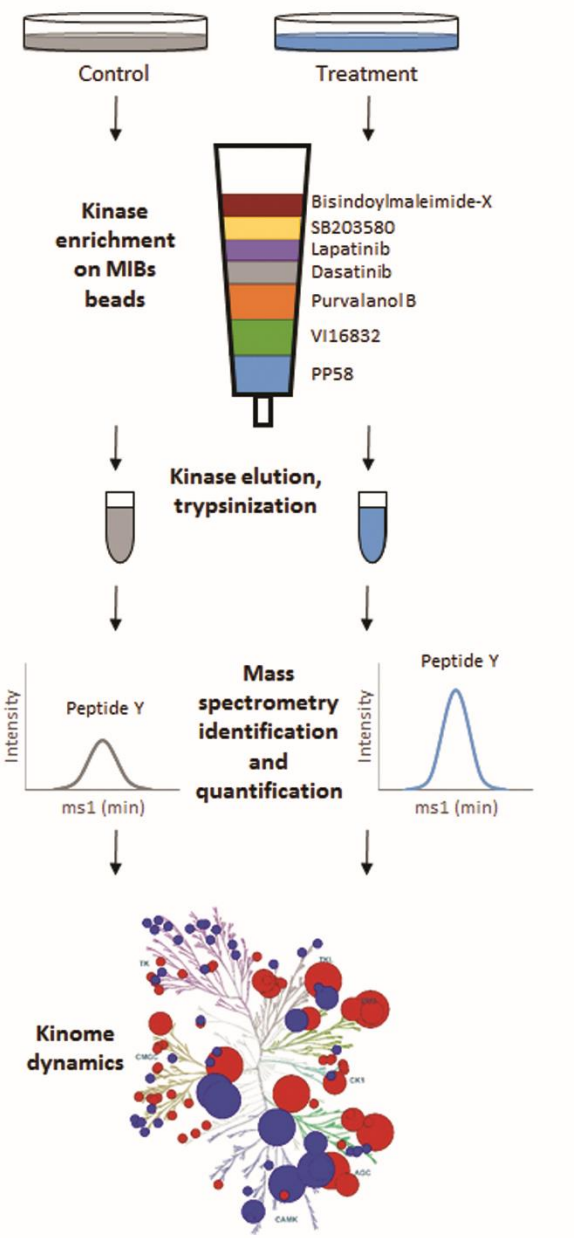

Figure 1.6: Graphical representation of MIB/MS
Control and treated cells are lysed and clarified by centrifugation prior to being passed over a column layered with kinase inhibitors immobilized on sepharose beads (MIBs). Kinases capture by MIBs is based on affinity of kinases for the immobilized inhibitors, kinase expression, and the activation state of the kinase. Bound kinases are eluted from the column and trypsinized to prepare samples for analysis by mass spectrometry (MS). Kinases in each sample are identified and quantified using quantitative MS and the relative abundance are calculated by isotobaric labeling or label free quantification of peptides. Kinome dynamics are determined by quantifying changes in MIB binding of hundreds of kinases simultaneously. Kinome tree illustration reproduced courtesy of Cell Signaling Technology, Inc. (www.cellsignal.com).

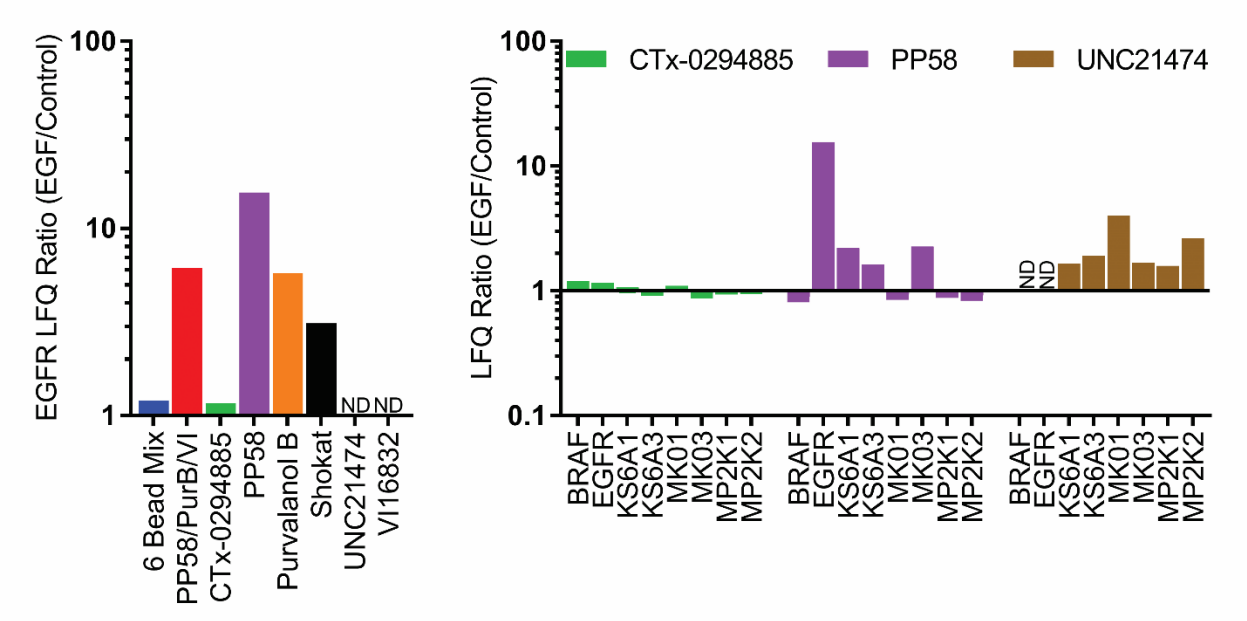

Figure 1.7: Inhibitor bead composition defines activity-dependent capture by MIB/MS
SUM159 cells were serum starved for 24 hours then treated for 15 minutes with 100 ng/mL EGF prior to kinase enrichment using multiplexed inhibitor beads (MIB) and label free quantification (LFQ) by mass spectrometry (MS). Short-term agonist treatment minimizes changes in protein abundance. The ratio of EGF stimulated over serum starved control cells are plotted for EGFR (left) or the indicated kinases (right). A value >1 indicates increased capture by MIBs in response to EGF stimulation. Failure to capture or quantify an indicated kinase is denoted with "ND" (Not Detected).

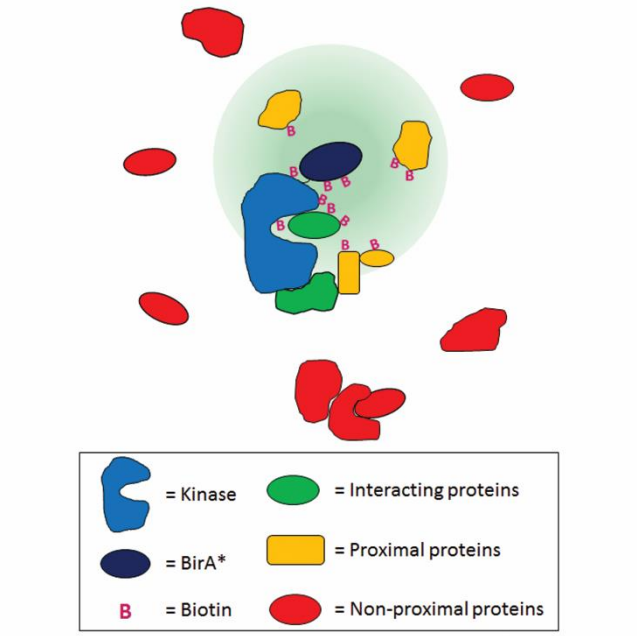

Figure 1.8: BioID schematic with BirA*-Kinase fusion protein
Autobiotinylation of the BirA*-Kinase fusion occurs. Interacting and proximal proteins that fall within the ~10 nm labeling radius (green circle) of BirA* are biotinylated. Direct interactors are not biotinylated if they are more than 10 nm from BirA*.

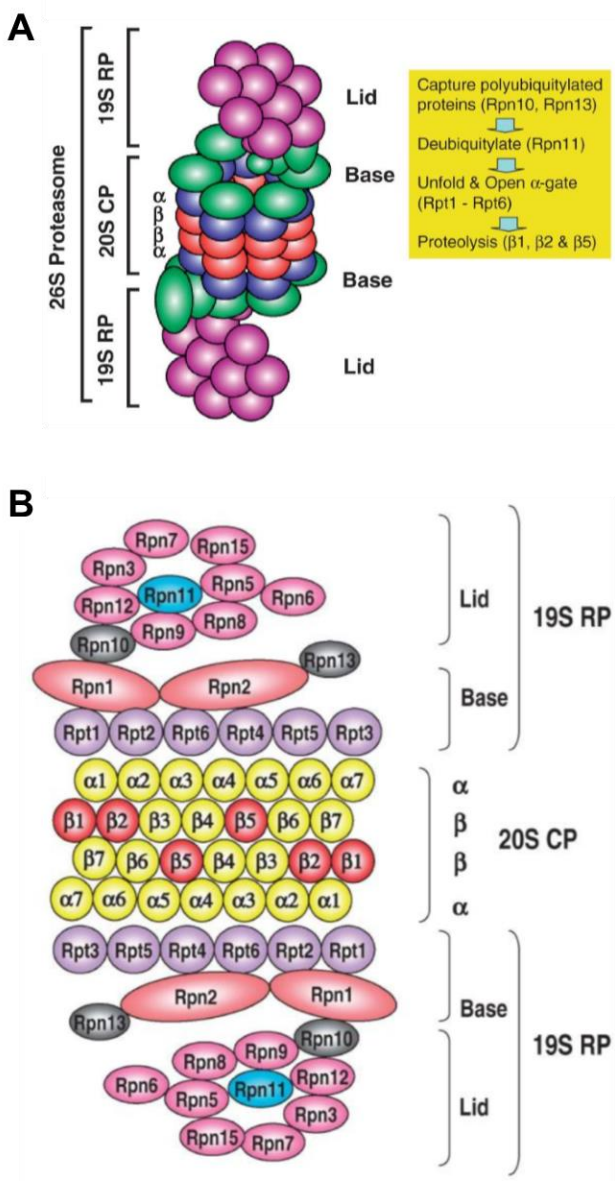

Figure 1.9: Structure of the 26S proteasome
(*A*) Schematic diagram of structure of and proteolysis by the 26S proteasome. (*B*) Schematic depicting a flattened subunit structure of the 26S proteasome. CP = core particle; RP = regulatory particle; Rpt = RP triple-ATPase; Rpn = RP non-ATPase. Figures adapted and reprinted with permission from the publisher (164).

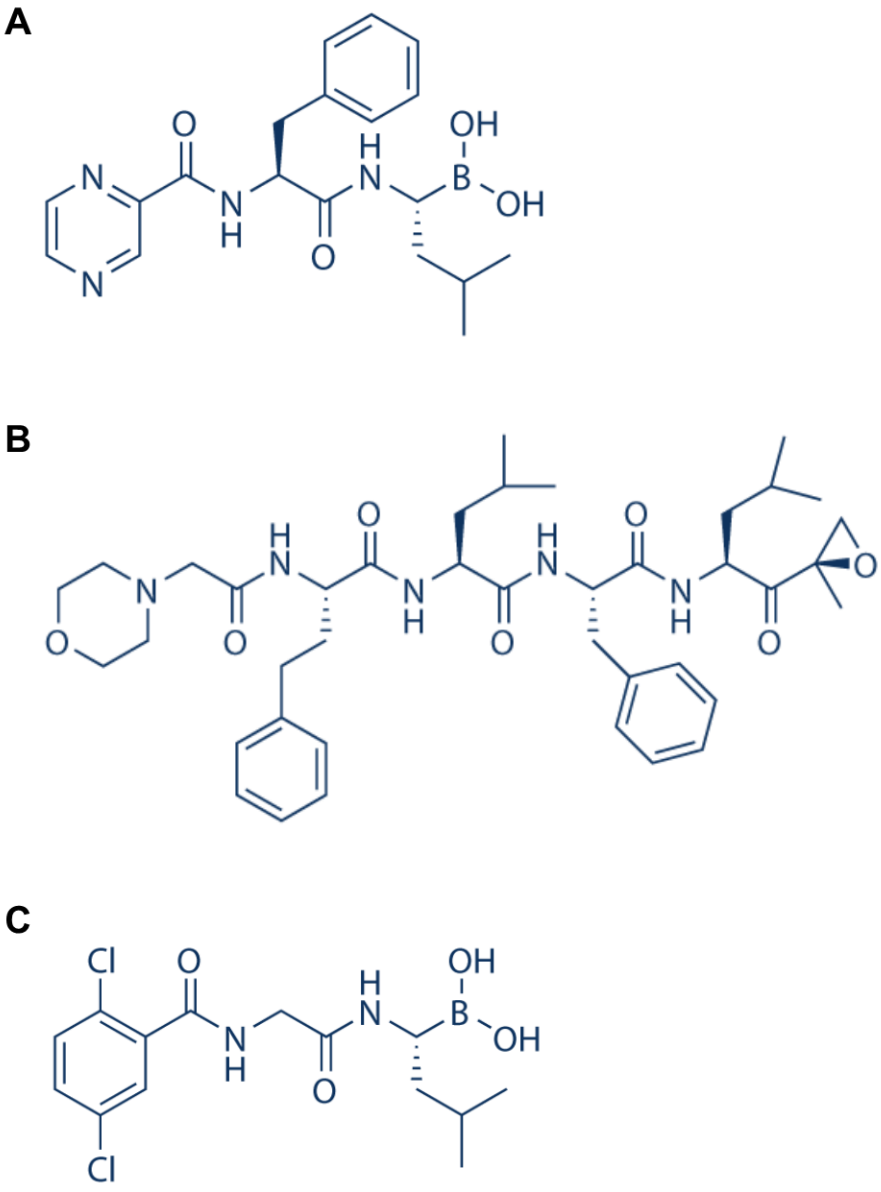

Figure 1.10: Chemical structures of proteasome inhibitors
Chemical structures of the proteasome inhibitors (*A*) bortezomib, (*B*) carfilzomib, and (*C*) ixazomib. Bortezomib, carfilzomib, and ixaxomib preferentially target the β5 subunit (ChL activity) of the proteasome.

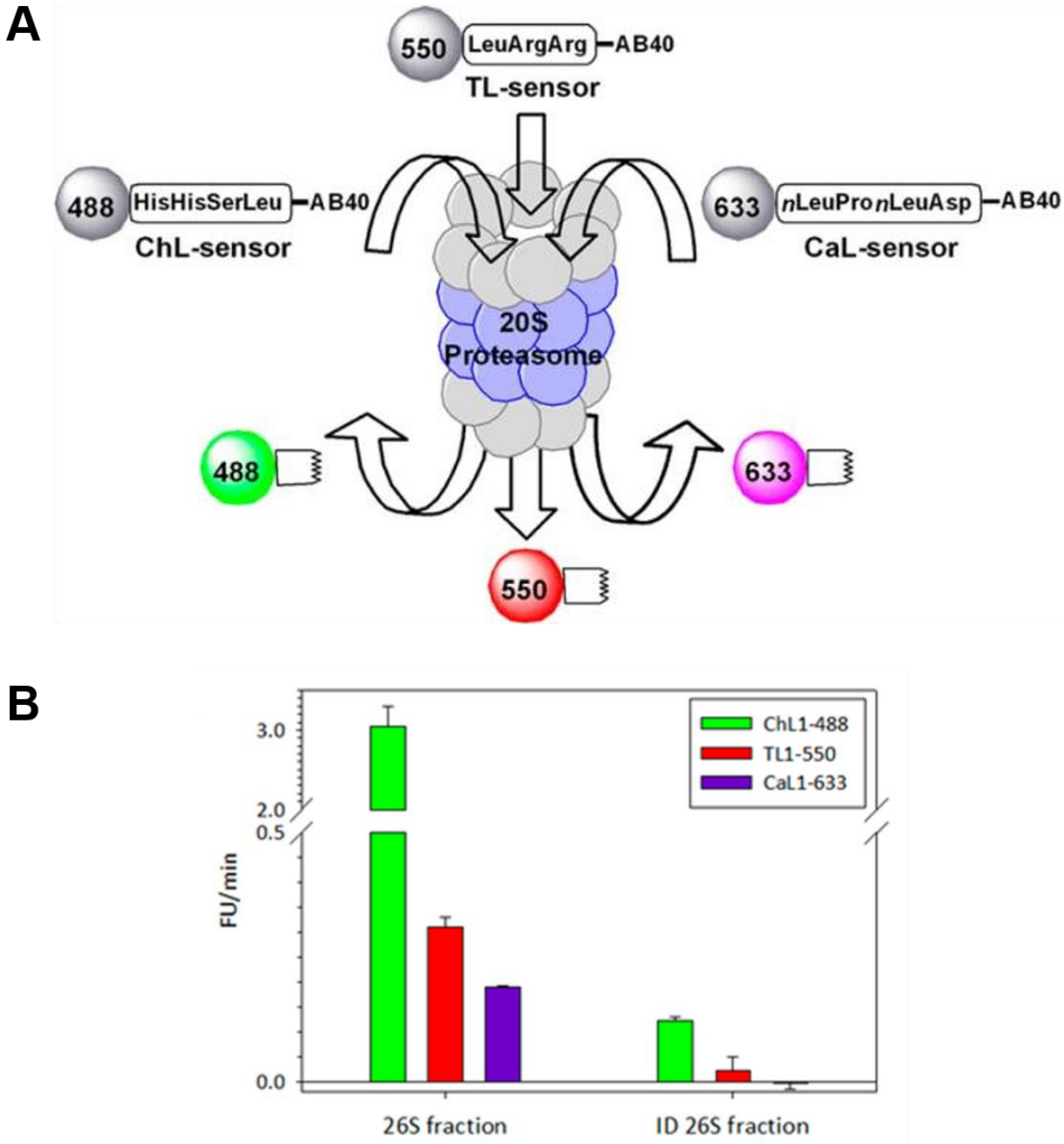

Figure 1.11: Proteasome activity determination by fluorescent sensors
(*A*) Multicolor monitoring of proteasome activity. ChL, chymotrypsin-like; TL, trypsin-like; CaL, caspase-like; AB40, acid blue 40. (*B*) Proteasome activities from different fractions of HeLa cell lysis procedure. "ID 26S fraction" indicates samples that were immunodepleted of the proteasome. Figure adapted and reprinted with permission from the publisher (213). Further permissions related to this figure should be directed to the American Chemical Society. The original article can be found at http://pubs.acs.org/doi/10.1021/cb5007322.

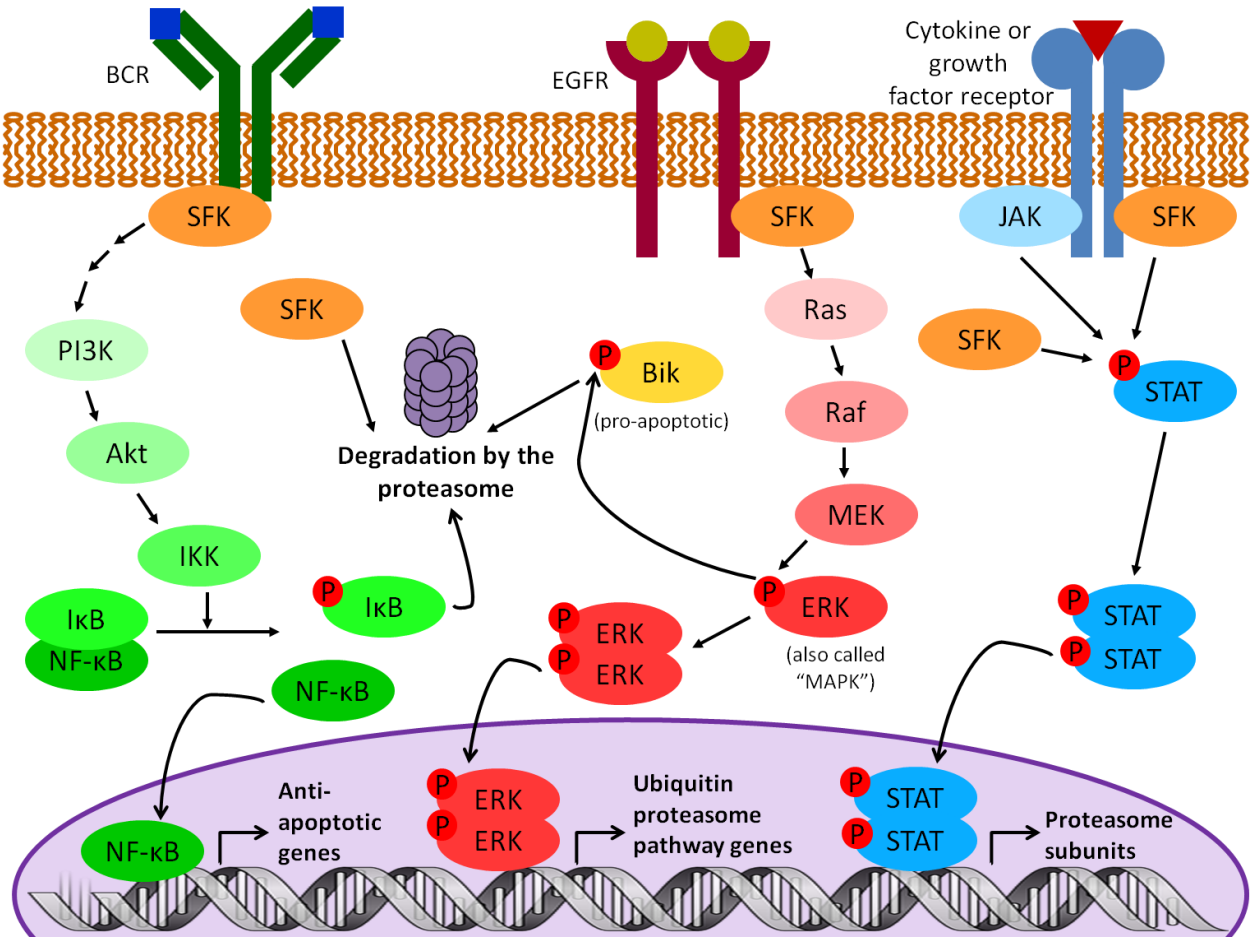

Figure 1.12: Possible mechanisms of cross talk between the SFKs and the proteasome
BCR, B-cell receptor; SFK, Src family kinase; EGFR, epidermal growth factor receptor.

CHAPTER 2: DASATINIB IS PREFERENTIALLY ACTIVE IN THE ACTIVATED B-CELL SUBTYPE OF DIFFUSE LARGE B-CELL LYMPHOMA[2]

2.1 Introduction

Non-Hodgkin lymphoma (NHL) is the seventh most common cancer in the United States, with diffuse large B-cell lymphoma (DLBCL) being the most common subtype (1-3). The standard treatment of DLBCL is a cocktail of chemotherapeutic agents called R-CHOP, which includes rituximab, cyclophosphamide, doxorubicin, vincristine, and prednisone. However, roughly 10% of DLBCL patients will be refractory (non-responsive) to this therapy, and a substantial 40% of DLBCL patients who do respond to R-CHOP will relapse within 5 years (7). Although the standard R-CHOP chemotherapy regimen has a relatively high cure rate for patients with a good prognosis (2,8), patients with refractory and relapsed DLBCL pose a significant challenge to effective treatment. By gene expression profiling, DLBCL patients can be categorized into two clinically relevant subtypes: activated B-cell (ABC) and germinal center B-cell (GCB) (4). Patients with ABC DLBCL generally have a much poorer prognosis than those with GCB DLBCL (5,6). Despite these distinctions, there are currently no established treatment differences between these two subtypes. Although some therapeutic agents have shown preferential activity in the poor prognosis ABC subtype (19), none of these agents are FDA-approved for use in DLBCL. Thus, a better understanding of the cellular processes that contribute to tumor progression and drug resistance in DLBCL would complement ongoing

[2] This chapter is in preparation to be submitted as an article in the Journal of Proteome Research. The original citation is as follows:
Cann ML, Herring LE, Gilbert TSK, Richards KL, Graves LM, Lawrence DS. Dasatinib is preferentially active in the activated B-cell subtype of diffuse large B-cell lymphoma. J Proteome Res. 2017. In preparation.

studies of promising therapeutic agents and could lead to the identification of additional therapeutic targets for the treatment of relapsed and refractory DLBCL.

Chronic, overactive signaling through the B-cell receptor (BCR) and the anti-apoptotic NF-κB pathway are hallmarks of the ABC but not the GCB DLBCL subtype (9,10), and may be particularly important for promoting tumor progression and drug resistance. Signaling through the BCR triggers the activation of many pro-survival and anti-apoptotic signaling pathways, including the NF-κB pathway. Important kinase mediators of BCR signaling are Syk and Btk, both of which have inhibitors in clinical trials for the treatment of DLBCL as well as other types of lymphoma (58). The Src family kinases (SFKs) are a family of nine nonreceptor tyrosine kinases that facilitate signaling from the BCR to Syk and Btk. The SFKs also play a role in signaling from many other receptors, facilitating several proliferation, survival, and cell motility pathways (22,23,29). Based on SFK involvement in these signaling pathways, it is not surprising that the SFKs have been implicated in progression and drug resistance in many cancers, including lymphoma (9,29,37,38).

We hypothesized that SFK inhibitors would provide a viable option for the treatment of the ABC subtype of DLBCL. Dasatinib (Sprycel) is an FDA-approved kinase inhibitor that broadly targets SFKs and other kinases, and is used for treatment of leukemia (228). We explored the effects of dasatinib and other SFK inhibitors in a panel of ABC and GCB DLBCL cell lines, and found that the ABC DLBCL cell lines are considerably more sensitive to dasatinib than the GCB DLBCL cell lines. However, both subtypes display inhibition of the SFKs in response to dasatinib after both short- and long-term treatment, as determined by western blot analysis. The difference in dasatinib sensitivities is due to either differences in signaling inhibition downstream of the SFKs or an off-target effect of dasatinib. We used a kinase

enrichment approach, multiplex inhibitor beads coupled to mass spectrometry (MIB/MS) (70), to determine the effects of dasatinib on the kinome. The MIB/MS technique revealed that a large number of kinases involved in cell cycle regulation are inhibited in the ABC DLBCL subtype, but not in the GCB DLBCL subtype, in response to long-term dasatinib treatment. Our findings highlight the potential use for dasatinib in the treatment of DLBCL.

2.2 Materials and Methods

2.2.1 Cell Culture

The Farage cell line was purchased from ATCC, the HBL-1 cell line was obtained from Ben Major, the HT, Karpas 422, OCI-Ly3 cell lines were obtained from Steven Park, and the OCI-Ly10 and TMD8 cell lines were obtained from Sandeep Dave. Cell culture media, fetal bovine serum (FBS), and penicillin-streptomycin were purchased from Corning Cellgro. All cell lines were maintained between $2x10^5$ – $1x10^6$ cells/mL in RPMI 1640 media containing 10% FBS supplemented with penicillin-streptomycin at 37 °C in a 5% CO_2 incubator.

2.2.2 Cell Viability Assays

Cell viability was determined using the CellTiter-Glo® 2.0 system (Promega) according to the manufacturer's protocol. Cells were seeded into 96-well plates at 5,000 cells/well, treated with the indicated concentrations of dasatinib, saracatinib, or ponatinib (Selleck Chemicals), and grown at 37 °C in a 5% CO_2 incubator. All inhibitors were dissolved in DMSO with a final concentration of 0.1% DMSO. After 72 h, plates were incubated at room temperature for 30 min, 100 μL of CellTiter-Glo® 2.0 was added per well and mixed, and plates were allowed to equilibrate for another 10 min. The plates were read on the Molecular Devices Spectra Max Gemini EM plate reader with the luminescent settings. All data is reported as the mean ±

standard error of triplicate assays. All data were fit to the standard EC_{50} equation and plotted using Sigmaplot.

2.2.3 Whole Cell Lysate Preparation

Cells were seeded at $2x10^5$ cells/mL in 75 cm^2 flasks and treated with dasatinib for the indicated times and concentrations. Cells were harvested and centrifuged at 1,000 x g for 5 min at 4 °C, then washed 3 times with ice cold 1X DPBS. Cell pellets were then lysed in M-PER + 5X Halt Protease & Phosphatase cocktail (EDTA-free; both from Thermo Fisher Scientific), rotated for 10 min at 4 °C, then centrifuged at 17,000 x g for 10 min at 4 °C. Supernatants were collected and protein concentration was determined using the Pierce BCA Protein Assay Kit (Thermo Scientific).

2.2.4 Western Blots

Phospho-Tyr416 SFK, phospho-Tyr527 SFK, Blk, Fgr, Fyn, Hck, Lck, Lyn, Src, Yes, GAPDH, phospho-Tyrosine, phospho-Syk, Syk, phospho-Erk, Erk, Aurora A kinase, Aurora B kinase, CDK4, and CDK6 antibodies were purchased from Cell Signaling Technologies. The cyclin A, B, D, and E antibodies were purchased from Abcam. Total SFK antibody was purchased from Millipore. All secondary antibodies were purchased from GE Healthcare. SDS-PAGE was performed using 4-15% polyacrylamide gels (Bio-Rad) and loading 20 μg (10 μL) of each sample per well. Gels were then transferred to polyvinylidene fluoride (PVDF) membranes overnight at 4 °C. Membranes were blocked with 5% BSA or milk in 1X Tris-buffered saline (TBS) + 0.1% Tween-20 for 2 h, then incubated with 1:500-1:1000 of the primary antibody in the blocking solution overnight at 4 °C. Membranes were washed with TBS + 0.1% Tween-20, incubated with 1:5000 HRP-conjugated secondary antibody for 1 h at room temperature, and washed again with TBS + 0.1% Tween-20. Secondary antibodies were detected using the Clarity

Western ECL Substrate (Bio-Rad) according to the manufacturer's protocol. Images were acquired by an Alpha Innotech FluorChem FC2, using the chemiluminescent settings. Densitometry analysis was performed in ImageJ.

2.2.5 Lyn Immunoprecipitation

Lyn antibody (12.5 uL, Santa Cruz) was incubated with 100 µL of 2.5 mg/mL whole cell lysate (250 µg protein) and rotated overnight at 4 °C. Protein A-Sepharose 4B beads (Invitrogen) were aliquoted into spin columns (Thermo Scientific) and washed with M-PER (Thermo Scientific). The lysate/antibody mixtures were added to the beads and rotated at 4 °C for 1 h to capture antibodies. Antibody-bound beads were washed again, and proteins were eluted from the beads via boiling in SDS-PAGE sample buffer.

2.2.6 Multiplexed Inhibitor Bead (MIB) Affinity Chromatography/MS Analysis

Kinases were isolated from cell lysates as previously described (70,132). Briefly, cells were harvested by centrifugation and washed 3 times with 1X DPBS, then flash frozen in liquid nitrogen. Cells were lysed in MIB Lysis Buffer (50 mM HEPES pH 7.5, 150 mM NaCl, 0.5% Triton X-100, 1 mM EDTA, 1 mM EGTA, 10 mM NaF, and 2.5 mM Na_3VO_4, supplemented with protease inhibitor cocktail (Roche) and phosphatase inhibitor cocktails 2 & 3 (Sigma-Aldrich)). Lysates were sonicated, clarified by centrifugation, and filtered through a 0.2-µm syringe filter. The amount of starting material was 5 mg protein, and was diluted to 1.25 mg/mL with MIB lysis buffer. Diluted lysates were passed over a mixture of 117 µL each of the following kinase inhibitors conjugated to ECH Sepharose beads: Purvalanol B, VI-16832, and PP58, layered from top to bottom respectively. The kinase inhibitor-bead conjugates were previously equilibrated in high salt buffer (50 mM HEPES pH 7.5, 1 M NaCl, 0.5% Triton X-100, 1 mM EDTA, and 1 mM EGTA). MIBs columns were sequentially washed with high salt

buffer, low salt buffer (50 mM HEPES pH 7.5, 150 mM NaCl, 0.5% Triton X-100, 1 mM EDTA, and 1 mM EGTA), and SDS buffer (50 mM HEPES pH 7.5, 150 mM NaCl, 0.5% Triton X-100, 1 mM EDTA, 1 mM EGTA, and 0.1% SDS). Proteins were eluted by boiling samples in elution buffer (100 mM Tris-HCl pH 6.8, 0.5% SDS, and 1% β-mercaptoethanol) for 15 min twice. Dithiothreitol (DTT) was added to a final concentration of 5 mM and samples were incubated at 60 °C for 25 min. Samples were then cooled to room temperature on ice and alkylated by adding iodoacetamide to a final concentration of 20 mM and incubating for 30 min in the dark at room temperature. Samples were then concentrated in 10K Amicon Ultra centrifugal concentrators (Millipore), followed by methanol and chloroform precipitation of proteins. The final protein pellets were re-suspended in 50 mM HEPES pH 8.0 and incubated with trypsin at 37 °C overnight. Residual detergent was removed by three sequential ethyl acetate extractions, then desalted using Pierce C-18 spin columns (Thermo Scientific) according to the manufacturer's protocol. Samples were stored at -80C until further analysis.

2.2.7 LC/MS/MS Analysis

Each sample was analyzed by LC-MS/MS using an Easy nLC 1000 coupled to a QExactive HF equipped with an Easy Spray source (Thermo Scientific). First, samples were reconstituted in loading buffer (1% ACN, 0.1% formic acid), and then loaded onto a PepMap 100 C18 column (75 μm inner diameter × 25 cm, 2 μm particle size) (Thermo Scientific). Peptides were separated over a gradient consisting of 5-32% mobile phase B over a 120-min method at a 250 nL/min flow rate, where mobile phase A was 0.1% formic acid in water and mobile phase B consisted of 0.1% formic acid in ACN. The QExactive HF was operated in data-dependent mode where the 15 most intense precursors were selected for subsequent fragmentation. Resolution for the precursor scan (m/z 400-1600) was set to 120,000 with a

target value of $3x10^6$ ions. For MS/MS scans with HCD (normalized collision energy 27%), resolution was set to 15,000 with a target value of $2x10^4$ ions. Peptide match was set to preferred, and precursors with unknown charge or a charge state of 1 and >7 were excluded.

2.2.8 Mass Spectrometry Data Processing and Analysis

Raw data files were processed using MaxQuant software (version 1.5.3.17). Data were searched against a reviewed human UniProt database (downloaded Feb 2017, containing 20,162 sequences) using the integrated Andromeda search engine (229). The following parameters were used to identify tryptic peptides for protein identification: up to two missed trypsin cleavage sites; carbamidomethylation (C) was set as a fixed modification; and oxidation (M) was set as a variable modification. A false discovery rate (FDR) of 1% was used to filter all results, and match between runs was enabled. Only proteins with >1 unique+razor peptide were used for label-free quantitation.

Statistical analysis (ANOVA), hierarchical clustering, and principal component analysis were performed using Perseus software (version 1.6.0.2). Bioinformatics analysis was performed using DAVID Bioinformatics Resources 6.8 functional annotation tool (230,231). Over-represented functional terms (UniProt biological processes) with p-value<0.05 were selected for further analysis. Lists of kinases in these functional clusters were further investigated using STRING 10.5 (232) to construct protein networks and analyze their associations.

2.2.9 Antibody Arrays

Antibody arrays for probing proteins involved in apoptosis were purchased from Ray Biotech and were used according to the manufacturer's protocol. Images were acquired by a

Bio-Rad ChemiDoc, using the chemiluminescent settings. Densitometry analysis was performed in ImageJ.

2.3 Results

2.3.1 ABC DLBCL cells are more sensitive to dasatinib than GCB DLBCL cells

The ABC subtype of DLBCL is characterized by chronic BCR signaling, which is heavily dependent on the Src family kinases (SFKs) (9,10). Therefore, we hypothesized that ABC DLBCL cells would be more sensitive to SFK inhibition than their GCB DLBCL counterparts. To investigate SFKs as potential targets for the treatment of ABC DLBCL, we examined sensitivity to SFK inhibitors in a panel of DLBCL cell lines: Farage, HBL-1, HT, Karpas 422, OCI-Ly3, OCI-Ly10, and TMD8. Of these cell lines, HBL-1, OCI-Ly3, OCI-Ly10, and TMD8 are classified as ABC DLBCL, and Farage, HT, and Karpas 422 are classified as GCB DLBCL (233). We tested the sensitivity of these 7 cell lines to the SFK inhibitors dasatinib, saracatinib, and ponatinib (Figure 2.1, Table 2.1). Interestingly, we found that the four ABC DLBCL cell lines are highly sensitive to dasatinib (EC_{50} between 6-81 nM), whereas the three GCB DLBCL cell lines are resistant (EC_{50}>2,500 nM). However, this disparity is much less pronounced with saracatinib and ponatinib, which are reported to be more specific for the SFKs than dasatinib (64,234,235).

2.3.2 ABC DLBCL cells have higher Lyn expression than GCB DLBCL cells

To characterize potential differences between ABC and GCB cell types, we determined the basal protein expression levels of several of the SFK members by western blotting (Figure 2.2). In general, we observed heterogeneous expression of the various SFK members across the panel of seven DLBCL cell lines. However, Lyn is more highly expressed in the ABC DLBCL

cell lines, whereas Fyn is more highly expressed in the GCB DLBCL cell lines. In addition, we noticed that the GCB DLBCL cell lines had higher levels of the inactive phospho-Y527 form of the SFKs. To complement these data, we utilized a proteomics-based method to examine the kinome of these cells: multiplexed inhibitor beads (MIB) combined with mass spectrometry (MS), or MIB/MS. The MIB/MS technique involves flowing whole cell lysates over columns of kinase inhibitors bound to sepharose beads (Figure 2.3) (70,132). The immobilized kinase inhibitors on the MIBs broadly capture kinases based on expression and, in some instances, activity (236). The captured kinases are then identified and quantified using MS. Using the MIB/MS technique, we analyzed the basal kinome in our panel of 7 cell lines, and evaluated the relative amount of SFKs in these cells (Figure 2.4). The relative amount of SFKs identified by MIB/MS closely reflect the expression we observed via western blotting, including higher Lyn expression in the ABC DLBCL cell lines and higher Fyn expression in the GCB DLBCL cell lines.

2.3.3 Dasatinib inhibits the SFKs in both ABC and GCB DLBCL cells after short-term treatment

Resistance of cells to kinase inhibitors is not uncommon, and can result from kinase overexpression, mutation, increased expression of efflux pumps, drug metabolism, or other mechanisms (237). Therefore, we questioned whether dasatinib was effectively penetrating the cells and inhibiting its target, the SFKs, in both DLBCL subtypes. We selected a representative cell line from each subtype: TMD8 for the ABC DLBCLs and HT for the GCB DLBCLs. These cells were treated with 100 nM dasatinib or DMSO for 30 min, were lysed, and the kinomes were analyzed by MIB/MS (Figure 2.5). Comparing the kinome data from the DMSO- and dasatinib-treated cells indicates that dasatinib affects the SFKs equivalently in both the TMD8

and HT cell lines, as both cell lines display reduced MIB binding of the SFKs in response to dasatinib treatment (Figure 2.6A). Furthermore, western blot analysis showed that short-term dasatinib treatment leads to a decrease in the level of phospho-active SFKs and a decrease in global tyrosine phosphorylation across all seven cell lines, without changes in Lyn expression (Figures 2.6B and 2.6C, respectively). These data suggest effective and similar inhibition of the SFKs in both DLBCL subtypes after short-term dasatinib treatment. In addition, western blot analysis shows a dose-dependent decrease in phosphorylation of the SFKs and downstream targets of the SFKs after short-term dasatinib treatment (Figure 2.7). Taken together, these data show that dasatinib is able to permeate the cell and bind to and inhibit the SFKs in both the ABC and GCB DLBCL cell lines.

2.3.4 Dasatinib inhibits the SFKs in both ABC and GCB DLBCL cells after long-term treatment

Another possible explanation for the differences in dasatinib sensitivity is that some of the SFKs may be recovering or adapting after long-term treatment with dasatinib. To determine if the SFKs are becoming resistant to long-term dasatinib treatment, we utilized MIB/MS to assess kinome changes in the HT and TMD8 cell lines after treatment with dasatinib for 24 h (Figure 2.8). Similar to the data obtained after short-term dasatinib treatment, MIB/MS analysis demonstrated reduced MIB binding of the SFKs in both the TMD8 and HT cell lines (Figure 2.9A). Western blot analysis of phospho-active SFK and global tyrosine phosphorylation also demonstrated SFK inhibition without impacting protein expression in all seven cell lines after 24 h of dasatinib treatment (Figures 2.9B and 2.9C, respectively). Using a lower dose of dasatinib, we also extended the treatment time to 72 h and assessed changes in the kinome via MIB/MS (Figure 2.10). Even at 72 h, the SFKs show reduced MIB binding in both the TMD8 and HT cell

lines (Figure 2.11), indicating that even after long-term treatment with dasatinib, the SFKs in both ABC and GCB DLBCL cell lines remain sensitive to dasatinib inhibition.

2.3.5 Dasatinib treatment induces changes in kinases other than the SFKs

Due to the sustained inhibition of the SFKs after both short- and long-term treatment with dasatinib, we examined if inhibition of other kinases might contribute to the differential sensitivities observed among our cell lines. Dasatinib is known to be a broadly selective kinase inhibitor (64), so we questioned the extent to which dasatinib affects non-Src-family kinases in our DLBCL cell lines. To evaluate this, we performed a principal component analysis (PCA) of the MIB/MS data from the 30-min and 24-h dasatinib treatment experiments (Figure 2.12). Interestingly, in the 30-min dataset, all of the HT samples cluster together and all of the TMD8 samples cluster together, regardless of DMSO or dasatinib treatment. However, in the 24-h dataset, the DMSO and dasatinib treatment groups cluster separately for each cell line. These data suggest that the 24-h dasatinib treatment alters the kinome to a greater extent compared to the 30-min dasatinib treatment. Comparing the 30-min and 24-hr MIB/MS analyses (Figures 2.5 and 2.8, respectively) reveals a noticeable difference in the kinase families affected by dasatinib across both cell lines. After 30 min, only the tyrosine kinase (TK) family of kinases were affected by dasatinib treatment in each cell line, as determined by a ±2-fold or higher change in MIB binding, relative to DMSO. In contrast, after 24 h, the kinases displaying a ±2-fold or higher change in MIB binding not only include the TK kinase family, but also the AGC and CAMK families, among other kinase families. Indeed, hierarchical clustering (ANOVA p-value <0.05) of the MIB/MS data from these experiments reveals several more clusters of differentially affected kinases at the 24-h timepoint relative to the 30-min timepoint (Figure 2.13).

2.3.6 Dasatinib inhibits several cell cycle kinases in ABC but not GCB DLBCL cell lines

To further understand the differences in dasatinib sensitivity between the ABC and GCB DLBCL cell lines, we sought to explore the non-Src-family kinases that are affected by dasatinib. These are kinases that could be impacted by dasatinib due to inhibition of signaling pathways downstream of the SFKs or to off-target effects of dasatinib. Only kinases showing statistical significance (ANOVA p-value <0.05) and a ±2-fold change upon dasatinib treatment compared to DMSO were further considered. Of the 24 kinases in the 30-min treatment groups that meet these criteria, 21 show reduced MIB binding in both the TMD8 and HT cell lines (the exceptions being CAMK4, FES, and MAP2K6). However, in the 24-h treatment groups, 54 kinases display various responses to dasatinib treatment in both cell lines. To identify which cellular processes were enriched in this group of kinases, we performed a functional annotation clustering analysis (Figure 2.14A). The predominant biological processes represented by the 54 kinases from the 24-h MIB/MS experiment are cell cycle (23.6% of the kinases), immunity (23.6%), and apoptosis (18.2%). Using STRING 10.5 (232), we constructed protein networks of the kinases from each of these processes to visualize how the kinases may associate with one another (Figure 2.14B-D). The immunity cluster includes several kinases, namely the SFKs and Btk, which are known to be involved in BCR signaling and other proliferation pathways. Many of the kinases in this network have decreased MIB binding in both cell lines after dasatinib treatment. The apoptosis cluster contains kinases with a variety of responses in the TMD8 and HT cell lines. In the cell cycle cluster, however, nearly all of the kinases have decreased MIBs binding in only the TMD8 cell line after dasatinib treatment, with the exception of GSG2 and Src, which have decreased MIBs binding in both cell lines. Interestingly, nearly all of the kinases in this cluster appear to have associations with several other kinases in the cluster.

Moreover, the canonical SFK member, Src, is also included in this network and associates with CDK4. These results implicate cell cycle kinases as possible players in mediating the sensitivity of ABC DLBCL cell lines to dasatinib.

To highlight the differences in MIB binding after dasatinib treatment between the TMD8 and HT cell lines, two sets of hierarchical clustering on the 24-h dataset were performed: 1) clustering based on the label-free quantification (LFQ) values of ANOVA-significant kinases from all samples and 2) clustering based on the MIBs binding ratios of the individual replicates from each cell line, filtered as described above (ANOVA-significant and 2-fold change in MIB binding) (Figure 2.15). In each cluster map, there is a cluster of kinases that are inhibited in the TMD8 cell line upon dasatinib treatment, but relatively unchanged in the HT cell line. There are 12 kinases in common between these two clusters, 9 (75%) are known to be involved with cell cycle signaling and another 2 are implicated in preventing apoptosis (Table 2.2). This result follows what we observed with the functional annotation analysis. We assessed changes in activation and/or expression of selected cell cycle kinases identified in the MIB/MS analysis (Figure 2.16) to determine if changes in cell cycle kinases could be observed in the other ABC DLBCL cell lines. Western blot analysis showed that total protein levels of Aurora kinase A, Aurora kinase B, CDK4, and CDK6 are decreased in the ABC DLBCL lines in response to 24-h dasatinib treatment. This suggests that the sensitivity of the ABC DLBCL cell lines to dasatinib may be in part due to its effects on the cell cycle, which are not apparent in the GCB DLBCL cell lines. Conversely, it is also possible that the reductions in cell cycle kinases is simply a manifestation of the ABC DLBCL cell lines' sensitivity to dasatinib.

2.3.7 Dasatinib induces cell death in TMD8 but not HT cell line

We also analyzed the effects of dasatinib on specific parameters of cell survival and apoptosis. Using antibody arrays of pro- and anti-apoptotic proteins (Figure 2.17), we found that dasatinib induces over a 2-fold reduction in expression of the pro-survival protein survivin (gene name BIRC5) in the TMD8 cell line, but does not affect survivin in the HT cell line. Survivin is known to interact with several of the cell cycle regulation kinases we identified by MIB/MS earlier, including AURKA, AURKB, CDK4, and PLK1 (238-241). We also assayed whether or not dasatinib induces cell death in either of the cell lines, as opposed to growth inhibition. We assessed apoptosis by staining cells with annexin-V and propidium iodide (PI) after treatment with dasatinib for 4 h or 24 h. Staining was analyzed via flow cytometry (Figure 2.18). These studies demonstrate that 100 nM dasatinib induces cell death within the TMD8 cell line, but not the HT cell line.

2.4 Discussion

Despite the fact that the current treatment for both the ABC and GCB subtypes of DLBCL is the same (R-CHOP), the ABC DLBCL subtype has a much worse prognosis (5,6). Thus, there is a need to find additional therapeutic agents for the treatment of ABC DLBCL. In this study, we explored the utility of the SFK inhibitor dasatinib for the treatment of DLBCL. Using established cell lines, we found that, although ABC DLBCL cell lines are more sensitive to dasatinib than GCB DLBCL cell lines, all cells exhibit significant inhibition of the SFKs after both short- and long-term treatment with dasatinib. This indicates that either signaling downstream of the SFKs or off-target effects of dasatinib are the likely causes of the differential sensitivities to dasatinib. Considering the dependency of ABC DLBCL cell lines on BCR

signaling (and consequently on the SFKs), impacts on signaling downstream of the SFKs as a result of dasatinib treatment is probable. Using MIB/MS and western blot analysis, we assessed changes in the kinome in response to dasatinib treatment, and found that several cell cycle kinases are downregulated in the ABC DLBCL cell lines, but not the GCB DLBCL cell lines. Correspondingly, we found a decrease in the cell survival protein survivin (BIRC5) and increased cell death in response to dasatinib in the ABC DLBCL cell line compared to the GCB DLBCL cell line. Thus, our results suggest that dasatinib has an effect on cell cycle regulation in the ABC DLBCL cell line, which may contribute to this subtype's enhanced sensitivity to dasatinib.

It is well known that dasatinib is a promiscuous kinase inhibitor, targeting Abl, EGFRs, c-Kit, and other kinases in addition to the SFKs (64). The SFK inhibitors saracatinib and ponatinib are reported to be more selective for the SFKs than dasatinib (64,234,235). Our dose-response studies demonstrate a large difference in dasatinib sensitivity between the ABC and GCB DLBCL cell lines, but this difference is less pronounced with saracatinib and ponatinib. This raises the question as to how and why the ABC DLBCLs respond more vigorously to dasatinib than the more selective inhibitors saracatinib and ponatinib. Our data show higher Lyn expression in the ABC DLBCL cell lines and higher Fyn expression in the GCB DLBCL cell lines. Interestingly, the work of Eguchi *et al.* provides evidence that a deficiency in Fyn protein can predispose cells to dasatinib sensitivity (242). From an enzymatic activity perspective, our results clearly demonstrate continued inhibition of all SFK members in both DLBCL subtypes, even after long-term treatment with dasatinib. Therefore, the notion that a deficiency in Fyn activity in the ABC DLBCL cell lines causes the sensitivity to dasatinib is unlikely, as Fyn is inhibited in the GCB DLBCL cell lines and yet they live. However, it should be noted that the

Eguchi *et al.* paper focused on a deficiency of Fyn *protein*, not activity. Thus, it is possible that the Fyn protein may play some sort of scaffolding function that impacts apoptotic pathways, causing differences in sensitivity to dasatinib between the ABC and GCB DLBCL cell lines.

Several of our experiments and analyses point to a potential role of cell cycle kinases in dasatinib sensitivity. We have shown that, of the kinases that display significant changes in MIBs binding after dasatinib treatment, many are involved in the cell cycle. Furthermore, of the kinases that show reduced MIBs binding in the TMD8 cell line (ABC DLBCL) but no change in the HT cell line (GCB DLBCL), the majority are cell cycle kinases. However, it is still unclear as to whether this inhibition of cell cycle proteins is a cause for dasatinib sensitivity or a result of dasatinib sensitivity. Furthermore, it remains to be shown whether the inhibition of cell cycle kinases is due to inhibition of signaling downstream of the SFKs, or a consequence of an off-target effect of dasatinib.

Our network analysis of the kinases listed in the cell cycle functional annotation cluster hinted at a possible link between the SFK member Src and the cell cycle kinase CDK4. There is evidence that Src can induce gene expression of cyclin D1 (243), which is a major activator of CDK4 and CDK6 (244,245). If this relationship exists in our ABC DLBCL cell lines, it makes sense that the changes we observe in the cell cycle kinase expression levels (particularly CDK 4 and CDK6) are not seen at 30 min, but rather at 24 h. In addition, there is evidence that some cells can proliferate in the absence of the cyclin D-CDK4/6 axis (246). Furthermore, a study in the GCB DLBCL cell line OCI-Ly18 demonstrated that OCI-Ly18 expresses cyclin D3, but not cyclins D1 and D2, and that knockdown of cyclin D3 did not affect cell viability or proliferation (247). Thus, it is possible that, in the ABC DLBCL cell lines, dasatinib-induced inhibition of the SFKs leads to inhibition of the cyclin D-CDK4/6 axis, which results in growth inhibition and cell

death. Moreover, it is possible that a lack of dependency on the cyclin D-CDK4/6 axis in the GCB DLBCL cell lines may contribute to their resistance to dasatinib. This should be explored in future studies.

It should be noted that several of the cell cycle kinases we identified are capable of interacting with, and even regulating, each other. For example, Polo-like kinase 1 (PLK1) can interact with AURKA, AURKB, BUB1, CDC7, or MYT1 to help regulate mitotic entry and spindle assembly (248-252), and AURKA can even activate PLK1 (249). In addition, survivin is known to interact with several of the cell cycle regulation kinases we identified, including AURKA, AURKB, CDK4, and PLK1 (238-241). Further studies should explore the mechanisms by which dasatinib leads to inhibition of these cell cycle proteins, and if inhibition of one may lead to the inhibition of others.

The Aurora kinases (AURKA and AURKB) are among the cell cycle kinases we identified as downregulated in the ABC DLBCL subtype after dasatinib treatment. Interestingly, there are ongoing studies for the use of Aurora kinase inhibitors in the treatment of DLBCL, particularly for more aggressive forms of the disease (253-255), and in general the Aurora kinases are gaining recognition as potential targets for the treatment of other cancers (256,257). Furthermore, some studies have demonstrated synergy between Aurora kinase inhibitors and dasatinib (258,259), and have even suggested that inhibition of the Aurora kinases can overcome resistance to other tyrosine kinase inhibitors (260). Considering the promiscuity of dasatinib and that there is currently no evidence in the literature to suggest interactions between the SFKs and the Aurora kinases, it is possible that dual inhibition of the SFKs and the Aurora kinases in the ABC DLBCL cell lines, but not the GCB DLBCL cell lines, causes the disparity in dasatinib sensitivity we have observed.

To our knowledge, this is the first study to demonstrate downregulation of several cell cycle kinases in response to dasatinib treatment in DLBCL. It is possible that some indirect or "downstream" effect of dasatinib leads to their inhibition rather than direct inhibition of these cell cycle kinases. Indeed, in several studies that examined direct targets of dasatinib *in vitro* and in cells, none identified the cell cycle kinases we found (64,261,262). However, one study in leukemia cells determined that CDK2 and CDK8 genes, among other cell cycle genes, were down-regulated in response to dasatinib treatment (227). It is important to note that inhibition of cell cycle kinases was predominantly observed in the ABC DLBCL cell lines, and not the GCB DLBCL cell lines. Therefore, it is likely that some mechanism other than direct inhibition by dasatinib is taking place, and it is of great interest to further examine this mechanism to better understand the sensitivity of the ABC DLBCL cell lines to dasatinib. This study clearly demonstrates that dasatinib has potent activity on the ABC DLBCL subtype, which warrants further exploration into the use of dasatinib to treat more refractory or resistant forms of DLBCL.

2.5 Tables and Figures

Cell Line	Dasatinib EC_{50} (nM)	Saracatinib EC_{50} (μM)	Ponatinib EC_{50} (nM)
Farage	>2,500.0	>10.0	>1,000.0
HT	>2,500.0	>10.0	>1,000.0
Karpas 422	>2,500.0	>10.0	>1,000.0
HBL-1	81.4	5.7	272.1
OCI-Ly3	6.7	0.7	88.8
OCI-Ly10	34.3	3.5	78.1
TMD8	20.5	2.4	14.9

Table 2.1: EC_{50} values of dasatinib, saracatinib, and ponatinib in DLBCL cell lines
All data are reported as the average EC_{50} of triplicate assays.

Gene Name	Protein Name	Major Cellular Pathways
ACVR1B	Activin receptor type-1B	Cytokine signaling (activins)
AURKA	Aurora kinase A	Cell cycle regulation (mitotic spindle)
AURKB	Aurora kinase B	Cell cycle regulation (cytokinesis checkpoint)
BUB1	Mitotic checkpoint serine/threonine-protein kinase BUB1	Cell cycle regulation (spindle assembly checkpoint and chromosome alignment)
CDC7	Cell division cycle 7-related protein kinase	Cell cycle regulation (promotes G1/S phase transition)
CDK4	Cyclin-dependent kinase 4	Cell cycle regulation (promotes G1/S phase transition)
CDK6	Cyclin-dependent kinase 6	Cell cycle regulation (promotes G1/S phase transition)
CHUK	Inhibitor of nuclear factor kappa-B kinase subunit alpha	Anti-apoptosis signaling (activates NF-κB)
MAP2K5	Dual specificity mitogen-activated protein kinase kinase 5	MAPK signaling (protection from apoptosis)
PKMYT1	Membrane-associated tyrosine- and threonine-specific cdc2-inhibitory kinase	Cell cycle regulation (inhibits G2/M checkpoint)
PLK1	Serine/threonine-protein kinase PLK1	Cell cycle regulation (M phase progression)
TTK	Dual specificity protein kinase TTK	Cell cycle regulation (mitotic checkpoint)

Table 2.2: Differential expression of kinases revealed by hierarchical clustering
Kinases that are inhibited in TMD8 but not HT after 100 nM treatment with dasatinib for 24 h. Kinases listed were those that were found in both clustering analyses described in Figure 2.15.

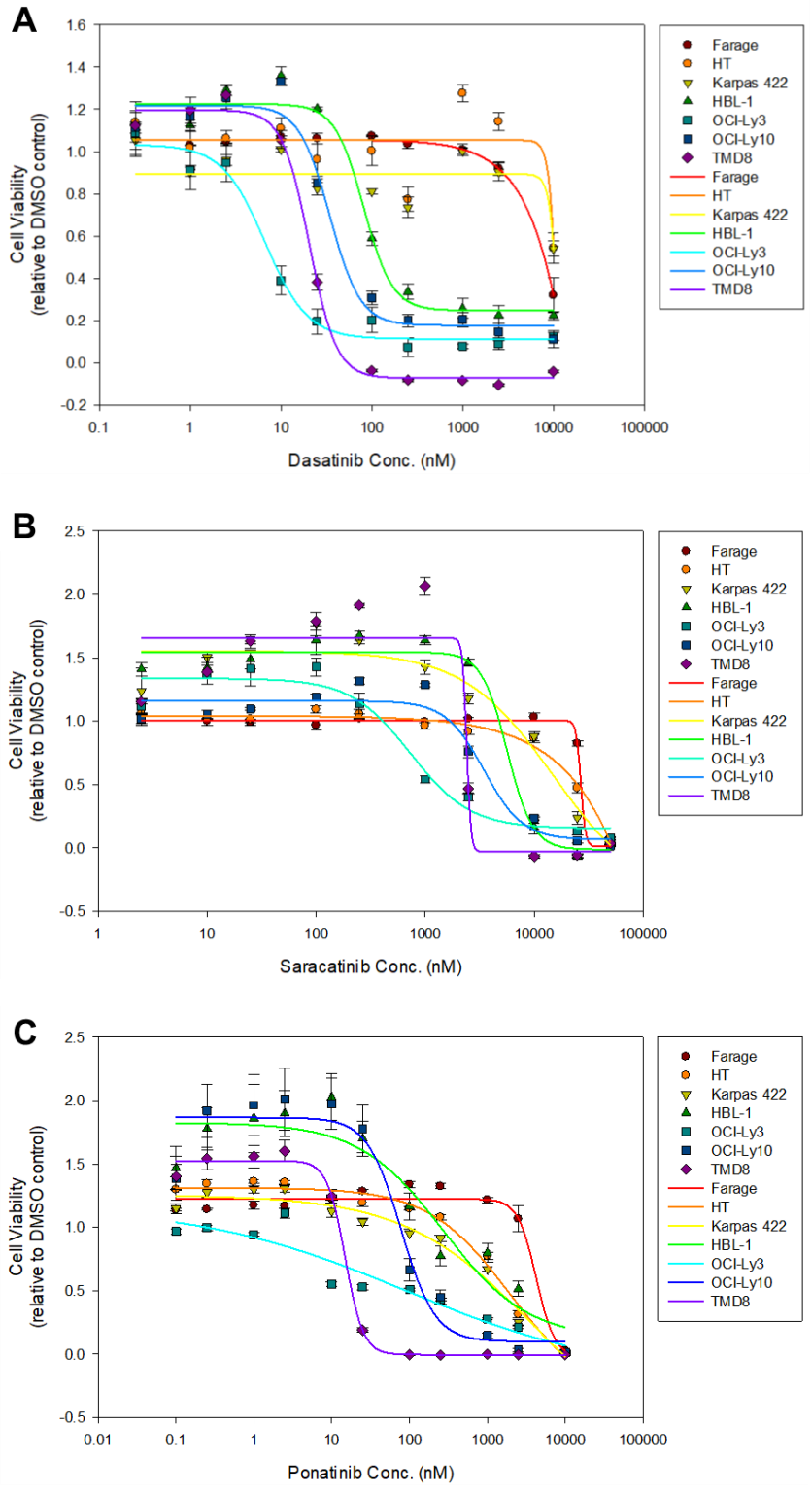

Figure 2.1: SFK inhibitor dose-response curves in DLBCL cell lines
Dose-response curves of cell viability for the panel of DLBCL cell lines treated with (*A*) dasatinib, (*B*) saracatinib, or (*C*) ponatinib. Cells were treated with the indicated concentration of drug for 72 h prior to measuring cell viability.

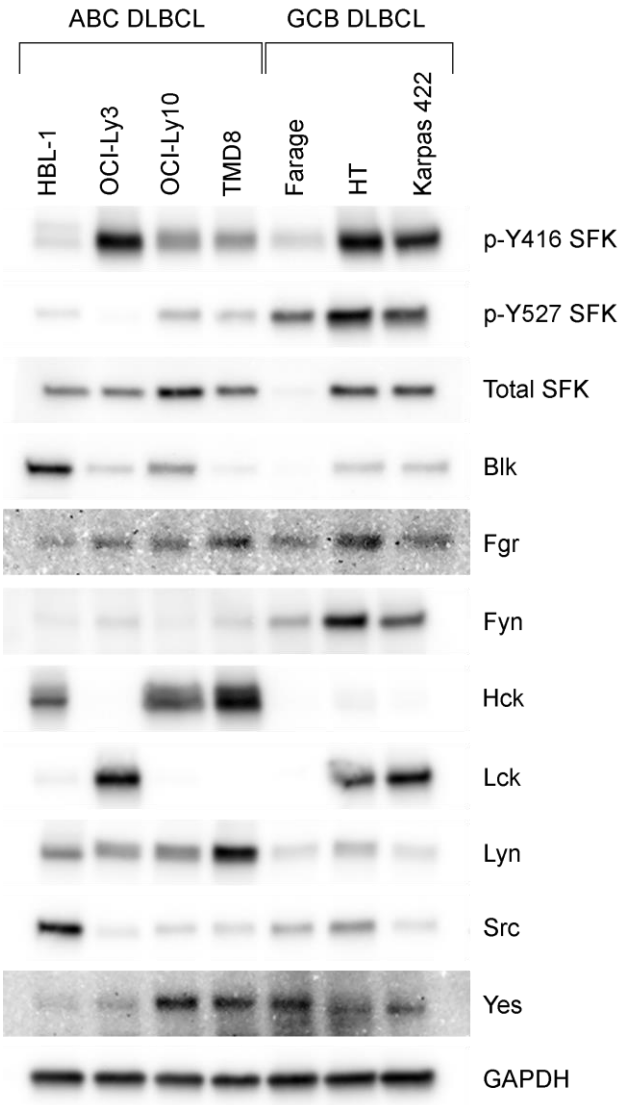

Figure 2.2: SFK member expression in DLBCL cell lines
Relative protein expression of the individual SFK members in the panel of DLBCL cell lines, as determined by western blotting.

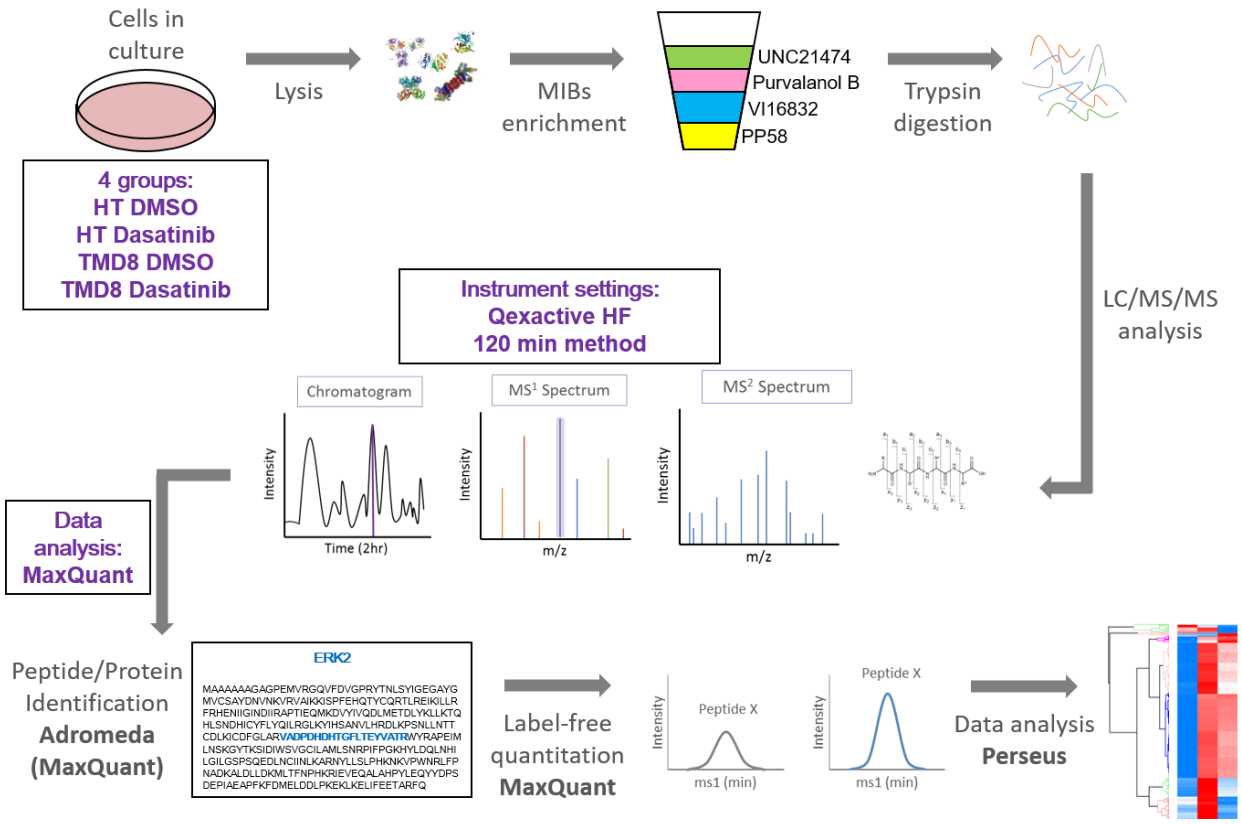

Figure 2.3: Schematic of proteomics workflow
Schematic representation of the MIB/MS technique. Cells are lysed, then lysates are flowed over a column of kinase inhibitor-bound beads to capture kinases. Bound kinases are then eluted, trypsinized, and identified by mass spectrometry.

	HBL-1	OCI-Ly3	OCI-Ly10	TMD8	Farage	HT	Karpas 422
BLK	2.52	0.50	1.18	0.18	0.15	1.71	0.77
FGR	0.09	-	0.04	0.01	0.02	5.41	1.44
FRK	5.51	0.07	0.38	0.74	0.28	0.01	-
FYN	0.11	0.05	0.02	0.17	0.57	4.59	1.48
HCK	0.55	0.00	1.38	5.07	0.00	0.00	0.00
LCK	0.15	2.74	0.06	0.00	0.00	1.72	2.32
LYN	1.24	0.74	0.88	2.89	0.37	0.70	0.18
SRC	1.81	0.00	0.33	0.15	0.52	3.14	1.04
YES1	0.69	0.40	1.85	1.77	1.58	0.71	-

Figure 2.4: Active SFKs in DLBCL cell lines
Relative expression of the individual SFK members in the panel of DLBCL cell lines, as determined by MIB/MS binding. Data are shown as normalized to the average of each SFK across all 7 cell lines. Red indicates higher MIBs binding, blue indicates less MIBs binding (relative to the average).

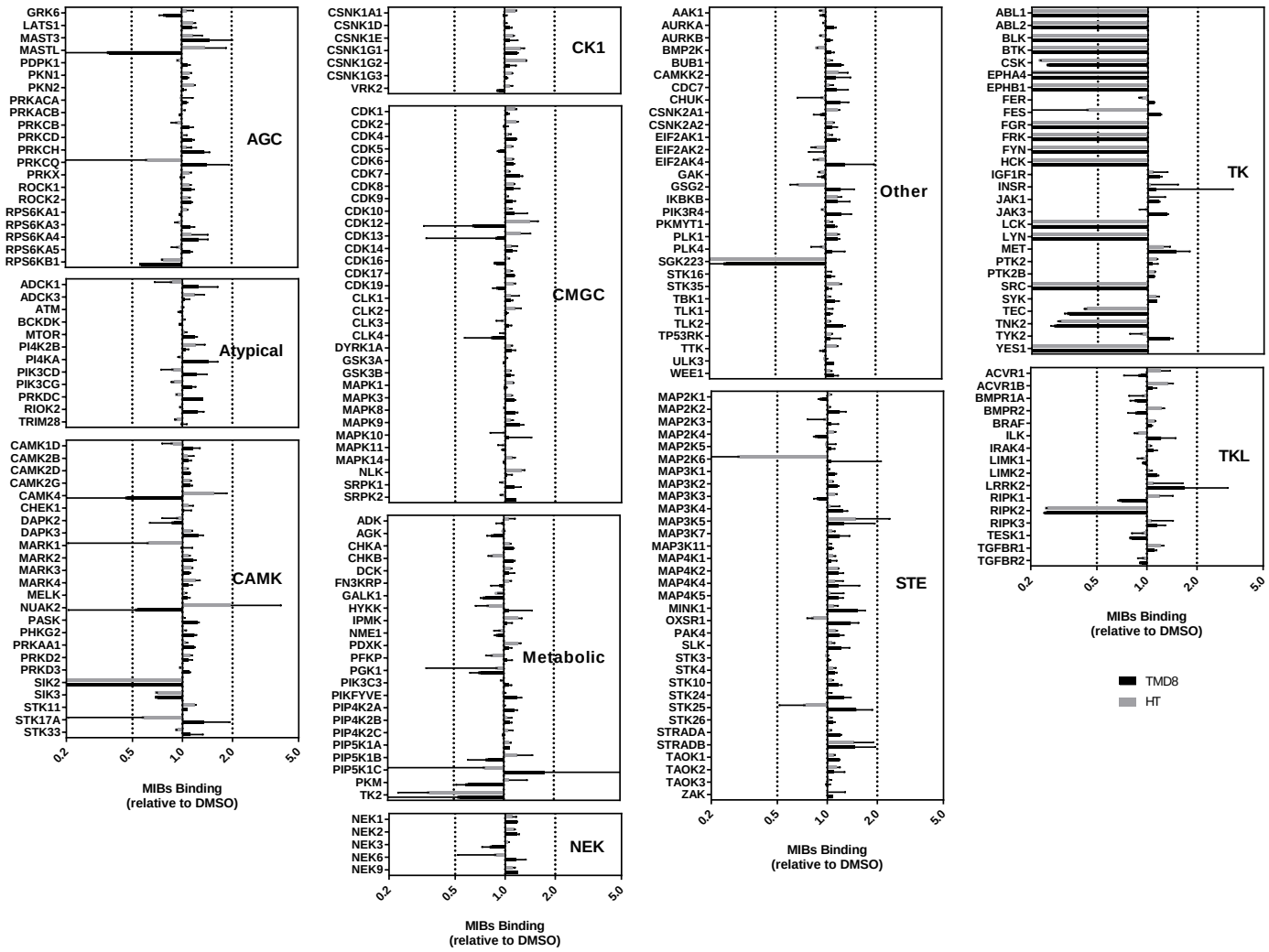

Figure 2.5: MIB/MS binding after treatment with 100 nM dasatinib for 30 min

TMD8 and HT cells were treated with DMSO or 100 nM dasatinib for 30 min, and kinome changes were analyzed by MIB/MS in three independent experiments. Data are shown as ratios of kinase binding in the dasatinib-treated cells relative to the DMSO-treated cells. Ratios <1 and >1 denote decreased and increased MIB binding of kinases from lysates, respectively.

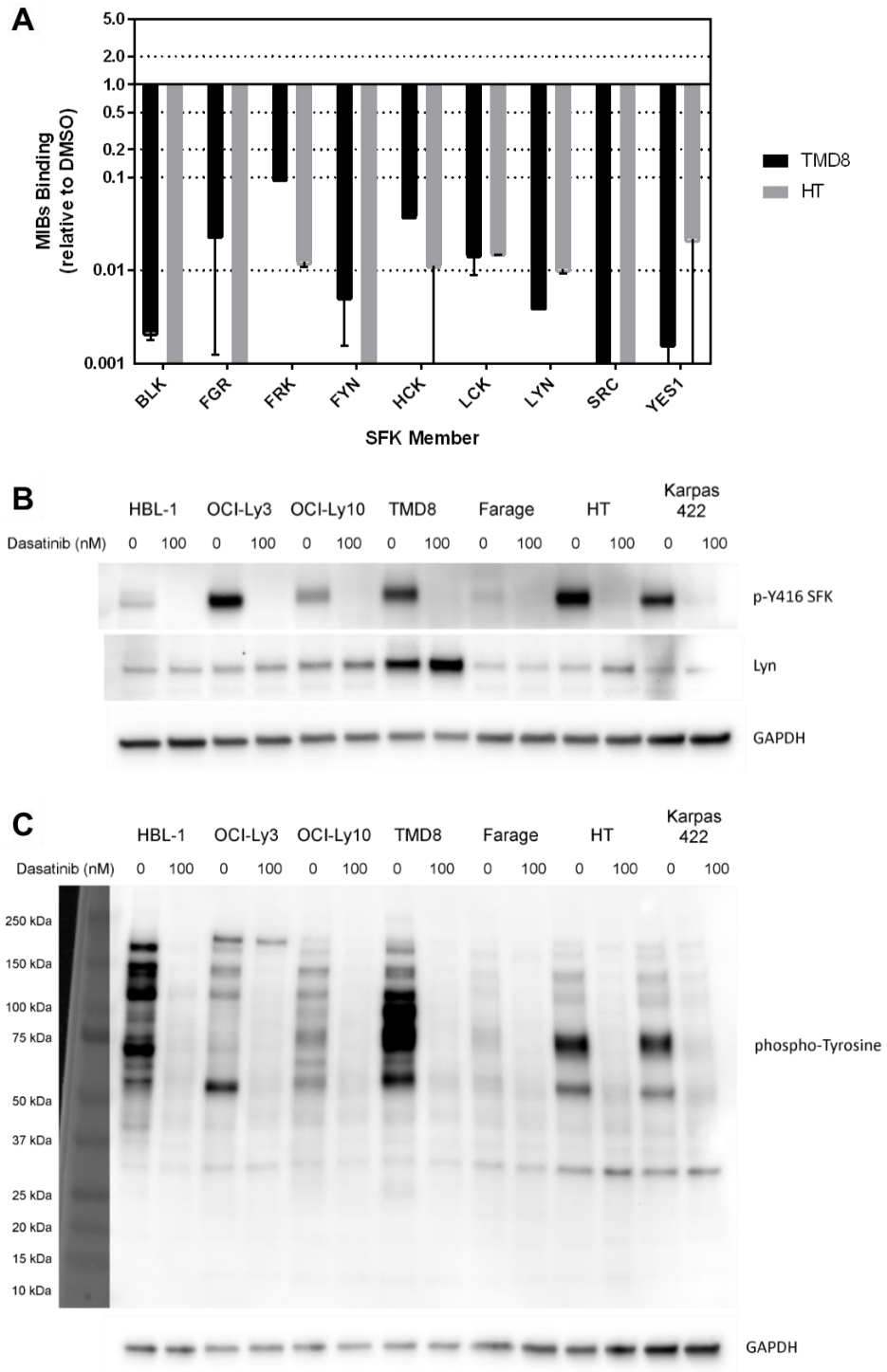

Figure 2.6: SFKs are inhibited by dasatinib after 30 min treatment
After treatment with 100 nM dasatinib for 30 min, cells were lysed and SFK inhibition was assessed via (*A*) changes in binding of the SFKs using the MIB/MS technique (<1 and >1 denote decreased and increased MIB binding of kinases from lysates, respectively), (*B*) changes in SFK phosphorylation status (western blot), or (*C*) changes in global phospho-tyrosine residues (western blot).

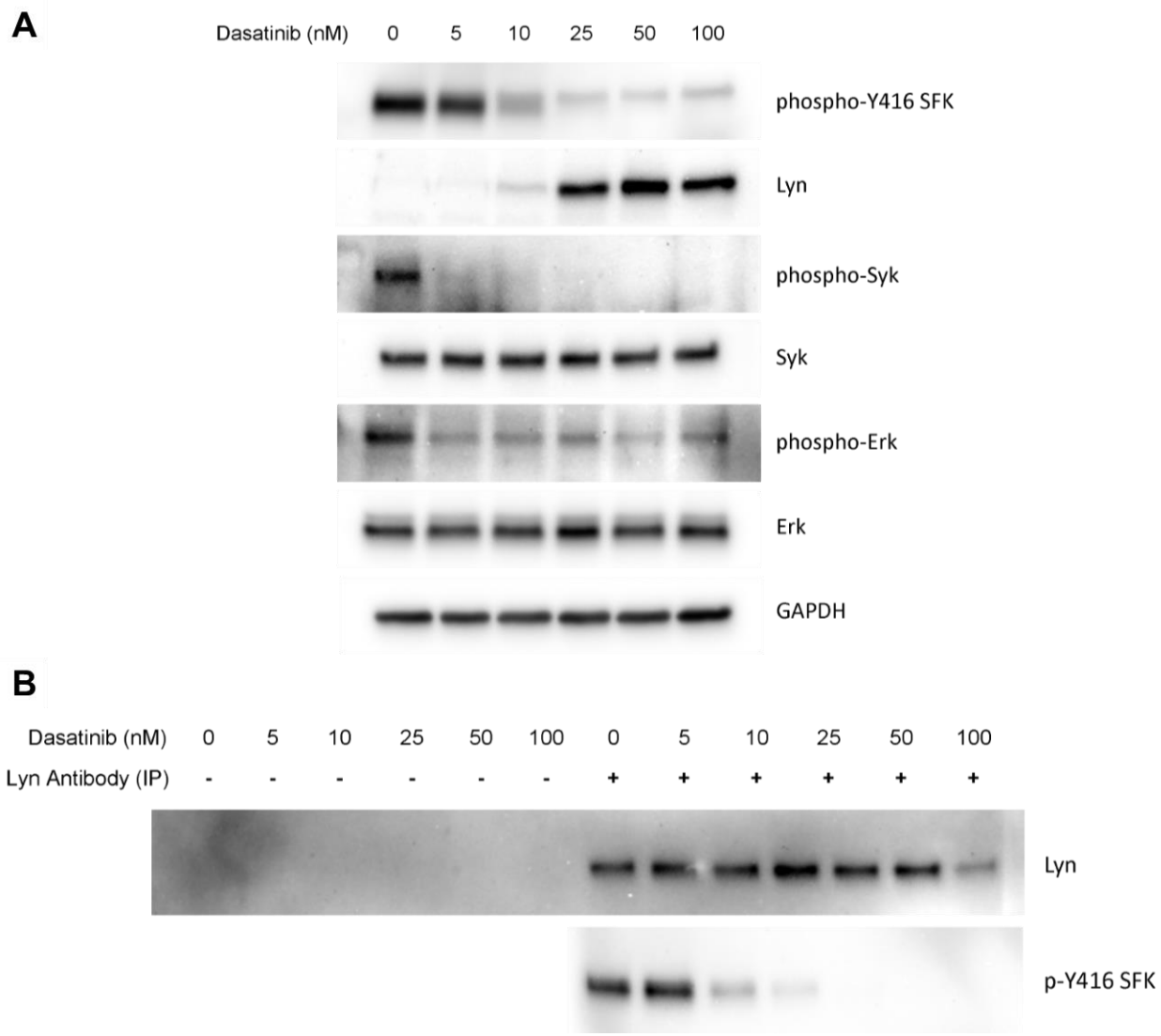

Figure 2.7: SFKs are inhibited by short-term dasatinib treatment in a dose-dependent manner

(*A*) Western blots of SFK downstream targets after 30 min treatment with dasatinib at the indicated concentrations. Western blots shown were from the OCI-Ly3 cell line. (*B*) Western blot of phospho-active Lyn from cells treated with dasatinib at the indicated concentrations for 30 min. After dasatinib treatment, cells were lysed and Lyn was immunoprecipitated from whole cell lysates. Immunoprecipitations and western blots were performed using the OCI-Ly3 cell line.

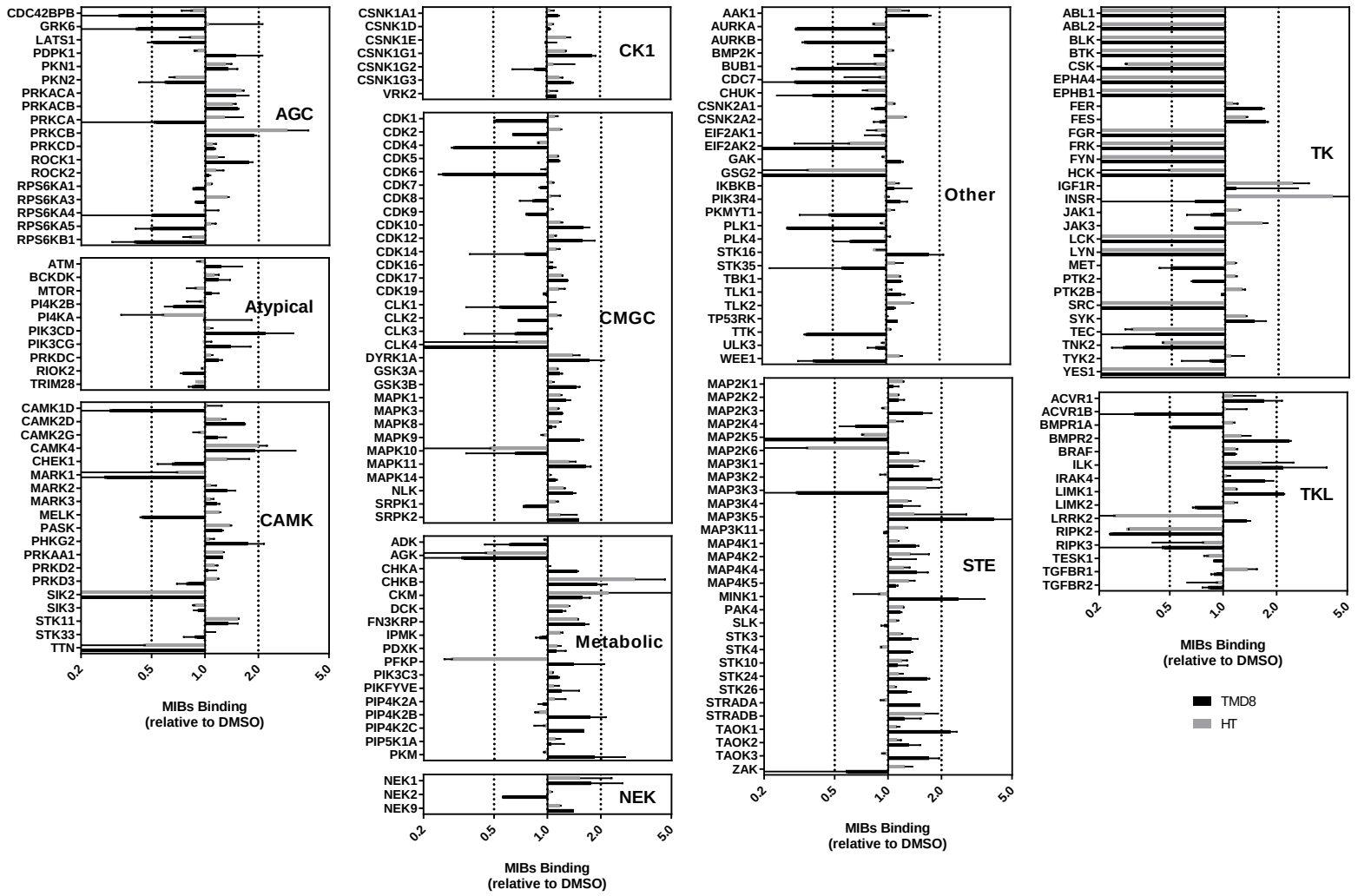

Figure 2.8: MIB/M4S binding after treatment with 100 nM dasatinib for 24 h

TMD8 and HT cells were treated with DMSO or 100 nM dasatinib for 24 h, and kinome changes were analyzed by MIB/MS in three independent experiments. Data are shown as ratios of kinase binding in the dasatinib-treated cells relative to the DMSO-treated cells. Ratios <1 and >1 denote decreased and increased MIB binding of kinases from lysates, respectively.

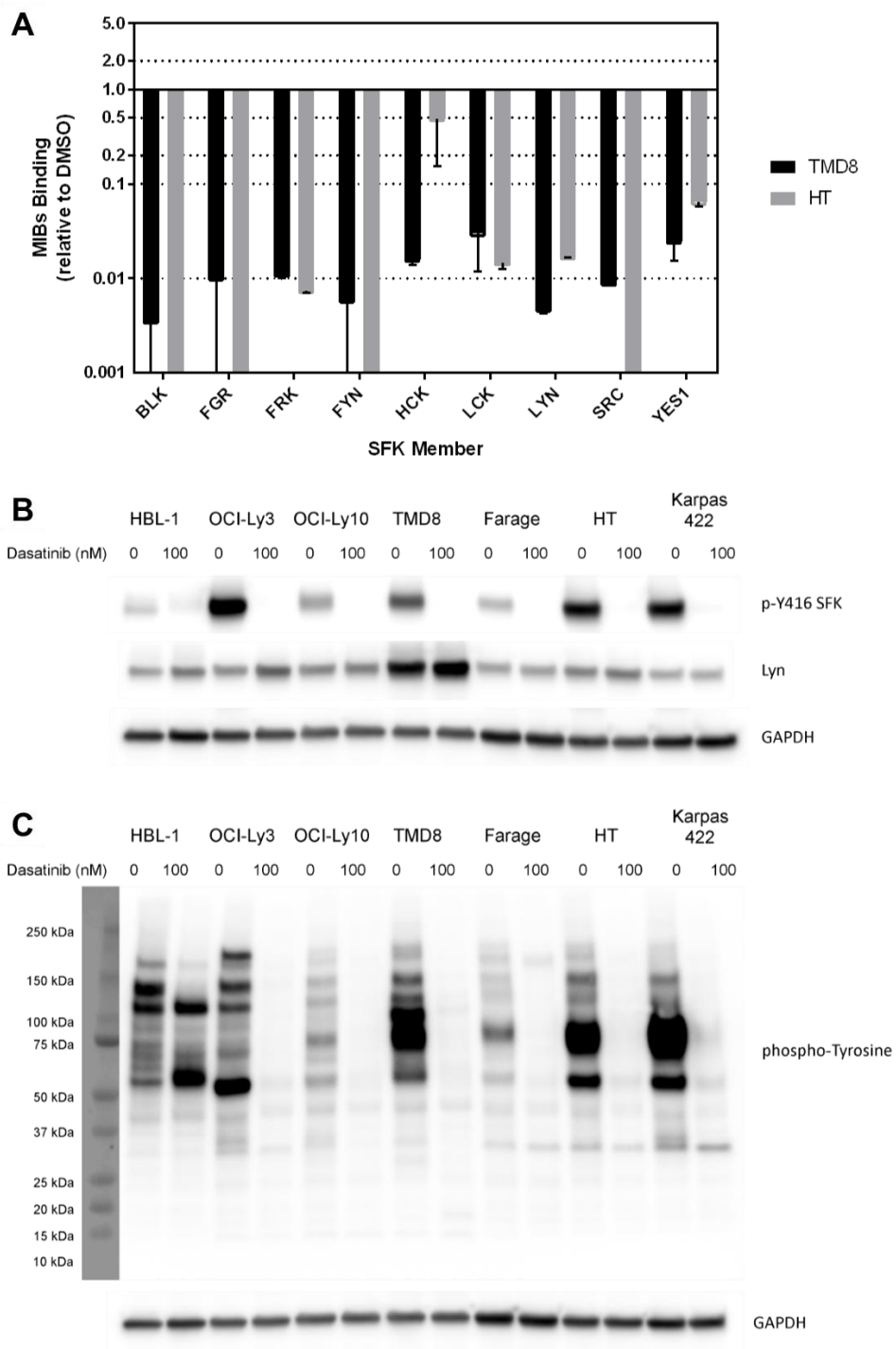

Figure 2.9: SFKs are inhibited by dasatinib after 24 h treatment
After treatment with 100 nM dasatinib for 24 h, cells were lysed and SFK inhibition was assessed via (*A*) changes in binding of the SFKs using the MIB/MS technique (<1 and >1 denote decreased and increased MIB binding of kinases from lysates, respectively), (*B*) changes in SFK phosphorylation status (western blot), or (*C*) changes in global phospho-tyrosine residues (western blot).

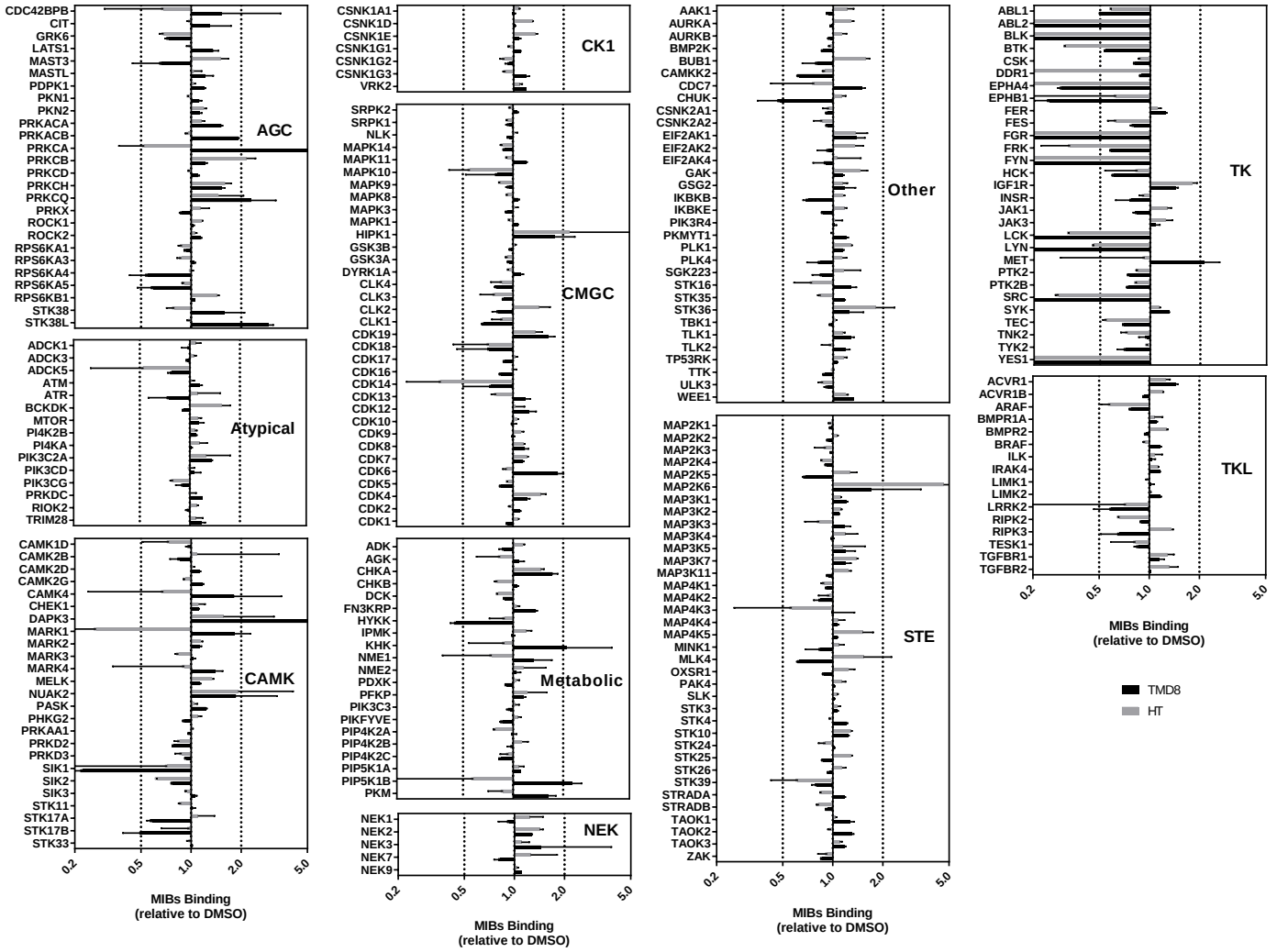

Figure 2.10: MIB/MS binding after treatment with 100 nM dasatinib for 72 h

TMD8 and HT cells were treated with DMSO or 10 nM dasatinib for 72 h, and kinome changes were analyzed by MIB/MS in three independent experiments. Data are shown as ratios of kinase binding in the dasatinib-treated cells relative to the DMSO-treated cells. Ratios <1 and >1 denote decreased and increased MIB binding of kinases from lysates, respectively.

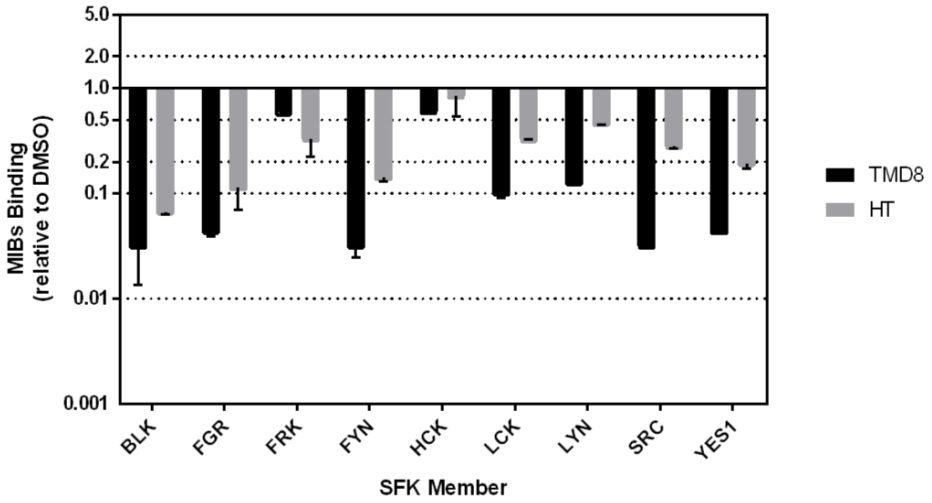

Figure 2.11: SFKs are inhibited by dasatinib after 72 h treatment
After treatment with 10 nM dasatinib for 72 h, cells were lysed and SFK inhibition was assessed via changes in binding of the SFKs using the MIB/MS technique (<1 and >1 denote decreased and increased MIB binding of kinases from lysates, respectively).

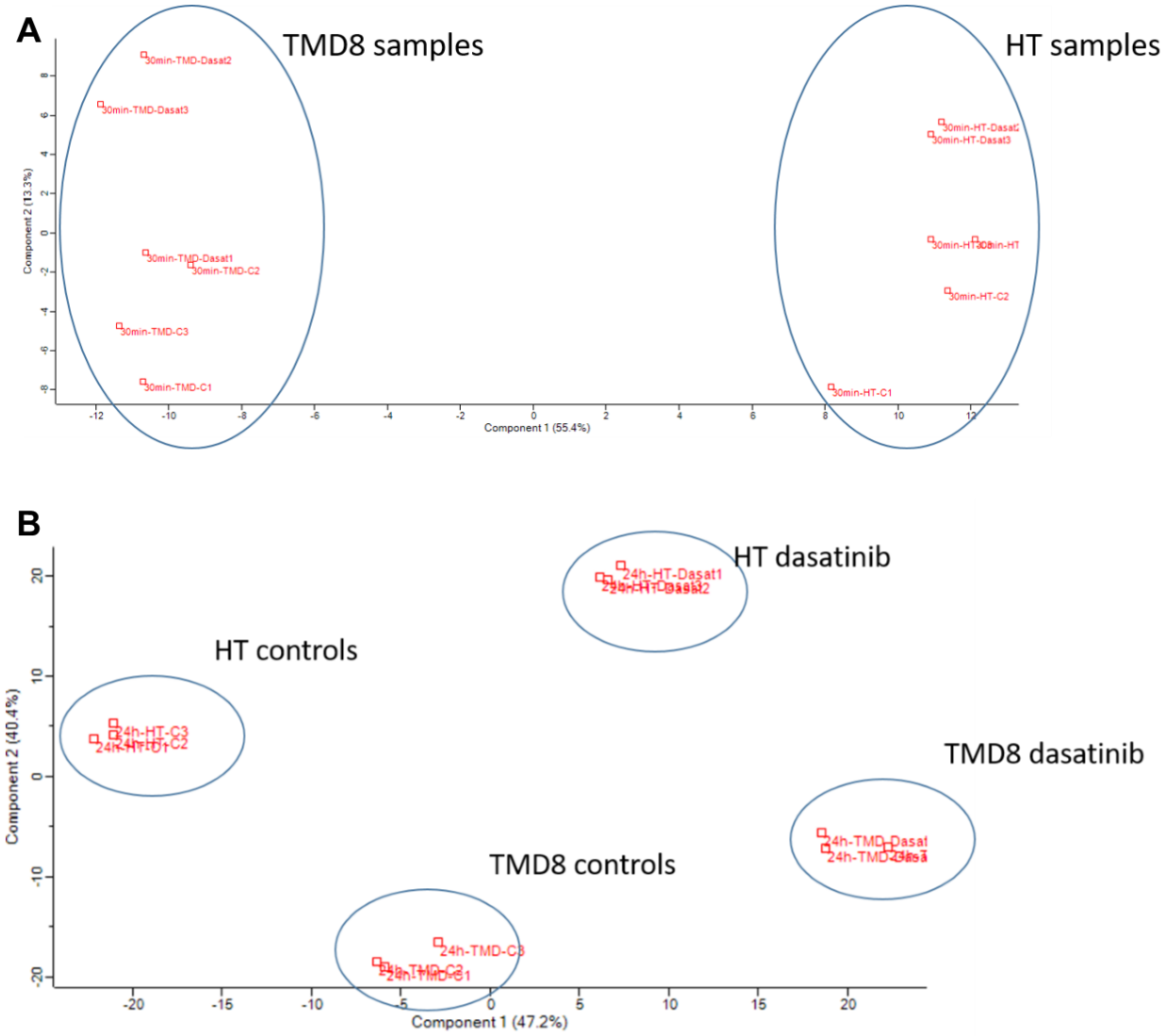

Figure 2.12: Long-term dasatinib treatment has more of an impact on the kinome than short-term dasatinib treatment

Principal component analysis of kinases identified by MIB/MS after treatment with 100 nM dasatinib for (*A*) 30 min or (*B*) 24 h.

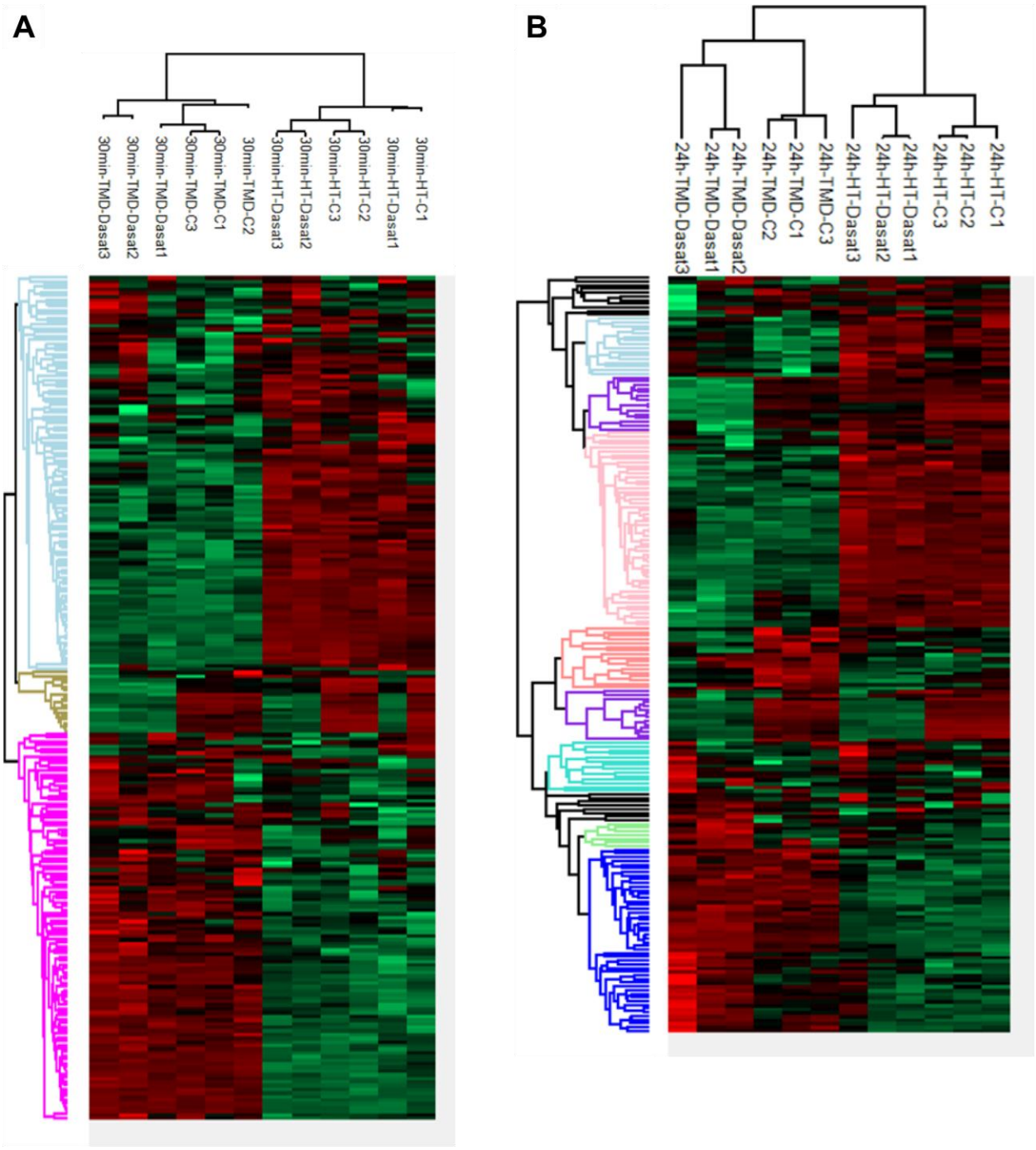

Figure 2.13: Dasatinib treatment induces different kinome responses
Hierarchical clustering of label-free quantification (LFQ) values for kinases identified by MIB/MS after treatment with 100 nM dasatinib for (*A*) 30 min (231 quantifiable kinases) or (*B*) 24 h (205 quantifiable kinases). Red = positive z-score; green = negative z-score.

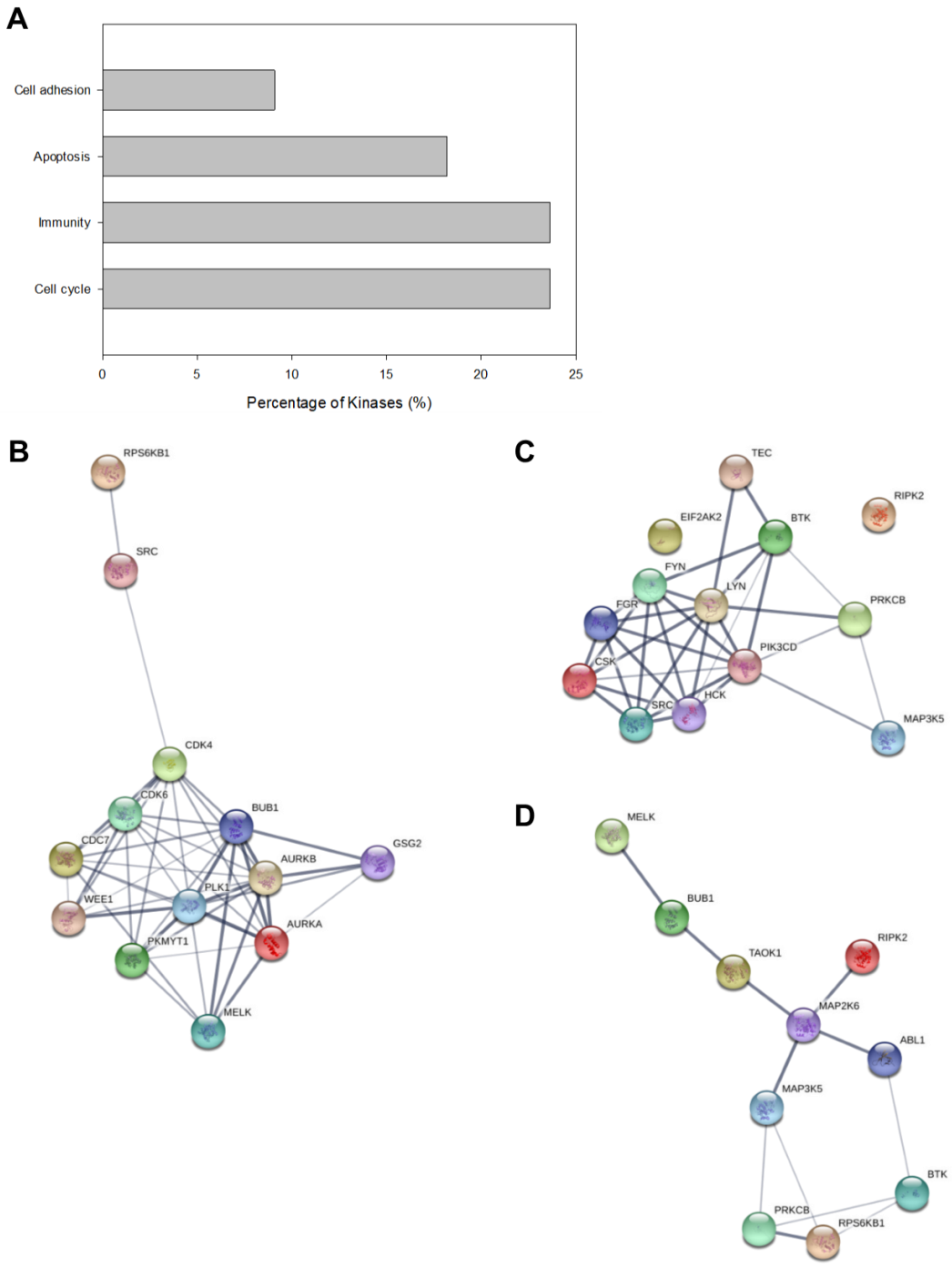

Figure 2.14: Functional annotation analysis of 24-h MIBs/MS results
(A) Functional annotation clusters of ANOVA-significant kinases with ±2-fold change or higher in MIB binding after dasatinib treatment. Assessment was generated using the DAVID functional annotation tool (230,231) and selecting for Uniprot keyword annotation terms for biological processes. (B-D) Association networks of proteins from the (B) cell cycle, (C) immunity, and (D) apoptosis clusters were analyzed using the online STRING (232) tool. Line thickness between nodes portrays the STRING calculated association confidence.

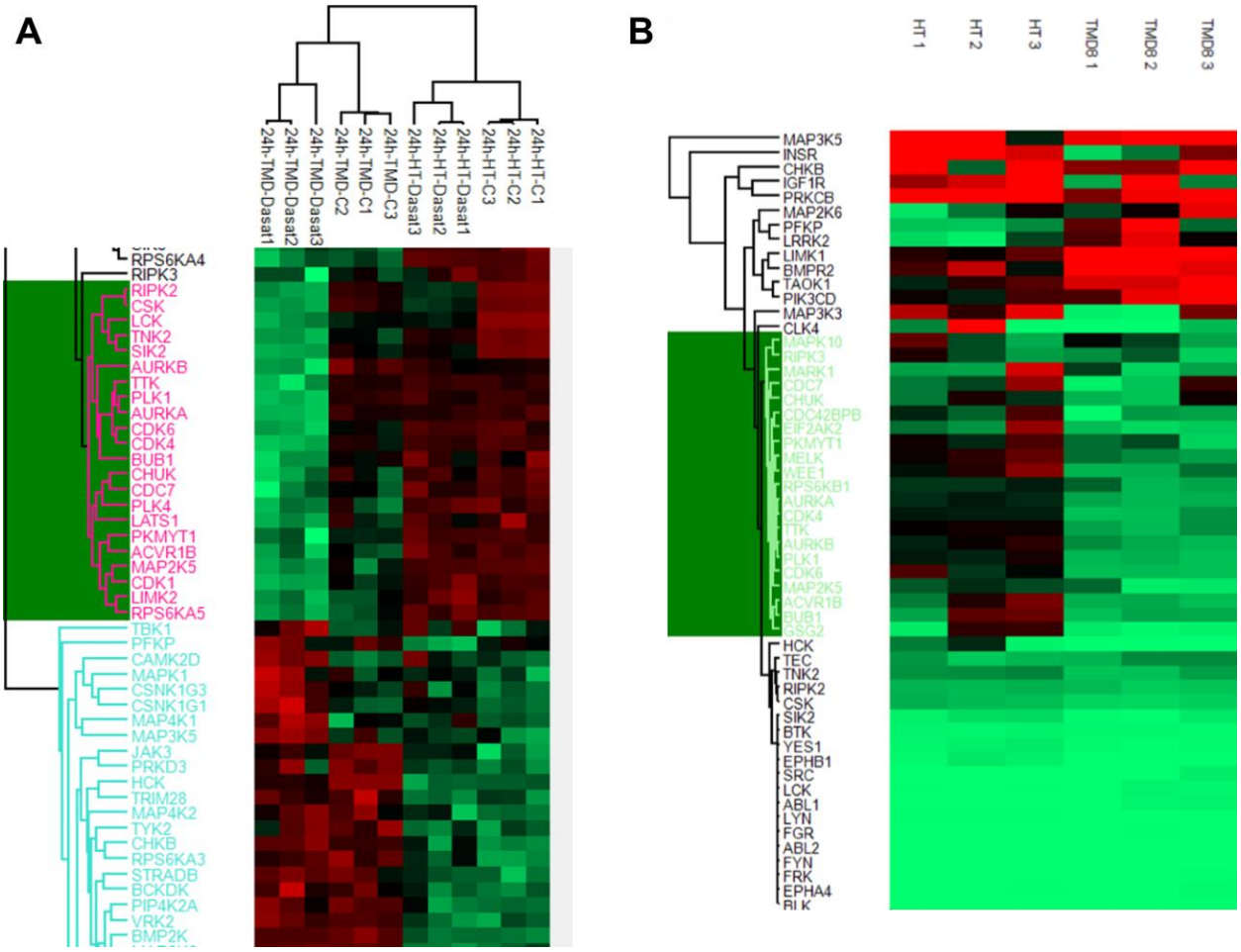

Figure 2.15: Hierarchical clustering of kinases inhibited in the TMD8 but not HT cell line after treatment with dasatinib

(*A*) Hierarchical clustering of label-free quantification (LFQ) values for kinases identified by MIB/MS after treatment with 100 nM dasatinib for 24 h (205 quantifiable kinases), zoomed in to show kinases inhibited by dasatinib in the TMD8 cell line. Red = positive z-score; green = negative z-score. (*B*) Hierarchical clustering of MIBs binding ratios of kinases identified by the MIB/MS technique after treatment with 100 nM dasatinib for 24 h. Kinases were filtered for those that were statistically significant (ANOVA $p<0.05$) and had binding ratios (dasatinib-treated relative to DMSO-treated) of less than 0.5 or greater than 2.0 in at least one of the cell lines. Hierarchical clustering was performed on 54 kinases, including all 9 SFK members. Red = binding ratio greater than 1; green = binding ratio less than 1.

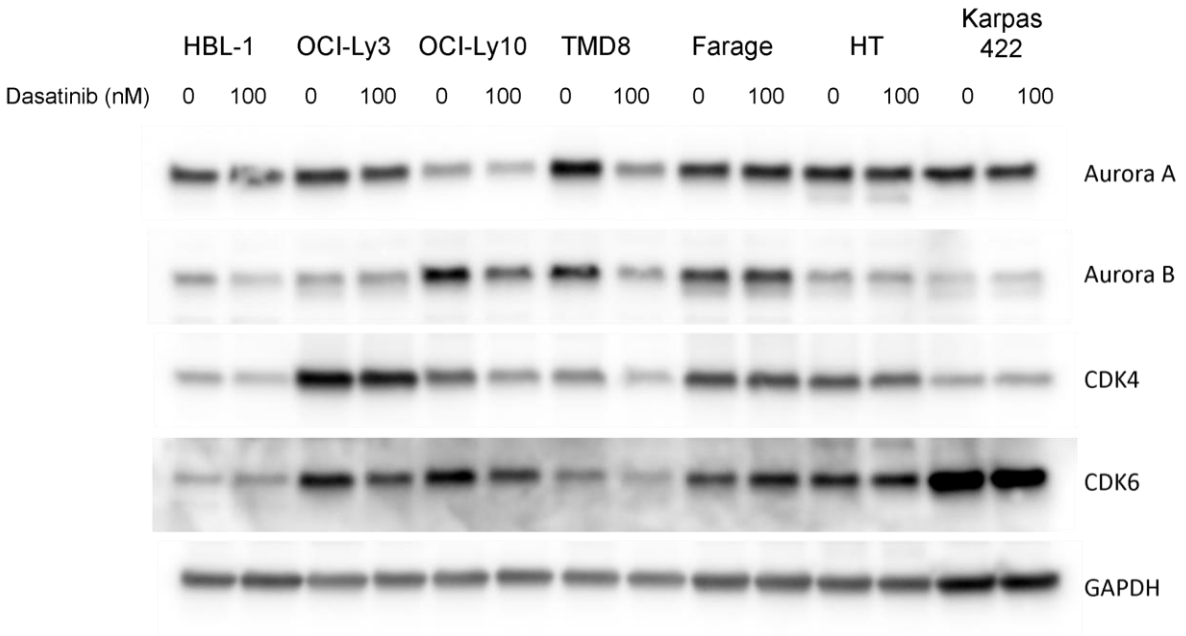

Figure 2.16: Decreased expression of cell cycle kinases in the ABC DLBCL cell lines after treatment with dasatinib
Western blot analysis of several cell cycle kinases in the panel of DLBCL cell lines after treatment with 100 nM dasatinib for 24 h.

A

	A	B	C	D	E	F	G	H	I	J	K	L	M	N
1	Positive	Positive	Negative	Negative	Blank	Blank	BAD	BAX	Bcl-2	Bcl-w	BID	BIM	Cleaved Caspase-3	Caspase-8
2	Positive	Positive	Negative	Negative	Blank	Blank	BAD	BAX	Bcl-2	Bcl-w	BID	BIM	Cleaved Caspase-3	Caspase-8
3	CD40	CD40 Ligand	cIAP-2	Cytoc C	DR6	Fas	Fas Ligand	Blank	HSP27	HSP60	HSP70	HTRA2	IGF-1	IGF-2
4	CD40	CD40 Ligand	cIAP-2	Cyto C	DR6	Fas	Fas Ligand	Blank	HSP27	HSP60	HSP70	HTRA2	IGF-1	IGF-2
5	IGFBP-1	IGFBP-2	IGFBP-3	IGFBP-4	IGFBP-5	IGFBP-6	IGF-1R	Livin	p21	p27	p53	SMAC	Survivin	TNF RI
6	IGFBP-1	IGFBP-2	IGFBP-3	IGFBP-4	IGFBP-5	IGFBP-6	IGF-1R	Livin	p21	p27	p53	SMAC	Survivin	TNF RI
7	TNF RII	TNF-alpha	TNF-beta	TRAIL R1	TRAIL R2	TRAIL R3	TRAIL R4	XIAP	Blank	Blank	Negative	Negative	Negative	Positive
8	TNF RII	TNF-alpha	TNF-beta	TRAIL R1	TRAIL R2	TRAIL R3	TRAIL R4	XIAP	Blank	Blank	Negative	Negative	Negative	Positive

pro-apoptotic
anti-apoptotic/pro-survival
mixed

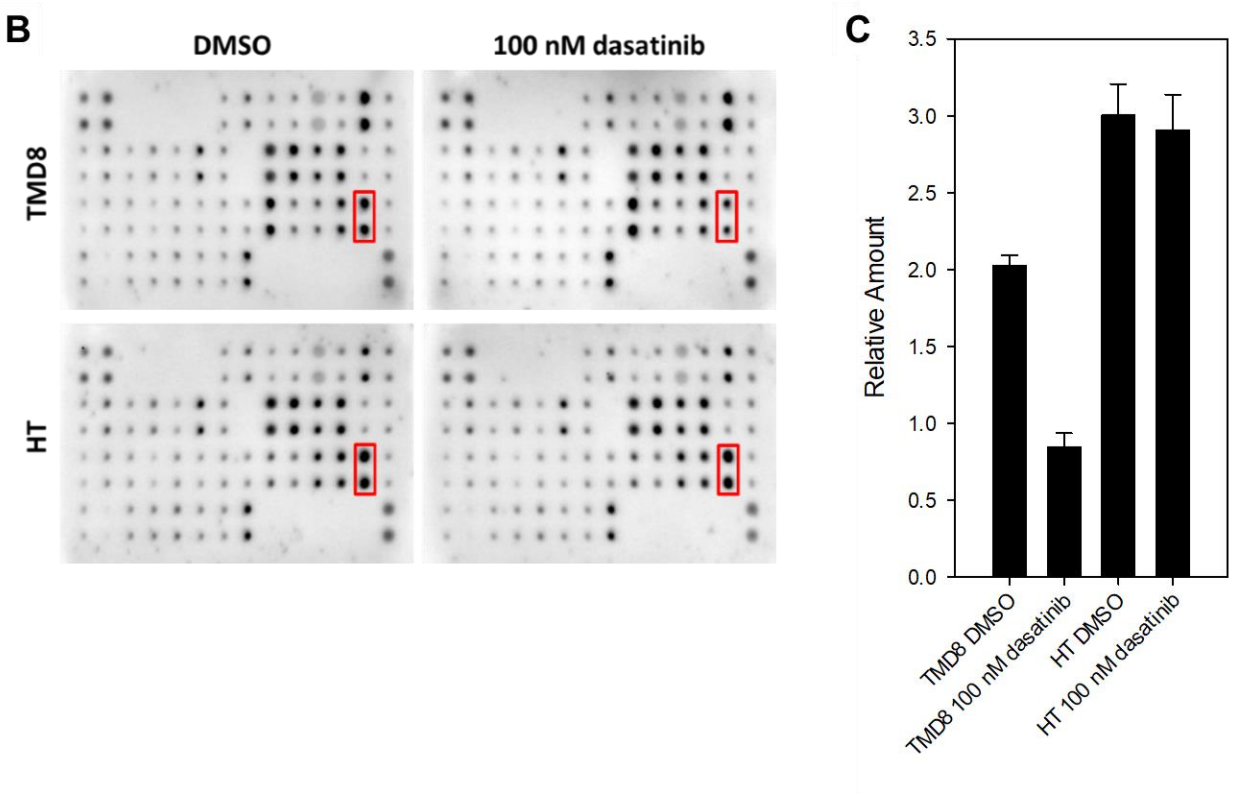

Figure 2.17: Dasatinib treatment decreases survivin expression in TMD8 but not HT cells
(*A*) Map of the proteins targeted by the apoptotic antibody arrays. Pink = pro-apoptotic, blue = anti-apoptotic/pro-survival, purple = mixed activity. (*B*) Antibody arrays of anti- or pro-apoptotic proteins of HT and TMD8 cells treated with 100 nM dasatinib for 24 h. Red boxes indicate survivin. (*C*) Quantification of survivin expression.

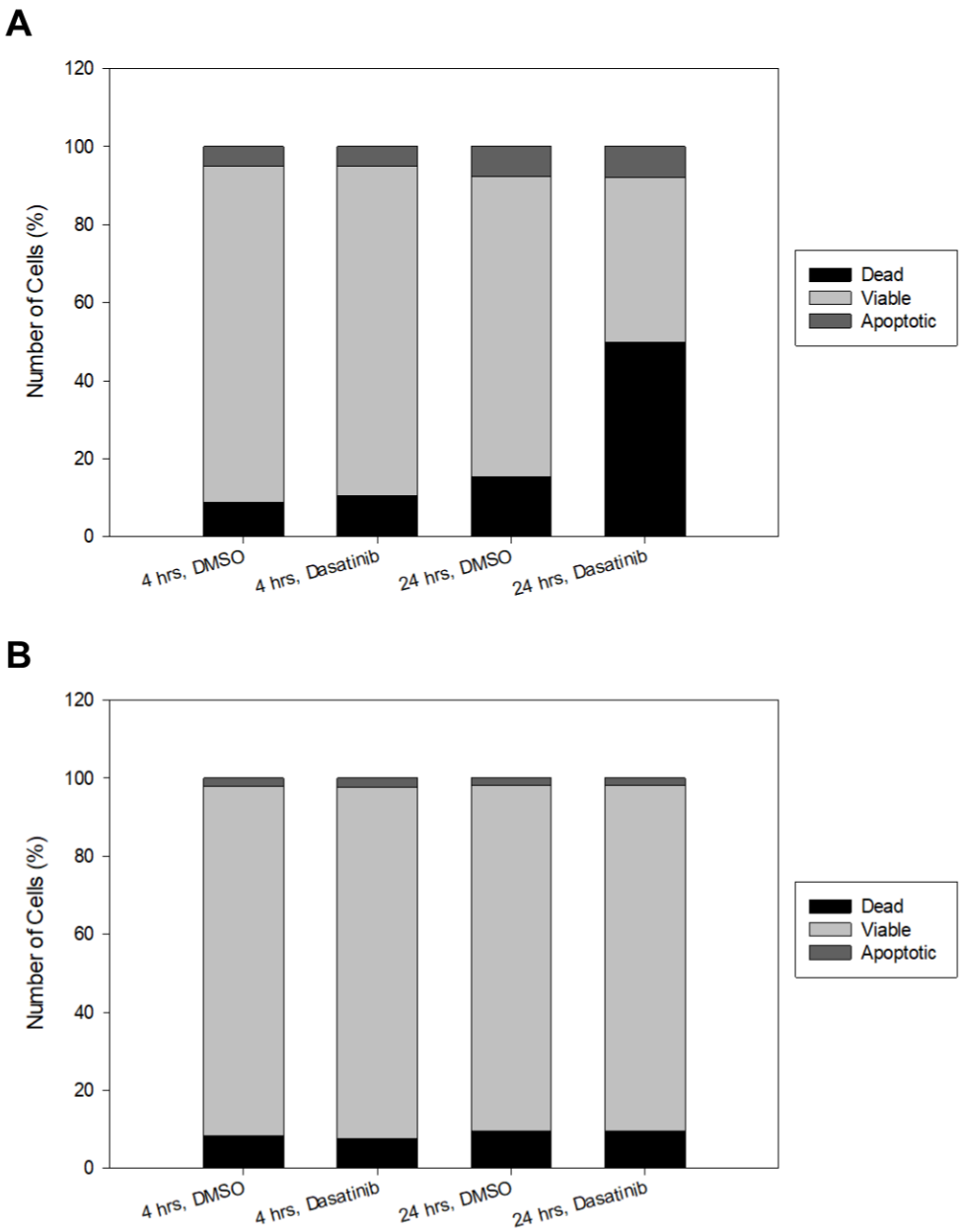

Figure 2.18: Dasatinib treatment induces cell death in TMD8 but not HT cell lines
Quantification of flow cytometry analysis of cells stained with annexin-V (AnnV) and propidium iodide (PI) after treatment with 100 nM dasatinib for 4 or 24 h. Dead = $AnnV^+$, PI^+; Viable = $AnnV^-$, PI^-; Apoptotic = $AnnV^+$, PI^-. (*A*) Analysis of TMD8 cell line. (*B*) Analysis of HT cell line.

CHAPTER 3: THE SRC FAMILY KINASES AS PROTEASOME REGULATORS IN ACTIVATED B-CELL DIFFUSE LARGE B-CELL LYMPHOMA

3.1 Introduction

Diffuse large B-cell lymphoma (DLBCL) is a heterogeneous disease that consists of different molecular subtypes based on gene expression profiling. Patients with DLBCL can be categorized into two clinically relevant subtypes: activated B-cell (ABC) and germinal center B-cell (GCB) (4). However, despite these distinctions, patients with ABC or GCB DLBCL are treated identically using a chemotherapy regimen called R-CHOP, which includes rituximab, cyclophosphamide, doxorubicin, vincristine, and prednisone. Although the R-CHOP regimen has a relatively high cure rate for patients with GCB DLBCL (2,8), patients with ABC DLBCL generally have a much poorer prognosis (5,6). Therefore, there is great interest in developing additional therapeutic agents for the treatment of ABC DLBCL.

As part of the distinctions between the ABC and GCB DLBCL subtypes, there are certain pathways that are known to be overactive in ABC, but not GCB, DLBCL. In particular, chronic, overactive signaling through the B-cell receptor (BCR) and the NF-κB pathway are hallmarks of the ABC but not the GCB DLBCL subtype (9,10). Signaling through the BCR can trigger many pro-survival and proliferation pathways, including initiation of the anti-apoptotic NF-κB pathway (10,263). This signaling is heavily dependent upon three key nonreceptor tyrosine kinases: Lyn, a member of the Src family kinases (SFKs); Syk; and Btk (32). Of these three, Lyn is first in line to help mediate BCR signaling (32-34). In addition, Lyn and the other SFKs play a role in signaling from many receptors, facilitating several proliferation, survival, and cell

motility pathways (22,23,29). Based on SFK involvement in these signaling pathways, it is not surprising that the SFKs have been implicated in progression and drug resistance in many cancers, including lymphoma (9,29,37,38). Therefore, the SFKs could be a viable target for the treatment of ABC DLBCL. In fact, some studies have demonstrated the potential for targeting the SFKs in lymphoma, showing that the SFK inhibitor dasatinib is capable of inhibiting proliferation in certain DLBCL and other B-cell lymphoma cell lines (9,37,38,215).

The cell's natural protein degradation machinery, the proteasome, has also been implicated in cancer and drug resistance due to its degradation of various antitumor-related proteins (11,180,181,216). In regards to DLBCL, the anti-apoptotic NF-κB signaling pathway is heavily dependent upon the proteasome because negative regulators of the NF-κB pathway are degraded by the proteasome. Previous work from our lab demonstrated that proteasome specific activity is higher in DLBCL cell lines compared to healthy, primary B-cells (213). This suggests the proteasome may also be of use as a target for the treatment of ABC DLBCL. In fact, the proteasome inhibitor bortezomib is currently in clinical trials for the treatment of ABC DLBCL. When combined with standard chemotherapy, bortezomib has a significant effect on ABC DLBCL but not on GCB DLBCL patients (12,190).

The proteasome is a proteolytic complex found in the nucleus and cytoplasm of all eukaryotic cells. It is generally comprised of a 20S core particle and one or two regulatory particles. The 20S core particle is a barrel-shaped structure comprised of two heteroheptameric outer α-rings and two heteroheptameric inner β-rings (164). It has three distinct proteolytic activities: caspase-like (CaL), trypsin-like (TL), and chymotrypsin-like (ChL), which are provided by its β1, β2, and β5 subunits, respectively (163). The 20S core particle can be capped

on either end by one of four possible regulatory particles: PA700 (also known as 19S), PA28αβ, PA28γ, and PA200 (163).

Interestingly, there is some evidence of potential mechanistic links between the SFKs and the proteasome. For example, the SFKs are involved in many signaling pathways that feed into the proteasome, such as NF-κB and MAPK/ERK signaling (217-220). In addition, the SFKs themselves are degraded by the proteasome (221,222). Moreover, the SFKs can promote Jak/STAT and EGF/MAPK signaling (226,227), both of which have been demonstrated to activate the proteasome (223-225). A recent study by Crawford *et al.* (192) demonstrated that treatment of chronic myelogenous leukemia cells with tyrosine kinase inhibitors and proteasome inhibitors produces a synergistic effect. Thus, it is possible that there is cross talk between the SFKs and the proteasome. However, to our knowledge, direct links between SFK activity and proteasome activation have not been studied.

We hypothesized that the SFKs activate the proteasome. Furthermore, since the proteasome and the SFKs are important particularly for ABC DLBCL over GCB DLBCL, we were particularly interested in studying the differences in SFK-mediated proteasome activation between the two subtypes. Using a set of novel peptide probes for the proteasome's three catalytic activities (213), we found that treatment with the SFK inhibitor dasatinib results in reduced proteasome activity in the ABC DLBCL cell lines tested, but has no effect on the GCB DLBCL cell lines. Furthermore, this reduction in activity is accompanied by a reduction in the amount of 19S regulatory particle in isolated proteasomes. However, the total levels of 19S regulatory particle are unchanged in whole lysates, indicating either a dissociation or disrupted assembly between the proteasome 20S core particle and 19S regulatory particle.

3.2 Materials and Methods

3.2.1 Materials

Dasatinib was purchased from SelleckChem. All other chemicals were from Fisher or Sigma unless otherwise noted.

3.2.2 Whole Cell Lysate Preparation

Approximately 72 h after seeding at $2x10^5$ cells/mL in 75 cm^2 flasks, cells from each cell line were used to prepare whole cell lysate and proteasome-enriched extracts (cells were split 50/50 for the two preparations after washing with 1X DPBS). Cells were harvested and centrifuged at 1,000 x g for 5 min at 4 °C, then washed 3 times with ice cold 1X DPBS. Cell pellets for the whole lysate preparation were then resuspended in M-PER + 5X Halt Protease & Phosphatase cocktail (EDTA-free), both purchased from Thermo Scientific, rotated for 10 min at 4 °C, then centrifuged at 17,000 x g for 10 min at 4 °C. Supernatants were collected and protein concentration was determined using the Pierce BCA Protein Assay Kit from Thermo Scientific.

3.2.3 Proteasome Enrichment

Approximately 72 h after seeding at $2x10^5$ cells/mL in 75 cm^2 flasks, cells from each cell line were used to prepare whole cell lysate and proteasome-enriched extracts (cells were split 50/50 for the two preparations after washing with 1X DPBS). Cells were harvested and centrifuged at 1,000 x g for 5 min at 4 °C, then washed 3 times with ice cold 1X DPBS. Cell pellets for the proteasome enrichment preparation were then resuspended in 4 volumes homogenization buffer (50 mM Tris, 250 mM sucrose, 5 mM $MgCl_2$, 1 mM ATP, 1 mM DTT, 0.5 mM EDTA, pH 7.5) with 0.025% digitonin, incubated on ice for 10 min, then centrifuged at 17,000 x g for 10 min at 4 °C. The supernatant was collected and ultracentrifuged at 180,000 x g for 4 h at 4 °C. The supernatant was removed and the pellet resuspended in homogenization

buffer without digitonin. Protein concentration was determined using the Pierce BCA Protein Assay Kit from Thermo Scientific.

3.2.4 Proteasome Activity Assays

The activities of all proteasome-enriched extracts were determined in assay buffer (50 mM Tris pH 7.5, 40 mM KCl, 4 mM $MgCl_2$, 1 mM ATP, 1 mM EDTA) and 0.05% bovine serum albumin (BSA) with 0.5 μM ChL-488, 1 μM TL-550, and 1 μM CaL-633 proteasome sensors, as described previously (213,264). The reactions were initiated with 10 μg of sample and the reaction progress monitored for 4 h at room temperature. Control assays without proteasome were run to ensure that the fluorescent change was due to proteasome activity and not hydrolysis. Fluorescence was monitored on a Molecular Devices Spectra Max Gemini EM plate reader with excitation wavelengths of 490 nm, 550 nm, and 625 nm and emission wavelengths of 515 nm, 575 nm, and 655 nm, respectively. Sigmaplot 12 software (serial number 775206611) was used for the analysis of all data. The rate of each assay was determined using a linear fit to the first 10% of substrate consumption. All data are reported as the mean ± standard deviation of triplicate assays.

3.2.5 Western Blots

Proteasome 20S α7 and 19S Rpn13 antibodies were purchased from Cell Signaling Technologies. Proteasome 20S β1, 20S β2, and 20S β5 antibodies were purchased from Enzo Life Sciences. Proteasome 20S β5i antibody was purchased from Thermo Fisher Scientific. All secondary antibodies were purchased from GE Healthcare. SDS-PAGE was performed using 4-15% SDS Tris-HCl gels (Bio-Rad) and loading 20 μg (10 μL) of each sample per well. Gels were then transferred to polyvinylidene fluoride (PVDF) membranes overnight at 4 °C. Membranes were blocked with 5% BSA in 1X Tris-buffered saline (TBS) + 0.1% Tween-20 for

2 h, then incubated with 1:500-1:1000 of the primary antibody in the blocking solution overnight at 4 °C. Membranes were washed with TBS + 0.1% Tween-20, incubated with 1:5000 HRP-conjugated secondary antibody for 1 h at room temperature, and washed again with TBS + 0.1% Tween-20. Secondary antibodies were detected using the Clarity Western ECL Substrate (Bio-Rad) according to the manufacturer's protocol. Images were acquired using an Alpha Innotech FluorChem FC2 using the chemiluminescent settings. Densitometry analysis was performed in ImageJ.

3.2.6 Trypsin digestion and phosphopeptide enrichment

For phosphoproteome analysis, 4 volumes of cold acetone were added to 1 mg of each lysate for protein precipitation. The samples were then reconstituted in 7 M urea, reduced, alkylated, and digested overnight with trypsin (Promega). Peptides were desalted using Sep-Pak C18 cartridges (Waters) according to the manufacturer's protocol, then dried down and stored at -80 °C until further use. Phosphopeptide enrichment was performed using the 200 µL TiO_2 Spin Columns from GL Sciences. Peptide samples were reconstituted with 80/20 ACN/lactic acid in 1% TFA, then loaded onto the TiO_2 spin column prewashed with 80% ACN, 1% TFA. Peptides were washed once with 80/20 ACN/lactic acid in 1% TFA and twice with 80% ACN, 1% TFA. Retained peptides were eluted twice with 20% ACN, 5% NH_4OH and acidified to pH <4 with formic acid. All phosphopeptide eluates were desalted using C18 Spin Columns (Thermo Fisher) then dried down and stored at -80 °C until further use.

3.2.7 LC/MS/MS Analysis

Each sample was analyzed by LC-MS/MS using an Easy nLC 1000 coupled to a QExactive HF equipped with an Easy Spray source (Thermo Scientific). First, samples were reconstituted in loading buffer (1% ACN, 0.1% formic acid), and then loaded onto a PepMap

100 C18 column (75 μm inner diameter × 25 cm, 2 μm particle size) (Thermo Scientific). Peptides were separated over a gradient consisting of 5-32% mobile phase B over a 120-min method at a 250 nL/min flow rate, where mobile phase A was 0.1% formic acid in water and mobile phase B consisted of 0.1% formic acid in ACN. The QExactive HF was operated in data-dependent mode where the 15 most intense precursors were selected for subsequent fragmentation. Resolution for the precursor scan (m/z 400-1600) was set to 120,000 with a target value of $3x10^6$ ions. For MS/MS scans with HCD (normalized collision energy 27%), resolution was set to 15,000 with a target value of $2x10^4$ ions. Peptide match was set to preferred, and precursors with unknown charge or a charge state of 1 and >7 were excluded.

3.2.8 Mass Spectrometry Data Processing and Analysis

Raw data files were processed using MaxQuant software (version 1.5.3.17). Data were searched against a reviewed human UniProt database (downloaded Feb 2017, containing 20,162 sequences) using the integrated Andromeda search engine (229). The following parameters were used to identify tryptic peptides for protein identification: up to two missed trypsin cleavage sites; carbamidomethylation (C) was set as a fixed modification; and oxidation (M) was set as a variable modification. A false discovery rate (FDR) of 1% was used to filter all results, and match between runs was enabled. Only proteins with >1 unique+razor peptide were used for label-free quantitation.

3.3 Results

3.3.1 Dasatinib treatment reduces proteasome activity in ABC DLBCL cells

We first assessed the potential for the SFKs to regulate the proteasome by examining the effects of treatment with the SFK inhibitor dasatinib. To do this, we utilized a set of novel

peptide probes for measuring proteasome activities. The 20S core particle of the proteasome has three proteolytic activities, caspase-like (CaL), trypsin-like (TL), and chymotrypsin-like (ChL), which are provided by its β1, β2, and β5 subunits, respectively (163). We have previously developed three distinct fluorogenic peptide-based sensors that can simultaneously measure each of these activities (213) (Figure 1.11). Each sensor is comprised of a fluorophore, a peptide specific for one of the three proteasome activities, and a quencher (acid blue 40, abbreviated AB40) (214). The ChL, TL, and CaL sensors have the following sequences: FAM-His-His-Ser-Leu-Lys(AB40), TAMRA-Leu-Arg-Arg-Lys(AB40), and DyLight633-nLeu-Pro-nLeu-Asp-Lys(AB40), respectively. In the intact sensor, the fluorescence of the fluorophore is internally quenched by a covalently appended dye (AB40), but upon proteolysis of the peptide, the fluorophore dissociates from the quencher and becomes fluorescent. In order to simultaneously measure each proteolytic activity, each sensor has a photophysically distinct fluorophore.

Cells were treated with our without dasatinib for 72 h, proteasomes were isolated, and proteasome activity was measured using the aforementioned probes, as described previously (213). To ensure our measurements were not compounded by significant cell death due to dasatinib, we selected doses for each cell line such that at least 75% of the cells were viable (Table 3.1). These doses were chosen based on dose-response curves performed in earlier work (Chapter 2). After assessing proteasome activity in response to dasatinib treatment, we found that dasatinib treatment induces significant reductions in proteasome ChL, TL, and CaL activity in the ABC DLBCL cell lines, but has no effect in the GCB DLBCL cell lines (Figure 3.1). In addition, this reduction in proteasome activity appears to be both time- and dose-dependent (Figure 3.2), becoming most readily apparent after 72 h of dasatinib treatment.

3.3.2 Dasatinib treatment does not significantly alter proteasome catalytic subunit protein expression

In order to assess the cause of the effects of dasatinib treatment on the proteasome, we first questioned whether dasatinib has a direct effect on proteasome activity. Purified proteasomes were mixed with varying concentrations of dasatinib, then proteasome activity was assessed as before. These studies demonstrated that dasatinib has no direct effect on proteasomal activity (data not shown).

Another possible explanation for the changes in proteasome activity is a change in the expression levels of its three catalytic subunits, β1, β2, and β5, which confer its CaL, TL, and ChL activities, respectively (163). We therefore assessed potential changes in protein expression of each of the constitutive proteasome catalytic subunits in response to dasatinib treatment (Figure 3.3). Expression levels were assessed in both isolated proteasomes (Figure 3.3A) and whole lysates (Figure 3.3B), using expression of the 20S α7 subunit as a loading control for total proteasome. Although there appears to be a minimal change in expression of the β5 proteasome subunit with dasatinib treatment in the ABC DLBCL cell lines, there does not appear to be any significant changes in expression of the β2 and β1 subunits in response to dasatinib treatment. In immune cells, the β1, β2, and β5 subunits can be replaced by the immunoproteasome subunits β1i, β2i, and β5i, respectively (163,165). This produces a proteasome with altered cleavage patterns favoring the production of peptides involved in antigen presentation (163,166,167). Since we found the ChL (β5/β5i) activity to be most dominant in our cell lines, and dasatinib induces the most robust changes in ChL (β5/β5i) activity, we also assessed changes in expression

of the β5i subunit of the immunoproteasome (Figure 3.3). Similar to the constitutive proteasome catalytic subunits, no significant change in β5i subunit expression was observed.

3.3.3 Dasatinib treatment reduces 19S regulatory particle levels in isolated proteasomes but not whole lysates

Binding of the 19S regulatory particle is known to enhance proteasome activity (265,266). Considering the observed changes in proteasome activity across all three catalytic activities in the ABC DLBCL cell lines in response to dasatinib, it is possible that this reduced proteasomal activity may be due to changes in the 19S regulatory particle. Therefore, we assessed changes in expression of Rpn13, a subunit of the 19S regulatory particle, in both isolated proteasomes and whole lysates (Figure 3.4). Interestingly, the isolated proteasomes from dasatinib-treated ABC DLBCL cell lines show a decrease in the amount of Rpn13, compared to DMSO controls. We at first thought this could indicate a general downregulation of Rpn13 expression. However, western blotting of the corresponding whole lysates demonstrates no change in Rpn13 expression between DMSO and dasatinib treatment in any of the cell lines. Therefore, it is possible the proteasome is undergoing a structural change that affects binding of the 19S regulatory particle to the 20S core particle. We have attempted immunoprecipitation and Native-PAGE experiments to confirm this notion. However, to date we have been unsuccessful in optimizing these techniques. Some of the challenges we have encountered include interference of the sepharose beads for immunoprecipitation with western blotting, as well as issues of similar molecular weights between the immunoprecipitation antibody light chains and proteasome subunits. In addition, we have yet to identify ideal gel polyacrylamide and running buffer concentrations to produce adequate separation of the 20S and 19S particles with sufficient band sharpness using Native-PAGE.

3.3.4 Dasatinib treatment leads to changes in proteasome subunit phosphorylation

To better understand the potential structural changes that might be occurring in the proteasome in response to dasatinib, a kinase inhibitor, we decided to evaluate changes in the phosphoproteome. We selected one representative cell line from each subtype: HT for the GCB DLBCL cell lines and TMD8 for the ABC DLBCL cell lines. Cells were treated with 100 nM dasatinib for 30 min, lysed, and the lysates subjected to phosphoproteomics analysis via mass spectrometry. We searched the results for proteasome proteins, and found phosphorylation results from 10 proteasome subunits and 2 proteasome-related proteins (Table 3.2). The identified proteasome subunits are two members of the 19S regulatory particle and a subunit from the 20S core particle. The two proteasome-related proteins identified are PSMF1, a known proteasome inhibitor (267,268), and PSMG2, a proteasome assembly chaperone (269). Nearly all of the identified phosphorylation sites have been reported previously (270-275), with Ser 152 of PSMF1 (PI31) being the exception. Comparing the HT cell line to the TMD8 cell line, changes in phosphorylation are most prominent for the proteasome 19S base subunit PSMD1 (Rpn2), the proteasome inhibitor protein PSMF1 (PI31), and the proteasome assembly chaperone PSMG1 (PAC1).

3.4 Discussion

Since patients with ABC DLBCL have a poorer prognosis than their GCB DLBCL counterparts (5,6), there is great interest in identifying effective drug targets for the treatment of this subtype. Both the SFKs and the proteasome are critical for signaling in the ABC DLBCL subtype, particularly in regards to overactive NF-κB signaling (10,11,32,180,263). Although there is evidence for potential cross talk between the SFKs and the proteasome, direct links

between these proteins have yet to be studied. In this study, we explored the potential role of the SFKs as regulators of the proteasome. Treatment of a panel of DLBCL cell lines with the SFK inhibitor dasatinib results in a marked decrease in the proteasome's ChL, TL, and CaL activities for the ABC DLBCL cell lines, whereas no changes are observed in the GCB DLBCL cell lines. Biochemical analyses demonstrate that while there is minimal change in expression of the β5 proteasome subunit, which is responsible for the proteasome's ChL activity, dasatinib treatment induces a decrease in expression of the proteasome 19S regulatory particle in isolated proteasomes. However, 19S expression remains unchanged in whole lysates, indicating that the SFKs could regulate proteasome assembly, possibly via phosphorylation or through a chaperone protein that helps assemble or stabilize proteasome complexes. A phosphoproteomics analysis demonstrated changes in the phosphorylation status of several proteasome subunits and proteasome-related proteins in response to dasatinib treatment. Our working hypothesis is that the SFKs, either directly or indirectly via proteasome-related proteins, help promote assembly or stability of the 20S core and 19S regulatory proteasome particles (Figure 3.5).

Several studies have examined the mechanism by which the 19S regulatory particle binds to the proteasome 20S core particle. The 19S regulatory particle is comprised of 18 different subunits, six of which are ATPases used for ATP-dependent protein unfolding (164). These six ATPases form the base of the 19S core particle and directly bind to the outer α-ring of the 20S core particle (276-278). In addition, the 19S lid subunit Rpn6 is described as having a pivotal role in stabilizing the interaction between the proteasome 20S core particle and 19S regulatory particle (279). There is evidence of phosphorylation of several of these key binding subunits, and some phosphorylation sites have been demonstrated to enhance proteasome activity (272,280-283). Unsurprisingly, the assembly of the 20S core particle and 19S regulatory particle

is facilitated by several chaperone proteins, such as Hsp90 (284), Nas6 (285), and the heterodimeric complex of PSMG1 (also known as PAC1) and PSMG2 (also known as PAC2) (269). Our phosphoproteomics data demonstrated changes in phosphorylation of Thr18 of the chaperone PSMG1 in response to dasatinib treatment, with a fold change of 1.40 for the HT cell line and 0.34 for the TMD8 cell line. Although other researchers have also identified this phosphorylation site (271), to our knowledge no functional analyses of its role in PSMG1 activity have been performed. It is possible that phosphorylation of Thr18 on PSMG1 activates the chaperone, thus promoting proper proteasome assembly. If this enhanced phosphorylation is present across all of the GCB DLBCL cell lines and reduced in the ABC DLBCL cell lines with dasatinib treatment, it could explain (at least in part) the differences in proteasome structure between the two subtypes in response to dasatinib. Future studies should explore changes in phosphorylation of Thr18 on PSMG1 after dasatinib treatment in all seven of the cell lines used in this study.

Dasatinib treatment also induces changes in phosphorylation status of Thr273 of the 19S regulatory particle base subunit Rpn2 (PSMD1), with a reduction of 0.67 in the HT cell line and an increase of 1.72 in the TMD8 cell line. Interestingly, Lee *et al.* demonstrated that phosphorylation of Thr273 by p38 MAPK causes inhibition of the proteasome (286), which could help explain the reduction in proteasome activity observed in the ABC DLBCL cell lines after dasatinib treatment. This should be confirmed by assessing phosphorylation of Thr273 on Rpn2 in all seven cell lines used in this study. On another note, one of the major functions of the Rpn2 subunit is docking for the ubiquitin-binding Rpn13 subunit (287-289). However, crystal structures demonstrate that the Thr273 residue is far from the Rpn13 binding site of Rpn2 (289), making it unlikely that phosphorylation at this residue would impact Rpn13 binding.

Nevertheless, it is worth noting that the representative 19S subunit we examined in this study was Rpn13, and it is possible that the apparent dissociation of the 19S regulatory particle from the 20S core particle in response to dasatinib treatment is merely an artifact of reduced binding of Rpn13 to Rpn2, and not dissociation of the entire 19S proteasome. Subsequent studies should be performed with antibodies directed against other 19S subunits to confirm our results. In addition, optimization of the immunoprecipitation or Native-PAGE techniques will also help shed light on the possible dissociation of the proteasome's 20S and 19S particles.

Lastly, we also observed a difference in phosphorylation of Ser152 of PI31 (PSMF1) after dasatinib treatment, with a reduction of 0.18 in the HT cell line and an increase of 8.91 in the TMD8 cell line. PI31 is known to inhibit the proteasome by disrupting association of the 20S and 19S core particles (267,268,290). To our knowledge, phosphorylation at Ser152 of PI31 has not been reported in previous studies, but phosphorylation at the adjacent Ser153 residue has been detected (271). The role of phosphorylation at these sites is currently unknown, and warrants further exploration. One could speculate that changes in phosphorylation of the PI31 proteasome inhibitor may help cause the dissociation of the proteasome 20S and 19S particles that we observed, but substantially more analyses will be required to confirm this.

Our data demonstrate a significant reduction in proteasome activity in ABC DLBCL cell lines after dasatinib treatment. So far, our studies indicate that dasatinib treatment results in the dissociation (or decreased assembly) of the 20S core and 19S regulatory particles. Further studies are needed to confirm this notion and determine the mechanism by which dasatinib induces this change in proteasome activity. Focus should be placed on determining which kinases phosphorylate Rpn2, PAC1, and PI31, and evaluating their potential links to the SFKs.

3.5 Tables and Figures

Cell Line	Dasatinib Conc. (nM)
HBL-1	55
OCI-Ly3	5
OCI-Ly10	30
TMD8	15
Farage	1000
HT	1000
Karpas 422	1000

Table 3.1: Dasatinib doses used to maintain at least 75% viability
Doses result in at least 75% viability of cells 72 h after dasatinib treatment (abbreviated as EC_{25} dose).

Gene Name	Protein Name	Major Function	Phosphorylation Site(s)	Identified Phosphorylated Peptide	Average Ratio of Change in Phosphorylation (Dasatinib/DMSO)	
					HT	TMD8
PSMA5	α5	20S CP α-ring	Ser16	^{11}GVNTF**pS**PEGR^{20}	1.03	0.71
PSMD1	Rpn2	19S RP base; Ubiquitin receptor (Rpn13) docking	Thr273	^{270}TVG**pT**PIASVPGSTNTGTVPGSEKD SDSMETEEK^{302}	0.67	1.71
PSMD2	Rpn1	19S RP base; Ubiquitin receptor (Rpn10) docking	Ser16	^{9}APVQPQQ**pS**PAAAPGGTDEKPSGK^{31}	1.16	0.79
PSMF1	Proteasome inhibitor PI31 subunit	Inhibits proteasome 20S CP association with PA28 and 19S RPs	Ser152, Ser153	^{149}ANV**pSpS**PHREFPPATAR^{164}	0.18, 0.43	8.91, 0.76
PSMG1	Proteasome assembly chaperone PAC 1	Assembly chaperone	Thr18	^{16}AG**pT**EDEEEEEEGRRETPEDR^{35}	1.40	0.34

Table 3.2: Changes in phosphorylation of proteasome subunits after dasatinib treatment

List of the proteasome 20S and regulatory particle subunits as well as known proteasome assembly chaperone proteins that display changes in phosphorylation after 30 min dasatinib treatment. CP = core particle; RP = regulatory particle;Rpn = RP non-ATPase; pS = phosphorylated serine; pT = phosphorylated threonine.

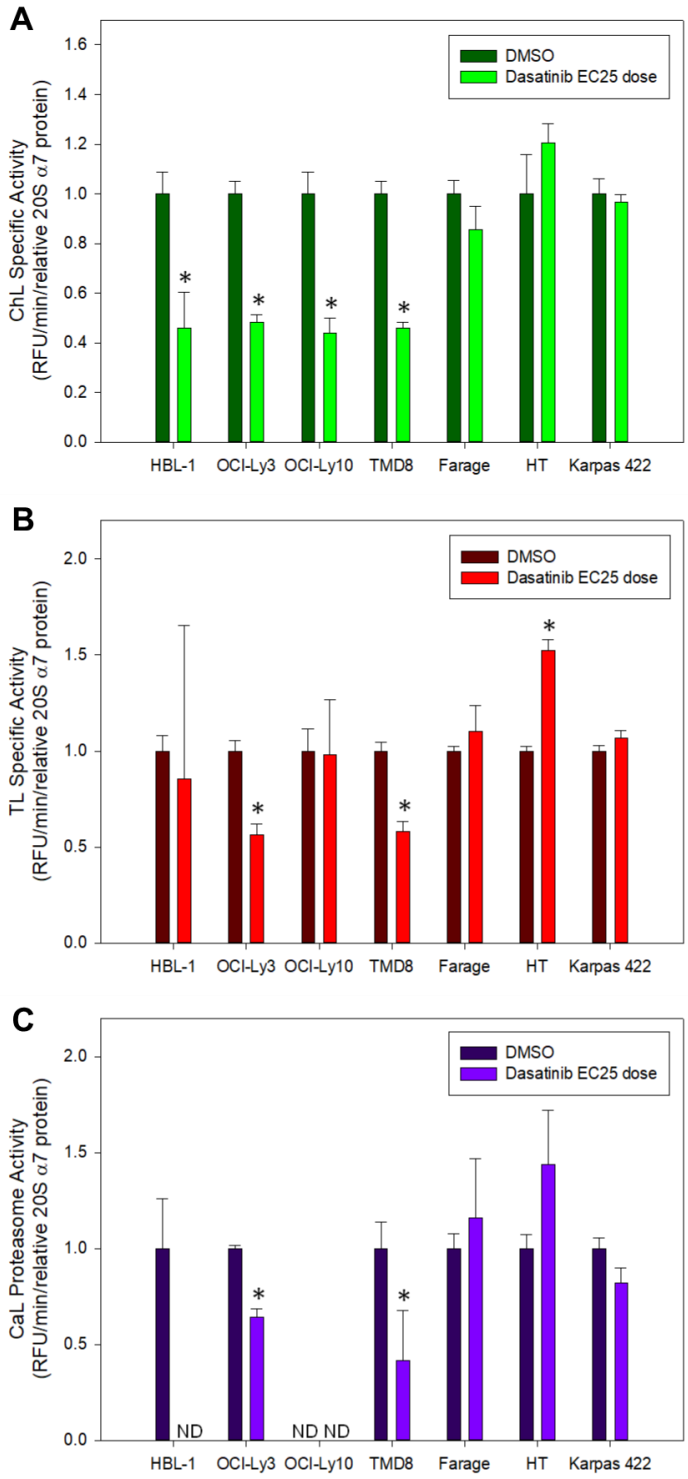

Figure 3.1: Dasatinib treatment reduces proteasome activity in ABC DLBCL cells
Proteasome (*A*) ChL, (*B*) TL, and (*C*) CaL activities, relative to 20S alpha7 expression and DMSO controls, with or without dasatinib treatment for 72 h. Data represent the average ± S.D. of triplicate experiments. * indicates $p<0.05$, versus control. ND = not detectable.

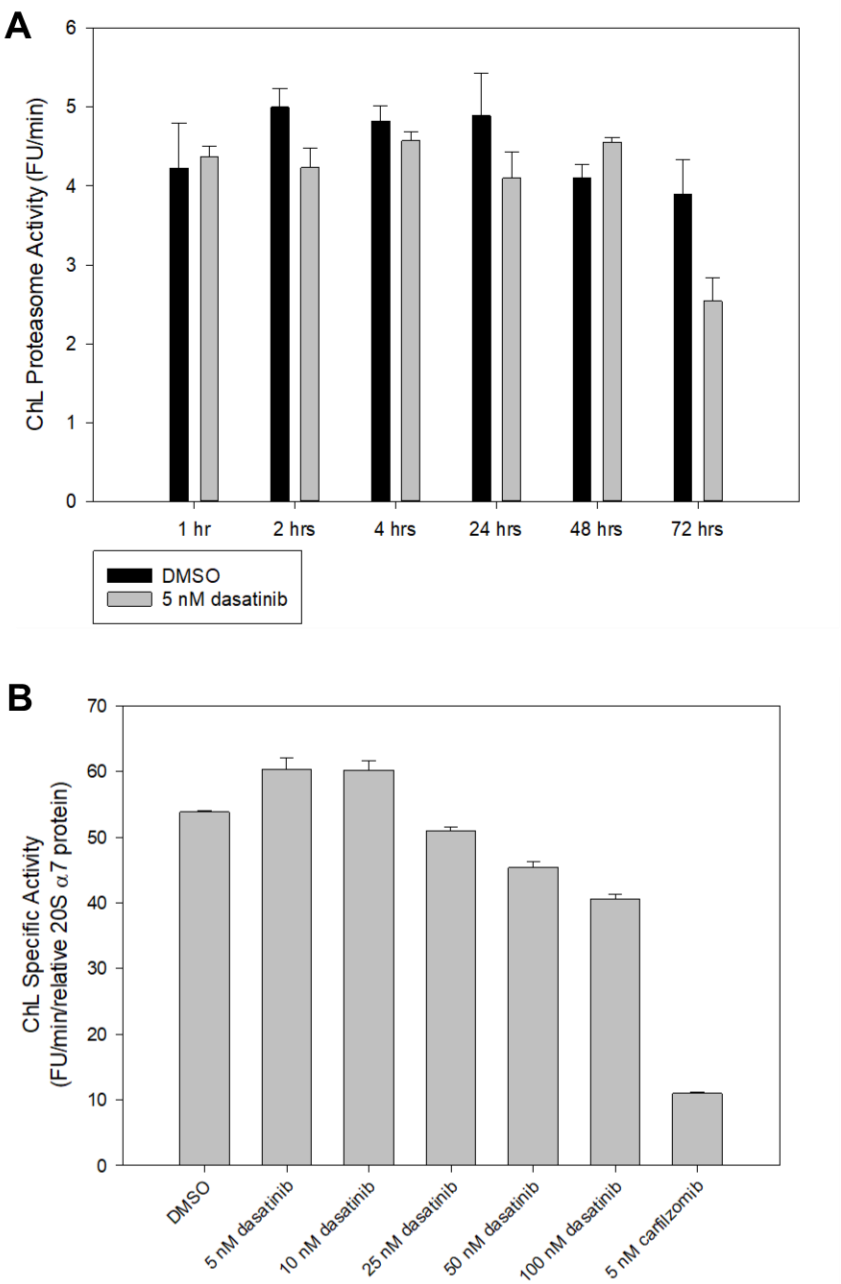

Figure 3.2: Dasatinib-induced changes in proteasome activity are time- and dose-dependent (*A*) ChL proteasome activity after treatment with DMSO or 5 nM dasatinib at the indicated times in the OCI-Ly3 cell line. (*B*) ChL proteasome activity after treatment with DMSO or the indicated concentrations of dasatinib or carfilzomib for 16 h in the OCI-Ly3 cell line.

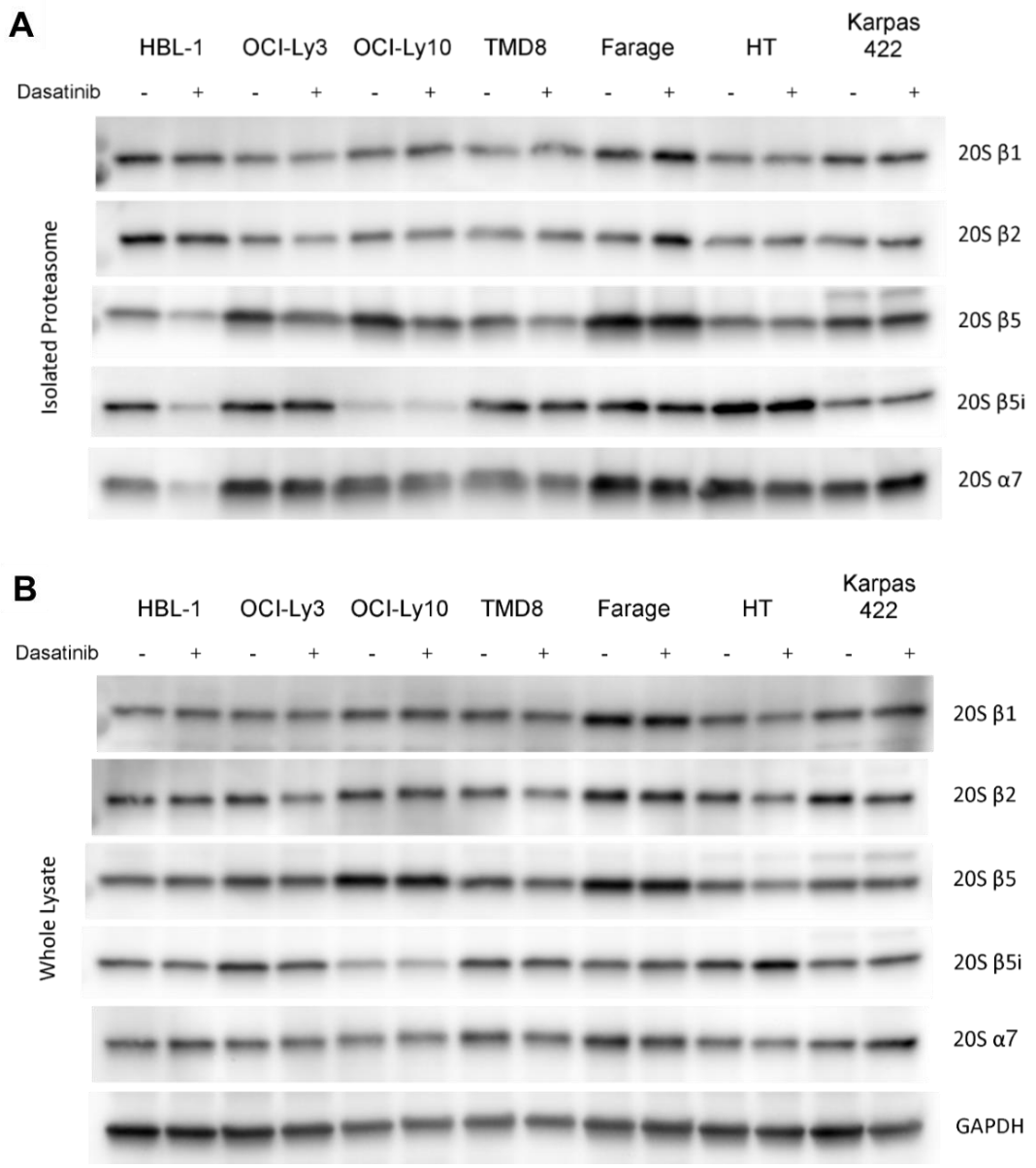

Figure 3.3: Dasatinib treatment does not alter proteasome catalytic subunit expression
Expression of several proteasome 20S subunits from (*A*) isolated proteasomes or (*B*) whole lysates after treatment with dasatinib for 72 h.

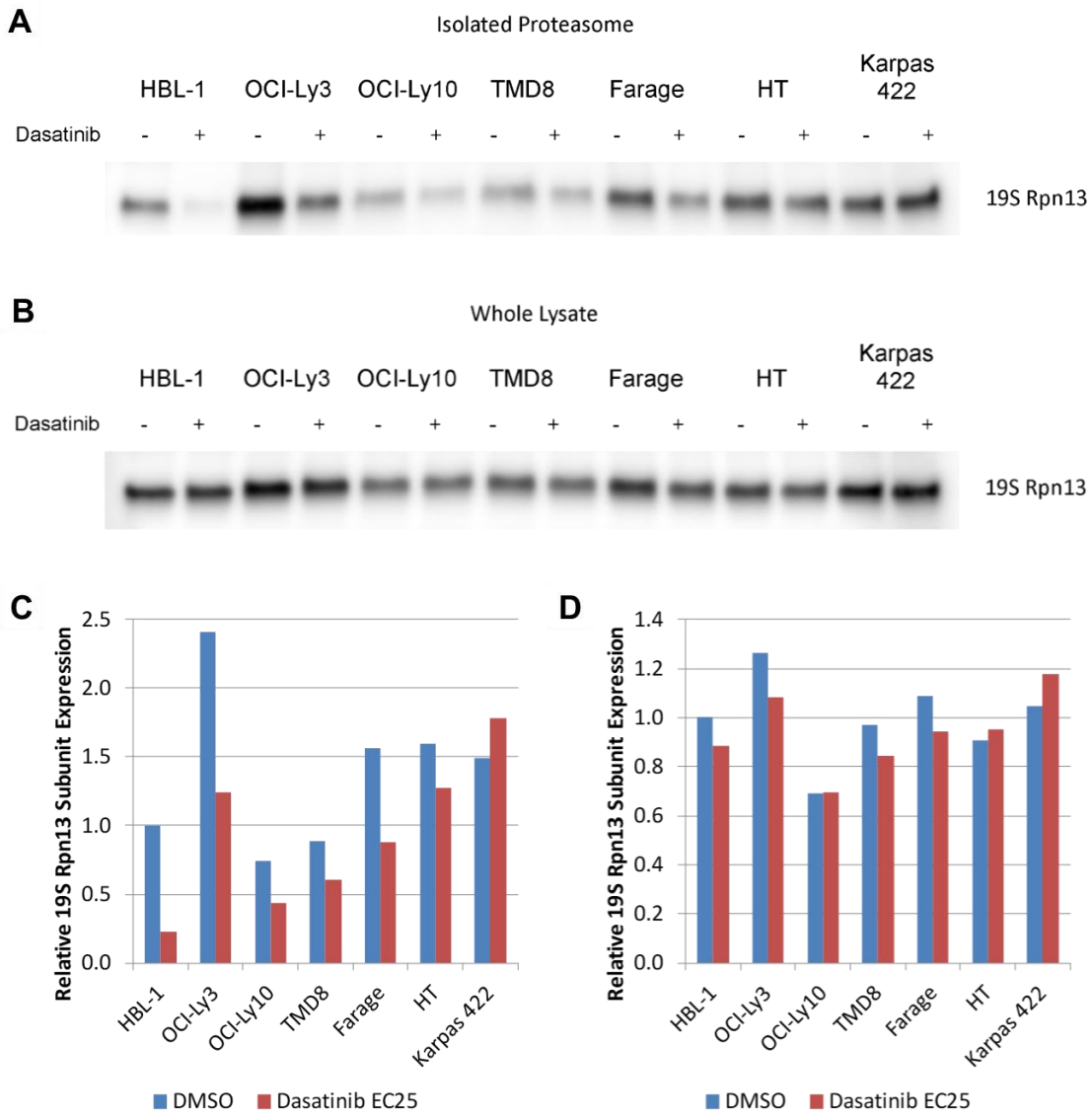

Figure 3.4: Dasatinib treatment reduces 19S regulatory particle levels in isolated proteasomes

(*A-B*) Expression of proteasome 19S Rpn13 subunits from (*A*) isolated proteasomes or (*B*) whole lysates after treatment with dasatinib for 72 h. (*C-D*) Quantification of 19S Rpn13 expression from (*C*) isolated proteasomes or (*D*) whole lysates.

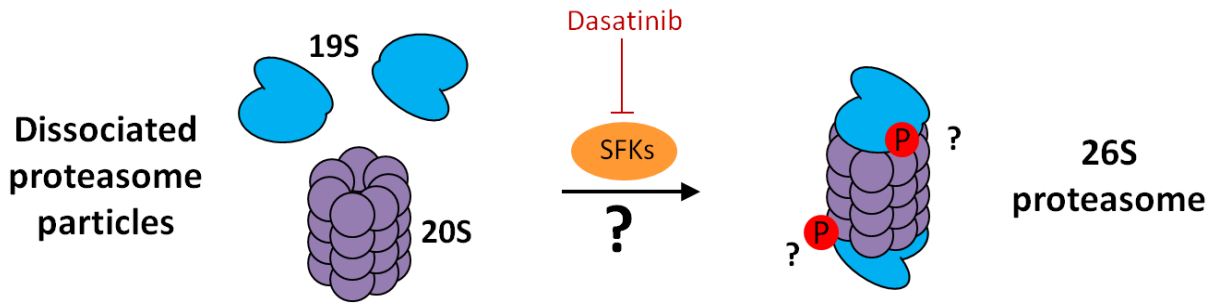

Figure 3.5: Schematic of working hypothesis
Based on our results so far, it appears that the SFKs (or other kinases) may play a role in stabilizing the interaction between the 20S core and 19S regulatory particles of the proteasome, possibly through phosphorylation of proteasome subunits. Treatment with dasatinib may disrupt this kinase activity, therefore destabilizing the proteasome, resulting in decreased proteasome activity.

CHAPTER 4: PROTEASOME CATALYTIC SIGNATURES AS PREDICTORS OF RESPONSIVENESS TO SITE-SPECIFIC PROTEASOME INHIBITORS[3]

4.1 Introduction

The proteasome is a key component of cellular machinery, and is critical for maintaining the health and viability of a cell (173). Acting as the garbage disposal of the cell, the proteasome is responsible for degrading proteins that are damaged or no longer needed. In addition, the proteasome plays a role in antigen processing within the immune system (166,167). Considering its essential role in a multitude of signaling pathways, such as cell cycle regulation (174), transcription (175), and signal transduction (176), it is not surprising that aberrant proteasome activity is linked with disease. For example, proteasome activity is often upregulated in cancer (172,177,178), but downregulated in neurodegenerative diseases (179). Consequently, there has been and continues to be a high level of interest in the proteasome as a therapeutic target.

The proteasome is a multi-subunit protein comprised of a 20S core particle and a regulatory cap particle. The 20S core particle is a barrel-shaped structure that harbors the protein's proteolytic activity. It is comprised of two outer α-rings and two inner β-rings. The core particle has three distinct proteolytic activities: caspase-like (CaL), trypsin-like (TL), and chymotrypsin-like (ChL), which are provided by its β1, β2, and β5 subunits, respectively (163). In immune cells, or in nonimmune cells in the presence of interferon or tumor necrosis factor, each of these subunits can be replaced by immunoproteasome subunits β1i, β2i, and β5i, respectively, resulting in either mixed proteasomes, with one or two subunits replaced, or the full

[3] This chapter is in preparation to be submitted to an academic journal. The original citation is as follows: Cann ML, Wang Q, Lawrence DS, Priestman MA. Proteasome catalytic signatures as predictors of responsiveness to site-specific proteasome inhibitors. In preparation.

immunoproteasome when all three are substituted (163,165). This produces a proteasome with altered cleavage patterns favoring the production of peptides involved in antigen presentation (163,166,167). Whereas the proteasome's 20S core particle acts as the degradation machinery, the regulatory particles serve as a lid to the 20S core particle and facilitate binding, unfolding, and entry of proteasome substrates. There are four different regulatory particles that can bind to the 20S core particle: PA700 (also known as 19S), PA28αβ, PA28γ, and PA200 (163). Considering the variety of regulatory particles and catalytic 20S subunits, there is potential for several forms of the proteasome to exist within a given tissue, or even within an individual cell (171,172).

There are currently three proteasome inhibitors approved for clinical use: bortezomib, carfilzomib, and ixazomib (182). All three are used for the treatment of multiple myeloma (and mantle cell lymphoma in the case of bortezomib), and are currently in clinical trials for other hematological and solid malignancies. These inhibitors preferentially target the β5 subunit of the proteasome, which confers the proteasome's ChL activity (183-185). Although these inhibitors are successful in the clinic, bortezomib is known to have numerous side effects, the most significant of which is peripheral neuropathy. Furthermore, there are many patients who are inherently resistant or develop resistance to the current proteasome inhibitors (291,292). This resistance has been ascribed to mutations in the β5 subunit or increased proteasome expression, and has the potential to be overcome by targeting multiple catalytic subunits (175,176). In an effort to combat drug resistance and unwanted side effects, a new generation of proteasome inhibitors that target the β2 (LU-102) (293) and β1 (NC-001) (294) subunits have been described. These β2 (TL) and β1 (CaL) inhibitors, while not reported to be cytotoxic alone in several cancer cell lines, do increase the susceptibility of these cells to β5 inhibitors (293-297).

Optimized combinations of site-specific proteasome inhibitors have the potential to increase the efficacy as well as reduce side effects of β5 inhibitors due to lower doses needed for clinical effectiveness. However, combination studies of these inhibitors have been primarily limited to multiple myeloma cell lines and patient samples, and there are currently no means for predicting which cell types will be sensitive to these inhibitors. We sought to explore the sensitivity of a panel of cancer cell lines to the TL and CaL proteasome inhibitors. Furthermore, we addressed whether there is a biochemical marker, such as proteasome subunit expression or activity, that could predict which cell types would be most sensitive to these inhibitors. Herein, we report that cell lines that have low TL and CaL activities relative to ChL activity are particularly sensitive to TL and CaL inhibitors, respectively, especially when employed in combination with ChL-targeted inhibitors.

4.2 Materials and Methods

4.2.1 Materials

Farage, HL60, HeLa, A549, MCF7 and DU145 cell lines were obtained from the tissue culture facility at the University of North Carolina at Chapel Hill. All reagents for cell culture media were purchased from Gibco. CellTiter-Glo® 2.0 was purchased from Promega. Bortezomib and carfilzomib were purchased from Enzo life sciences. LU-12 and NC-001 were gifts from Dr. H. Overkleeft at the University of Leiden in the Netherlands. The BCA kit from Thermo Scientific was used to quantify the protein content of all lysates. M-PER and Halt-protease cocktail were from Thermo-Fisher. All other chemicals were from Fisher or Sigma unless otherwise noted.

4.2.2 Cell Culture

HeLa, A549, MCF7 and DU145 cell lines were passaged by treatment with 0.05% trypsin + 0.53 mM EDTA before reaching confluence and maintained in DMEM containing 10% fetal bovine serum (FBS), non-essential amino acids and penicillin-streptomycin at 37 °C in a 5% CO_2 incubator. Farage and HL60 cell lines were maintained between $3x10^5$ – $1x10^6$ in RPMI 1640 media containing 15% FBS supplemented with penicillin-streptomycin at 37 °C in a 5% CO_2 incubator.

4.2.3 Proteasome Enriched Cell Extracts

One 90% confluent 75 cm^2 flask of HeLa, A549, MCF7 or DU145 cell lines or 50 mL of Farage or HL60 cell lines at $6x10^5$ were used to isolate a cell fraction to monitor proteasome activity while removing other protease activity (213,264). Isolated cells were resuspended in ice cold PBS, centrifuged at 1,000 x g for 5 min at 4 °C for 3 cycles. Cells were then resuspended in 4 volumes homogenization buffer (50 mM Tris, 250 mM sucrose, 5 mM $MgCl_2$, 1 mM ATP, 1 mM DTT, 0.5 mM EDTA, pH 7.5) with 0.025% digitonin, incubated on ice for 10 min, followed by centrifugation at 17,000 x g for 10 min at 4 °C. The supernatant was then ultracentrifuged at 180,000 x g for 4 h at 4 ˚°C. The supernatant was removed and the pellet resuspended in homogenization buffer without digitonin. Protein concentration was determined using the BCA kit from Thermo Scientific.

4.2.4 Assessment of Proteasome Activity

The activities of all proteasome enriched extracts were determined in assay buffer (50 mM Tris pH 7.5, 40 mM KCl, 4 mM $MgCl_2$, 1 mM ATP, 1 mM EDTA) and 0.05% bovine serum albumin (BSA) (213,264) with 0.5 µM ChL-488, 1 µM TL-550, and 1 µM CaL-633 proteasome sensors. The reactions were initiated with 10 µg of sample and the reaction progress

monitored for 2 h at room temperature. Control assays without proteasome were run to ensure that the fluorescent change was due to proteasome activity and not hydrolysis. Fluorescence was monitored on Molecular Devices Spectra Max Gemini EM plate reader with excitation at 490 nm, 550 nm, and 625 nm with emission at 515 nm, 575 nm, and 655 nm, respectively. Sigmaplot 12 (serial number 775206611) was used for the analysis of all data. The rate of each assay was determined using a linear fit to the first 10% of substrate consumption. All data is reported as the mean ± standard deviation of triplicate assays where FU is fluorescent units.

4.2.5 Western Blots

Proteasome 20S α7, 19S Rpn13, PA28α, and ubiquitin antibodies were purchased from Cell Signaling Technologies. Proteasome 20S β1, 20S β2, and 20S β5 antibodies were purchased from Enzo Life Sciences. Proteasome 20S β1i and 20S β5i antibodies were purchased from Thermo Fisher Scientific. Proteasome 20S β2i and PA200 antibodies were purchased from Novus Biologicals. All secondary antibodies were purchased from GE Healthcare. SDS-PAGE was performed using 4-15% SDS Tris-HCl gels (Bio-Rad) and loading 20 μL of each sample per well. Gels were then transferred to polyvinylidene fluoride (PVDF) membranes overnight at 4 °C. Membranes were blocked with 5% BSA in 1X Tris-buffered saline (TBS) + 0.1% Tween-20 for 2 h, then incubated with 1:500-1:1000 of the primary antibody in the blocking solution overnight at 4 °C. Membranes were washed with TBS + 0.1% Tween-20, incubated with 1:5000 HRP-conjugated secondary antibody for 1 h at room temperature, and washed again with TBS + 0.1% Tween-20. Secondary antibodies were detected using the Clarity Western ECL Substrate (Bio-Rad) according to the manufacturer's protocol. Images were acquired using an Alpha Innotech FluorChem FC2 using the chemiluminescent settings.

4.2.6 Cell Viability Studies

CellTiter-Glo® 2.0 was used to monitor cell viability according to published Promega protocols. Inhibitors concentration for the viability assays were 0-400 nM bortezomib, 0-400 nM carfilizomib, 0-5000 nM NC-001, and/ or 0-5000 nM LU-102. All inhibitors were dissolved in DMSO with a final concentration of DMSO of 1% in every well. Cells were plated at 2,000 cell/well in a 96 well plate with 100 µl media +/- inhibitors and grown for 48 h at 37 °C in a 5% CO_2 incubator. After incubation 100 µl of CellTiter-Glo® 2.0 was added to each well and incubated at room temperature for 30 min. The plates were read on the Molecular Devices Spectra Max Gemini EM plate reader with the luminescent settings. All data is reported as the mean ± standard deviation of triplicate assays. All data was fit to the standard IC_{50} equation and plotted using Sigmaplot.

4.2.7 Proteasome Inhibition and Total Ubiquitination

All inhibitors were dissolved in DMSO with a final concentration of DMSO of 1% in every well. Inhibitor concentrations for the viability assays were 5 nM bortezomib, 50 nM carfilizomib, 500-5000 nM NC-001, or 500-5000 nM LU-102. Cells were plated at 50,000 cell/well in 2 ml media in a 6 well plate and grown overnight at 37 °C in a 5% CO_2 incubator. Inhibitors were added to the media and the plates were incubated at 37 °C in a 5% CO_2 incubator for 6 h. The media was removed and the cells were washed with PBS before lysis with MPER + Halt protease cocktail. Western blots were run as previously described.

4.2.8 Correlation Assessments

Correlation assessments were performed using the Pearson's correlation coefficient, Spearman's rank correlation coefficient, or Kendall's rank correlation coefficient. The Pearson's correlation coefficient was determined using the following equation:

$$r = \frac{\sum_{i=1}^{n}(x_i - \bar{x})(y_i - \bar{y})}{\sqrt{\sum_{i=1}^{n}(x_i - \bar{x})^2}\sqrt{\sum_{i=1}^{n}(y_i - \bar{y})^2}}$$

where x and y are the datasets being compared (x_i being an individual data point and $\bar{x}$ being the mean of dataset 1, and analogously for y_i and $\bar{y}$) and n is the total number of data points in each set (i.e. the number of cell lines). The Spearman's rank correlation coefficient was determined by first assigning the values in each dataset a rank (1-6), where the smallest value was assigned a rank of 1 and the largest a rank of 6. The Pearson's correlation equation was then applied to the ranked values of each dataset to give the Spearman's rank correlation coefficient (ρ). The Kendall's rank correlation coefficient was determined using the same ranking system described above and the following equation:

$$\tau = \frac{(C - D)}{n(n-1)/2}$$

where C is the number of concordant (x, y) pairs from dataset x and dataset y, D is the number of discordant (x, y) pairs from dataset x and dataset y, and n is the total number of data points in each set (i.e. the number of cell lines).

4.3 Results and Discussion

4.3.1 Sensitivity to Site-Specific Proteasome Inhibitors

Bortezomib and carfilzomib are two proteasome inhibitors that are clinically approved for the treatment of multiple myeloma. Both bortezomib and carfilzomib preferentially target the

ChL activity of the proteasome (183-185). However, due to significant side effects and the development of resistance to these inhibitors, there have also been efforts to develop inhibitors that selectively target the TL and CaL sites, such as the TL inhibitor LU-102 (293) and the CaL inhibitor NC-001 (294). In the current study, we sought to examine the sensitivity of several cancer cell lines to site-specific proteasome inhibitors, and to determine if there is a marker that can predict inhibitor sensitivity. The cell lines used were: Farage, a B-cell lymphoma cell line; HL60, a leukemia cell line; HeLa, a cervical cancer cell line; A549, a lung carcinoma cell line; DU145, a prostate cancer cell line; and MCF7, a breast adenocarcinoma cell line. We began by generating dose-response curves with bortezomib, carfilzomib, LU-102, and NC-001 for our panel of cell lines to determine each cell line's sensitivity to the various compounds (Table 4.1, Figure 4.1). However, due to solubility issues with LU-102 and NC-001, we were unable to determine EC_{50}s for several of the cell lines, and instead report the percent viability of each cell line at 5 μM of each compound. EC_{50} values that could be determined for NC-001 and LU-102 are reported in Table 4.2. The six cell lines respond similarly to bortezomib and carfilzomib, with EC_{50} values ranging from about 3 nM to 30 nM for bortezomib and about 10 nM to 70 nM for carfilzomib. The cell lines display a wider range of sensitivities to the TL and CaL inhibitors LU-102 and NC-001, respectively, with percent viabilities at 5 μM ranging from 4% to 100% for LU-102 and 26% to 100% for NC-001, respectively. Although previous studies have reported synergy of LU-102 and NC-001 with ChL inhibitors, only limited single-agent toxicities have been described for these compounds to date (293,294,296,297). We discovered that the TL inhibitor LU-102 and CaL inhibitor NC-001 alone are cytotoxic in several cell lines, indicating their potential use for cancer treatment in the clinic.

To determine if LU-102 or NC-001 resistance by some cell lines is due to lack of cellular proteasome inhibition, we investigated total protein ubiquitination. Proteins are targeted for degradation by the proteasome by labeling with ubiquitin chains (163). Consequently, an accumulation of ubiquitin is indicative of proteasome inhibition. We assessed ubiquitin accumulation in response to the various site-specific proteasome inhibitors (Figure 4.2). Short-term treatment of cells with bortezomib or carfilzomib produced ubiquitin accumulation in all cell lines. Interestingly, the TL inhibitor LU-102 and CaL inhibitor NC-001 induce ubiquitin accumulation in all cell lines at a concentration of 5 μM. This indicates that the site-specific proteasome inhibitors are penetrating all of the cancer cell lines tested and inhibiting proteasome activity, even if this inhibition does not produce a cytotoxic effect.

4.3.2 Proteasome Subunit Expression and Inhibitor Sensitivity

Our dose-response curve data demonstrate that the sensitivity to TL and CaL proteasome inhibitors varies among our cell lines. However, methods for predicting these sensitivities have yet to be explored. To determine if there is a biochemical marker that can predict site-specific proteasome inhibitor sensitivity, we first examined the expression of the proteasome's 20S catalytic subunits (β1, β2, β5, β1i, β2i, and β5i). We also assessed the presence of the proteasome's regulatory particle subunits (19S/PA700, PA28, or PA200), as binding of the regulatory particles is known to enhance proteasome activity (265,266). We found that both proteasome catalytic subunit expression and regulatory particle expression varies among the six cell lines (Figure 4.3). To determine if expression of any of these proteins correlates with site-specific proteasome inhibitor sensitivity, we assessed possible relationships using the Pearson's correlation method, the Spearman's rank correlation method, and the Kendall's rank correlation method (Tables 4.3 and 4.4). We found that neither proteasome 20S catalytic subunit expression

nor regulatory particle subunit expression correlate with sensitivity to any of the proteasome inhibitors. Therefore, proteasome protein expression is not a suitable biomarker for predicting inhibitor sensitivity.

4.3.3 Proteasome Catalytic Activity and Inhibitor Sensitivity

Moving forward in our search for predictors of proteasome inhibitor sensitivity, we next considered the individual activities of the ChL, TL, and CaL proteasome subunits. The subunit composition and activity of the proteasome has been found to vary depending on the type of malignancy, as was observed in a recent study describing differences in expression of the β-subunits in acute lymphoblastic leukemia (ALL) and acute myelogenous leukemia (AML) cell lines (298). Additionally, total activity of the ChL, TL, and CaL sites differs due to proteasome composition, tissue type, or disease state (202,298). For example, some studies suggest that ChL activity is higher in cancerous cells lines relative to normal cells (172,299). However, Driessen and colleagues failed to observe any correlation between ChL activity and cancer in leukemia patients (300). In these previous reports, proteasome activity was monitored by methods that precluded simultaneous real-time monitoring of all three catalytic activities. We've designed a set of internally quenched fluorescent peptides that enable simultaneous monitoring of the ChL, TL, and CaL activities of the proteasome (Figure 4.4) (213). These proteasome sensors possess photochemically distinct fluorophores: fluorescein (λ_{ex} = 488 nm) for ChL, tetramethylrhodamine (λ_{ex} = 550 nm) for TL, and DyLight633 (λ_{ex} = 633 nm) for CaL, appended to the N-terminus of the recognition sequences selective for each proteasomal activity [ChL: Fluorophore-His-His-Ser-Leu-Lys(Quencher); TL: Fluorophore-Leu-Arg-Arg-Lys(Quencher); CaL: Fluorophore-norLeu-Pro-norLeu-Asp-Lys(Quencher)]. A broad-spectrum quencher, an acid blue 40 derivative (AB40) (214), is appended to the C-terminal lysine residue on each

sensor. Proteolysis liberates the fluorophore from the quencher and furnishes a fluorescent enhancement of 30- to 140-fold for each peptide.

Using our proteasome sensor triad, we assessed the relative activities of the ChL, TL, and CaL proteasome subunits in each of our cell lines (Figure 4.5a, Figure 4.6). Although the relative catalytic activities vary across the six cell lines, the ChL activity is consistently higher than the TL and CaL activities in all cell lines. Indeed, many investigators believe that ChL activity is most important for protein degradation, and higher levels of ChL activity relative to TL and CaL activities have been observed in previous studies (213,301). However, it should be noted that the importance of the TL and CaL activities is gaining recognition (294,295,301,302). To this end, we next determined if any correlations exist between proteasome activity and inhibitor sensitivity (Tables 4.3 and 4.5). Similar to protein expression, proteasome activity does not correlate with inhibitor sensitivity. Thus, proteasome activity is also not a suitable biomarker for predicting inhibitor sensitivity. Furthermore, proteasome protein expression levels do not correlate with subunit activity (Table 4.6, Figure 4.7), indicating that protein expression does not always reflect enzymatic activity. This furthers the notion that activity, not protein level, is a key consideration when contemplating the use of an inhibitor.

4.3.4 Proteasome Catalytic Signature and Inhibitor Sensitivity

In our previous work, we found that the proteasome has a unique "catalytic signature" (or ratio of catalytic activities) depending on cell type, source, or disease state (213). We therefore questioned whether the proteasome's catalytic signature could serve as a predictor of proteasome inhibitor sensitivity. We determined the catalytic signature of each cell line by calculating the TL/ChL, CaL/ChL, and TL/CaL activity ratios (Figure 4.5b, Figure 4.8), which are independent of the amount of proteasome in each sample, and therefore provide a consistent and reliable

measurement that can be compared between samples. These individual catalytic ratios vary across the six cell lines. In the case of TL/CaL, the ratio is as low as 0.2 in Farage and as high as 1 in DU145. By contrast, the dynamic range of the TL/ChL and CaL/ChL ratios is narrower, given the prominent ChL activity in all cell lines. Nonetheless, these ratios vary as well, with the hematological cell lines (Farage and HL60) at the low end and the solid tumors (HeLa, DU145, and MCF7) at the high end. We then assessed the correlation between the proteasome's catalytic signature and proteasome inhibitor sensitivity (Table 4.3, Table 4.7), and found that the ratios of the catalytic activities do correlate with site-specific inhibitor sensitivity. All three correlation methods reveal that the TL/ChL ratio is significantly positively correlated with cell viability after treatment with the TL inhibitor LU-102 (Pearson: 0.979; Spearman: 1.000; Kendall: 1.000; Tables 4.3 and 4.7, Figure 4.9a). Likewise, the CaL/ChL ratio is significantly positively correlated with cell viability after treatment with the CaL inhibitor NC-001 (Pearson: 0.892; Spearman: 1.000; Kendall: 1.000; Tables 4.3 and 4.7, Figure 4.9b). These data indicate that, although proteasome activities and subunit expression levels do not predict sensitivity to site-specific inhibitors, the TL/ChL and the CaL/ChL ratios of proteasome activity do serve as barometers of sensitivity to the TL inhibitor LU-102 and the CaL inhibitor NC-001, respectively. In particular, the lower the proteasomal TL/ChL ratio in a given cell line, the more sensitive that cell line will be to the TL inhibitor LU-102. An analogous relationship is observed for the CaL/ChL ratio and the CaL inhibitor NC-001. In short, these results are consistent with the notion that, in spite of the depressed CaL and TL proteolytic activities in certain cell lines, these activities remain essential to cell viability. It is tempting to speculate that drug sensitivity is accentuated under conditions in which the targeted pathway is catalytically subdued. It is

possible that, in these cells, there are key protein targets that require TL- or CaL-mediated degradation in order for the cell to survive.

4.3.5 Synergy of ChL and TL or CaL Site-Specific Inhibitors

Previous studies have demonstrated synergy between TL or CaL inhibitors and ChL inhibitors (293-295,297). However, these studies have been primarily limited to hematological cells, particularly those derived from multiple myeloma. Considering our observations of single-agent cytotoxicity of LU-102 and NC-001, we next sought to explore the potential synergy between the site-specific TL and CaL inhibitors and the commercially available proteasome inhibitors bortezomib (Table 4.8, Figure 4.10) and carfilzomib (Table 4.9, Figure 4.11) in our panel of cell lines. Both of these inhibitors target the ChL site in proteasomes. The addition of the TL inhibitor LU-102 induces up to a 12-fold decrease in bortezomib EC_{50} values. Only the MCF7 cell line, which displays the largest TL/ChL ratio, is resistant to the synergistic impact of LU-102. In an analogous vein, the CaL inhibitor NC-001 reduces the EC_{50} of bortezomib, albeit not to the same extent as LU-102. However, with both inhibitors, the cell lines with the lowest TL/ChL and CaL/ChL ratios display the greatest synergy. We also examined the impact of NC-001 and LU-102 on the efficacy of carfilzomib (Table 4.9). Once again, cell lines with low TL/ChL and CaL/ChL ratios are significantly more susceptible to combination therapy than the corresponding cell lines with more robust relative TL and CaL activities. Our data demonstrate that the LU-102 and NC-001 site-specific proteasome inhibitors display synergy with ChL proteasome inhibitors. Interestingly, the TL inhibitor LU-102 generates a more robust synergistic effect with both bortezomib and carfilzomib than the CaL inhibitor NC-001, a phenomenon that has also been observed in a previous study (297). These results, along with the single-agent sensitivities described above, suggest that cell lines with low TL and CaL

proteasome activities relative to ChL activity are nonetheless dependent upon these activities for survival.

4.3.6 Conclusions

The proteasome serves as the major degradation machinery for cellular proteins, and plays an important role in many cellular processes. It is a validated anticancer target, and the current clinically approved proteasome inhibitors primarily target its ChL activity. Although studies have shown that targeting the TL or CaL activity can sensitize cells to ChL inhibition, these studies have been primarily limited to hematological cell lines. We have assessed inhibitors of TL and CaL activity in a variety of cancer cell lines, and found both inhibitors capable of single-agent cytotoxicity, with a range of sensitivities among the different cell lines. We have determined that neither proteasome subunit expression nor TL, CaL, or ChL activity correlate with sensitivity to proteasome inhibitors. However, the ratios of the catalytic activities do correlate with site-specific inhibitor sensitivity. Cells with the lowest TL/ChL and CaL/ChL activity ratios are most sensitive to the TL and CaL site-specific inhibitors, respectively. Furthermore, synergy between TL or CaL inhibitors and bortezomib or carfilzomib is evident in all of the cell lines we studied, and is particularly strong for the hematological cell lines.

Contemporary cancer therapies are typically designed to disrupt the action of upregulated biochemical targets. However, our results show it is also important to consider more modest biochemical activities that are nonetheless crucial. In short, a transformed cell's addiction to certain prioritized biochemical actions might render it susceptible to the interference of related, but significantly less robust, activities. In the case of the proteasome, cell lines that prioritize ChL proteasome activity over TL and CaL activity are particularly sensitive to TL and CaL inhibitors, especially when employed in combination with ChL-targeted inhibitors. These cells

have very little TL and CaL activities to start, and it is clear that what little activity they do have is crucial for cell survival. Moreover, although the current approvals and clinical trials for proteasome inhibitors focus mainly on hematological malignancies, our study demonstrates the potential utility for dual inhibition of proteasome subunits in solid malignancies in addition to hematological malignancies.

4.4 Tables and Figures

Cell Line	EC_{50} Bortezomib (nM)	EC_{50} Carfilzomib (nM)	Viability LU-102 (%)	Viability NC-001 (%)
Farage	3.6 ± 0.1	27.6 ± 5.5	4.2 ± 0.8	26.6 ± 5.9
HL60	4.2 ± 0.1	10.8 ± 2.9	28.5 ± 4.3	58.7 ± 16.5
HeLa	5.6 ± 0.1	61.6 ± 2.0	62.0 ± 3.3	90.7 ± 2.5
A549	5.7 ± 0.1	38.3 ± 4.0	44.7 ± 2.7	48.4 ± 3.1
DU145	31.2 ± 4.0	61.0 ± 4.8	101.3 ± 5.3	94.2 ± 2.4
MCF7	25.2 ± 1.9	67.5± 3.9	89.8 ± 11.4	100.6 ± 4.8

Table 4.1: Cell viability of cancer cell lines when exposed to single proteasome inhibitors
For bortezomib and carfilzomib, data are reported as EC_{50} ± S.D. For LU-102 and NC-001, data are reported as % viability ± S.D. at 5 μM inhibitor. Solubility issues with the compounds prevented determination of EC_{50} for several cell lines. All assays were run in triplicate.

Cell Line	EC_{50} LU-102 (nM)	EC_{50} NC-001 (nM)
Farage	600 ± 50	1200 ± 140
HL60	1780 ± 210	> 5000
HeLa	> 5000	> 5000
A549	3910 ± 100	4970 ± 120
DU145	> 5000	> 5000
MCF7	> 5000	> 5000

Table 4.2: Cell viability of cancer cell lines when exposed to the proteasome inhibitors LU-102 or NC-001
All data are reported as EC_{50} ± S.D. of triplicate assays.

Inhibitor Toxicity	Subunit Expression			Activities			Catalytic Signature		
	β2 (TL)	β1 (CaL)	β5 (ChL)	TL	CaL	ChL	TL/ChL	CaL/ChL	TL/CaL
LU-102	-0.05	-0.71	0.14	0.20	-0.83	-0.80	0.99	0.82	0.72
NC-001	-0.35	-0.69	-0.16	-0.13	-0.83	-0.95	0.82	0.96	0.45

Table 4.3: Correlation between proteasome activity, catalytic signatures, and subunit expression with site-specific inhibitor toxicity

Data are reported as the average of Pearson's, Spearman's, and Kendall's correlation coefficients. A coefficient equal to 1 indicates positive correlation, equal to 0 indicates no correlation, and equal to -1 indicates negative correlation. A correlation coefficient greater than or equal to 0.89 (or less than or equal to -0.89) indicates statistically significant correlation with 99% confidence.

Inhibitor Toxicity	Correlation Coefficient	Subunit Expression		
		β2 (TL)	β1 (CaL)	β5 (ChL)
LU-102	Pearson's	-0.012	-0.760	0.007
	Spearman's	-0.086	-0.771	0.200
	Kendall's	-0.067	-0.600	0.200
NC-001	Pearson's	-0.297	-0.710	-0.208
	Spearman's	-0.429	-0.771	-0.200
	Kendall's	-0.333	-0.600	-0.067
Bortezomib	Pearson's	-0.002	-0.834	-0.196
	Spearman's	0.143	-0.657	0.314
	Kendall's	0.067	-0.467	0.333
Carfilzomib	Pearson's	-0.278	-0.851	-0.035
	Spearman's	-0.543	-0.886	-0.143
	Kendall's	-0.467	-0.733	-0.200

Table 4.4: Correlation between proteasome subunit expression and inhibitor toxicity
Data are reported as the correlation coefficient for each correlation test. A coefficient equal to 1 indicates positive correlation, equal to 0 indicates no correlation, and equal to -1 indicates negative correlation. A correlation coefficient greater than or equal to 0.89 (or less than or equal to -0.89) indicates statistically significant correlation with 99% confidence.

Inhibitor Toxicity	Correlation Coefficient	Activity		
		TL	CaL	ChL
LU-102	Pearson's	0.185	-0.859	-0.795
	Spearman's	0.200	-0.886	-0.886
	Kendall's	0.200	-0.733	-0.733
NC-001	Pearson's	-0.118	-0.925	-0.848
	Spearman's	-0.200	-0.829	-1.000
	Kendall's	-0.067	-0.733	-1.000
Bortezomib	Pearson's	0.093	-0.628	-0.509
	Spearman's	0.314	-0.714	-0.771
	Kendall's	0.333	-0.600	-0.600
Carfilzomib	Pearson's	0.043	-0.589	-0.505
	Spearman's	-0.143	-0.600	-0.771
	Kendall's	-0.200	-0.333	-0.600

Table 4.5: Correlation between proteasome activity and inhibitor toxicity
Data are reported as the correlation coefficient for each correlation test. A coefficient equal to 1 indicates positive correlation, equal to 0 indicates no correlation, and equal to -1 indicates negative correlation. A correlation coefficient greater than or equal to 0.89 (or less than or equal to -0.89) indicates statistically significant correlation with 99% confidence.

Proteasome Subunit Expression	Correlation Coefficient	Activity		
		TL	CaL	ChL
β1	Pearson	-	0.429	-
	Spearman	-	0.600	-
	Kendall	-	0.333	-
β2	Pearson	0.900	-	-
	Spearman	0.829	-	-
	Kendall	0.733	-	-
β5	Pearson	-	-	-0.164
	Spearman	-	-	0.200
	Kendall	-	-	0.067

Table 4.6: Correlation between proteasome activity and subunit expression
Data are reported as the correlation coefficient for each correlation test. A coefficient equal to 1 indicates positive correlation, equal to 0 indicates no correlation, and equal to -1 indicates negative correlation. A correlation coefficient greater than or equal to 0.89 (or less than or equal to -0.89) indicates statistically significant correlation with 99% confidence.

Inhibitor Toxicity	Correlation Coefficient	Catalytic signature		
		TL/ChL	CaL/ChL	TL/CaL
LU-102	Pearson's	0.979	0.851	0.776
	Spearman's	1.000	0.886	0.771
	Kendall's	1.000	0.733	0.600
NC-001	Pearson's	0.857	0.892	0.583
	Spearman's	0.886	1.000	0.429
	Kendall's	0.733	1.000	0.333
Bortezomib	Pearson's	0.910	0.733	0.674
	Spearman's	0.943	0.771	0.829
	Kendall's	0.867	0.600	0.733
Carfilzomib	Pearson's	0.744	0.722	0.499
	Spearman's	0.771	0.771	0.429
	Kendall's	0.600	0.600	0.200

Table 4.7: Correlation between proteasome catalytic signatures and inhibitor toxicity
Data are reported as the correlation coefficient for each correlation test. A coefficient equal to 1 indicates positive correlation, equal to 0 indicates no correlation, and equal to -1 indicates negative correlation. A correlation coefficient greater than or equal to 0.89 (or less than or equal to -0.89) indicates statistically significant correlation with 99% confidence.

Cell Line	75 nM LU-102	2000 nM LU-102	150 nM NC-001	2000 nM NC-001
Farage	12 ± 0.4	N.D.	4.5 ± 0.2	N.D.
HL60	4.7 ± 0.2	N.D.	1.1 ± 0.1	6.0 ± 0.2
HeLa	1.1 ± 0.3	9.3 ± 0.2	1.1 ± 0.1	2.8 ± 0.1
A549	1.7 ± 0.1	7.1 ± 0.4	2.1 ± 0.1	2.1 ± 0.1
DU145	1.5 ± 0.1	5.0 ± 0.3	1.3 ± 0.2	1.3 ± 0.1
MCF7	1.3 ± 0.2	1.8 ± 0.2	1.1 ± 0.2	1.1 ± 0.2

Table 4.8: Synergy of site-specific inhibitors with bortezomib
Fold decrease in EC_{50} of cell viability of cancer cell lines when exposed to bortezomib ± NC-001 or LU-102. All data are reported as fold changes ± S.D. of triplicate assays. N.D. = not determined.

Cell Line	75 nM LU-102	2000 nM LU-102	150 nM NC-001	2000 nM NC-001
Farage	15 ± 0.1	N.D.	8.0 ± 0.1	N.D.
HL60	6.5 ± 0.1	N.D.	1.0 ± 0.1	12 ± 0.1
HeLa	1.5 ± 0.1	17 ± 0.1	1.3 ± 0.3	7.0 ± 0.3
A549	1.7 ± 0.1	12 ± 0.1	2.1 ± .02	9.7 ± 0.1
DU145	1.2 ± 0.1	5.1 ± 0.4	1.2 ± 0.1	6.1 ± 0.1
MCF7	1.2 ± 0.1	2.2 ± 0.2	1.2 ± 0.1	2.4 ± 0.2

Table 4.9: Synergy of site-specific inhibitors with carfilzomib
Fold decrease in EC_{50} of cell viability of cancer cell lines when exposed to carfilzomib ± NC-001 or LU-102. All data are reported as fold changes ± S.D. of triplicate assays. N.D. = not determined.

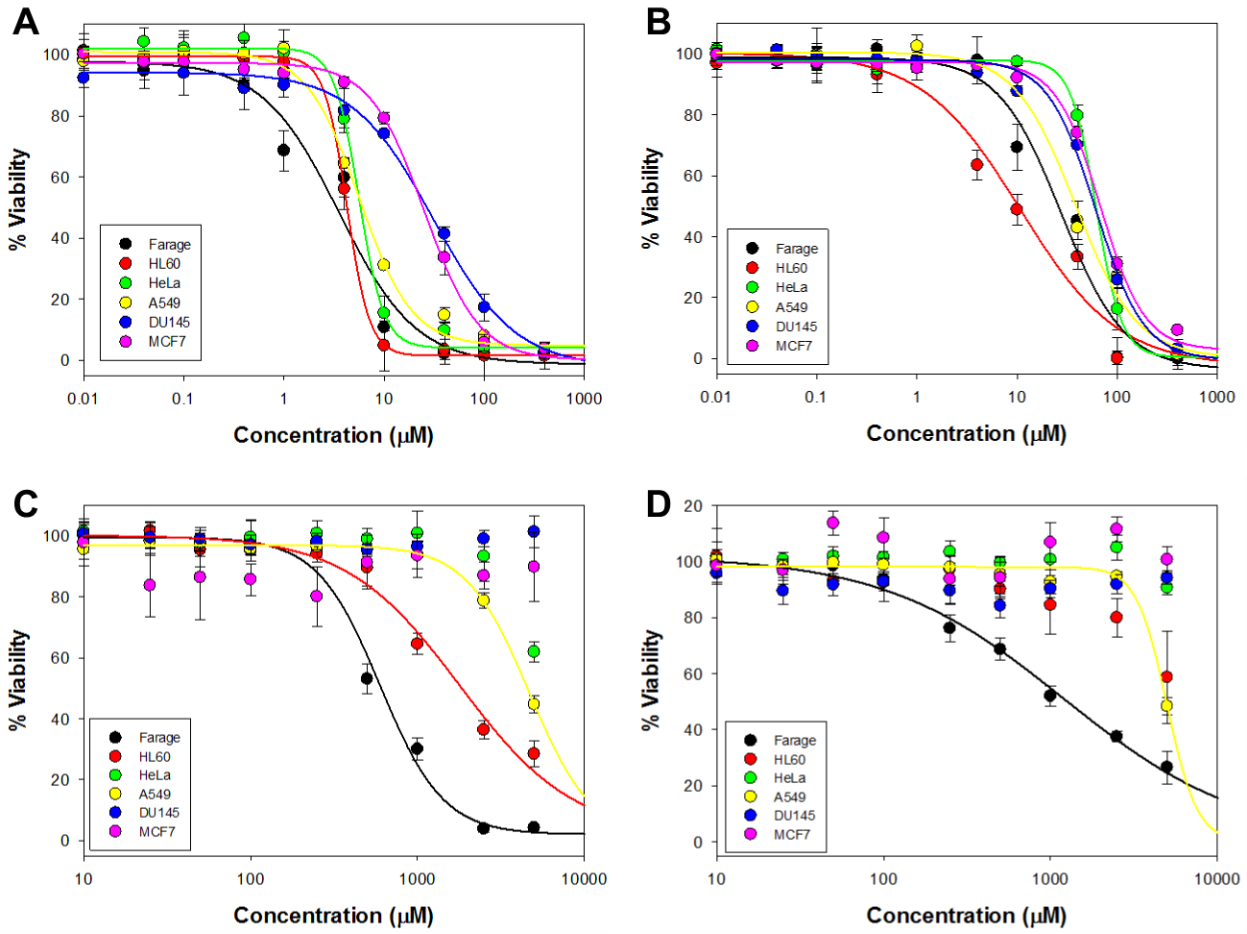

Figure 4.1: Dose-response curves of cell viability of cancer cell lines when exposed to the proteasome inhibitors
Inhibitors: (*A*) bortezomib, (*B*) carfilzomib, (*C*) LU-102, and (*D*) NC-001. Cell lines: Farage (black), HL60 (red), HeLa (green), A549 (yellow), DU145 (blue), and MCF7 (pink). All assays were run in triplicate.

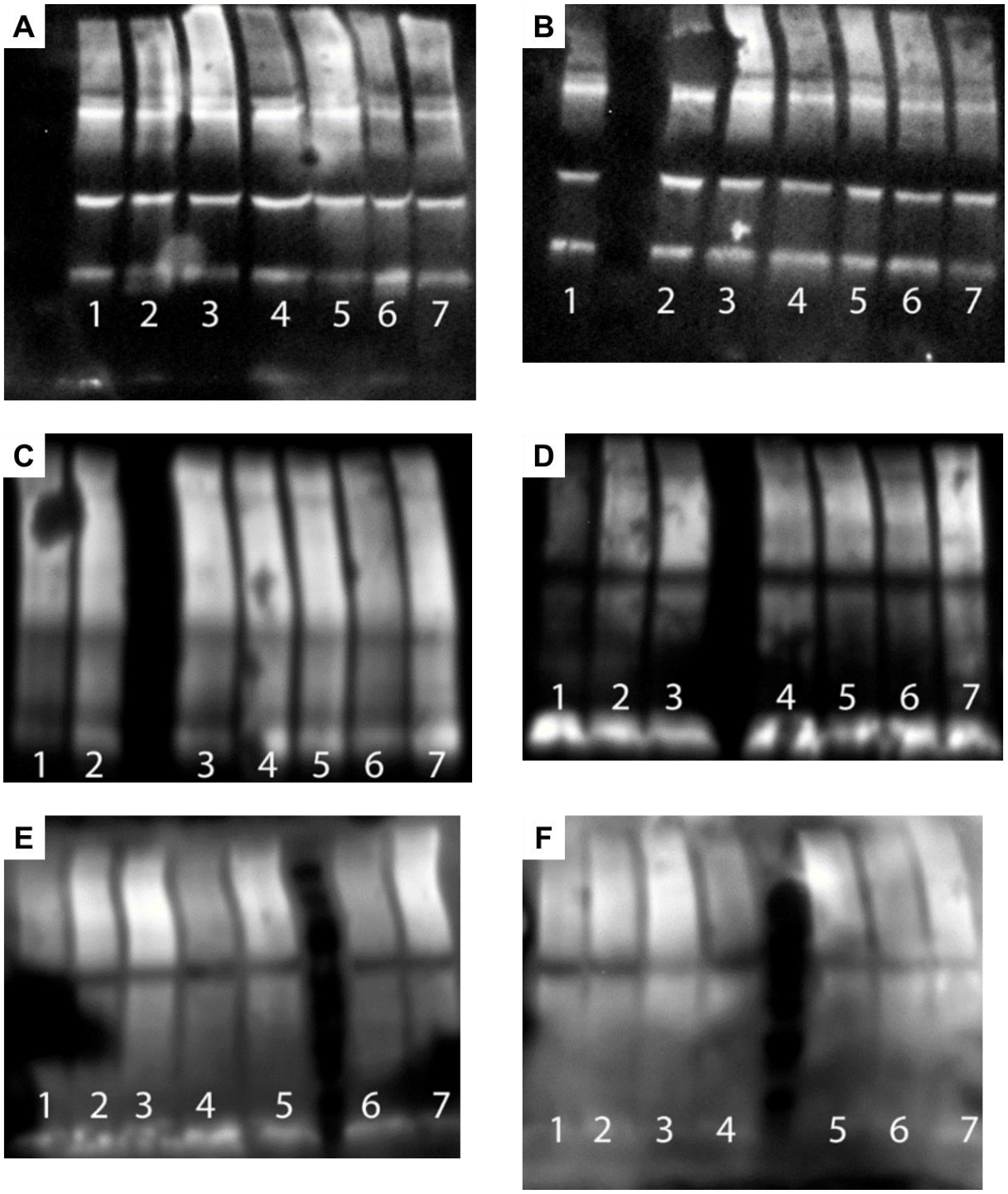

Figure 4.2: Western blots for total ubiquitination in cancer cell lines ± proteasome inhibitors

Lane 1: no inhibitor, lane 2: 5 nM bortezomib, lane 3: 50 nM carfilzomib, lane 4: 500 nM LU-102, lane 5: 5000 nM LU-102, lane 6: 500 nM NC-001, lane 7: 5000 nM NC-001. Cell lines: (*A*) Farage, (*B*) HL60, (*C*) HeLa, (*D*) A549, (*E*) DU145, and (*F*) MCF7. Cells were treated ± proteasome inhibitors for 6 h before lysis.

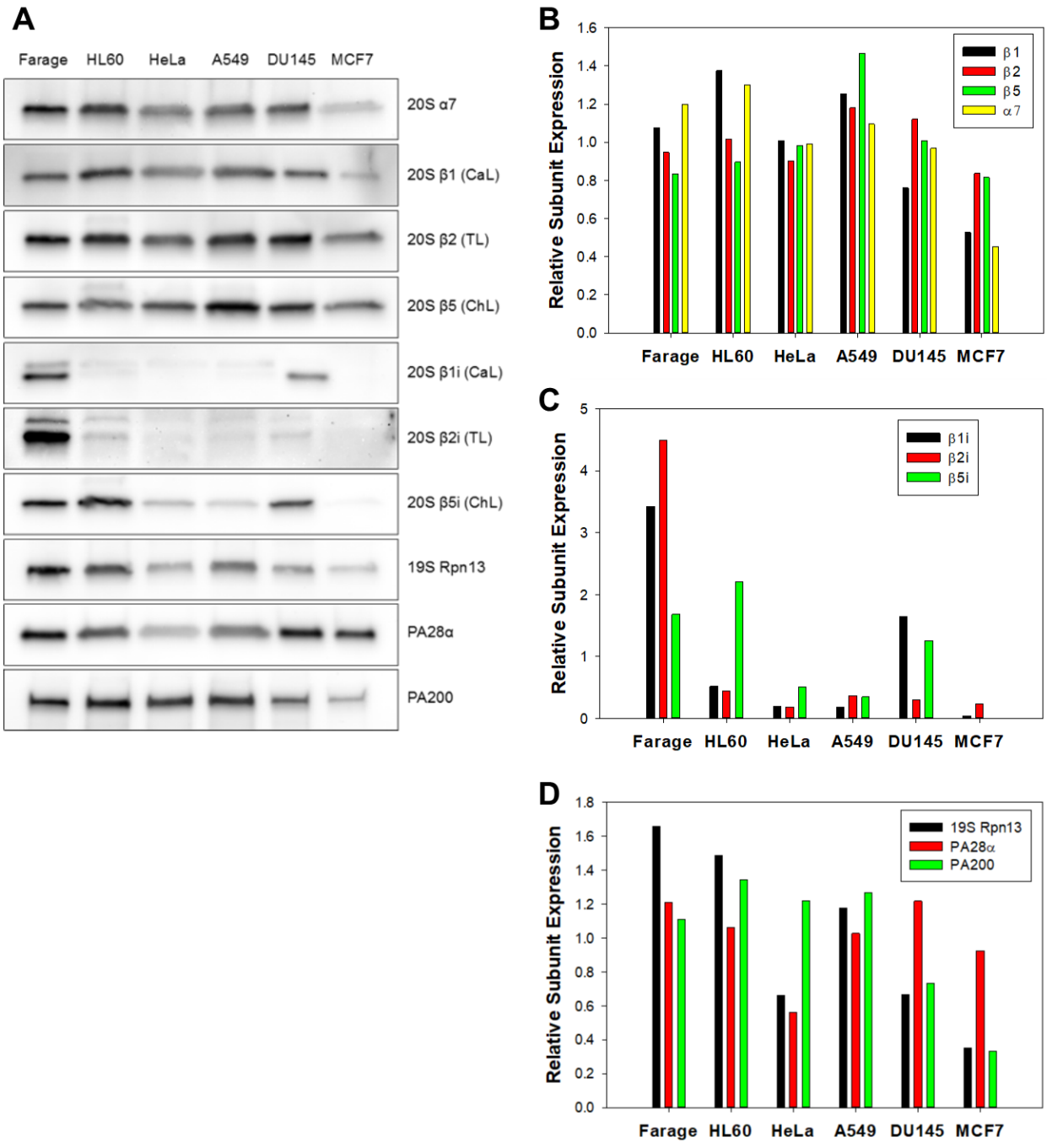

Figure 4.3: Proteasome protein expression from various cancer cell lines
(*A*) Western blots of several proteasome subunits from the core particle and regulatory particles. (*B-D*) Quantification of western blots for (*B*) regular 20S core particle subunits, (*C*) immunoproteasome 20S core particle subunits, and (*D*) different regulatory particle subunits. Quantification is represented relative to the average expression (across all cell lines) of each subunit.

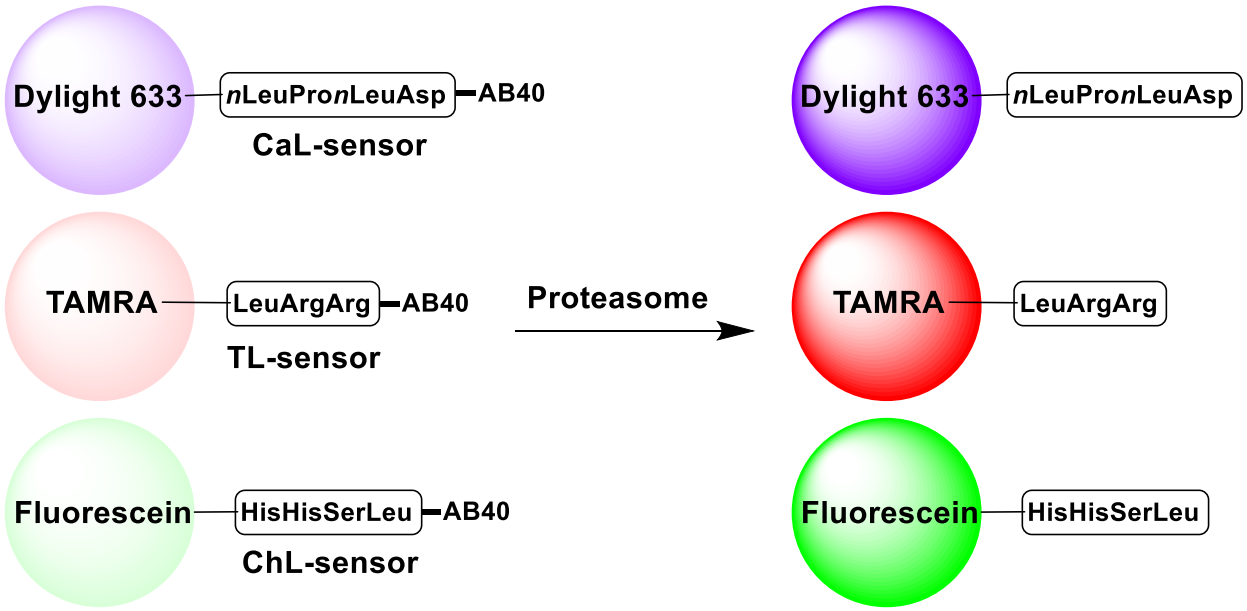

Figure 4.4: Schematic of proteasome sensors
Full chemical structures can be found in Priestman *et al*. (213).

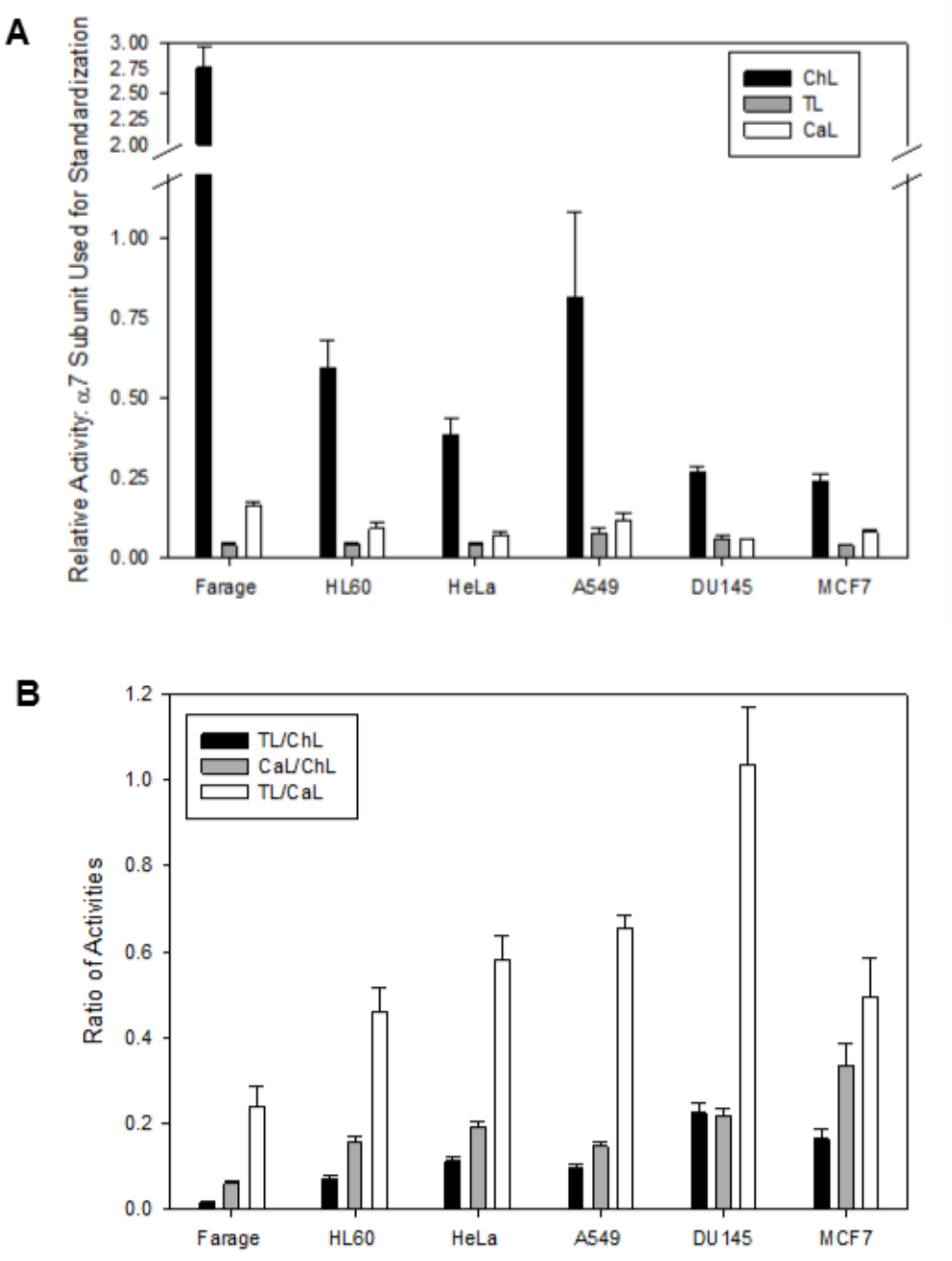

Figure 4.5: Proteasome catalytic activity from various cancer cell lines
(*A*) Site-specific activity of proteasome from cancer cell lines with ChL (black), TL (grey) and CaL (white) activity sensors. Activity is represented as relative activity compared to the amount of α7 proteasome subunit present in each sample. (*B*) Proteasome catalytic signatures, ratio of TL:ChL (black), CaL:ChL (grey), and TL:CaL (white) vary in different cancer cell lines. All data represents the average ± S.D. of 4-5 independently purified samples.

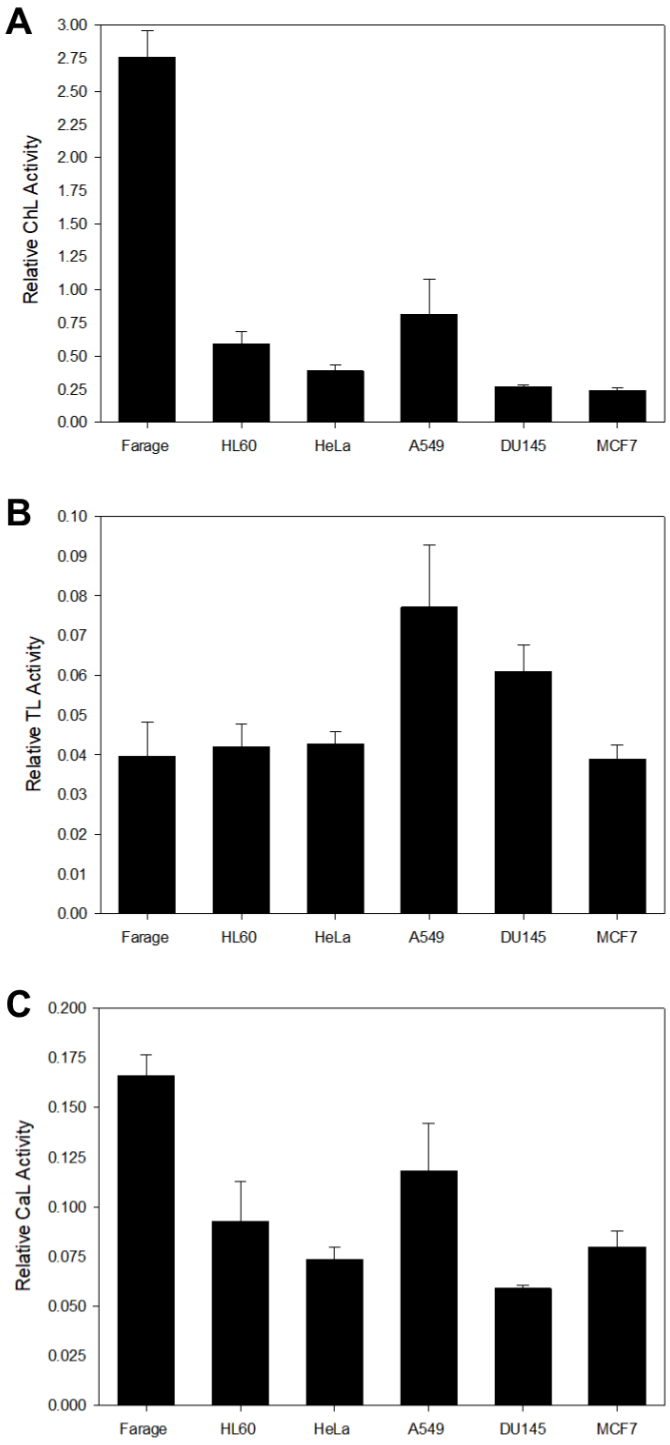

Figure 4.6: Proteasome catalytic activities
Site-specific ChL (*A*), TL (*B*), and CaL (*C*) proteasome activities from cancer cells. Activity is represented as relative activity standardized to the amount of α7 proteasome subunit present in each sample. Data represent the average ± S.D. of 4-5 proteasome preparations and triplicate assays for each preparation.

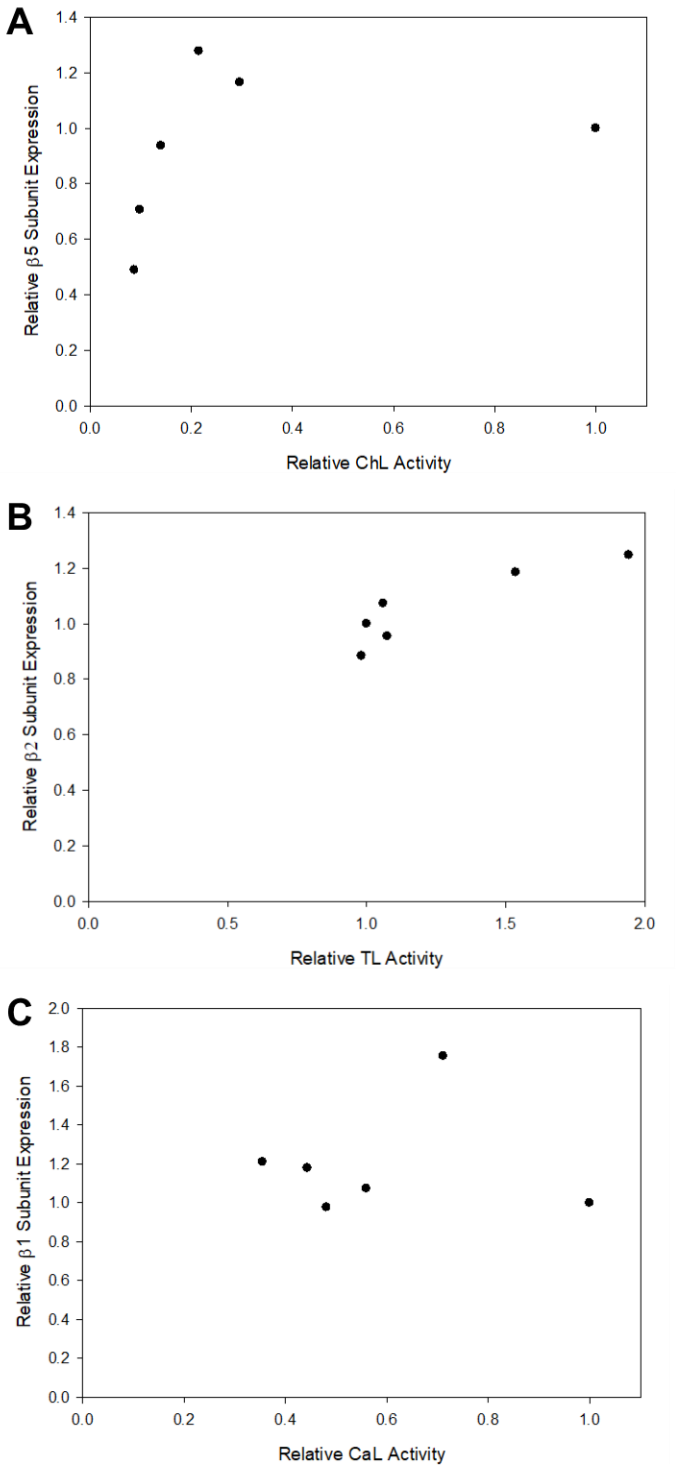

Figure 4.7: Lack of correlation between proteasome activity and subunit expression
Comparison of site-specific ChL (*A*), TL (*B*), and CaL (*C*) proteasome activities to β5 (*A*), β2 (*B*), and β1 (*C*) subunit expression. All data are shown relative to the Farage proteasome preparations.

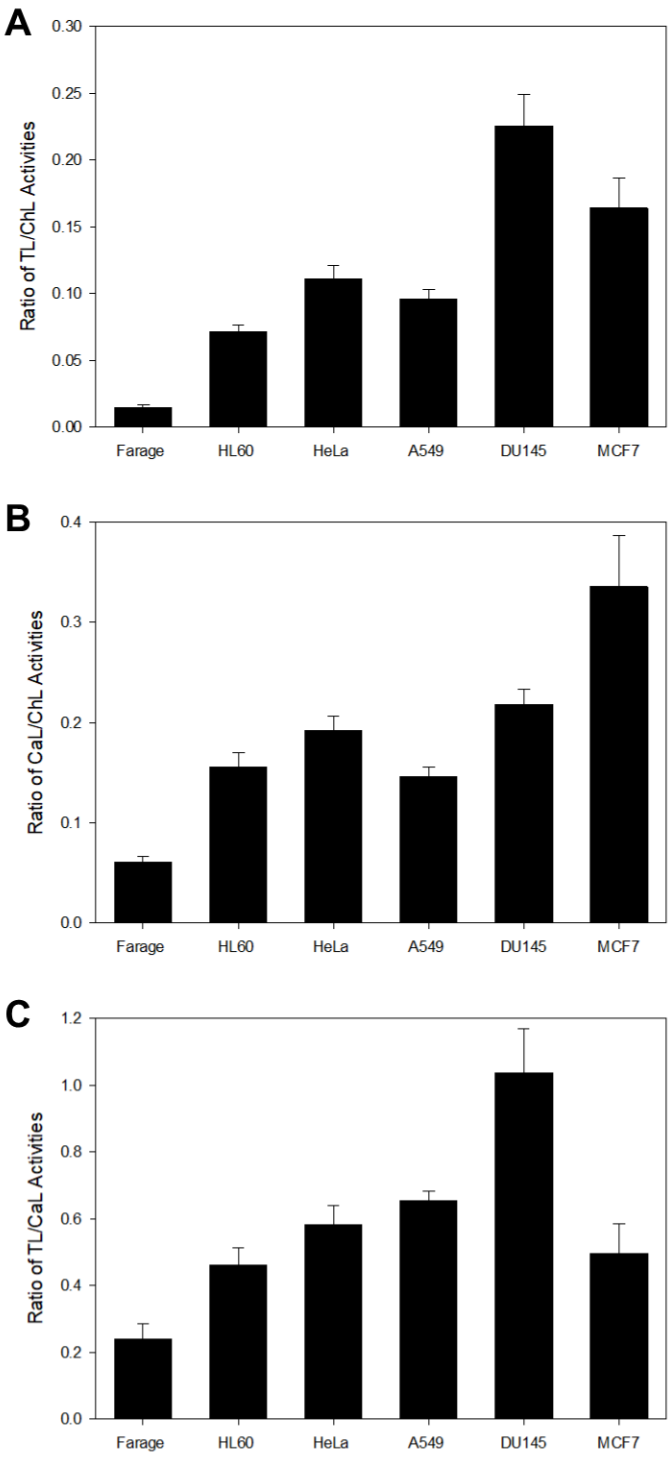

Figure 4.8: Proteasome catalytic ratios
Ratios of TL:ChL (*A*), CaL:ChL (*B*), and TL:CaL (*C*) proteasome activities vary in different cancer cell lines. Data represents the average ± S.D. of 4-5 proteasome preparations and triplicate assays for each preparation.

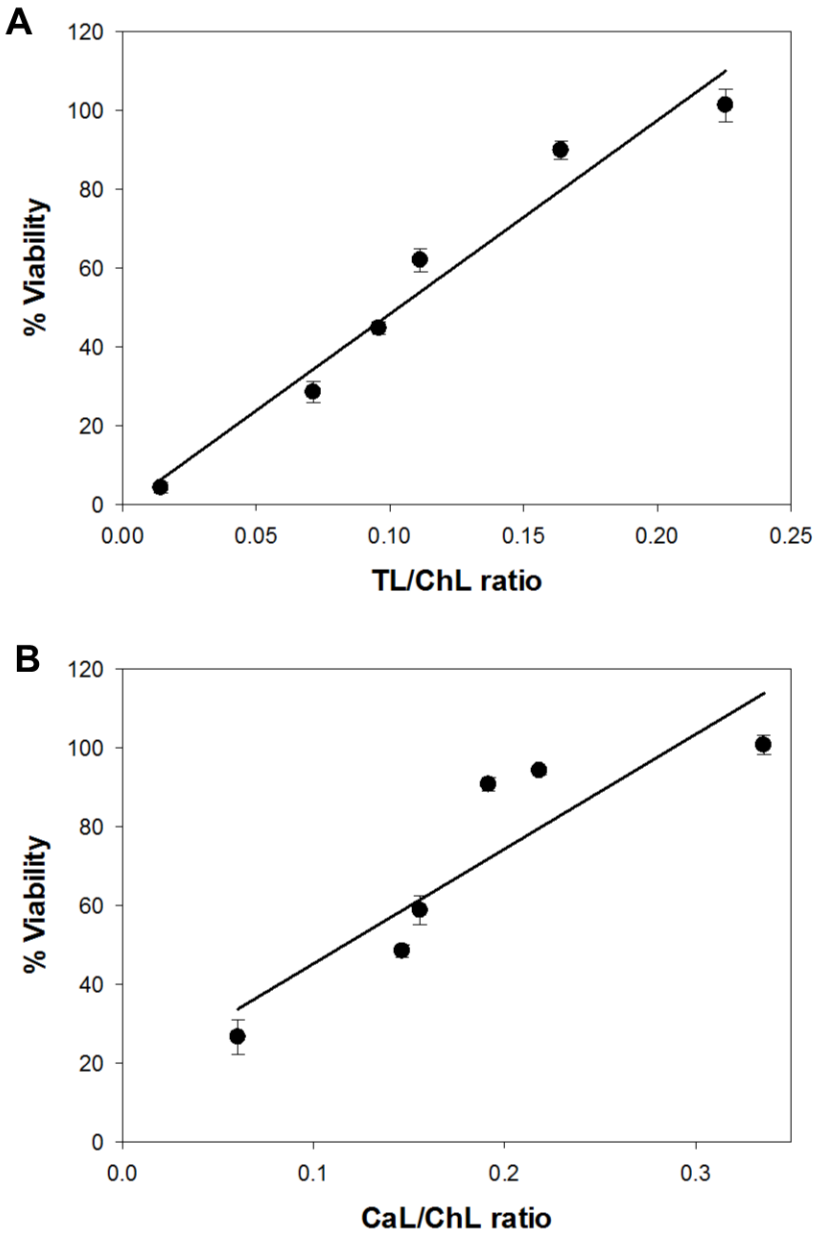

Figure 4.9: Correlation of proteasome inhibitor sensitivity vs. catalytic activity ratios
(*A*) Graph of TL inhibitor viability (percent viability of cells after treatment with 5 μM LU-102) vs. TL/ChL proteasome activity ratio. (*B*) Graph of CaL inhibitor viability (percent viability of cells after treatment with 5 μM NC-001) vs. CaL/ChL proteasome activity ratio.

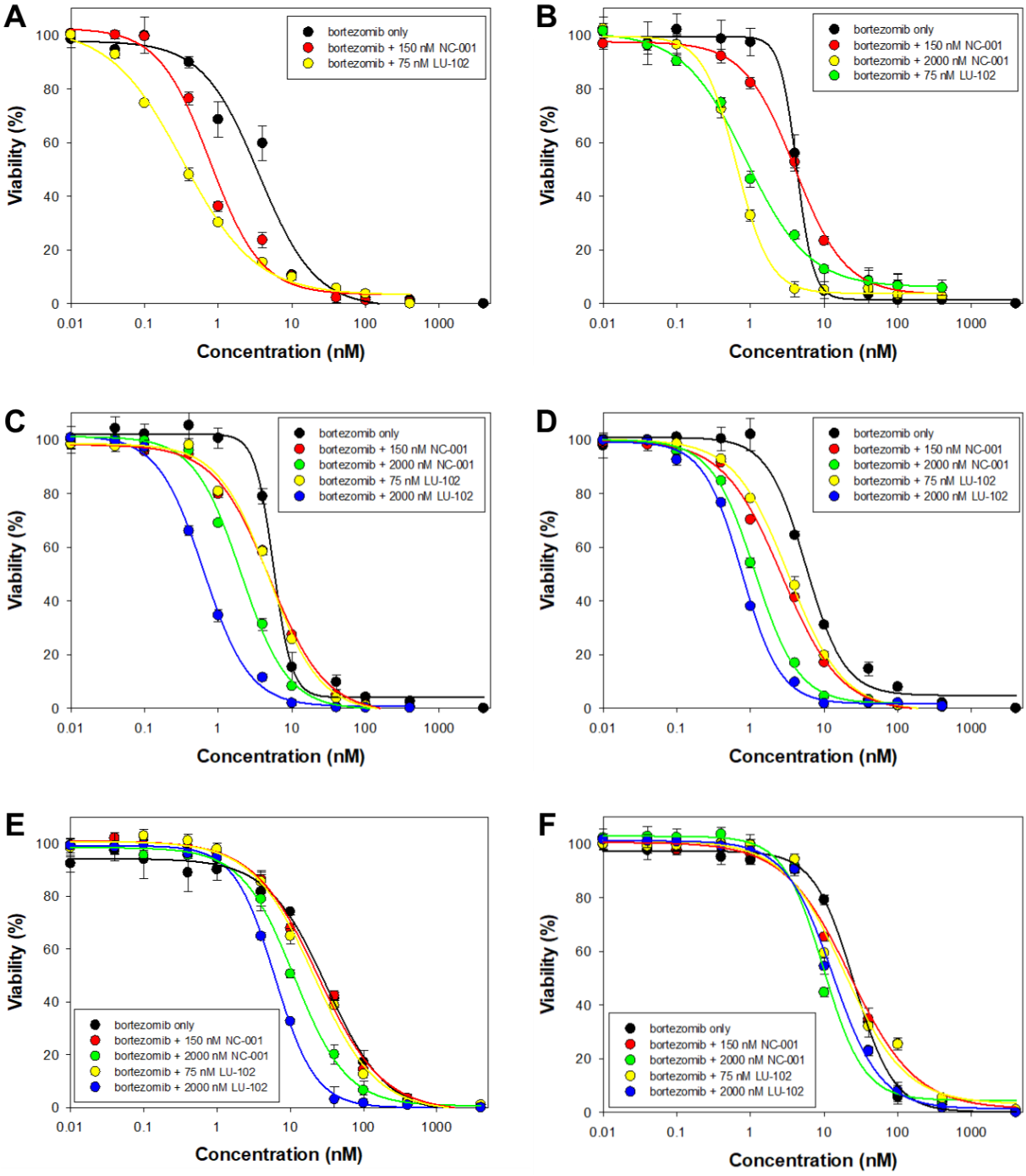

Figure 4.10: Synergy between site-specific proteasome inhibitors and bortezomib
Dose-response curves of cell viability of cancer cell lines when exposed to bortezomib (black) ± NC-001 (red = 150 nM, green = 2000 nM) or LU-102 (yellow = 75 nM, blue = 2000 nM). Cell lines: (*A*) Farage, (*B*) HL60, (*C*) HeLa, (*D*) A549, (*E*) DU145, and (*F*) MCF7. All assays were run in triplicate.

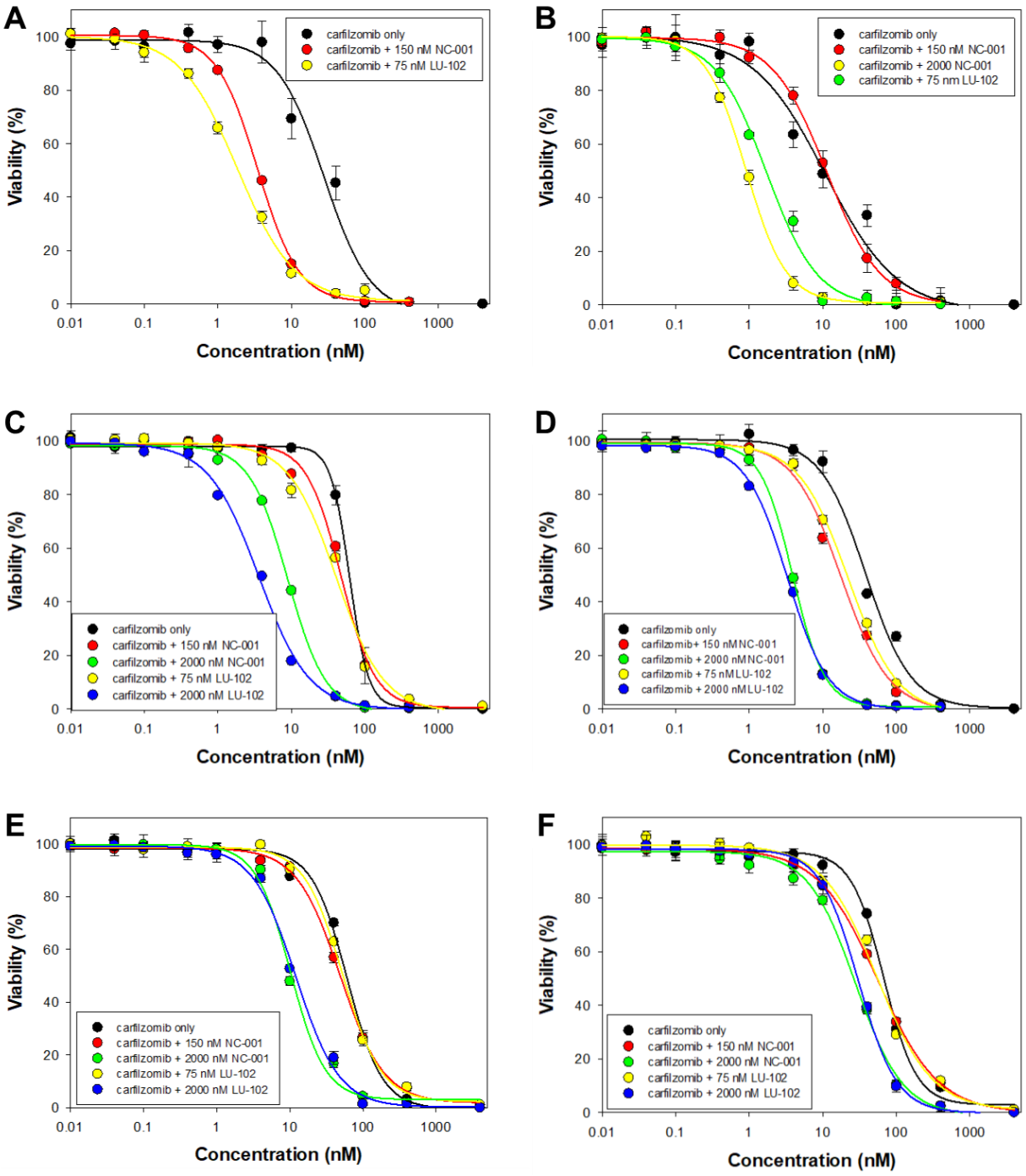

Figure 4.11: Synergy between site-specific proteasome inhibitors and carfilzomib
Dose-response curves of cell viability of cancer cell lines when exposed to carfilzomib (black) ± NC-001 (red = 150 nM, green = 2000 nM) or LU-102 (yellow = 75 nM, blue = 2000 nM). Cell lines: (*A*) Farage, (*B*) HL60, (*C*) HeLa, (*D*) A549, (*E*) DU145, and (*F*) MCF7. All assays were run in triplicate.

CHAPTER 5: CONCLUDING REMARKS

5.1 Summary

Diffuse large B-cell lymphoma (DLBCL) is a heterogeneous disease, with at least one-third of its patients not responding to the current chemotherapy regimen, R-CHOP. By gene expression profiling, patients with DLBCL can be categorized into two clinically relevant subtypes: activated B-cell (ABC) DLBCL and germinal center B-cell (GCB). Patients with ABC DLBCL have a worse prognosis, and are defined by chronic, overactive signaling through the B-cell receptor and NF-κB pathways. These pathways are heavily dependent upon the Src family kinases (SFKs) for their signaling, and the NF-κB pathway is also dependent upon the proteasome for its signaling. The purpose of my thesis work was to identify additional therapeutic targets for the treatment of DLBCL, namely the ABC subtype, and we chose to focus on the SFKs and the proteasome as potential drug targets for this disease.

In Chapter 2, we examined the effects of the SFK inhibitor dasatinib in a panel of ABC and GCB DLBCL cell lines, and found that the ABC DLBCL cell lines are much more sensitive to dasatinib than the GCB DLBCL cell lines. However, using multiplexed inhibitor bead coupled to mass spectrometry (MIB/MS) kinome profiling and western blot analysis, we found that both subtypes display inhibition of the SFKs in response to dasatinib after both short- and long-term treatment. The MIB/MS analyses revealed several cell cycle kinases, including CDK4, CDK6, and the Aurora kinases, are downregulated by dasatinib treatment in the ABC DLBCL subtype, but not in the GCB DLBCL subtype. The present findings have important

implications for the clinical use of dasatinib for the treatment of ABC DLBCL, either alone or in combination with other agents.

In Chapter 3, we examined the effects of the SFK inhibitor dasatinib on the proteasome in the same panel of DLBCL cell lines. Using a set of novel peptide probes for the proteasome's three catalytic activities, we found that treatment with dasatinib results in reduced proteasome activity in the ABC DLBCL cell lines tested, but had no effect on the GCB DLBCL cell lines. Furthermore, this reduction in activity is accompanied by a reduction in the amount of 19S regulatory particle in isolated proteasomes. However, the total levels of 19S regulatory particle are unchanged in whole lysates, indicating either a dissociation or disrupted assembly between the proteasome 20S core particle and 19S regulatory particle. Furthermore, phosphoproteomics analyses showed several proteasome subunits and proteasome-related proteins to have changes in phosphorylation in response to dasatinib treatment. This study demonstrates a potential role for the SFKs in regulating the proteasome, and hints at the proteasome being a potential target for the treatment of ABC DLBCL.

In Chapter 4, we explored the utility of site-specific inhibitors of the proteasome's trypsin-like (TL) and caspase-like (CaL) activities in a variety of cell lines. We found that, while proteasome subunit expression or total activity does not correlate with proteasome activity, the TL/ChL and CaL/ChL ratios of proteasome activity correlate with sensitivity to TL and CaL inhibitors, respectively. Furthermore, the combination of the TL or CaL site-specific inhibitors with bortezomib or carfilzomib is synergistic in all cell lines examined. This suggests that the proteasome's catalytic signature is useful for predicting sensitivity to site-specific inhibitors of the proteasome, and that dual inhibition of proteasome subunits may be a viable option for the treatment of both hematological and solid malignancies. Moreover, the two cell lines that were

most sensitive to the site-specific proteasome inhibitors were hematological cell lines, with the DLBCL cell line Farage being the most sensitive overall. It is possible that site-specific proteasome inhibition might be a viable treatment option for DLBCL.

These findings have important implications for the use of dasatinib for the treatment of ABC DLBCL, either alone or in combination with other agents. In addition, the proteasome also appears to be a promising target for the treatment of DLBCL, potentially for both subtypes.

5.2 Future Directions

The studies discussed in Chapter 2 lay the groundwork for potential uses of the SFK inhibitor dasatinib for the treatment of ABC DLBCL. However, there is much that still remains unclear. We have demonstrated that ABC DLBCL cell lines are more sensitive to dasatinib than GCB DLBCL cell lines. Treatment with dasatinib inhibits the SFKs in both ABC and GCB DLBCL cell lines, and inhibits several cell cycle kinases in ABC DLBCL cell lines. However, we do not know whether the inhibition of cell cycle kinases is a cause of the dasatinib sensitivity observed in ABC DLBCL cell lines or if it is a result of the dasatinib sensitivity. Do the cells die because the cell cycle kinases are inhibited, or are the cell cycle kinases inhibited because the cells are dying? Furthermore, we are still unsure of the mechanism that is leading to inhibition of the cell cycle kinases. It is possible that they are inhibited due to inhibition of signaling pathways downstream of the SFKs, but it is also possible that the cell cycle kinases are inhibited due to off-target effects of dasatinib. Future studies should explore this mechanism.

In Chapter 3, we highlighted a potential role for the SFKs as regulators of the proteasome, but more studies are needed to confirm these results. Most importantly, either immunoprecipitation or Native-PAGE techniques need to be optimized in order to confirm the

dissociation (or failure to associate) between the proteasome 20S core particle and 19S regulatory particle in response to dasatinib treatment. Furthermore, additional studies are needed to further elucidate the mechanism by which dasatinib disrupts proteasome activity. Some focus could be paid to the proteasome inhibitory protein PI31, the proteasome assembly chaperone, PSMG1, and the proteasome 19S subunit Rpn2, as these showed changes in phosphorylation in response to dasatinib treatment.

In Chapter 4, we identified a method for predicting sensitivity to inhibitors of the β1 (CaL) and β2 (TL) proteasome subunits. Moreover, we found that the two hematological cell lines we tested had the highest sensitivity to the site-specific inhibitors. In particular, the DLBCL cell line was the most sensitive. Future studies should assess the sensitivity of our panel of seven DLBCL cell lines to these site-specific inhibitors, and assess potential differences in sensitivity between the ABC and GCB DLBCL subtypes. We already know one GCB DLBCL cell line is very responsive to these inhibitors. Will the ABC DLBCL cell lines be more sensitive?

The overall goal of this thesis work was to identify additional therapeutic agents for the treatment of DLBCL, and particularly the ABC DLBCL subtype. We have found a lot of potential for the SFK inhibitor dasatinib, as well as potential for the site-specific proteasome inhibitors. The most important future studies will entail testing these inhibitors in *in vivo* models of lymphoma, as well as human patient samples. These compounds could be tested alone, but should also be tested as combination therapies with the standard of care for DLBCL, R-CHOP. Synergy studies between the SFK and proteasome inhibitors could also be explored. Our hope is that one day, dasatinib and the site-specific proteasome inhibitors will become a routine part of chemotherapy for the patients who will truly benefit from their use.

REFERENCES

1. Siegel, R. L., Miller, K. D., and Jemal, A. (2017) Cancer Statistics, 2017. *CA Cancer J Clin* **67**, 7-30

2. Shankland, K. R., Armitage, J. O., and Hancock, B. W. (2012) Non-Hodgkin lymphoma. *Lancet* **380**, 848-857

3. Rogers, B. B. (2006) Overview of non-Hodgkin's lymphoma. *Semin Oncol Nurs* **22**, 67-72

4. Alizadeh, A. A., Eisen, M. B., Davis, R. E., Ma, C., Lossos, I. S., Rosenwald, A., Boldrick, J. C., Sabet, H., Tran, T., Yu, X., Powell, J. I., Yang, L., Marti, G. E., Moore, T., Hudson, J., Jr., Lu, L., Lewis, D. B., Tibshirani, R., Sherlock, G., Chan, W. C., Greiner, T. C., Weisenburger, D. D., Armitage, J. O., Warnke, R., Levy, R., Wilson, W., Grever, M. R., Byrd, J. C., Botstein, D., Brown, P. O., and Staudt, L. M. (2000) Distinct types of diffuse large B-cell lymphoma identified by gene expression profiling. *Nature* **403**, 503-511

5. Rosenwald, A., Wright, G., Chan, W. C., Connors, J. M., Campo, E., Fisher, R. I., Gascoyne, R. D., Muller-Hermelink, H. K., Smeland, E. B., Giltnane, J. M., Hurt, E. M., Zhao, H., Averett, L., Yang, L., Wilson, W. H., Jaffe, E. S., Simon, R., Klausner, R. D., Powell, J., Duffey, P. L., Longo, D. L., Greiner, T. C., Weisenburger, D. D., Sanger, W. G., Dave, B. J., Lynch, J. C., Vose, J., Armitage, J. O., Montserrat, E., Lopez-Guillermo, A., Grogan, T. M., Miller, T. P., LeBlanc, M., Ott, G., Kvaloy, S., Delabie, J., Holte, H., Krajci, P., Stokke, T., Staudt, L. M., and Lymphoma/Leukemia Molecular Profiling, P. (2002) The use of molecular profiling to predict survival after chemotherapy for diffuse large-B-cell lymphoma. *N Engl J Med* **346**, 1937-1947

6. Lenz, G., Wright, G., Dave, S. S., Xiao, W., Powell, J., Zhao, H., Xu, W., Tan, B., Goldschmidt, N., Iqbal, J., Vose, J., Bast, M., Fu, K., Weisenburger, D. D., Greiner, T. C., Armitage, J. O., Kyle, A., May, L., Gascoyne, R. D., Connors, J. M., Troen, G., Holte, H., Kvaloy, S., Dierickx, D., Verhoef, G., Delabie, J., Smeland, E. B., Jares, P., Martinez, A., Lopez-Guillermo, A., Montserrat, E., Campo, E., Braziel, R. M., Miller, T. P., Rimsza, L. M., Cook, J. R., Pohlman, B., Sweetenham, J., Tubbs, R. R., Fisher, R. I., Hartmann, E., Rosenwald, A., Ott, G., Muller-Hermelink, H. K., Wrench, D., Lister, T. A., Jaffe, E. S., Wilson, W. H., Chan, W. C., Staudt, L. M., and Lymphoma/Leukemia Molecular Profiling, P. (2008) Stromal gene signatures in large-B-cell lymphomas. *N Engl J Med* **359**, 2313-2323

7. Coiffier, B. (2002) Rituximab in combination with CHOP improves survival in elderly patients with aggressive non-Hodgkin's lymphoma. *Semin Oncol* **29**, 18-22

8. Sehn, L. H., Donaldson, J., Chhanabhai, M., Fitzgerald, C., Gill, K., Klasa, R., MacPherson, N., O'Reilly, S., Spinelli, J. J., Sutherland, J., Wilson, K. S., Gascoyne, R. D., and Connors, J. M. (2005) Introduction of combined CHOP plus rituximab therapy dramatically improved outcome of diffuse large B-cell lymphoma in British Columbia. *J Clin Oncol* **23**, 5027-5033

9. Davis, R. E., Ngo, V. N., Lenz, G., Tolar, P., Young, R. M., Romesser, P. B., Kohlhammer, H., Lamy, L., Zhao, H., Yang, Y., Xu, W., Shaffer, A. L., Wright, G., Xiao, W., Powell, J., Jiang, J. K., Thomas, C. J., Rosenwald, A., Ott, G., Muller-Hermelink, H. K., Gascoyne, R. D., Connors, J. M., Johnson, N. A., Rimsza, L. M., Campo, E., Jaffe, E. S., Wilson, W. H., Delabie, J., Smeland, E. B., Fisher, R. I., Braziel, R. M., Tubbs, R. R., Cook, J. R., Weisenburger, D. D.,

Chan, W. C., Pierce, S. K., and Staudt, L. M. (2010) Chronic active B-cell-receptor signalling in diffuse large B-cell lymphoma. *Nature* **463**, 88-92

10. Davis, R. E., Brown, K. D., Siebenlist, U., and Staudt, L. M. (2001) Constitutive nuclear factor kappaB activity is required for survival of activated B cell-like diffuse large B cell lymphoma cells. *J Exp Med* **194**, 1861-1874

11. Bu, R., Hussain, A. R., Al-Obaisi, K. A., Ahmed, M., Uddin, S., and Al-Kuraya, K. S. (2014) Bortezomib inhibits proteasomal degradation of IkappaBalpha and induces mitochondrial dependent apoptosis in activated B-cell diffuse large B-cell lymphoma. *Leuk Lymphoma* **55**, 415-424

12. Dunleavy, K., Pittaluga, S., Czuczman, M. S., Dave, S. S., Wright, G., Grant, N., Shovlin, M., Jaffe, E. S., Janik, J. E., Staudt, L. M., and Wilson, W. H. (2009) Differential efficacy of bortezomib plus chemotherapy within molecular subtypes of diffuse large B-cell lymphoma. *Blood* **113**, 6069-6076

13. Younes, A., Thieblemont, C., Morschhauser, F., Flinn, I., Friedberg, J. W., Amorim, S., Hivert, B., Westin, J., Vermeulen, J., Bandyopadhyay, N., de Vries, R., Balasubramanian, S., Hellemans, P., Smit, J. W., Fourneau, N., and Oki, Y. (2014) Combination of ibrutinib with rituximab, cyclophosphamide, doxorubicin, vincristine, and prednisone (R-CHOP) for treatment-naive patients with CD20-positive B-cell non-Hodgkin lymphoma: a non-randomised, phase 1b study. *Lancet Oncol* **15**, 1019-1026

14. Cheng, S., Coffey, G., Zhang, X. H., Shaknovich, R., Song, Z., Lu, P., Pandey, A., Melnick, A. M., Sinha, U., and Wang, Y. L. (2011) SYK inhibition and response prediction in diffuse large B-cell lymphoma. *Blood* **118**, 6342-6352

15. Nowakowski, G. S., LaPlant, B., Macon, W. R., Reeder, C. B., Foran, J. M., Nelson, G. D., Thompson, C. A., Rivera, C. E., Inwards, D. J., Micallef, I. N., Johnston, P. B., Porrata, L. F., Ansell, S. M., Gascoyne, R. D., Habermann, T. M., and Witzig, T. E. (2015) Lenalidomide combined with R-CHOP overcomes negative prognostic impact of non-germinal center B-cell phenotype in newly diagnosed diffuse large B-Cell lymphoma: a phase II study. *J Clin Oncol* **33**, 251-257

16. Robertson, M. J., Kahl, B. S., Vose, J. M., de Vos, S., Laughlin, M., Flynn, P. J., Rowland, K., Cruz, J. C., Goldberg, S. L., Musib, L., Darstein, C., Enas, N., Kutok, J. L., Aster, J. C., Neuberg, D., Savage, K. J., LaCasce, A., Thornton, D., Slapak, C. A., and Shipp, M. A. (2007) Phase II study of enzastaurin, a protein kinase C beta inhibitor, in patients with relapsed or refractory diffuse large B-cell lymphoma. *J Clin Oncol* **25**, 1741-1746

17. Younes, A., Romaguera, J., Fanale, M., McLaughlin, P., Hagemeister, F., Copeland, A., Neelapu, S., Kwak, L., Shah, J., de Castro Faria, S., Hart, S., Wood, J., Jayaraman, R., Ethirajulu, K., and Zhu, J. (2012) Phase I study of a novel oral Janus kinase 2 inhibitor, SB1518, in patients with relapsed lymphoma: evidence of clinical and biologic activity in multiple lymphoma subtypes. *J Clin Oncol* **30**, 4161-4167

18. Yahiaoui, A., Meadows, S. A., Sorensen, R. A., Cui, Z. H., Keegan, K. S., Brockett, R., Chen, G., Queva, C., Li, L., and Tannheimer, S. L. (2017) PI3Kdelta inhibitor idelalisib in combination with BTK inhibitor ONO/GS-4059 in diffuse large B cell lymphoma with acquired resistance to PI3Kdelta and BTK inhibitors. *PLoS One* **12**, e0171221

19. Wilson, W. H. (2013) Treatment strategies for aggressive lymphomas: what works? *Hematology Am Soc Hematol Educ Program* **2013**, 584-590

20. Amin, A. D., Peters, T. L., Li, L., Rajan, S. S., Choudhari, R., Puvvada, S. D., and Schatz, J. H. (2017) Diffuse large B-cell lymphoma: can genomics improve treatment options for a curable cancer? *Cold Spring Harb Mol Case Stud* **3**, a001719

21. Yeatman, T. J. (2004) A renaissance for SRC. *Nat Rev Cancer* **4**, 470-480

22. Thomas, S. M., and Brugge, J. S. (1997) Cellular functions regulated by Src family kinases. *Annu Rev Cell Dev Biol* **13**, 513-609

23. Brown, M. T., and Cooper, J. A. (1996) Regulation, substrates and functions of src. *Biochim Biophys Acta* **1287**, 121-149

24. Martin, G. S. (2001) The hunting of the Src. *Nat Rev Mol Cell Biol* **2**, 467-475

25. Parsons, S. J., and Parsons, J. T. (2004) Src family kinases, key regulators of signal transduction. *Oncogene* **23**, 7906-7909

26. Bolen, J. B., and Brugge, J. S. (1997) Leukocyte protein tyrosine kinases: potential targets for drug discovery. *Annu Rev Immunol* **15**, 371-404

27. Xu, W., Harrison, S. C., and Eck, M. J. (1997) Three-dimensional structure of the tyrosine kinase c-Src. *Nature* **385**, 595-602

28. Yamaguchi, H., and Hendrickson, W. A. (1996) Structural basis for activation of human lymphocyte kinase Lck upon tyrosine phosphorylation. *Nature* **384**, 484-489

29. Wheeler, D. L., Iida, M., and Dunn, E. F. (2009) The role of Src in solid tumors. *Oncologist* **14**, 667-678

30. Hecker, T. P., Grammer, J. R., Gillespie, G. Y., Stewart, J., Jr., and Gladson, C. L. (2002) Focal adhesion kinase enhances signaling through the Shc/extracellular signal-regulated kinase pathway in anaplastic astrocytoma tumor biopsy samples. *Cancer Res* **62**, 2699-2707

31. Abram, C. L., and Courtneidge, S. A. (2000) Src family tyrosine kinases and growth factor signaling. *Exp Cell Res* **254**, 1-13

32. Dal Porto, J. M., Gauld, S. B., Merrell, K. T., Mills, D., Pugh-Bernard, A. E., and Cambier, J. (2004) B cell antigen receptor signaling 101. *Mol Immunol* **41**, 599-613

33. Gauld, S. B., and Cambier, J. C. (2004) Src-family kinases in B-cell development and signaling. *Oncogene* **23**, 8001-8006

34. Hendriks, R. W. (2011) Drug discovery: New Btk inhibitor holds promise. *Nat Chem Biol* **7**, 4-5

35. Pleiman, C. M., Abrams, C., Gauen, L. T., Bedzyk, W., Jongstra, J., Shaw, A. S., and Cambier, J. C. (1994) Distinct p53/56lyn and p59fyn domains associate with nonphosphorylated and phosphorylated Ig-alpha. *Proc Natl Acad Sci U S A* **91**, 4268-4272

36. Kurosaki, T. (1999) Genetic analysis of B cell antigen receptor signaling. *Annu Rev Immunol* **17**, 555-592

37. Ke, J., Chelvarajan, R. L., Sindhava, V., Robertson, D. A., Lekakis, L., Jennings, C. D., and Bondada, S. (2009) Anomalous constitutive Src kinase activity promotes B lymphoma survival and growth. *Mol Cancer* **8**, 132

38. Yang, C., Lu, P., Lee, F. Y., Chadburn, A., Barrientos, J. C., Leonard, J. P., Ye, F., Zhang, D., Knowles, D. M., and Wang, Y. L. (2008) Tyrosine kinase inhibition in diffuse large B-cell lymphoma: molecular basis for antitumor activity and drug resistance of dasatinib. *Leukemia* **22**, 1755-1766

39. Hanahan, D., and Weinberg, R. A. (2011) Hallmarks of cancer: the next generation. *Cell* **144**, 646-674

40. Irby, R. B., Mao, W., Coppola, D., Kang, J., Loubeau, J. M., Trudeau, W., Karl, R., Fujita, D. J., Jove, R., and Yeatman, T. J. (1999) Activating SRC mutation in a subset of advanced human colon cancers. *Nat Genet* **21**, 187-190

41. Sugimura, M., Kobayashi, K., Sagae, S., Nishioka, Y., Ishioka, S., Terasawa, K., Tokino, T., and Kudo, R. (2000) Mutation of the SRC gene in endometrial carcinoma. *Jpn J Cancer Res* **91**, 395-398

42. Nilbert, M., and Fernebro, E. (2000) Lack of activating c-SRC mutations at codon 531 in rectal cancer. *Cancer Genet Cytogenet* **121**, 94-95

43. Laghi, L., Bianchi, P., Orbetegli, O., Gennari, L., Roncalli, M., and Malesci, A. (2001) Lack of mutation at codon 531 of SRC in advanced colorectal cancers from Italian patients. *Br J Cancer* **84**, 196-198

44. Ishizawar, R., and Parsons, S. J. (2004) c-Src and cooperating partners in human cancer. *Cancer Cell* **6**, 209-214

45. Nam, S., Kim, D., Cheng, J. Q., Zhang, S., Lee, J. H., Buettner, R., Mirosevich, J., Lee, F. Y., and Jove, R. (2005) Action of the Src family kinase inhibitor, dasatinib (BMS-354825), on human prostate cancer cells. *Cancer Res* **65**, 9185-9189

46. Goldenberg-Furmanov, M., Stein, I., Pikarsky, E., Rubin, H., Kasem, S., Wygoda, M., Weinstein, I., Reuveni, H., and Ben-Sasson, S. A. (2004) Lyn is a target gene for prostate cancer: sequence-based inhibition induces regression of human tumor xenografts. *Cancer Res* **64**, 1058-1066

47. Xu, W., Allbritton, N., and Lawrence, D. S. (2012) SRC kinase regulation in progressively invasive cancer. *PLoS One* **7**, e48867

48. Aligayer, H., Boyd, D. D., Heiss, M. M., Abdalla, E. K., Curley, S. A., and Gallick, G. E. (2002) Activation of Src kinase in primary colorectal carcinoma: an indicator of poor clinical prognosis. *Cancer* **94**, 344-351

49. Pena, S. V., Melhem, M. F., Meisler, A. I., and Cartwright, C. A. (1995) Elevated c-yes tyrosine kinase activity in premalignant lesions of the colon. *Gastroenterology* **108**, 117-124

50. Tauzin, S., Ding, H., Khatib, K., Ahmad, I., Burdevet, D., van Echten-Deckert, G., Lindquist, J. A., Schraven, B., Din, N. U., Borisch, B., and Hoessli, D. C. (2008) Oncogenic association of the Cbp/PAG adaptor protein with the Lyn tyrosine kinase in human B-NHL rafts. *Blood* **111**, 2310-2320

51. Dos Santos, C., Demur, C., Bardet, V., Prade-Houdellier, N., Payrastre, B., and Recher, C. (2008) A critical role for Lyn in acute myeloid leukemia. *Blood* **111**, 2269-2279

52. Donato, N. J., Wu, J. Y., Stapley, J., Gallick, G., Lin, H., Arlinghaus, R., and Talpaz, M. (2003) BCR-ABL independence and LYN kinase overexpression in chronic myelogenous leukemia cells selected for resistance to STI571. *Blood* **101**, 690-698

53. Roginskaya, V., Zuo, S., Caudell, E., Nambudiri, G., Kraker, A. J., and Corey, S. J. (1999) Therapeutic targeting of Src-kinase Lyn in myeloid leukemic cell growth. *Leukemia* **13**, 855-861

54. Wilson, M. B., Schreiner, S. J., Choi, H. J., Kamens, J., and Smithgall, T. E. (2002) Selective pyrrolo-pyrimidine inhibitors reveal a necessary role for Src family kinases in Bcr-Abl signal transduction and oncogenesis. *Oncogene* **21**, 8075-8088

55. Benati, D., and Baldari, C. T. (2008) SRC family kinases as potential therapeutic targets for malignancies and immunological disorders. *Curr Med Chem* **15**, 1154-1165

56. Danhauser-Riedl, S., Warmuth, M., Druker, B. J., Emmerich, B., and Hallek, M. (1996) Activation of Src kinases p53/56lyn and p59hck by p210bcr/abl in myeloid cells. *Cancer Res* **56**, 3589-3596

57. Wang, Q., Zimmerman, E. I., Toutchkine, A., Martin, T. D., Graves, L. M., and Lawrence, D. S. (2010) Multicolor monitoring of dysregulated protein kinases in chronic myelogenous leukemia. *ACS Chem Biol* **5**, 887-895

58. Niemann, C. U., and Wiestner, A. (2013) B-cell receptor signaling as a driver of lymphoma development and evolution. *Semin Cancer Biol* **23**, 410-421

59. Cheng, A. M., Rowley, B., Pao, W., Hayday, A., Bolen, J. B., and Pawson, T. (1995) Syk tyrosine kinase required for mouse viability and B-cell development. *Nature* **378**, 303-306

60. Nishizumi, H., Taniuchi, I., Yamanashi, Y., Kitamura, D., Ilic, D., Mori, S., Watanabe, T., and Yamamoto, T. (1995) Impaired proliferation of peripheral B cells and indication of autoimmune disease in lyn-deficient mice. *Immunity* **3**, 549-560

61. Khan, W. N., Sideras, P., Rosen, F. S., and Alt, F. W. (1995) The role of Bruton's tyrosine kinase in B-cell development and function in mice and man. *Ann N Y Acad Sci* **764**, 27-38

62. Lombardo, L. J., Lee, F. Y., Chen, P., Norris, D., Barrish, J. C., Behnia, K., Castaneda, S., Cornelius, L. A., Das, J., Doweyko, A. M., Fairchild, C., Hunt, J. T., Inigo, I., Johnston, K., Kamath, A., Kan, D., Klei, H., Marathe, P., Pang, S., Peterson, R., Pitt, S., Schieven, G. L., Schmidt, R. J., Tokarski, J., Wen, M. L., Wityak, J., and Borzilleri, R. M. (2004) Discovery of N-(2-chloro-6-methyl- phenyl)-2-(6-(4-(2-hydroxyethyl)- piperazin-1-yl)-2-methylpyrimidin-4-ylamino)thiazole-5-carboxamide (BMS-354825), a dual Src/Abl kinase inhibitor with potent antitumor activity in preclinical assays. *J Med Chem* **47**, 6658-6661

63. Shah, N. P., Tran, C., Lee, F. Y., Chen, P., Norris, D., and Sawyers, C. L. (2004) Overriding imatinib resistance with a novel ABL kinase inhibitor. *Science* **305**, 399-401

64. Karaman, M. W., Herrgard, S., Treiber, D. K., Gallant, P., Atteridge, C. E., Campbell, B. T., Chan, K. W., Ciceri, P., Davis, M. I., Edeen, P. T., Faraoni, R., Floyd, M., Hunt, J. P., Lockhart, D. J., Milanov, Z. V., Morrison, M. J., Pallares, G., Patel, H. K., Pritchard, S., Wodicka, L. M., and Zarrinkar, P. P. (2008) A quantitative analysis of kinase inhibitor selectivity. *Nat Biotechnol* **26**, 127-132

65. Ple, P. A., Green, T. P., Hennequin, L. F., Curwen, J., Fennell, M., Allen, J., Lambert-Van Der Brempt, C., and Costello, G. (2004) Discovery of a new class of anilinoquinazoline inhibitors with high affinity and specificity for the tyrosine kinase domain of c-Src. *J Med Chem* **47**, 871-887

66. O'Hare, T., Pollock, R., Stoffregen, E. P., Keats, J. A., Abdullah, O. M., Moseson, E. M., Rivera, V. M., Tang, H., Metcalf, C. A., 3rd, Bohacek, R. S., Wang, Y., Sundaramoorthi, R., Shakespeare, W. C., Dalgarno, D., Clackson, T., Sawyer, T. K., Deininger, M. W., and Druker, B. J. (2004) Inhibition of wild-type and mutant Bcr-Abl by AP23464, a potent ATP-based oncogenic protein kinase inhibitor: implications for CML. *Blood* **104**, 2532-2539

67. Brognard, J., and Hunter, T. (2011) Protein kinase signaling networks in cancer. *Curr Opin Genet Dev* **21**, 4-11

68. Fleuren, E. D., Zhang, L., Wu, J., and Daly, R. J. (2016) The kinome 'at large' in cancer. *Nat Rev Cancer* **16**, 83-98

69. Graves, L. M., Duncan, J. S., Whittle, M. C., and Johnson, G. L. (2013) The dynamic nature of the kinome. *Biochem J* **450**, 1-8

70. Duncan, J. S., Whittle, M. C., Nakamura, K., Abell, A. N., Midland, A. A., Zawistowski, J. S., Johnson, N. L., Granger, D. A., Jordan, N. V., Darr, D. B., Usary, J., Kuan, P. F., Smalley, D. M., Major, B., He, X., Hoadley, K. A., Zhou, B., Sharpless, N. E., Perou, C. M., Kim, W. Y., Gomez, S. M., Chen, X., Jin, J., Frye, S. V., Earp, H. S., Graves, L. M., and Johnson, G. L. (2012) Dynamic reprogramming of the kinome in response to targeted MEK inhibition in triple-negative breast cancer. *Cell* **149**, 307-321

71. Stuhlmiller, T. J., Earp, H. S., and Johnson, G. L. (2014) Adaptive reprogramming of the breast cancer kinome. *Clin Pharmacol Ther* **95**, 413-415

72. Workman, P. (2005) Drugging the cancer kinome: progress and challenges in developing personalized molecular cancer therapeutics. *Cold Spring Harb Symp Quant Biol* **70**, 499-515

73. Casnellie, J. E., and Krebs, E. G. (1984) The use of synthetic peptides for defining the specificity of tyrosine protein kinases. *Adv Enzyme Regul* **22**, 501-515

74. Casnellie, J. E. (1991) Assay of protein kinases using peptides with basic residues for phosphocellulose binding. *Methods Enzymol* **200**, 115-120

75. Glickman, J. F. (2004) Assay Development for Protein Kinase Enzymes. in *Assay Guidance Manual* (Sittampalam, G. S., Coussens, N. P., Brimacombe, K., Grossman, A., Arkin, M., Auld, D., Austin, C., Baell, J., Bejcek, B., Chung, T. D. Y., Dahlin, J. L., Devanaryan, V., Foley, T. L.,

Glicksman, M., Hall, M. D., Hass, J. V., Inglese, J., Iversen, P. W., Lal-Nag, M., Li, Z., McGee, J., McManus, O., Riss, T., Trask, O. J., Jr., Weidner, J. R., Xia, M., and Xu, X. eds.), Eli Lilly & Company and the National Center for Advancing Translational Sciences, Bethesda (MD). pp

76. Zhang, L., and Daly, R. J. (2012) Targeting the human kinome for cancer therapy: current perspectives. *Crit Rev Oncog* **17**, 233-246

77. Schmelzle, K., and White, F. M. (2006) Phosphoproteomic approaches to elucidate cellular signaling networks. *Curr Opin Biotechnol* **17**, 406-414

78. Newman, R. H., Zhang, J., and Zhu, H. (2014) Toward a systems-level view of dynamic phosphorylation networks. *Front Genet* **5**, 263

79. Tan, C. S., and Linding, R. (2009) Experimental and computational tools useful for (re)construction of dynamic kinase-substrate networks. *Proteomics* **9**, 5233-5242

80. Diks, S. H., Kok, K., O'Toole, T., Hommes, D. W., van Dijken, P., Joore, J., and Peppelenbosch, M. P. (2004) Kinome profiling for studying lipopolysaccharide signal transduction in human peripheral blood mononuclear cells. *J Biol Chem* **279**, 49206-49213

81. Kemp, B. E., and Pearson, R. B. (1991) Design and use of peptide substrates for protein kinases. *Methods Enzymol* **200**, 121-134

82. Miller, C. J., and Turk, B. E. (2016) Rapid Identification of Protein Kinase Phosphorylation Site Motifs Using Combinatorial Peptide Libraries. *Methods Mol Biol* **1360**, 203-216

83. Leung, G. C., Murphy, J. M., Briant, D., and Sicheri, F. (2009) Characterization of kinase target phosphorylation consensus motifs using peptide SPOT arrays. *Methods Mol Biol* **570**, 187-195

84. Wang, Y., and Ma, H. (2015) Protein kinase profiling assays: a technology review. *Drug Discov Today Technol* **18**, 1-8

85. Gonzalez-Vera, J. A. (2012) Probing the kinome in real time with fluorescent peptides. *Chem Soc Rev* **41**, 1652-1664

86. Jia, Y., Quinn, C. M., Kwak, S., and Talanian, R. V. (2008) Current in vitro kinase assay technologies: the quest for a universal format. *Curr Drug Discov Technol* **5**, 59-69

87. Hemmila, I. I. (1999) LANCEtrade mark: Homogeneous Assay Platform for HTS. *J Biomol Screen* **4**, 303-308

88. Jia, Y. (2008) Current status of HTRF((R)) technology in kinase assays. *Expert Opin Drug Discov* **3**, 1461-1474

89. Mathis, G. (1995) Probing molecular interactions with homogeneous techniques based on rare earth cryptates and fluorescence energy transfer. *Clin Chem* **41**, 1391-1397

90. Ullman, E. F., Kirakossian, H., Singh, S., Wu, Z. P., Irvin, B. R., Pease, J. S., Switchenko, A. C., Irvine, J. D., Dafforn, A., Skold, C. N., and Wagner, D. B. (1994) Luminescent oxygen channeling immunoassay: measurement of particle binding kinetics by chemiluminescence. *Proc Natl Acad Sci U S A* **91**, 5426-5430

91. Warner, G., Illy, C., Pedro, L., Roby, P., and Bosse, R. (2004) AlphaScreen kinase HTS platforms. *Curr Med Chem* **11**, 721-730

92. Owicki, J. C. (2000) Fluorescence polarization and anisotropy in high throughput screening: perspectives and primer. *J Biomol Screen* **5**, 297-306

93. Seethala, R., and Menzel, R. (1997) A homogeneous, fluorescence polarization assay for src-family tyrosine kinases. *Anal Biochem* **253**, 210-218

94. Gaudet, E. A., Huang, K. S., Zhang, Y., Huang, W., Mark, D., and Sportsman, J. R. (2003) A homogeneous fluorescence polarization assay adaptable for a range of protein serine/threonine and tyrosine kinases. *J Biomol Screen* **8**, 164-175

95. Morgan, A. G., McCauley, T. J., Stanaitis, M. L., Mathrubutham, M., and Millis, S. Z. (2004) Development and validation of a fluorescence technology for both primary and secondary screening of kinases that facilitates compound selectivity and site-specific inhibitor determination. *Assay Drug Dev Technol* **2**, 171-181

96. Xia, W., Rininsland, F., Wittenburg, S. K., Shi, X., Achyuthan, K. E., McBranch, D. W., and Whitten, D. G. (2004) Applications of fluorescent polymer superquenching to high throughput screening assays for protein kinases. *Assay Drug Dev Technol* **2**, 183-192

97. Koresawa, M., and Okabe, T. (2004) High-throughput screening with quantitation of ATP consumption: a universal non-radioisotope, homogeneous assay for protein kinase. *Assay Drug Dev Technol* **2**, 153-160

98. Charter, N. W., Kauffman, L., Singh, R., and Eglen, R. M. (2006) A generic, homogenous method for measuring kinase and inhibitor activity via adenosine 5'-diphosphate accumulation. *J Biomol Screen* **11**, 390-399

99. Singh, P., Harden, B. J., Lillywhite, B. J., and Broad, P. M. (2004) Identification of kinase inhibitors by an ATP depletion method. *Assay Drug Dev Technol* **2**, 161-169

100. Zhang, J., Ma, Y., Taylor, S. S., and Tsien, R. Y. (2001) Genetically encoded reporters of protein kinase A activity reveal impact of substrate tethering. *Proc Natl Acad Sci U S A* **98**, 14997-15002

101. Ting, A. Y., Kain, K. H., Klemke, R. L., and Tsien, R. Y. (2001) Genetically encoded fluorescent reporters of protein tyrosine kinase activities in living cells. *Proc Natl Acad Sci U S A* **98**, 15003-15008

102. Violin, J. D., Zhang, J., Tsien, R. Y., and Newton, A. C. (2003) A genetically encoded fluorescent reporter reveals oscillatory phosphorylation by protein kinase C. *J Cell Biol* **161**, 899-909

103. Kunkel, M. T., Ni, Q., Tsien, R. Y., Zhang, J., and Newton, A. C. (2005) Spatio-temporal dynamics of protein kinase B/Akt signaling revealed by a genetically encoded fluorescent reporter. *J Biol Chem* **280**, 5581-5587

104. Sato, M., Kawai, Y., and Umezawa, Y. (2007) Genetically encoded fluorescent indicators to visualize protein phosphorylation by extracellular signal-regulated kinase in single living cells. *Anal Chem* **79**, 2570-2575

105. Yeh, R. H., Yan, X., Cammer, M., Bresnick, A. R., and Lawrence, D. S. (2002) Real time visualization of protein kinase activity in living cells. *J Biol Chem* **277**, 11527-11532

106. Chen, C. A., Yeh, R. H., Yan, X., and Lawrence, D. S. (2004) Biosensors of protein kinase action: from in vitro assays to living cells. *Biochim Biophys Acta* **1697**, 39-51

107. Sharma, V., Wang, Q., and Lawrence, D. S. (2008) Peptide-based fluorescent sensors of protein kinase activity: design and applications. *Biochim Biophys Acta* **1784**, 94-99

108. Shults, M. D., and Imperiali, B. (2003) Versatile fluorescence probes of protein kinase activity. *J Am Chem Soc* **125**, 14248-14249

109. Veldhuyzen, W. F., Nguyen, Q., McMaster, G., and Lawrence, D. S. (2003) A light-activated probe of intracellular protein kinase activity. *J Am Chem Soc* **125**, 13358-13359

110. Szoko, E., and Tabi, T. (2010) Analysis of biological samples by capillary electrophoresis with laser induced fluorescence detection. *J Pharm Biomed Anal* **53**, 1180-1192

111. Cohen, C. B., Chin-Dixon, E., Jeong, S., and Nikiforov, T. T. (1999) A microchip-based enzyme assay for protein kinase A. *Anal Biochem* **273**, 89-97

112. Yoon, S., Han, K. Y., Nam, H. S., Nga le, V., and Yoo, Y. S. (2004) Determination of protein phosphorylation and the translocation of green fluorescence protein-extracellular signal-regulated kinase 2 by capillary electrophoresis using laser induced fluorescence detection. *J Chromatogr A* **1056**, 237-242

113. Proctor, A., Herrera-Loeza, S. G., Wang, Q., Lawrence, D. S., Yeh, J. J., and Allbritton, N. L. (2014) Measurement of protein kinase B activity in single primary human pancreatic cancer cells. *Anal Chem* **86**, 4573-4580

114. Rauf, F., Huang, Y., Muhandiramlage, T. P., and Aspinwall, C. A. (2010) Analysis of protein kinase A activity in insulin-secreting cells using a cell-penetrating protein substrate and capillary electrophoresis. *Anal Bioanal Chem* **397**, 3359-3367

115. Manning, G., Whyte, D. B., Martinez, R., Hunter, T., and Sudarsanam, S. (2002) The protein kinase complement of the human genome. *Science* **298**, 1912-1934

116. Charboneau, L., Tory, H., Chen, T., Winters, M., Petricoin, E. F., 3rd, Liotta, L. A., and Paweletz, C. P. (2002) Utility of reverse phase protein arrays: applications to signalling pathways and human body arrays. *Brief Funct Genomic Proteomic* **1**, 305-315

117. Nishizuka, S. S., and Mills, G. B. (2016) New era of integrated cancer biomarker discovery using reverse-phase protein arrays. *Drug Metab Pharmacokinet* **31**, 35-45

118. Zhang, H., Shi, X., and Pelech, S. (2016) Monitoring Protein Kinase Expression and Phosphorylation in Cell Lysates with Antibody Microarrays. *Methods Mol Biol* **1360**, 107-122

119. Jacoby, E., Tresadern, G., Bembenek, S., Wroblowski, B., Buyck, C., Neefs, J. M., Rassokhin, D., Poncelet, A., Hunt, J., and van Vlijmen, H. (2015) Extending kinome coverage by analysis of kinase inhibitor broad profiling data. *Drug Discov Today* **20**, 652-658

120. Godl, K., Wissing, J., Kurtenbach, A., Habenberger, P., Blencke, S., Gutbrod, H., Salassidis, K., Stein-Gerlach, M., Missio, A., Cotten, M., and Daub, H. (2003) An efficient proteomics method to identify the cellular targets of protein kinase inhibitors. *Proc Natl Acad Sci U S A* **100**, 15434-15439

121. Oppermann, F. S., Gnad, F., Olsen, J. V., Hornberger, R., Greff, Z., Keri, G., Mann, M., and Daub, H. (2009) Large-scale proteomics analysis of the human kinome. *Mol Cell Proteomics* **8**, 1751-1764

122. Bantscheff, M., Eberhard, D., Abraham, Y., Bastuck, S., Boesche, M., Hobson, S., Mathieson, T., Perrin, J., Raida, M., Rau, C., Reader, V., Sweetman, G., Bauer, A., Bouwmeester, T., Hopf, C., Kruse, U., Neubauer, G., Ramsden, N., Rick, J., Kuster, B., and Drewes, G. (2007) Quantitative chemical proteomics reveals mechanisms of action of clinical ABL kinase inhibitors. *Nat Biotechnol* **25**, 1035-1044

123. Bantscheff, M., Hopf, C., Kruse, U., and Drewes, G. (2007) Proteomics-based strategies in kinase drug discovery. *Ernst Schering Found Symp Proc* **3**, 1-28

124. Daub, H. (2015) Quantitative proteomics of kinase inhibitor targets and mechanisms. *ACS Chem Biol* **10**, 201-212

125. Gholami, A. M., Hahne, H., Wu, Z., Auer, F. J., Meng, C., Wilhelm, M., and Kuster, B. (2013) Global proteome analysis of the NCI-60 cell line panel. *Cell Rep* **4**, 609-620

126. Medard, G., Pachl, F., Ruprecht, B., Klaeger, S., Heinzlmeir, S., Helm, D., Qiao, H., Ku, X., Wilhelm, M., Kuehne, T., Wu, Z., Dittmann, A., Hopf, C., Kramer, K., and Kuster, B. (2015) Optimized chemical proteomics assay for kinase inhibitor profiling. *J Proteome Res* **14**, 1574-1586

127. Zhang, L., Holmes, I. P., Hochgrafe, F., Walker, S. R., Ali, N. A., Humphrey, E. S., Wu, J., de Silva, M., Kersten, W. J., Connor, T., Falk, H., Allan, L., Street, I. P., Bentley, J. D., Pilling, P. A., Monahan, B. J., Peat, T. S., and Daly, R. J. (2013) Characterization of the novel broad-spectrum kinase inhibitor CTx-0294885 as an affinity reagent for mass spectrometry-based kinome profiling. *J Proteome Res* **12**, 3104-3116

128. Ruprecht, B., Zaal, E. A., Zecha, J., Wu, W., Berkers, C. R., Kuster, B., and Lemeer, S. (2017) Lapatinib Resistance in Breast Cancer Cells Is Accompanied by Phosphorylation-Mediated Reprogramming of Glycolysis. *Cancer Res* **77**, 1842-1853

129. Daub, H., Olsen, J. V., Bairlein, M., Gnad, F., Oppermann, F. S., Korner, R., Greff, Z., Keri, G., Stemmann, O., and Mann, M. (2008) Kinase-selective enrichment enables quantitative phosphoproteomics of the kinome across the cell cycle. *Mol Cell* **31**, 438-448

130. Lemeer, S., Zorgiebel, C., Ruprecht, B., Kohl, K., and Kuster, B. (2013) Comparing immobilized kinase inhibitors and covalent ATP probes for proteomic profiling of kinase expression and drug selectivity. *J Proteome Res* **12**, 1723-1731

131. Urisman, A., Levin, R. S., Gordan, J. D., Webber, J. T., Hernandez, H., Ishihama, Y., Shokat, K. M., and Burlingame, A. L. (2017) An Optimized Chromatographic Strategy for Multiplexing In Parallel Reaction Monitoring Mass Spectrometry: Insights from Quantitation of Activated Kinases. *Mol Cell Proteomics* **16**, 265-277

132. Cooper, M. J., Cox, N. J., Zimmerman, E. I., Dewar, B. J., Duncan, J. S., Whittle, M. C., Nguyen, T. A., Jones, L. S., Ghose Roy, S., Smalley, D. M., Kuan, P. F., Richards, K. L., Christopherson, R. I., Jin, J., Frye, S. V., Johnson, G. L., Baldwin, A. S., and Graves, L. M. (2013) Application of multiplexed kinase inhibitor beads to study kinome adaptations in drug-resistant leukemia. *PLoS One* **8**, e66755

133. Stuhlmiller, T. J., Miller, S. M., Zawistowski, J. S., Nakamura, K., Beltran, A. S., Duncan, J. S., Angus, S. P., Collins, K. A., Granger, D. A., Reuther, R. A., Graves, L. M., Gomez, S. M., Kuan, P. F., Parker, J. S., Chen, X., Sciaky, N., Carey, L. A., Earp, H. S., Jin, J., and Johnson, G. L. (2015) Inhibition of Lapatinib-Induced Kinome Reprogramming in ERBB2-Positive Breast Cancer by Targeting BET Family Bromodomains. *Cell Rep* **11**, 390-404

134. Zawistowski, J. S., Bevill, S. M., Goulet, D. R., Stuhlmiller, T. J., Beltran, A. S., Olivares-Quintero, J. F., Singh, D., Sciaky, N., Parker, J. S., Rashid, N. U., Chen, X., Duncan, J. S., Whittle, M. C., Angus, S. P., Velarde, S. H., Golitz, B. T., He, X., Santos, C., Darr, D. B., Gallagher, K., Graves, L. M., Perou, C. M., Carey, L. A., Earp, H. S., and Johnson, G. L. (2017) Enhancer Remodeling during Adaptive Bypass to MEK Inhibition Is Attenuated by Pharmacologic Targeting of the P-TEFb Complex. *Cancer Discov* **7**, 302-321

135. McNeill, R. S., Canoutas, D. A., Stuhlmiller, T. J., Dhruv, H. D., Irvin, D. M., Bash, R. E., Angus, S. P., Herring, L. E., Simon, J. M., Skinner, K. R., Limas, J. C., Chen, X., Schmid, R. S., Siegel, M. B., Van Swearingen, A. E., Hadler, M. J., Sulman, E. P., Sarkaria, J. N., Anders, C. K., Graves, L. M., Berens, M. E., Johnson, G. L., and Miller, C. R. (2017) Combination therapy with potent PI3K and MAPK inhibitors overcomes adaptive kinome resistance to single agents in preclinical models of glioblastoma. *Neuro Oncol*, [epub ahead of print]

136. Kurimchak, A. M., Shelton, C., Duncan, K. E., Johnson, K. J., Brown, J., O'Brien, S., Gabbasov, R., Fink, L. S., Li, Y., Lounsbury, N., Abou-Gharbia, M., Childers, W. E., Connolly, D. C., Chernoff, J., Peterson, J. R., and Duncan, J. S. (2016) Resistance to BET Bromodomain Inhibitors Is Mediated by Kinome Reprogramming in Ovarian Cancer. *Cell Rep* **16**, 1273-1286

137. Ruprecht, B., Zecha, J., Heinzlmeir, S., Medard, G., Lemeer, S., and Kuster, B. (2015) Evaluation of Kinase Activity Profiling Using Chemical Proteomics. *ACS Chem Biol* **10**, 2743-2752

138. Fedorov, O., Muller, S., and Knapp, S. (2010) The (un)targeted cancer kinome. *Nat Chem Biol* **6**, 166-169

139. Arend, K. C., Lenarcic, E. M., Vincent, H. A., Rashid, N., Lazear, E., McDonald, I. M., Gilbert, T. S., East, M. P., Herring, L. E., Johnson, G. L., Graves, L. M., and Moorman, N. J. (2017) Kinome Profiling Identifies Druggable Targets for Novel Human Cytomegalovirus (HCMV) Antivirals. *Mol Cell Proteomics* **16**, S263-S276

140. Werth, E. G., McConnell, E. W., Gilbert, T. S., Couso Lianez, I., Perez, C. A., Manley, C. K., Graves, L. M., Umen, J. G., and Hicks, L. M. (2017) Probing the global kinome and phosphoproteome in Chlamydomonas reinhardtii via sequential enrichment and quantitative proteomics. *Plant J* **89**, 416-426

141. Treindl, F., Ruprecht, B., Beiter, Y., Schultz, S., Dottinger, A., Staebler, A., Joos, T. O., Kling, S., Poetz, O., Fehm, T., Neubauer, H., Kuster, B., and Templin, M. F. (2016) A bead-based western for high-throughput cellular signal transduction analyses. *Nat Commun* **7**, 12852

142. Patricelli, M. P., Nomanbhoy, T. K., Wu, J., Brown, H., Zhou, D., Zhang, J., Jagannathan, S., Aban, A., Okerberg, E., Herring, C., Nordin, B., Weissig, H., Yang, Q., Lee, J. D., Gray, N. S., and Kozarich, J. W. (2011) In situ kinase profiling reveals functionally relevant properties of native kinases. *Chem Biol* **18**, 699-710

143. Patricelli, M. P., Szardenings, A. K., Liyanage, M., Nomanbhoy, T. K., Wu, M., Weissig, H., Aban, A., Chun, D., Tanner, S., and Kozarich, J. W. (2007) Functional interrogation of the kinome using nucleotide acyl phosphates. *Biochemistry* **46**, 350-358

144. Shi, T., Song, E., Nie, S., Rodland, K. D., Liu, T., Qian, W. J., and Smith, R. D. (2016) Advances in targeted proteomics and applications to biomedical research. *Proteomics* **16**, 2160-2182

145. Graves, L. M., and Litchfield, D. W. (2011) "Going KiNativ": probing the Native Kinome. *Chem Biol* **18**, 683-684

146. Shah, K., and Shokat, K. M. (2003) A chemical genetic approach for the identification of direct substrates of protein kinases. *Methods Mol Biol* **233**, 253-271

147. Lopez, M. S., Kliegman, J. I., and Shokat, K. M. (2014) The logic and design of analog-sensitive kinases and their small molecule inhibitors. *Methods Enzymol* **548**, 189-213

148. Zhao, Q., Ouyang, X., Wan, X., Gajiwala, K. S., Kath, J. C., Jones, L. H., Burlingame, A. L., and Taunton, J. (2017) Broad-Spectrum Kinase Profiling in Live Cells with Lysine-Targeted Sulfonyl Fluoride Probes. *J Am Chem Soc* **139**, 680-685

149. Roux, K. J., Kim, D. I., Raida, M., and Burke, B. (2012) A promiscuous biotin ligase fusion protein identifies proximal and interacting proteins in mammalian cells. *J Cell Biol* **196**, 801-810

150. Kwon, K., and Beckett, D. (2000) Function of a conserved sequence motif in biotin holoenzyme synthetases. *Protein Sci* **9**, 1530-1539

151. Choi-Rhee, E., Schulman, H., and Cronan, J. E. (2004) Promiscuous protein biotinylation by Escherichia coli biotin protein ligase. *Protein Sci* **13**, 3043-3050

152. Kim, D. I., Birendra, K. C., Zhu, W., Motamedchaboki, K., Doye, V., and Roux, K. J. (2014) Probing nuclear pore complex architecture with proximity-dependent biotinylation. *Proc Natl Acad Sci U S A* **111**, E2453-2461

153. Hesketh, G. G., Youn, J. Y., Samavarchi-Tehrani, P., Raught, B., and Gingras, A. C. (2017) Parallel Exploration of Interaction Space by BioID and Affinity Purification Coupled to Mass Spectrometry. *Methods Mol Biol* **1550**, 115-136

154. Lambert, J. P., Tucholska, M., Go, C., Knight, J. D., and Gingras, A. C. (2015) Proximity biotinylation and affinity purification are complementary approaches for the interactome mapping of chromatin-associated protein complexes. *J Proteomics* **118**, 81-94

155. Kim, D. I., Jensen, S. C., Noble, K. A., Kc, B., Roux, K. H., Motamedchaboki, K., and Roux, K. J. (2016) An improved smaller biotin ligase for BioID proximity labeling. *Mol Biol Cell* **27**, 1188-1196

156. Kazazian, K., Go, C., Wu, H., Brashavitskaya, O., Xu, R., Dennis, J. W., Gingras, A. C., and Swallow, C. J. (2017) Plk4 Promotes Cancer Invasion and Metastasis through Arp2/3 Complex Regulation of the Actin Cytoskeleton. *Cancer Res* **77**, 434-447

157. Zhou, N., Zhao, W. D., Liu, D. X., Liang, Y., Fang, W. G., Li, B., and Chen, Y. H. (2011) Inactivation of EphA2 promotes tight junction formation and impairs angiogenesis in brain endothelial cells. *Microvasc Res* **82**, 113-121

158. Caballe, A., Wenzel, D. M., Agromayor, M., Alam, S. L., Skalicky, J. J., Kloc, M., Carlton, J. G., Labrador, L., Sundquist, W. I., and Martin-Serrano, J. (2015) ULK3 regulates cytokinetic abscission by phosphorylating ESCRT-III proteins. *Elife* **4**, e06547

159. Zhou, Z., Rawnsley, D. R., Goddard, L. M., Pan, W., Cao, X. J., Jakus, Z., Zheng, H., Yang, J., Arthur, J. S., Whitehead, K. J., Li, D., Zhou, B., Garcia, B. A., Zheng, X., and Kahn, M. L. (2015) The cerebral cavernous malformation pathway controls cardiac development via regulation of endocardial MEKK3 signaling and KLF expression. *Dev Cell* **32**, 168-180

160. Varnaite, R., and MacNeill, S. A. (2016) Meet the neighbors: Mapping local protein interactomes by proximity-dependent labeling with BioID. *Proteomics* **16**, 2503-2518

161. Kim, D. I., and Roux, K. J. (2016) Filling the Void: Proximity-Based Labeling of Proteins in Living Cells. *Trends Cell Biol* **26**, 804-817

162. Miao, W., Xiao, Y., Guo, L., Jiang, X., Huang, M., and Wang, Y. (2016) A High-Throughput Targeted Proteomic Approach for Comprehensive Profiling of Methylglyoxal-Induced Perturbations of the Human Kinome. *Anal Chem* **88**, 9773-9779

163. Marques, A. J., Palanimurugan, R., Matias, A. C., Ramos, P. C., and Dohmen, R. J. (2009) Catalytic mechanism and assembly of the proteasome. *Chem Rev* **109**, 1509-1536

164. Tanaka, K. (2009) The proteasome: overview of structure and functions. *Proc Jpn Acad Ser B Phys Biol Sci* **85**, 12-36

165. Adams, J. (2004) The proteasome: a suitable antineoplastic target. *Nat Rev Cancer* **4**, 349-360

166. Basler, M., Kirk, C. J., and Groettrup, M. (2013) The immunoproteasome in antigen processing and other immunological functions. *Curr Opin Immunol* **25**, 74-80

167. Heemels, M. T., and Ploegh, H. (1995) Generation, translocation, and presentation of MHC class I-restricted peptides. *Annu Rev Biochem* **64**, 463-491

168. Groll, M., Bajorek, M., Kohler, A., Moroder, L., Rubin, D. M., Huber, R., Glickman, M. H., and Finley, D. (2000) A gated channel into the proteasome core particle. *Nat Struct Biol* **7**, 1062-1067

169. Tomko, R. J., Jr., and Hochstrasser, M. (2013) Molecular architecture and assembly of the eukaryotic proteasome. *Annu Rev Biochem* **82**, 415-445

170. Rabl, J., Smith, D. M., Yu, Y., Chang, S. C., Goldberg, A. L., and Cheng, Y. (2008) Mechanism of gate opening in the 20S proteasome by the proteasomal ATPases. *Mol Cell* **30**, 360-368

171. Fabre, B., Lambour, T., Garrigues, L., Ducoux-Petit, M., Amalric, F., Monsarrat, B., Burlet-Schiltz, O., and Bousquet-Dubouch, M. P. (2014) Label-free quantitative proteomics reveals the dynamics of proteasome complexes composition and stoichiometry in a wide range of human cell lines. *J Proteome Res* **13**, 3027-3037

172. Frisan, T., Levitsky, V., and Masucci, M. G. (2000) Variations in proteasome subunit composition and enzymatic activity in B-lymphoma lines and normal B cells. *Int J Cancer* **88**, 881-888

173. Heinemeyer, W., Kleinschmidt, J. A., Saidowsky, J., Escher, C., and Wolf, D. H. (1991) Proteinase yscE, the yeast proteasome/multicatalytic-multifunctional proteinase: mutants unravel its function in stress induced proteolysis and uncover its necessity for cell survival. *EMBO J* **10**, 555-562

174. Teixeira, L. K., and Reed, S. I. (2013) Ubiquitin ligases and cell cycle control. *Annu Rev Biochem* **82**, 387-414

175. Geng, F., Wenzel, S., and Tansey, W. P. (2012) Ubiquitin and proteasomes in transcription. *Annu Rev Biochem* **81**, 177-201

176. Lu, Z., and Hunter, T. (2009) Degradation of activated protein kinases by ubiquitination. *Annu Rev Biochem* **78**, 435-475

177. Hoeller, D., and Dikic, I. (2009) Targeting the ubiquitin system in cancer therapy. *Nature* **458**, 438-444

178. Chen, L., and Madura, K. (2005) Increased proteasome activity, ubiquitin-conjugating enzymes, and eEF1A translation factor detected in breast cancer tissue. *Cancer Res* **65**, 5599-5606

179. Keck, S., Nitsch, R., Grune, T., and Ullrich, O. (2003) Proteasome inhibition by paired helical filament-tau in brains of patients with Alzheimer's disease. *J Neurochem* **85**, 115-122

180. Voorhees, P. M., Dees, E. C., O'Neil, B., and Orlowski, R. Z. (2003) The proteasome as a target for cancer therapy. *Clin Cancer Res* **9**, 6316-6325

181. Mani, A., and Gelmann, E. P. (2005) The ubiquitin-proteasome pathway and its role in cancer. *J Clin Oncol* **23**, 4776-4789

182. Kisselev, A. F., van der Linden, W. A., and Overkleeft, H. S. (2012) Proteasome inhibitors: an expanding army attacking a unique target. *Chem Biol* **19**, 99-115

183. Screen, M., Britton, M., Downey, S. L., Verdoes, M., Voges, M. J., Blom, A. E., Geurink, P. P., Risseeuw, M. D., Florea, B. I., van der Linden, W. A., Pletnev, A. A., Overkleeft, H. S., and Kisselev, A. F. (2010) Nature of pharmacophore influences active site specificity of proteasome inhibitors. *J Biol Chem* **285**, 40125-40134

184. Huber, E. M., and Groll, M. (2012) Inhibitors for the immuno- and constitutive proteasome: current and future trends in drug development. *Angew Chem Int Ed Engl* **51**, 8708-8720

185. Demo, S. D., Kirk, C. J., Aujay, M. A., Buchholz, T. J., Dajee, M., Ho, M. N., Jiang, J., Laidig, G. J., Lewis, E. R., Parlati, F., Shenk, K. D., Smyth, M. S., Sun, C. M., Vallone, M. K., Woo, T.

M., Molineaux, C. J., and Bennett, M. K. (2007) Antitumor activity of PR-171, a novel irreversible inhibitor of the proteasome. *Cancer Res* **67**, 6383-6391

186. Adams, J., Behnke, M., Chen, S., Cruickshank, A. A., Dick, L. R., Grenier, L., Klunder, J. M., Ma, Y. T., Plamondon, L., and Stein, R. L. (1998) Potent and selective inhibitors of the proteasome: dipeptidyl boronic acids. *Bioorg Med Chem Lett* **8**, 333-338

187. Muz, B., Ghazarian, R. N., Ou, M., Luderer, M. J., Kusdono, H. D., and Azab, A. K. (2016) Spotlight on ixazomib: potential in the treatment of multiple myeloma. *Drug Des Devel Ther* **10**, 217-226

188. Gupta, S. V., Hertlein, E., Lu, Y., Sass, E. J., Lapalombella, R., Chen, T. L., Davis, M. E., Woyach, J. A., Lehman, A., Jarjoura, D., Byrd, J. C., and Lucas, D. M. (2013) The proteasome inhibitor carfilzomib functions independently of p53 to induce cytotoxicity and an atypical NF-kappaB response in chronic lymphocytic leukemia cells. *Clin Cancer Res* **19**, 2406-2419

189. Zhang, L., Pham, L. V., Newberry, K. J., Ou, Z., Liang, R., Qian, J., Sun, L., Blonska, M., You, Y., Yang, J., Lin, X., Rollo, A., Tamayo, A. T., Lee, J., Ford, R. J., Zhao, X., Kwak, L. W., Yi, Q., and Wang, M. (2013) In vitro and in vivo therapeutic efficacy of carfilzomib in mantle cell lymphoma: targeting the immunoproteasome. *Mol Cancer Ther* **12**, 2494-2504

190. Ruan, J., Martin, P., Furman, R. R., Lee, S. M., Cheung, K., Vose, J. M., Lacasce, A., Morrison, J., Elstrom, R., Ely, S., Chadburn, A., Cesarman, E., Coleman, M., and Leonard, J. P. (2011) Bortezomib plus CHOP-rituximab for previously untreated diffuse large B-cell lymphoma and mantle cell lymphoma. *J Clin Oncol* **29**, 690-697

191. Gatti, L., Zuco, V., Zaffaroni, N., and Perego, P. (2013) Drug combinations with proteasome inhibitors in antitumor therapy. *Curr Pharm Des* **19**, 4094-4114

192. Crawford, L. J., Chan, E. T., Aujay, M., Holyoake, T. L., Melo, J. V., Jorgensen, H. G., Suresh, S., Walker, B., and Irvine, A. E. (2014) Synergistic effects of proteasome inhibitor carfilzomib in combination with tyrosine kinase inhibitors in imatinib-sensitive and -resistant chronic myeloid leukemia models. *Oncogenesis* **3**, e90

193. de Queiroz Crusoe, E., Maiso, P., Fernandez-Lazaro, D., San-Segundo, L., Garayoa, M., Garcia-Gomez, A., Gutierrez, N. C., Delgado, M., Colado, E., Martin-Sanchez, J., Lee, F. Y., and Ocio, E. M. (2012) Transcriptomic rationale for the synergy observed with dasatinib + bortezomib + dexamethasone in multiple myeloma. *Ann Hematol* **91**, 257-269

194. Dasmahapatra, G., Patel, H., Dent, P., Fisher, R. I., Friedberg, J., and Grant, S. (2013) The Bruton tyrosine kinase (BTK) inhibitor PCI-32765 synergistically increases proteasome inhibitor activity in diffuse large-B cell lymphoma (DLBCL) and mantle cell lymphoma (MCL) cells sensitive or resistant to bortezomib. *Br J Haematol* **161**, 43-56

195. Lamothe, B., Cervantes-Gomez, F., Sivina, M., Wierda, W. G., Keating, M. J., and Gandhi, V. (2015) Proteasome inhibitor carfilzomib complements ibrutinib's action in chronic lymphocytic leukemia. *Blood* **125**, 407-410

196. Liggett, A., Crawford, L. J., Walker, B., Morris, T. C., and Irvine, A. E. (2010) Methods for measuring proteasome activity: current limitations and future developments. *Leuk Res* **34**, 1403-1409

197. Kisselev, A. F., Akopian, T. N., Castillo, V., and Goldberg, A. L. (1999) Proteasome active sites allosterically regulate each other, suggesting a cyclical bite-chew mechanism for protein breakdown. *Mol Cell* **4**, 395-402

198. Kisselev, A. F., Garcia-Calvo, M., Overkleeft, H. S., Peterson, E., Pennington, M. W., Ploegh, H. L., Thornberry, N. A., and Goldberg, A. L. (2003) The caspase-like sites of proteasomes, their substrate specificity, new inhibitors and substrates, and allosteric interactions with the trypsin-like sites. *J Biol Chem* **278**, 35869-35877

199. Orlowski, M., Cardozo, C., Hidalgo, M. C., and Michaud, C. (1991) Regulation of the peptidylglutamyl-peptide hydrolyzing activity of the pituitary multicatalytic proteinase complex. *Biochemistry* **30**, 5999-6005

200. Moravec, R. A., O'Brien, M. A., Daily, W. J., Scurria, M. A., Bernad, L., and Riss, T. L. (2009) Cell-based bioluminescent assays for all three proteasome activities in a homogeneous format. *Anal Biochem* **387**, 294-302

201. Berkers, C. R., Verdoes, M., Lichtman, E., Fiebiger, E., Kessler, B. M., Anderson, K. C., Ploegh, H. L., Ovaa, H., and Galardy, P. J. (2005) Activity probe for in vivo profiling of the specificity of proteasome inhibitor bortezomib. *Nat Methods* **2**, 357-362

202. Berkers, C. R., van Leeuwen, F. W., Groothuis, T. A., Peperzak, V., van Tilburg, E. W., Borst, J., Neefjes, J. J., and Ovaa, H. (2007) Profiling proteasome activity in tissue with fluorescent probes. *Mol Pharm* **4**, 739-748

203. Bogyo, M. (2005) Screening for selective small molecule inhibitors of the proteasome using activity-based probes. *Methods Enzymol* **399**, 609-622

204. Li, N., Kuo, C. L., Paniagua, G., van den Elst, H., Verdoes, M., Willems, L. I., van der Linden, W. A., Ruben, M., van Genderen, E., Gubbens, J., van Wezel, G. P., Overkleeft, H. S., and Florea, B. I. (2013) Relative quantification of proteasome activity by activity-based protein profiling and LC-MS/MS. *Nat Protoc* **8**, 1155-1168

205. Luker, G. D., Pica, C. M., Song, J., Luker, K. E., and Piwnica-Worms, D. (2003) Imaging 26S proteasome activity and inhibition in living mice. *Nat Med* **9**, 969-973

206. Gross, S., and Piwnica-Worms, D. (2005) Monitoring proteasome activity in cellulo and in living animals by bioluminescent imaging: technical considerations for design and use of genetically encoded reporters. *Methods Enzymol* **399**, 512-530

207. Deng, S., Zhou, H., Xiong, R., Lu, Y., Yan, D., Xing, T., Dong, L., Tang, E., and Yang, H. (2007) Over-expression of genes and proteins of ubiquitin specific peptidases (USPs) and proteasome subunits (PSs) in breast cancer tissue observed by the methods of RFDD-PCR and proteomics. *Breast Cancer Res Treat* **104**, 21-30

208. Wada, M., Kosaka, M., Saito, S., Sano, T., Tanaka, K., and Ichihara, A. (1993) Serum concentration and localization in tumor cells of proteasomes in patients with hematologic malignancy and their pathophysiologic significance. *J Lab Clin Med* **121**, 215-223

209. Majetschak, M., and Sorell, L. T. (2008) Immunological methods to quantify and characterize proteasome complexes: development and application. *J Immunol Methods* **334**, 91-103

210. Verdoes, M., Willems, L. I., van der Linden, W. A., Duivenvoorden, B. A., van der Marel, G. A., Florea, B. I., Kisselev, A. F., and Overkleeft, H. S. (2010) A panel of subunit-selective activity-based proteasome probes. *Org Biomol Chem* **8**, 2719-2727

211. Wakata, A., Lee, H. M., Rommel, P., Toutchkine, A., Schmidt, M., and Lawrence, D. S. (2010) Simultaneous fluorescent monitoring of proteasomal subunit catalysis. *J Am Chem Soc* **132**, 1578-1582

212. Carmony, K. C., and Kim, K. B. (2013) Activity-based imaging probes of the proteasome. *Cell Biochem Biophys* **67**, 91-101

213. Priestman, M. A., Wang, Q., Jernigan, F. E., Chowdhury, R., Schmidt, M., and Lawrence, D. S. (2015) Multicolor monitoring of the proteasome's catalytic signature. *ACS Chem Biol* **10**, 433-440

214. Jernigan, F. E., and Lawrence, D. S. (2013) A broad spectrum dark quencher: construction of multiple colour protease and photolytic sensors. *Chem Commun (Camb)* **49**, 6728-6730

215. Nowak, D., Boehrer, S., Hochmuth, S., Trepohl, B., Hofmann, W., Hoelzer, D., Hofmann, W. K., Mitrou, P. S., Ruthardt, M., and Chow, K. U. (2007) Src kinase inhibitors induce apoptosis and mediate cell cycle arrest in lymphoma cells. *Anticancer Drugs* **18**, 981-995

216. Perez-Galan, P., Roue, G., Villamor, N., Montserrat, E., Campo, E., and Colomer, D. (2006) The proteasome inhibitor bortezomib induces apoptosis in mantle-cell lymphoma through generation of ROS and Noxa activation independent of p53 status. *Blood* **107**, 257-264

217. Chen, Y. J., Yeh, M. H., Yu, M. C., Wei, Y. L., Chen, W. S., Chen, J. Y., Shih, C. Y., Tu, C. Y., Chen, C. H., Hsia, T. C., Chien, P. H., Liu, S. H., Yu, Y. L., and Huang, W. C. (2013) Lapatinib-induced NF-kappaB activation sensitizes triple-negative breast cancer cells to proteasome inhibitors. *Breast Cancer Res* **15**, R108

218. Fan, G., Simmons, M. J., Ge, S., Dutta-Simmons, J., Kucharczak, J., Ron, Y., Weissmann, D., Chen, C. C., Mukherjee, C., White, E., and Gelinas, C. (2010) Defective ubiquitin-mediated degradation of antiapoptotic Bfl-1 predisposes to lymphoma. *Blood* **115**, 3559-3569

219. Lopez, J., Hesling, C., Prudent, J., Popgeorgiev, N., Gadet, R., Mikaelian, I., Rimokh, R., Gillet, G., and Gonzalo, P. (2012) Src tyrosine kinase inhibits apoptosis through the Erk1/2- dependent degradation of the death accelerator Bik. *Cell Death Differ* **19**, 1459-1469

220. Dai, Z., Quackenbush, R. C., Courtney, K. D., Grove, M., Cortez, D., Reuther, G. W., and Pendergast, A. M. (1998) Oncogenic Abl and Src tyrosine kinases elicit the ubiquitin-dependent degradation of target proteins through a Ras-independent pathway. *Genes Dev* **12**, 1415-1424

221. Hakak, Y., and Martin, G. S. (1999) Ubiquitin-dependent degradation of active Src. *Curr Biol* **9**, 1039-1042

222. Harris, K. F., Shoji, I., Cooper, E. M., Kumar, S., Oda, H., and Howley, P. M. (1999) Ubiquitin-mediated degradation of active Src tyrosine kinase. *Proc Natl Acad Sci U S A* **96**, 13738-13743

223. Vangala, J. R., Dudem, S., Jain, N., and Kalivendi, S. V. (2014) Regulation of PSMB5 protein and beta subunits of mammalian proteasome by constitutively activated signal transducer and

activator of transcription 3 (STAT3): potential role in bortezomib-mediated anticancer therapy. *J Biol Chem* **289**, 12612-12622

224. Grimm, S., Ott, C., Horlacher, M., Weber, D., Hohn, A., and Grune, T. (2012) Advanced-glycation-end-product-induced formation of immunoproteasomes: involvement of RAGE and Jak2/STAT1. *Biochem J* **448**, 127-139

225. Liu, G., Rogers, J., Murphy, C. T., and Rongo, C. (2011) EGF signalling activates the ubiquitin proteasome system to modulate C. elegans lifespan. *EMBO J* **30**, 2990-3003

226. Jacobs, C., and Rubsamen, H. (1983) Expression of pp60c-src protein kinase in adult and fetal human tissue: high activities in some sarcomas and mammary carcinomas. *Cancer Res* **43**, 1696-1702

227. Nunoda, K., Tauchi, T., Takaku, T., Okabe, S., Akahane, D., Sashida, G., Ohyashiki, J. H., and Ohyashiki, K. (2007) Identification and functional signature of genes regulated by structurally different ABL kinase inhibitors. *Oncogene* **26**, 4179-4188

228. (2006) Sprycel (dasatinib) NDA 21-986 approval letter, June 28, 2006. (U.S. Food and Drug Administration, C. f. D. E. a. R. ed.

229. Cox, J., and Mann, M. (2008) MaxQuant enables high peptide identification rates, individualized p.p.b.-range mass accuracies and proteome-wide protein quantification. *Nat Biotechnol* **26**, 1367-1372

230. Huang da, W., Sherman, B. T., and Lempicki, R. A. (2009) Bioinformatics enrichment tools: paths toward the comprehensive functional analysis of large gene lists. *Nucleic Acids Res* **37**, 1-13

231. Huang da, W., Sherman, B. T., and Lempicki, R. A. (2009) Systematic and integrative analysis of large gene lists using DAVID bioinformatics resources. *Nat Protoc* **4**, 44-57

232. Szklarczyk, D., Morris, J. H., Cook, H., Kuhn, M., Wyder, S., Simonovic, M., Santos, A., Doncheva, N. T., Roth, A., Bork, P., Jensen, L. J., and von Mering, C. (2017) The STRING database in 2017: quality-controlled protein-protein association networks, made broadly accessible. *Nucleic Acids Res* **45**, D362-D368

233. Walsh, K., McKinney, M. S., Love, C., Liu, Q., Fan, A., Patel, A., Smith, J., Beaven, A., Jima, D. D., and Dave, S. S. (2013) PAK1 mediates resistance to PI3K inhibition in lymphomas. *Clin Cancer Res* **19**, 1106-1115

234. Roskoski, R., Jr. (2015) Src protein-tyrosine kinase structure, mechanism, and small molecule inhibitors. *Pharmacol Res* **94**, 9-25

235. Okumu, D. O., East, M. P., Levine, M., Herring, L. E., Zhang, R., Gilbert, T. S. K., Litchfield, D. W., Zhang, Y., and Graves, L. M. (2017) BIRC6 mediates imatinib resistance independently of Mcl-1. *PLoS One* **12**, e0177871

236. Cann, M. L., McDonald, I. M., East, M. P., Johnson, G. L., and Graves, L. M. (2017) Measuring Kinase Activity-A Global Challenge. *J Cell Biochem*

237. Barouch-Bentov, R., and Sauer, K. (2011) Mechanisms of drug resistance in kinases. *Expert Opin Investig Drugs* **20**, 153-208

238. Kamran, M., Long, Z. J., Xu, D., Lv, S. S., Liu, B., Wang, C. L., Xu, J., Lam, E. W., and Liu, Q. (2017) Aurora kinase A regulates Survivin stability through targeting FBXL7 in gastric cancer drug resistance and prognosis. *Oncogenesis* **6**, e298

239. Furuya, M., Tsuji, N., Kobayashi, D., and Watanabe, N. (2009) Interaction between survivin and aurora-B kinase plays an important role in survivin-mediated up-regulation of human telomerase reverse transcriptase expression. *Int J Oncol* **34**, 1061-1068

240. Ito, T., Shiraki, K., Sugimoto, K., Yamanaka, T., Fujikawa, K., Ito, M., Takase, K., Moriyama, M., Kawano, H., Hayashida, M., Nakano, T., and Suzuki, A. (2000) Survivin promotes cell proliferation in human hepatocellular carcinoma. *Hepatology* **31**, 1080-1085

241. Colnaghi, R., and Wheatley, S. P. (2010) Liaisons between survivin and Plk1 during cell division and cell death. *J Biol Chem* **285**, 22592-22604

242. Eguchi, R., Kubo, S., Takeda, H., Ohta, T., Tabata, C., Ogawa, H., Nakano, T., and Fujimori, Y. (2012) Deficiency of Fyn protein is prerequisite for apoptosis induced by Src family kinase inhibitors in human mesothelioma cells. *Carcinogenesis* **33**, 969-975

243. Aziz, N., Cherwinski, H., and McMahon, M. (1999) Complementation of defective colony-stimulating factor 1 receptor signaling and mitogenesis by Raf and v-Src. *Mol Cell Biol* **19**, 1101-1115

244. Dong, Y., Sui, L., Sugimoto, K., Tai, Y., and Tokuda, M. (2001) Cyclin D1-CDK4 complex, a possible critical factor for cell proliferation and prognosis in laryngeal squamous cell carcinomas. *Int J Cancer* **95**, 209-215

245. Musgrove, E. A., Caldon, C. E., Barraclough, J., Stone, A., and Sutherland, R. L. (2011) Cyclin D as a therapeutic target in cancer. *Nat Rev Cancer* **11**, 558-572

246. Kozar, K., and Sicinski, P. (2005) Cell cycle progression without cyclin D-CDK4 and cyclin D-CDK6 complexes. *Cell Cycle* **4**, 388-391

247. Gumina, M. R., Xu, C., and Chiles, T. C. (2010) Cyclin D3 is dispensable for human diffuse large B-cell lymphoma survival and growth: evidence for redundancy with cyclin E. *Cell Cycle* **9**, 820-828

248. Asteriti, I. A., De Mattia, F., and Guarguaglini, G. (2015) Cross-Talk between AURKA and Plk1 in Mitotic Entry and Spindle Assembly. *Front Oncol* **5**, 283

249. Macurek, L., Lindqvist, A., Lim, D., Lampson, M. A., Klompmaker, R., Freire, R., Clouin, C., Taylor, S. S., Yaffe, M. B., and Medema, R. H. (2008) Polo-like kinase-1 is activated by aurora A to promote checkpoint recovery. *Nature* **455**, 119-123

250. O'Connor, A., Maffini, S., Rainey, M. D., Kaczmarczyk, A., Gaboriau, D., Musacchio, A., and Santocanale, C. (2015) Requirement for PLK1 kinase activity in the maintenance of a robust spindle assembly checkpoint. *Biol Open* **5**, 11-19

251. Jia, L., Li, B., and Yu, H. (2016) The Bub1-Plk1 kinase complex promotes spindle checkpoint signalling through Cdc20 phosphorylation. *Nat Commun* **7**, 10818

252. Nakajima, H., Toyoshima-Morimoto, F., Taniguchi, E., and Nishida, E. (2003) Identification of a consensus motif for Plk (Polo-like kinase) phosphorylation reveals Myt1 as a Plk1 substrate. *J Biol Chem* **278**, 25277-25280

253. Friedberg, J. W., Mahadevan, D., Cebula, E., Persky, D., Lossos, I., Agarwal, A. B., Jung, J., Burack, R., Zhou, X., Leonard, E. J., Fingert, H., Danaee, H., and Bernstein, S. H. (2014) Phase II study of alisertib, a selective Aurora A kinase inhibitor, in relapsed and refractory aggressive B- and T-cell non-Hodgkin lymphomas. *J Clin Oncol* **32**, 44-50

254. Choudary, I., Barr, P. M., and Friedberg, J. (2015) Recent advances in the development of Aurora kinases inhibitors in hematological malignancies. *Ther Adv Hematol* **6**, 282-294

255. Mahadevan, D., Morales, C., Cooke, L. S., Manziello, A., Mount, D. W., Persky, D. O., Fisher, R. I., Miller, T. P., and Qi, W. (2014) Alisertib added to rituximab and vincristine is synthetic lethal and potentially curative in mice with aggressive DLBCL co-overexpressing MYC and BCL2. *PLoS One* **9**, e95184

256. Yan, M., Wang, C., He, B., Yang, M., Tong, M., Long, Z., Liu, B., Peng, F., Xu, L., Zhang, Y., Liang, D., Lei, H., Subrata, S., Kelley, K. W., Lam, E. W., Jin, B., and Liu, Q. (2016) Aurora-A Kinase: A Potent Oncogene and Target for Cancer Therapy. *Med Res Rev* **36**, 1036-1079

257. D'Assoro, A. B., Haddad, T., and Galanis, E. (2015) Aurora-A Kinase as a Promising Therapeutic Target in Cancer. *Front Oncol* **5**, 295

258. Ratushny, V., Pathak, H. B., Beeharry, N., Tikhmyanova, N., Xiao, F., Li, T., Litwin, S., Connolly, D. C., Yen, T. J., Weiner, L. M., Godwin, A. K., and Golemis, E. A. (2012) Dual inhibition of SRC and Aurora kinases induces postmitotic attachment defects and cell death. *Oncogene* **31**, 1217-1227

259. Petersen, W., Liu, J., Yuan, L., Zhang, H., Schneiderjan, M., Cho, Y. J., and MacDonald, T. J. (2014) Dasatinib suppression of medulloblastoma survival and migration is markedly enhanced by combining treatment with the aurora kinase inhibitor AT9283. *Cancer Lett* **354**, 68-76

260. Illert, A. L., Seitz, A. K., Rummelt, C., Kreutmair, S., Engh, R. A., Goodstal, S., Peschel, C., Duyster, J., and von Bubnoff, N. (2014) Inhibition of Aurora kinase B is important for biologic activity of the dual inhibitors of BCR-ABL and Aurora kinases R763/AS703569 and PHA-739358 in BCR-ABL transformed cells. *PLoS One* **9**, e112318

261. Shi, H., Zhang, C. J., Chen, G. Y., and Yao, S. Q. (2012) Cell-based proteome profiling of potential dasatinib targets by use of affinity-based probes. *J Am Chem Soc* **134**, 3001-3014

262. Li, J., Rix, U., Fang, B., Bai, Y., Edwards, A., Colinge, J., Bennett, K. L., Gao, J., Song, L., Eschrich, S., Superti-Furga, G., Koomen, J., and Haura, E. B. (2010) A chemical and phosphoproteomic characterization of dasatinib action in lung cancer. *Nat Chem Biol* **6**, 291-299

263. Ngo, V. N., Davis, R. E., Lamy, L., Yu, X., Zhao, H., Lenz, G., Lam, L. T., Dave, S., Yang, L., Powell, J., and Staudt, L. M. (2006) A loss-of-function RNA interference screen for molecular targets in cancer. *Nature* **441**, 106-110

264. Kisselev, A. F., and Goldberg, A. L. (2005) Monitoring activity and inhibition of 26S proteasomes with fluorogenic peptide substrates. *Methods Enzymol* **398**, 364-378

265. Adams, G. M., Crotchett, B., Slaughter, C. A., DeMartino, G. N., and Gogol, E. P. (1998) Formation of proteasome-PA700 complexes directly correlates with activation of peptidase activity. *Biochemistry* **37**, 12927-12932

266. Adams, G. M., Falke, S., Goldberg, A. L., Slaughter, C. A., DeMartino, G. N., and Gogol, E. P. (1997) Structural and functional effects of PA700 and modulator protein on proteasomes. *J Mol Biol* **273**, 646-657

267. Chu-Ping, M., Slaughter, C. A., and DeMartino, G. N. (1992) Purification and characterization of a protein inhibitor of the 20S proteasome (macropain). *Biochim Biophys Acta* **1119**, 303-311

268. Tanahashi, N., Kawahara, H., Murakami, Y., and Tanaka, K. (1999) The proteasome-dependent proteolytic system. *Mol Biol Rep* **26**, 3-9

269. Hirano, Y., Hendil, K. B., Yashiroda, H., Iemura, S., Nagane, R., Hioki, Y., Natsume, T., Tanaka, K., and Murata, S. (2005) A heterodimeric complex that promotes the assembly of mammalian 20S proteasomes. *Nature* **437**, 1381-1385

270. Claverol, S., Burlet-Schiltz, O., Girbal-Neuhauser, E., Gairin, J. E., and Monsarrat, B. (2002) Mapping and structural dissection of human 20 S proteasome using proteomic approaches. *Mol Cell Proteomics* **1**, 567-578

271. Zhou, H., Di Palma, S., Preisinger, C., Peng, M., Polat, A. N., Heck, A. J., and Mohammed, S. (2013) Toward a comprehensive characterization of a human cancer cell phosphoproteome. *J Proteome Res* **12**, 260-271

272. Wang, X., Chen, C. F., Baker, P. R., Chen, P. L., Kaiser, P., and Huang, L. (2007) Mass spectrometric characterization of the affinity-purified human 26S proteasome complex. *Biochemistry* **46**, 3553-3565

273. Mayya, V., Lundgren, D. H., Hwang, S. I., Rezaul, K., Wu, L., Eng, J. K., Rodionov, V., and Han, D. K. (2009) Quantitative phosphoproteomic analysis of T cell receptor signaling reveals system-wide modulation of protein-protein interactions. *Sci Signal* **2**, ra46

274. Bian, Y., Song, C., Cheng, K., Dong, M., Wang, F., Huang, J., Sun, D., Wang, L., Ye, M., and Zou, H. (2014) An enzyme assisted RP-RPLC approach for in-depth analysis of human liver phosphoproteome. *J Proteomics* **96**, 253-262

275. Olsen, J. V., Vermeulen, M., Santamaria, A., Kumar, C., Miller, M. L., Jensen, L. J., Gnad, F., Cox, J., Jensen, T. S., Nigg, E. A., Brunak, S., and Mann, M. (2010) Quantitative phosphoproteomics reveals widespread full phosphorylation site occupancy during mitosis. *Sci Signal* **3**, ra3

276. Smith, D. M., Chang, S. C., Park, S., Finley, D., Cheng, Y., and Goldberg, A. L. (2007) Docking of the proteasomal ATPases' carboxyl termini in the 20S proteasome's alpha ring opens the gate for substrate entry. *Mol Cell* **27**, 731-744

277. Kim, Y. C., and DeMartino, G. N. (2011) C termini of proteasomal ATPases play nonequivalent roles in cellular assembly of mammalian 26 S proteasome. *J Biol Chem* **286**, 26652-26666

278. Park, S., Li, X., Kim, H. M., Singh, C. R., Tian, G., Hoyt, M. A., Lovell, S., Battaile, K. P., Zolkiewski, M., Coffino, P., Roelofs, J., Cheng, Y., and Finley, D. (2013) Reconfiguration of the proteasome during chaperone-mediated assembly. *Nature* **497**, 512-516

279. Pathare, G. R., Nagy, I., Bohn, S., Unverdorben, P., Hubert, A., Korner, R., Nickell, S., Lasker, K., Sali, A., Tamura, T., Nishioka, T., Forster, F., Baumeister, W., and Bracher, A. (2012) The proteasomal subunit Rpn6 is a molecular clamp holding the core and regulatory subcomplexes together. *Proc Natl Acad Sci U S A* **109**, 149-154

280. Rush, J., Moritz, A., Lee, K. A., Guo, A., Goss, V. L., Spek, E. J., Zhang, H., Zha, X. M., Polakiewicz, R. D., and Comb, M. J. (2005) Immunoaffinity profiling of tyrosine phosphorylation in cancer cells. *Nat Biotechnol* **23**, 94-101

281. Brill, L. M., Salomon, A. R., Ficarro, S. B., Mukherji, M., Stettler-Gill, M., and Peters, E. C. (2004) Robust phosphoproteomic profiling of tyrosine phosphorylation sites from human T cells using immobilized metal affinity chromatography and tandem mass spectrometry. *Anal Chem* **76**, 2763-2772

282. Lokireddy, S., Kukushkin, N. V., and Goldberg, A. L. (2015) cAMP-induced phosphorylation of 26S proteasomes on Rpn6/PSMD11 enhances their activity and the degradation of misfolded proteins. *Proc Natl Acad Sci U S A* **112**, E7176-7185

283. Liu, X., Huang, W., Li, C., Li, P., Yuan, J., Li, X., Qiu, X. B., Ma, Q., and Cao, C. (2006) Interaction between c-Abl and Arg tyrosine kinases and proteasome subunit PSMA7 regulates proteasome degradation. *Mol Cell* **22**, 317-327

284. Yamano, T., Mizukami, S., Murata, S., Chiba, T., Tanaka, K., and Udono, H. (2008) Hsp90-mediated assembly of the 26 S proteasome is involved in major histocompatibility complex class I antigen processing. *J Biol Chem* **283**, 28060-28065

285. Sokolova, V., Li, F., Polovin, G., and Park, S. (2015) Proteasome Activation is Mediated via a Functional Switch of the Rpt6 C-terminal Tail Following Chaperone-dependent Assembly. *Sci Rep* **5**, 14909

286. Lee, S. H., Park, Y., Yoon, S. K., and Yoon, J. B. (2010) Osmotic stress inhibits proteasome by p38 MAPK-dependent phosphorylation. *J Biol Chem* **285**, 41280-41289

287. Hamazaki, J., Iemura, S., Natsume, T., Yashiroda, H., Tanaka, K., and Murata, S. (2006) A novel proteasome interacting protein recruits the deubiquitinating enzyme UCH37 to 26S proteasomes. *EMBO J* **25**, 4524-4536

288. Yao, T., Song, L., Xu, W., DeMartino, G. N., Florens, L., Swanson, S. K., Washburn, M. P., Conaway, R. C., Conaway, J. W., and Cohen, R. E. (2006) Proteasome recruitment and activation of the Uch37 deubiquitinating enzyme by Adrm1. *Nat Cell Biol* **8**, 994-1002

289. Lu, X., Nowicka, U., Sridharan, V., Liu, F., Randles, L., Hymel, D., Dyba, M., Tarasov, S. G., Tarasova, N. I., Zhao, X. Z., Hamazaki, J., Murata, S., Burke, T. R., Jr., and Walters, K. J. (2017)

Structure of the Rpn13-Rpn2 complex provides insights for Rpn13 and Uch37 as anticancer targets. *Nat Commun* **8**, 15540

290. McCutchen-Maloney, S. L., Matsuda, K., Shimbara, N., Binns, D. D., Tanaka, K., Slaughter, C. A., and DeMartino, G. N. (2000) cDNA cloning, expression, and functional characterization of PI31, a proline-rich inhibitor of the proteasome. *J Biol Chem* **275**, 18557-18565

291. Franke, N. E., Niewerth, D., Assaraf, Y. G., van Meerloo, J., Vojtekova, K., van Zantwijk, C. H., Zweegman, S., Chan, E. T., Kirk, C. J., Geerke, D. P., Schimmer, A. D., Kaspers, G. J., Jansen, G., and Cloos, J. (2012) Impaired bortezomib binding to mutant beta5 subunit of the proteasome is the underlying basis for bortezomib resistance in leukemia cells. *Leukemia* **26**, 757-768

292. Kale, A. J., and Moore, B. S. (2012) Molecular mechanisms of acquired proteasome inhibitor resistance. *J Med Chem* **55**, 10317-10327

293. Kraus, M., Bader, J., Geurink, P. P., Weyburne, E. S., Mirabella, A. C., Silzle, T., Shabaneh, T. B., van der Linden, W. A., de Bruin, G., Haile, S. R., van Rooden, E., Appenzeller, C., Li, N., Kisselev, A. F., Overkleeft, H., and Driessen, C. (2015) The novel beta2-selective proteasome inhibitor LU-102 synergizes with bortezomib and carfilzomib to overcome proteasome inhibitor resistance of myeloma cells. *Haematologica* **100**, 1350-1360

294. Britton, M., Lucas, M. M., Downey, S. L., Screen, M., Pletnev, A. A., Verdoes, M., Tokhunts, R. A., Amir, O., Goddard, A. L., Pelphrey, P. M., Wright, D. L., Overkleeft, H. S., and Kisselev, A. F. (2009) Selective inhibitor of proteasome's caspase-like sites sensitizes cells to specific inhibition of chymotrypsin-like sites. *Chem Biol* **16**, 1278-1289

295. Mirabella, A. C., Pletnev, A. A., Downey, S. L., Florea, B. I., Shabaneh, T. B., Britton, M., Verdoes, M., Filippov, D. V., Overkleeft, H. S., and Kisselev, A. F. (2011) Specific cell-permeable inhibitor of proteasome trypsin-like sites selectively sensitizes myeloma cells to bortezomib and carfilzomib. *Chem Biol* **18**, 608-618

296. Geurink, P. P., van der Linden, W. A., Mirabella, A. C., Gallastegui, N., de Bruin, G., Blom, A. E., Voges, M. J., Mock, E. D., Florea, B. I., van der Marel, G. A., Driessen, C., van der Stelt, M., Groll, M., Overkleeft, H. S., and Kisselev, A. F. (2013) Incorporation of non-natural amino acids improves cell permeability and potency of specific inhibitors of proteasome trypsin-like sites. *J Med Chem* **56**, 1262-1275

297. Weyburne, E. S., Wilkins, O. M., Sha, Z., Williams, D. A., Pletnev, A. A., de Bruin, G., Overkleeft, H. S., Goldberg, A. L., Cole, M. D., and Kisselev, A. F. (2017) Inhibition of the Proteasome beta2 Site Sensitizes Triple-Negative Breast Cancer Cells to beta5 Inhibitors and Suppresses Nrf1 Activation. *Cell Chem Biol* **24**, 218-230

298. Niewerth, D., Franke, N. E., Jansen, G., Assaraf, Y. G., van Meerloo, J., Kirk, C. J., Degenhardt, J., Anderl, J., Schimmer, A. D., Zweegman, S., de Haas, V., Horton, T. M., Kaspers, G. J., and Cloos, J. (2013) Higher ratio immune versus constitutive proteasome level as novel indicator of sensitivity of pediatric acute leukemia cells to proteasome inhibitors. *Haematologica* **98**, 1896-1904

299. Masdehors, P., Merle-Beral, H., Maloum, K., Omura, S., Magdelenat, H., and Delic, J. (2000) Deregulation of the ubiquitin system and p53 proteolysis modify the apoptotic response in B-CLL lymphocytes. *Blood* **96**, 269-274

300. Kraus, M., Ruckrich, T., Reich, M., Gogel, J., Beck, A., Kammer, W., Berkers, C. R., Burg, D., Overkleeft, H., Ovaa, H., and Driessen, C. (2007) Activity patterns of proteasome subunits reflect bortezomib sensitivity of hematologic malignancies and are variable in primary human leukemia cells. *Leukemia* **21**, 84-92

301. Oberdorf, J., Carlson, E. J., and Skach, W. R. (2001) Redundancy of mammalian proteasome beta subunit function during endoplasmic reticulum associated degradation. *Biochemistry* **40**, 13397-13405

302. Kisselev, A. F., Callard, A., and Goldberg, A. L. (2006) Importance of the different proteolytic sites of the proteasome and the efficacy of inhibitors varies with the protein substrate. *J Biol Chem* **281**, 8582-8590